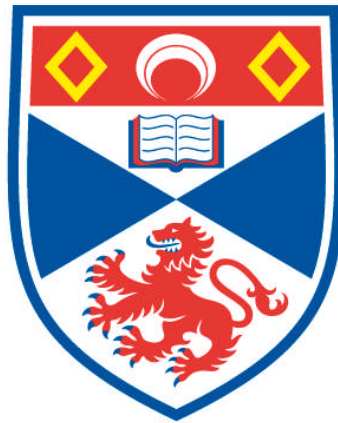


**A THEORETICAL STUDY OF POPULATION II CEPHEIDS
WITH PERIODS IN THE RANGE 10-20 DAYS**

Alan Bridger

**A Thesis Submitted for the Degree of PhD
at the
University of St Andrews**



1984

**Full metadata for this item is available in
Research@StAndrews:FullText
at:**

<http://research-repository.st-andrews.ac.uk/>

Please use this identifier to cite or link to this item:

<http://hdl.handle.net/10023/4009>

This item is protected by original copyright

A THEORETICAL STUDY OF POPULATION II CEPHEIDS WITH
PERIODS IN THE RANGE 10 - 20 DAYS

ALAN BRIDGER

UNIVERSITY OF ST. ANDREWS



! ASBTRACT

A theoretical study of population II variables with periods in the range 10 - 20 days (W Virginis variables) is presented. A modified hydrodynamic Christy code is used in conjunction with the Carson opacities, in preference to the Los Alamos tables, following the work of Carson, Stothers and Vemury on the shorter period BL Herculis variables. Twenty-five survey models are presented, along with nine other comparison models of varying masses and opacities.

A study of the observations shows that the division of these variables into two types by observers might be explained by a slightly different mass for each type, thus making the division dependent on the star's previous evolution.

The non-linear results obtained by this study show that a mass of $0.6 M_{\odot}$ is a good one to use, and that $M = 0.5 M_{\odot}$ makes little difference (although $M = 0.8 M_{\odot}$ seems to be too high). The results in general compare well with the observations, as both also show the split into two types of light curve. Three good models of individual stars are presented, on a par with the models of BL Herculis published by Carson, Stothers and Vemury. The bumps in the light and velocity curves of many of the models seem to be real, caused by the Christy "echo".

A few of the models show some RV Tauri behaviour. One in particular shows very strange behaviour, involving a violent alternation of light curve shapes. Models constructed using the Los Alamos opacities do not produce results as consistent with observations as those of the main survey.

The study shows that these stars can be represented by hydrodynamic models of mass $0.6 M_{\odot}$, using the Carson opacities, but also that convection may be important in the cooler stars in order to model them accurately. This indicates the direction in which further theoretical work may lie.

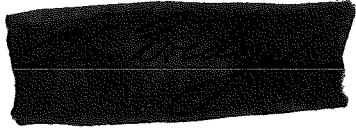
CERTIFICATE

I certify that Mr Alan Bridger has spent nine terms in research in the Department of Astronomy, University of St Andrews, that he has fulfilled the conditions of Ordinance General No. 12 and Senate Regulations under Resolution of the University Court, 1967, No. 1, and that he is qualified to submit the accompanying thesis in application for the degree of PhD.


A black rectangular redaction mark covering the signature of the supervisor.

T R Carson
Supervisor

I Alan Bridger hereby certify that this thesis which is approximately 40,000 words in length has been written by me, that it is the record of work carried out by me, and that it has not been submitted in any previous application for a higher degree.

date *15th August 1983* Signature of Candidate 

I was admitted as a research student under Ordinance No. 12 on *1st October 1979* and as a candidate for the degree of Ph.D. on *1st October 1980*, the higher study for which this is a record was carried out in the University of St Andrews between 1979 and 1982.

date *15th August 1983* signature of candidate 

In submitting this thesis to the University of St Andrews I understand that I am giving permission for it to be made available for use in accordance with the regulations of the University Library for the time being in force, subject to any copyright vested in the work not being affected thereby. I also understand that the title and abstract will be published, and that a copy of the work may be made and supplied to any bona fide library or research worker.

I would like to thank my supervisor, Dr. T.R.Carson, for suggesting the subject of this thesis, for making his opacity tables available to me, and especially for his help and encouragement throughout the work.

I would also like to thank Professor D.W.N.Stibbs for making available to me the facilities at the St. Andrews University Observatory.

Finally I would like to thank the many people who have assisted me during my study, especially C.S.Jeffery (in particular for the loan of his program to calculate convective stellar envelopes), A.D.MacFadzean, C.M.Scott, J.K.Worrell, TANO Corporation of New Orleans, and last (but certainly not least) my wife Elizabeth, whose proof-reading, typing and endless patience have been a great benefit.

ASBTRACT

A theoretical study of population II variables with periods in the range 10 - 20 days (W Virginis variables) is presented. A modified hydrodynamic Christy code is used in conjunction with the Carson opacities, in preference to the Los Alamos tables, following the work of Carson, Stothers and Vemury on the shorter period BL Herculis variables. Twenty-five survey models are presented, along with nine other comparison models of varying masses and opacities.

A study of the observations shows that the division of these variables into two types by observers might be explained by a slightly different mass for each type, thus making the division dependent on the star's previous evolution.

The non-linear results obtained by this study show that a mass of $0.6 M_{\odot}$ is a good one to use, and that $M = 0.5 M_{\odot}$ makes little difference (although $M = 0.8 M_{\odot}$ seems to be too high). The results in general compare well with the observations, as both also show the split into two types of light curve. Three good models of individual stars are presented, on a par with the models of BL Herculis published by Carson, Stothers and Vemury. The bumps in the light and velocity curves of many of the models seem to be real, caused by the Christy "echo".

A few of the models show some RV Tauri behaviour. One in particular shows very strange behaviour, involving a violent alternation of light curve shapes. Models constructed using the Los Alamos opacities do not produce results as consistent with observations as those of the main survey.

The study shows that these stars can be represented by hydrodynamic models of mass $0.6 M_{\odot}$, using the Carson opacities, but also that convection may be important in the cooler stars in order to model them accurately. This indicates the direction in which further theoretical work may lie.

CONTENTS

| | | |
|-----------|---|-----|
| CHAPTER 1 | INTRODUCTION | |
| CHAPTER 2 | PULSATION AND POPULATION II CEPHEIDS | |
| 2.1 | THE PULSATION THEORY OF VARIABLE STARS | 5 |
| 2.2 | OBSERVATIONAL AND EVOLUTIONARY ASPECTS OF POPULATION II CEPHEIDS | 18 |
| 2.3 | THEORETICAL ASPECTS OF POPULATION II CEPHEIDS | 31 |
| 2.3.1 | Introduction | 31 |
| 2.3.2 | The BL Herculis Variables And Blue Edges | 32 |
| 2.3.3 | The W Virginis Variables | 38 |
| CHAPTER 3 | THE EQUATIONS OF STELLAR PULSATION | |
| 3.1 | THE BASIC EQUATIONS | 43 |
| 3.2 | THE BOUNDARY CONDITIONS | 45 |
| 3.3 | THE DIFFERENCE EQUATIONS | 47 |
| 3.4 | THE SOLUTION OF THE IMPLICIT FORM OF THE ENERGY EQUATION | 54 |
| 3.5 | THE LUMINOSITY INTERPOLATION | 57 |
| 3.6 | THE TIME STEP. | 60 |
| 3.7 | THE INITIAL MODEL | 61 |
| 3.8 | TESTING FOR A PERIOD | 66 |
| 3.9 | NUMERICAL PROBLEMS | 67 |
| CHAPTER 4 | THE STATIC MODEL | |
| CHAPTER 5 | THE STELLAR PHYSICS | |
| 5.1 | THE EQUATION OF STATE | 76 |
| 5.2 | THE OPACITY | 83 |
| 5.2.1 | The Carson Opacities And Their Use | 83 |
| 5.2.2 | The Effect Of The Opacity | 86 |
| CHAPTER 6 | RESULTS | |
| 6.1 | THE RED EDGE OF THE INSTABILITY STRIP | 88 |
| 6.2 | THE TEST MODEL | 90 |
| 6.3 | THE INSTABILITY STRIP SURVEY | 92 |
| 6.4 | THE STATIC MODELS | 95 |
| 6.5 | GENERAL FEATURES OF THE SURVEY MODELS | 95 |
| 6.6 | THE PERIOD-MASS-RADIUS RELATION | 99 |
| 6.7 | THE LIGHT AND VELOCITY CURVES | 103 |
| 6.8 | TRENDS IN THE LIGHT AND VELOCITY CURVES | 107 |
| 6.9 | THE DRIVING REGIONS | 110 |
| 6.10 | ANALYSIS OF THE MODELS - THE CAUSES OF THE SECONDARY BUMPS | 112 |
| 6.11 | MODELS OF OBSERVED STARS | 118 |
| 6.12 | RV TAURI AND OTHER "PECULIAR" BEHAVIOUR | 120 |
| 6.13 | THE EFFECTS OF VARYING MASS AND OPACITY | 124 |

CHAPTER 7

CONCLUSION

CHAPTER 8

REFERENCES

CHAPTER 1

INTRODUCTION

It has been known since ancient times that some of the stars in the night sky vary in their brightness. However, the discovery that many of these variable stars show periodic variations that are cyclic, semi-regular or regular had to wait until about the sixteenth century. By 1800 only sixteen variable stars were known (two of these were later found to be eclipsing binaries and five were novae), of which two were classical cepheids, δ Cephei and η Aquilae. Now about 25000 intrinsic variable stars are known in this Galaxy, the vast majority of which are pulsating variables. Only about one star in $10^5 - 10^6$ is such a variable, so stellar pulsation is quite rare. Nevertheless, it is very important in astrophysics. For instance, many of these stars follow strict Period-Luminosity relationships, first determined for classical cepheids by Leavitt (Pickering 1912). These relationships provide us with basic distance indicators, both in the Galaxy and the Universe.

The theoretical study of pulsating variables is important in providing us with a test for our theories of stellar structure. Without it, the tests would be left to simple models of static stars and to the slow processes of stellar

evolution. Only stellar pulsation provides us with dynamic and observable properties (concerning a large part of the stellar envelope) which can be modelled.

Previous modellers of pulsating variables have studied the classical cepheids, RR Lyrae stars and many of the other types. Most of these studies have used the opacities calculated by A.N.Cox and his various co-workers, but recently a new set of stellar opacities has been calculated by Carson (1976). These opacities have been used successfully to model RR Lyrae stars, classical cepheids and BL Herculis variables. In many cases the new opacities seem to produce better results than those obtained with the Cox opacities; however, as there is some debate as to the validity of ^{various} ~~the Carson~~ opacities, it is important to use them to model as many different types of variable stars as possible, to see how they handle these variations. With this in mind, this study has been made of the W Virginis variables, also known as population II cepheids, with periods between 10 and 20 days. These stars are the population II counterparts of the classical cepheids, although they do not seem to show quite the same trends as are seen in the latter. In particular there is no counterpart to the so-called Hertzsprung progression.

Because of their faintness, observations of W Virginis variables are not as good as those of classical cepheids, and in fact observations of the velocity curves are almost non-existent. However, it has been possible to classify the light curves of these stars in many ways because some of them do have secondary bumps. The most recent classification by Kwee divided them into two groups.

In this study the W Virginis stars are modelled using the Carson opacities in an attempt to reproduce the observed light curves, and in particular the dichotomy of the light curves observed by Kwee. These variables have not been studied very extensively theoretically heretofore, so this work provides not only a test of the new opacities, but also a further test of pulsation theory.

This study follows on from that of Carson, Stothers and Vemury (1981) and Carson and Stothers (1982), who modelled the BL Herculis stars (population II cepheids with periods between 1 and 10 days). One aim of those works was to reproduce the observed light curves in some detail. This aim was achieved with a good model of BL Herculis itself, which reproduces both the light and velocity curves very well, and may be the best published model of an individual star. This aim is continued in this work, as the reproduction of the observed properties of variable stars is surely one of the most important aims of the theoretical study of pulsation. Since true light and velocity curves can only be obtained by hydrodynamic modelling, that is the method used here.

In section 2 a review of pulsating stars is presented in three parts; a summary of pulsation theory in general, a study of the available observations of W Virginis stars (with a review of current evolutionary ideas about these variables), and a review of the application of pulsation theory to the BL Herculis and W Virginis variables. In section 3 non-linear pulsation theory is discussed, and the method used is presented. Section 4 describes the procedure used to calculate the static model which served as a starting point. In section

5 the equation of state and the opacity are discussed. The results of the models and an extensive discussion of them is presented in section 6. Section 7 concludes the study, and suggests improvements and further areas for study.

CHAPTER 2

PULSATION AND POPULATION II CEPHEIDS

2.1 THE PULSATION THEORY OF VARIABLE STARS

The hypothesis that cyclic pulsations could account for the variability of many stars was put forward in the Nineteenth century. Shapley (1914) put the theory onto a firmer base, and then Eddington (1918a, 1918b, 1926) established the mathematical foundations of the theory of adiabatic free radial oscillations of gaseous spheres. He showed that free oscillations would quickly decay, contrary to observations, and therefore that a driving mechanism was required to keep the star pulsating. Eddington discussed two possible driving mechanisms, one of which (the "valve" mechanism) provided the basis for our present understanding of stellar pulsation. Reviews of the early history of the pulsation theory may be found in Rosseland (1949), Ledoux and Walraven (1958) and Zhevakin (1963).

In looking for possible driving agents for the pulsation of cepheids, Eddington ^{first suggested} ~~believed~~ that the nuclear reactions towards the stellar centre were the cause of the instability; in particular, that the increase in energy output on

compression would cause expansion, and the corresponding drop in nuclear energy production would allow subsequent compression and thus the maintenance of the cycle. This mechanism has now been shown to be untenable, since the pulsation amplitude towards the centre of the star is about 10^6 times smaller than that at the surface (Epstein 1950; J.P.Cox 1955).

The other possible cause discussed by Eddington was the "valve" mechanism in which the outer layers of the star behave rather like a thermodynamic heat engine. If a mass element in a star can absorb heat on compression, and release it on expansion, then it will act as a driving force, pushing the pulsation. Regions which act in the opposite manner will thus tend to damp the motion. It is this modulation of the heat flow through the layers of the star that modern theories are based on, though the way in which a driving region works varies according to the way heat energy is "trapped". Various ways of trapping heat energy on compression (which thus cause driving) are discussed later.

The basic equations used in the study of stellar pulsation are those of stellar structure, with time dependent terms added (compare section 3.1). These equations, in differential form, and with the variables defined as in section 3.1 are given here.

Continuity of Mass

$$\frac{dM_r}{dr} = 4\pi r^2 \rho(r) \quad (2.1)$$

Equation of Motion (or Hydrodynamic equilibrium)

$$\frac{\partial^2 r}{\partial t^2} = -\frac{GM_r}{r^2} - \frac{1}{\rho} \frac{\partial P}{\partial r} \quad (2.2)$$

$$\frac{\partial E}{\partial t} + P \frac{\partial V}{\partial t} = \epsilon - \frac{dL}{4\pi r^2 \rho dr} \quad (2.3)$$

and the luminosity is given (in the diffusion approximation) by;

$$L_r = - \frac{4\pi r^2 \rho \sigma}{3 \kappa(\rho, T)} \frac{d(T^4)}{dr} \quad (2.4)$$

These equations, along with formulae (or tables) for the opacity $\kappa(\rho, T)$, energy generation $\epsilon(\rho, T)$ and equation of state $P = P(\rho, T)$ and suitable boundary conditions can be solved for the radial pulsations of a star, neglecting convection, rotation, and magnetic fields, and assuming that the diffusion approximation for energy transfer holds throughout. For most problems the central core of the star can be ignored, since it has been shown that this region plays very little part in the pulsation. In this case the energy generation, ϵ , can be put equal to zero in equation (2.3). Using modern fast digital computers the problem is usually solved by linear or non-linear methods, both of which require an initial static solution of the equations as a starting point (see section 4). Reviews of modern work on stellar pulsation can be found in Christy (1966c), and J.P.Cox (1974, 1980).

In the linear theory, the pulsation equations are linearized and we thus consider small-amplitude oscillations about the equilibrium state (as defined by the static model). For many stars the motion is nearly adiabatic throughout the star, and so by simply assuming adiabatic heat changes (the Linear Adiabatic Theory) it is possible to obtain some quite good results for the dynamical aspects of the pulsation. Using

adiabatic theory, periods can be predicted, along with the dynamical stability and the relative pulsational amplitudes inside the star. However, since the heat changes are adiabatic it is not possible to obtain information regarding either the pulsational stability of the star or the luminosity variations. Only by using non-adiabatic changes can we determine the stability or instability of a star against pulsation. It is near the surface, where the heat capacity becomes very small, that the non-adiabatic effects are most noticeable. In the linear treatment the star is divided into some number of mass zones, just as in the non-linear treatment used here, but with many more zones. By measuring the change, $\Delta\tau_m$, in kinetic energy in each zone over one period it is possible to find which of the zones are driving and which are damping, since a driving region gains heat at maximum compression and a damping region loses heat at maximum compression. So $\Delta\tau_m > 0$ indicates driving while $\Delta\tau_m < 0$ shows damping. Summing over all of the mass zones we obtain the change $\Delta\tau$ in kinetic energy for the whole star. Since the gravitational energy term is conservative we can put $\Delta\tau = W$, where W is the PdV work done by all of the mass zones in one period. So for the whole star, $\Delta\tau = W > 0$ indicates pulsational instability, or the growth of pulsations, and $\Delta\tau < 0$ indicates pulsational stability, or the damping of any pulsations. It is also possible to determine the e-folding time τ_d for decay of the pulsations (the time required for the amplitude to decay to $1/e$ of its former value). This is defined by

$$\frac{1}{\tau_d} = -\frac{1}{2} \frac{\langle \frac{dW}{dt} \rangle}{\langle \delta\psi \rangle} \quad (2.5)$$

where $\delta\psi$ is the total pulsation energy of the star (kinetic

and potential)). The angular brackets indicate means over a period. For the linear theory (i.e. small amplitudes) we define the stability coefficient κ ,

$$\kappa = 1/\tau_d$$

So $\kappa > 0$ indicates stability and $\kappa < 0$ indicates instability. Typical values of the damping time, τ_d , for variable stars range (in units of P , the fundamental pulsation period) from 1 - 10 for the long period red variables to 10^4 to 10^6 for the short period δ scuti stars. For classical cepheids $\tau_d/P \sim 10^2 - 10^3$ and for population II cepheids $\tau_d/P \sim 10 - 20$. Using linear, non-adiabatic methods, much can be learned about the pulsations of variable stars; the mode and cause of pulsation can be established, along with the instability/stability of the star. Thus linear theory is very useful in determining the areas of pulsational instability in the HR diagram, the "blue edges" of instability regions, and if convection is included in some way, the "red edges" also. However, because the treatment is linear and the amplitudes are small, the linear theory cannot usually describe individual stars very well, particularly those with moderate to large amplitudes. At these amplitudes non-linear effects enter; they cause the light and velocity curves to deviate from pure sine waves, and have other effects such as lengthening the pulsation period. This is where non-linear methods are superior; in the modelling of individual stars and in trying to reproduce observed light and velocity curves.

Before discussing the non-linear methods used it is appropriate to discuss the possible driving mechanisms that may cause pulsational instability in stars. These are the

descendants of Eddington's original valve mechanism, and they all rely on the fact that the ionization of a constituent of the stellar envelope can modulate the flux variations. When such a region is gaining heat on compression and losing it on expansion maximum pressure occurs after maximum density, thus causing a "pumping up" of the pulsation. In most stars the luminosity variation $\delta L_r/L_r$ increases outwards; thus each zone is losing energy on compression, giving what is termed radiative damping. This behaviour is due to the fact that on compression the opacity usually decreases, allowing the heat to leak out. In most stars the important ionization zones in the envelope are those of hydrogen, neutral helium and single ionized helium. These three will usually only comprise two regions of ionization, the He II one at about 4×10^4 K and the combined region of H and He I ionization at about $1-1.5 \times 10^4$ K. The latter acts very much like a single region and is frequently simply called the H-ionization zone. In an ionization zone the adiabatic exponent $\bar{\gamma}_3 - 1$ becomes very small, as most of the energy on compression is going into ionizing the material, not raising the temperature. The smaller temperature variations also cause $\delta L_r/L_r$ to be small (since $L_r \propto T^4$), and thus the radiation is effectively "dammed" on compression. Then, on expansion, the temperature rises more than would be the case in adiabatic motion, and so does the pressure, which causes the driving of any incipient pulsation. This driving mechanism is called the γ -mechanism (Cox, Cox, Olsen, King and Eilers 1966).

Another mechanism, called by Baker and Kippenhahn (1962) the κ -mechanism, is caused by the possibility that for an opacity law of the form $\kappa \propto \rho^n T^{-s}$ ($n, s > 0$) the opacity may increase on compression if $\sqrt{3} - 1$ (and so $\delta T/T$) is small, i.e. in a region of ionization. This local opacity increase dams the radiation on compression, causing further driving.

Stellingwerf (1978, 1979) notes another possible cause of driving, which he called the bump-mechanism. If, in the above opacity dependence, s is large and negative (or even just less positive) as happens in the H-ionization zone, then there can be a damming of radiation on compression even if $\sqrt{3} - 1$ is close to its normal value of $5/3$. This may be important in the driving of some stars.

Whether or not a particular ionization region will cause driving in an actual star depends on where it lies in the stellar envelope in relation to a region known as the transition region, which divides the quasi-adiabatic interior from the non-adiabatic exterior. As the radius of a star increases (for given mass, luminosity and composition) the transition region moves outwards in mass. Above the transition region, in the non-adiabatic zones, the luminosity variations tend to be "frozen-in". There is no variation of $\delta L_r/L_r$ with space. If both ionization zones lie in this region then the star remains stable, since $\delta L_r/L_r$ remains constant, despite the variation of $(\delta L_r/L_r)_a$, the adiabatic variation. For a star with larger radius the He II ionization region may coincide with the transition region. In this case in the inner portion of the He II ionization zone the luminosity variation follows the adiabatic variation, whilst in the outer portion the

variation $\delta L_r/L_r$ is still constant in space, frozen at the small value it had in the middle of the zone. So the damping effect of the outer regions is eliminated and the driving of the inner portion can make the star unstable. The H-ionization zone still lies too far out to have a large effect. This coincidence of He II ionization zone and transition region seems to be the cause of pulsation in the whole cepheid instability strip in the HR diagram.

As the radius increases further (moving redwards in the HR diagram) the H-ionization region moves into coincidence with the transition region, potentially causing very strong driving. However, by this stage convection has usually appeared to damp the driving, bringing a return to stability and defining a "red edge". The effect of convection on pulsation is discussed later.

After suggestions by Zhevakin (1953, 1954a,b), Cox and Whitney (1958) and Aleshin (1959) that second helium ionization might be the scene of the valve mechanism of Eddington, work by Baker and Kippenhahn (1962) and J.P.Cox (1963) confirmed the effectiveness of He II ionization as a driving mechanism. Many studies have since reconfirmed this. It has also been suggested that H-ionization may be the major driving agent in the red variables.

Since most real stars are obviously non-linear (the non-sinusoidal light curves evidence this), only by solving the full set of non-linear equations can we hope to describe the pulsation of individual stars, including the light curves, velocity curves, limiting amplitudes etc. However, the set of non-linear equations is not soluble analytically except in a

few, totally unrealistic cases. (For adiabatic motion with constant Γ_1 and the homogenous model with constant Γ_1). However, some one zone non-linear models are relatively simple, and can help our understanding of some of the features of pulsation (for example Baker 1966; Usher and Whitney 1968; Rudd and Rosenberg 1970; and Stellingwerf 1972).

Most non-linear methods treat the equations as an initial value problem, integrating the equations forward in time from some initial conditions, usually a model envelope in hydrostatic and thermal equilibrium. The usual treatment is to divide the star between 25 to 50 mass zones and put the equations into difference form. Given sufficient computer time these methods provide information about the limiting amplitude, the growth (or decay) of the pulsations, the non-linear effects, the light and velocity curves, etc. The methods used by different investigators vary widely with no way of telling the "best" method, leaving the study looking somewhat like an art form. One problem associated with all non-linear approaches is the need to use an artificial viscosity, to spread the H-ionization front over several zones. The form that this takes is almost arbitrary, including at least one unknown parameter. The techniques used in this study originated with Christy (1964, 1966a, 1967) and have been used and modified by many authors since.

Aleshin's (1964) non-linear method was a little different. He just treated the region $T < \sim 5 \times 10^4$ K (normally most methods use $r > R_*/10$ or $T < \sim 10^6$ K), and he used only 10 zones, with the inner boundary having a sinusoidal oscillation with period and luminosity variations obtained from the linear

theory. The results were rather limited, but the inner boundary of sinusoidal variation has since been used by Stellingwerf (1974) in his non-linear scheme. Stellingwerf's scheme is a modification of that proposed by Baker and von Sengbusch (1969), and von Sengbusch (1973). In the von Sengbusch approach 10^4 linear equations are solved for 4 variables in J zones for K time-steps in a period. This gives $4J(K+1)+1$ unknowns, including the period. The solution is iterated until exact periodic repetition is obtained. The non-linear calculation is in fact treated as an eigenvalue problem with the period being a solution.

Stellingwerf's approach is a compromise between the usual Christy techniques and the von Sengbusch method. An initial model is found in the usual way, and an estimate of the period is made. A normal non-linear code then integrates through one period. Corrections are then made to the period and the physical variables, and the code integrates another period. This iteration proceeds until exact repetition is achieved. On convergence the non-linear code can be run for a time to allow complete analysis. Each mode can be studied in this manner, and the time taken to reach full amplitude is generally considerably shorter than with the usual e-folding growth approach. For stars that are not fully periodic, or aperiodic, this approach is limited. This is the case with certain population II cepheids, and in any case their growth rates are large enough (10-20 periods) so as to make any time-saving minimal.

Another approach to the problem is due to Castor, and is described by Castor, Davis and Davison (1977) and Davis and Davison (1978). In this approach the static Lagrangian mass zoning is replaced by a dynamic zoning in which the zones move during the time integration so as to keep a large number of zones in the hydrogen ionization front. This method produces a far better resolution of the ionization front, eliminating some of the spurious bumps sometimes seen in the light curves produced by normal Lagrangian codes.

One problem experienced in all attempts to solve the pulsation equations is the question of what to use as an external boundary condition, and where to apply it. Unno (1965) made a study of some boundary conditions. Most studies use a form of the perfect reflection (or standing wave) boundary condition. Here in the linear form, we have,

$$\left(\frac{d\delta P}{dr}\right)_{\text{surface}} = 0 \quad (2.6)$$

This assumes that the gas density vanishes at the surface. Equation (2.6) is correct for radiation pressure being negligible or significant. The equivalent non-linear boundary conditions are $P_{\text{tot}} = 0$ or $P_g = 0$. These "standing wave" boundary conditions give perfect reflection at the stellar surface and are the ones used in this study.

Another dynamic boundary condition is the "running wave" condition, where the reflection is not perfect, and some of the pulsational energy is allowed to run into a corona surrounding the star.

For the surface boundary condition on the heat equation we assume that there is some surface in the stellar atmosphere where there is no radiation incident from outside, and where the optical depth τ is zero. In the thermal diffusion approximation we can assume the Eddington relation,

$$T^4 = \frac{3}{4} T_e^4 (\tau + 2/3)$$

Baker and Kippenhahn (1965) applied their outer boundary condition at the photosphere, i.e. at $\tau = 2/3$. However, it is much better to apply the condition at small τ , $\tau \simeq 0$ (sometimes called the Castor-Iben boundary condition). This is what most investigators now choose. Another approach is to treat the optically thin zones using radiative transfer, and not diffusion theory, (Davis 1972). This is more correct, and the boundary condition on the radiation flow is obtained automatically. However, the increased complexity naturally increases the computing time required.

Until recently the effect of convection on pulsation has only been studied in an elementary way. There are two effects to consider, the change in the static structure and the interaction with the pulsation. One treatment, using linear methods, is to create a static model including convection and then ignore the convective flux variations. (Baker and Kippenhahn, 1965, for example). The problem with including convection in the pulsation itself is that of the time dependence. Some attempts have been made to include time-dependence in the conventional mixing-length theory, by (for example) Gough (1977) and Unno (1967). Gough's work has been applied to RR Lyrae variables (Baker and Gough 1979), concluding that convection has a negligible effect near the

blue edge, but that it can be responsible for the return to stability at the red edge. Baker and Gough's linear work provided a red edge in about the right place. Convection has largely been ignored in non-linear work, but Deupree included convection in a new fundamental way in a series of papers (1977a,b,c,d). He treats two spatial dimensions, allowing the formation of two-dimensional eddies, in a non-linear Euler-Lagrange formulation, which makes no assumption about the time behaviour of convection, and makes no use of the mixing length theory. The limitations of the approach are that only two space dimensions are used, and that Deupree had to introduce an eddy viscosity coefficient to treat the break up of large eddies and the conversion of convective kinetic energy into heat. More recently Stellingwerf (1982a,b) derived a scheme for treating non-local convection in a conventional spherically symmetric non-linear code. This approach is also different from the conventional mixing length theory. Turbulent pressure and viscosity are included in the treatment. Stellingwerf has also applied his work to the RR Lyrae variables.

All of the studies using convection indicate that convection has little effect near the blue edge of the instability strip, and can thus be safely ignored for the hotter models. However, on approaching the red edge, convection plays an increasing part, and the studies of Baker and Gough, Deupree, and Stellingwerf all indicate a return to stability here, as the convective motions increase. Stellingwerf has not determined the red edge of the RR Lyrae strip, but the edges obtained by Deupree (1977a) and Baker and Gough (1979) are essentially in agreement. According to

Deupree's work it seems that at maximum compression the convection causes the energy stored in the driving regions by the κ - and γ -mechanisms to leak out, thus reducing the driving. It seems that only a small amount of convection in an ionization zone is necessary to bring about stability.

Thus the problems of including convection in pulsation are beginning to be solved, although much useful work can still be done without the inclusion of convection; it generally only has a large effect near the red edge, and has only a small effect on the light and velocity curves of the stars. For the cooler models it probably limits the growth of the pulsation, possibly to a large extent near the red edge.

2.2 OBSERVATIONAL AND EVOLUTIONARY ASPECTS OF POPULATION II CEPHEIDS

Population II cepheids were first noticed as being distinct from the population I "classical" cepheids by virtue of their light curves, which are usually very different from those of classical cepheids of similar periods. Payne-Gaposchkin (1956) points out that this was noticed as a deviation from the Hertzsprung progression of classical cepheids. Having drawn this distinction, the position of many of these variables far from the galactic plane (as well as spectroscopic analysis) identified them as population II objects. As such they are also found in globular clusters, along with those other population II variables, RR Lyrae stars.

The periods of type II cepheids (also frequently called W Virginis stars, although it might be better to restrict this title to a specific class of these stars, those with $10 < P < 20$ days), range from 1 day up to about 50 days, where at the upper end the range overlaps that of the so-called RV Tauri variables, also population II objects. However, there are minima in the Period-Frequency distribution of population II cepheids, one between $P \sim 6$ days and $P \sim 10$ days, and another at $P \sim 22$ days. (See Kraft 1972). The first gap seems to be related to the evolutionary mechanisms for feeding the stars into the instability strip.

Iben and Rood (1970) have shown that as population II stars evolve off the horizontal branch, they move upwards in the HR diagram before moving towards the asymptotic giant branch, giving rise to the short period group of variables ($1 < P < \sim 6$ days), or AHB cepheids (for "above the horizontal branch"). Then as the star ascends the asymptotic giant branch, evolutionary studies have shown that the helium burning shell source undergoes a series of "flashes", or thermal instabilities, causing the star to execute a blue loop in the HR diagram (similar to the case for classical cepheids) which might take it through the population II instability strip (Schwarzschild and Harm 1970; Mengel 1973; Sweigart 1973). In particular, Mengel shows that an asymptotic giant branch star, of mass $0.6M_{\odot}$, undergoing thermal relaxation cycles, may make several blueward loops, but only for the later relaxation cycles, at higher luminosities and lower envelope mass.

These evolutionary ideas seem in general to explain the presence of type II cepheids in globular clusters, though many details still have to be explained (among them an explanation for the gap at $P \sim 22$ days).

If these current theories of post horizontal branch evolution in globular clusters are correct, then the masses and helium abundances of population II cepheids must be constrained to the ranges $0.5 \leq M/M_{\odot} \leq 0.7$, and $0.2 \leq Y \leq 0.3$. Bohm-Vitense et al. (1974) add more weight to this argument, giving a range for M/M_{\odot} of $0.47 - 0.8$, where the lower limit is the minimum likely mass of the helium core in a star undergoing the helium flash on the Red-Giant branch, and the upper limit is the currently accepted mass of a cluster star at the main sequence turn-off.

For the short period type II cepheids (often referred to as the BL Herculis stars) many of their light and velocity curves show bumps, reminiscent of the bump in the Hertzsprung progression for classical cepheids. Petersen's (1980) analysis of 18 BL Herculis stars with bumps on their light curves yielded a mean "bump mass" of 0.60 ± 0.09 , in good agreement with the expected evolutionary masses (a situation very different from that previously experienced with classical bump cepheids!).

Observations of those stars with periods of 10 days and upwards are very scarce, with the possible exception of W Virginis itself. Payne-Gaposchkin (1956) reviews the light curves of several, and the series of papers by Kwee (1967a, 1967b, 1968) and Kwee and Braun (1967) produce fairly good light curves for some field variables (see figure 2.1), and

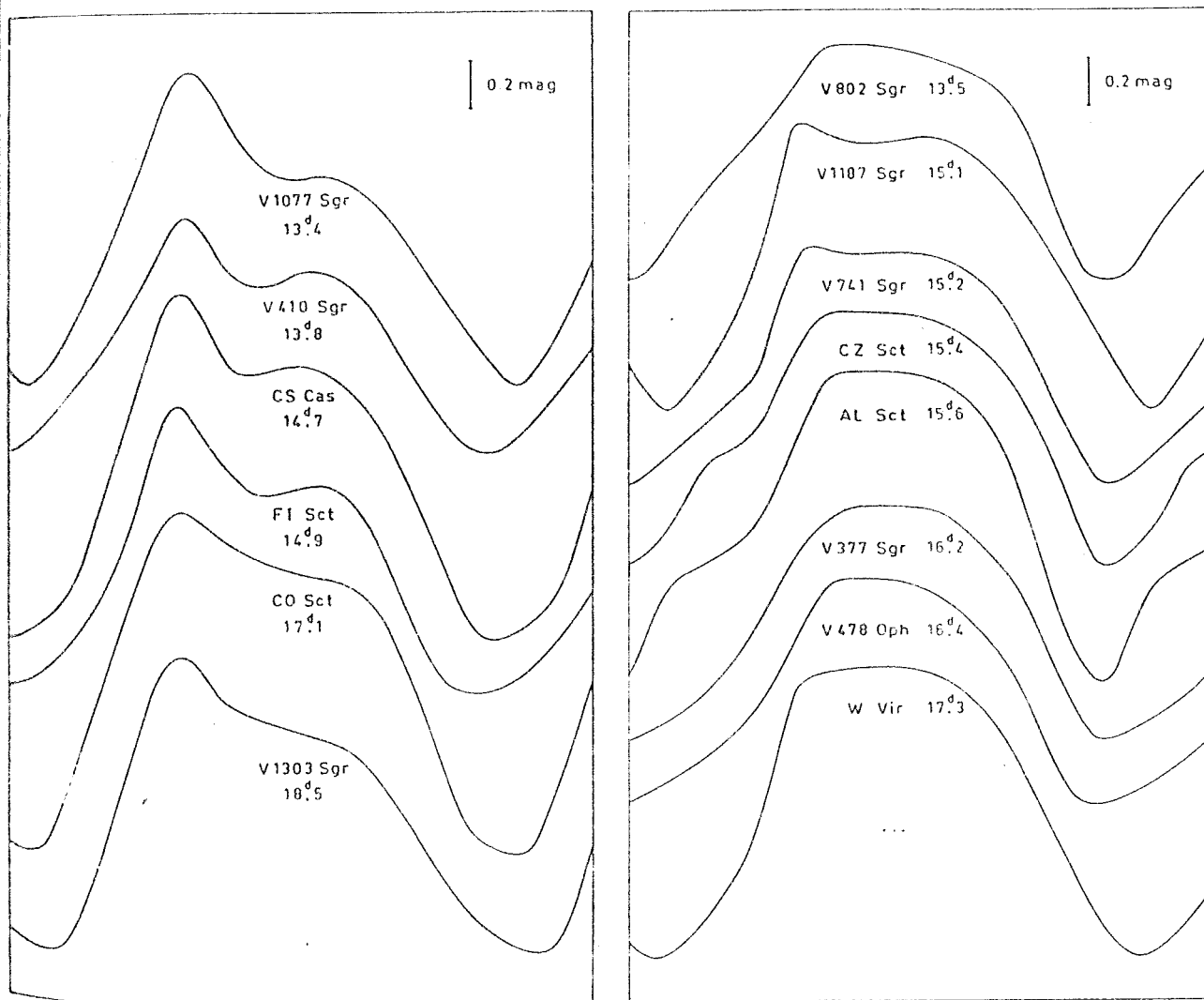


Figure 2.1 Observed crested and flat-topped light curves
(taken from Kwee 1967, figures 4 and 5)

compares the observations with those of previous observers, generally getting good agreement. W Virginis itself has been studied in detail by a few authors, in particular Abt (1954) and Barker et al. (1971). Apart from W Virginis, the only radial velocity observations available in this period range would appear to be by Joy (1949), sufficient for only rough curves of two stars.

Kwee (1967b) divided the type II cepheids observed by Kwee and Braun (1967) into three groups (most were type II cepheids, with three RR Lyrae stars and five classical cepheids, the latter largely being used for comparison). Those with $1 < P < 3$ days were called short period population II cepheids (now the BL Herculis stars), and those with $13 < P < 20$ days were divided, by the shape of their light curves, into crested and flat-topped variables. A similar classification had been made by Payne-Gaposchkin (1956), though the groupings were very different. Those with $3 < P < 13$ days were scarce and had generally featureless curves.

The light curve of a crested variable (hereafter sometimes referred to as c-type) is characterized by a distinct maximum, followed by a shoulder or bump on the descending branch, and a faster rise to maximum than fall to minimum. The flat-topped variables (hereafter sometimes called f-type) do indeed have a flat top to their light curves - a difficult to define maximum, and in general less asymmetry. However this classification must still be regarded with some doubt. For example, Kwee classifies the light curve of V1187 Sgr as flat-topped. Could it not be justifiably be called crested? The observations still leave in many cases a margin of error in the shape of the

light curve. Sometimes earlier observations would suggest a different classification. Since Kwee's observations cover only field stars the question arises as to whether the cluster variables divide in the same manner. Observations of the cluster variables by several authors (in particular Arp 1955; Demers 1969; Demers and Wehlau 1971; Fernie 1963) seem to confirm the dichotomy, though still with the reservations noted above.

Also as noted above, radial velocity curves for W Virginis stars are scarce, Abt's study of W Virignis probably providing the best available. However, from the data available, and from observations of longer period population II variables (e.g. Wallerstein 1958), some conclusions can be drawn. On rising light most of these stars, particularly those with periods of about 16 - 20 days, show hydrogen emission lines, frequently quite bright. This effect is not seen in the observations of classical cepheids (though it may be apparent in the ultra-violet). Also, related to this, the velocity curves are discontinuous, with double lines appearing in the spectra at maximum light. Both the emission lines and the discontinuous velocity curves can be explained in terms of a shock wave moving out through the atmosphere at, and just before, maximum light (Abt 1954, Wallerstein 1959, and references therein). So it is likely that any models of these stars should show a large outward velocity on approach to maximum light.

The population II cepheids follow a period-luminosity relation rather like that of the classical cepheids, though with a slightly different gradient and lying lower in the period-luminosity diagram. Arp (1955) first demonstrated the

existence of two period-luminosity relations for the cepheids, though his observational errors were rather large. Demers and Wehlau (1971) studied cluster population II variables, producing a $P-M_V$ relation which was later improved by the study of Demers and Harris (1974, equation [2.7]).

$$\langle M_V \rangle = - (0.08 \pm 0.09) - (1.59 \pm 0.11) \log P \quad (2.7)$$

Demers and Harris used equation (2.7) to estimate the absolute visual magnitudes of 11 field variables, whose colour excesses had been estimated from UBV photometry. Mean colours for the stars were already known since the field variables could be placed on a colour-magnitude diagram. The cluster variables already had UBV data (except for some which were not observed in the UBV system. These had been transformed by Kwee 1968). The combined colour-magnitude diagram for field and cluster population II variables shows a wide instability strip situated below that of the classical cepheids, and about three times the width.

Using the tables of Bohm-Vitense (1973), Demers and Harris converted their $(M_V, B-V)$ values into $(\log(L/L_\odot), \log T_e)$ values so that the instability strip could be plotted on an HR diagram (figure 2.2). The boundaries of their instability strip are defined by

$$\log(L/L_\odot) = - 10.75 \log T_e + \begin{matrix} 43.5 & \text{(blue edge)} \\ 42.4 & \text{(red edge)} \end{matrix} \quad (2.8)$$

Also plotted in figure 2.2 are estimates of $(\log(L/L_\odot), \log T_e)$ for 11 population II cepheids by Bohm-Vitense et al. (1974). All but two of the stars studied by Bohm-Vitense et al. are also studied by Demers and Harris, but the agreement

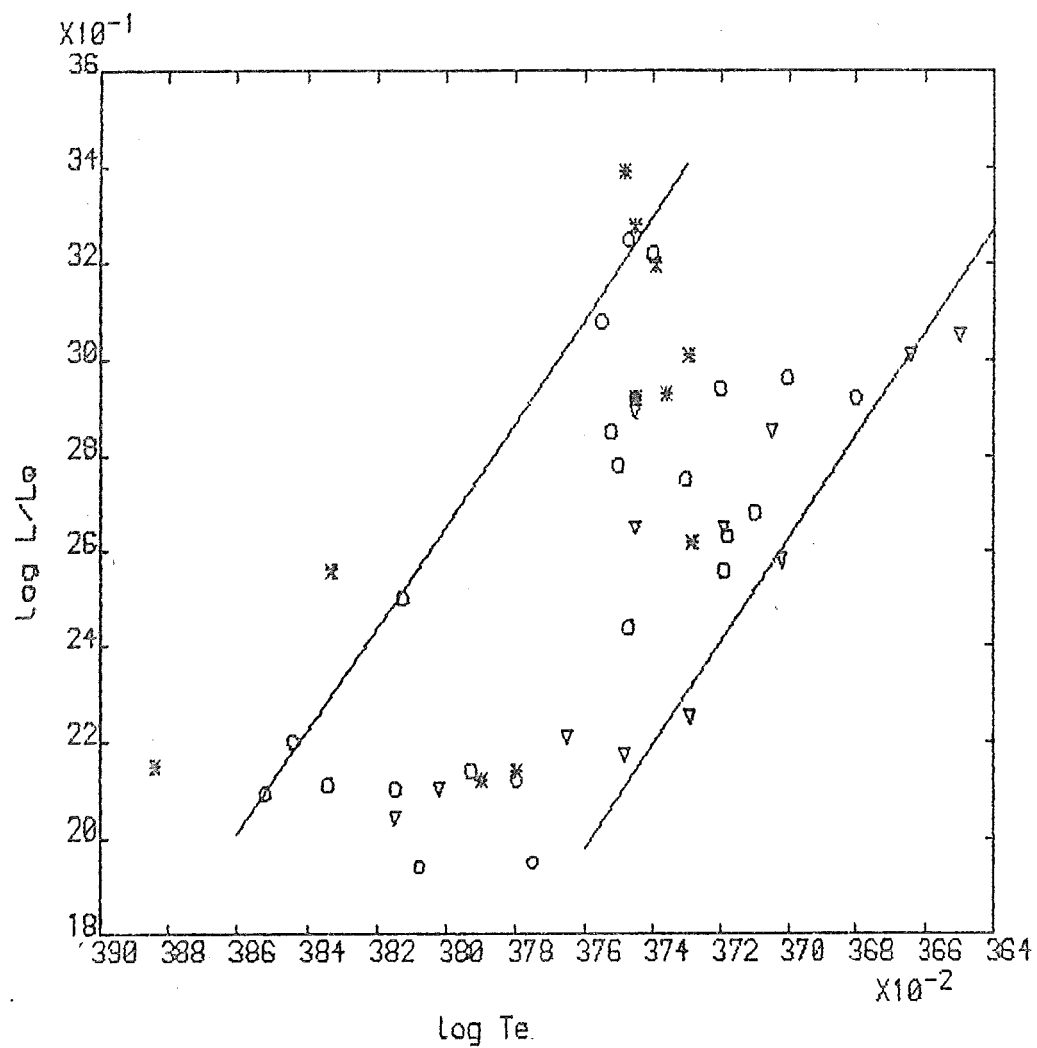


Figure 2.2 The observed Instability Strip

Edges from Demers & Harris (1974)
 o cluster stars
 ∇ field stars
 * from Bohm-Vitense et al. (1974)

is not in general very close; for instance, their estimates for the $\log T_e$ of W Vir differ by over 0.03. This would seem to indicate a possible error on the Demers and Harris blue edge of about ± 0.03 in $\log T_e$, or more.

In figure 2.2 the distinction between the short-period ($P < \sim 3$ days) BL Herculis variables and the longer period ($P > \sim 6$ days) W Virginis variables can be clearly seen. The BL Herculis stars form a definite group at $\log(L/L_\odot) < 2.3$, whilst the W Virginis stars cover a wide luminosity range above $\log(L/L_\odot) \simeq 2.5$. This wide spread of luminosities can be explained by the fact that the phase of asymptotic giant branch evolution at which the star executes a "blue loop" is very sensitive to the mass, so a small range of masses suffices to provide the large observed spread in luminosity (Mengel 1973).

Two stars (M13 no. 2 and ω Cen no. 48) fall in the gap with periods of 5.12 and 4.48 days. Demers and Harris state that about 6% of the cluster population II variables have $3 < P < 6$ days and that a similar percentage of the field variables seem to fall in this range. Thus we see that the period distribution and the appearance of the variables on the HR diagram confirm the division of the variables into the two groups.

Since the radial velocity data for the stars with $10 < P < 20$ days is very scarce, the light curves and periods are the only observational data that theoretical work can aim at reproducing. Even here there are problems. Several authors (Kwee 1967a, 1967b; Vasiljanovskaja and Erleksova 1968; Coutts 1973; and Stobie 1975, for example), have noted that the W Virginis variables show variations in period and light curves

from cycle to cycle. Sometimes their variations are regular, providing a period doubling effect somewhat like that of the RV Tauri variables. More often it is apparently random (though some of the observations may be insufficient to find any regularity if it exists), consisting of small period changes and/or slight changes in the shape of the light curve. Possibly, in marginal cases, this may even change its classification from crested to flat-topped and vice versa (for instance, see the plots of the light curve of V741 Sgr given in Payne-Gaposchkin [1956] and in Kwee [1967b]). Also for the star AP Her, Kwee and Braun's observations give a classification of x (i.e. no distinctive features, neither c- nor f-type), but those of Michslowska-Smak and Smak (1965) suggest that AP Her has a slight shoulder or incipient bump, and may be at least xc. RU Cam appears to be an extreme example of irregularity. In 1964 it stopped pulsating (Demers and Fernie 1966), but it has since restarted (Broglia and Guerrero 1973).

In tables 2.1a and b are presented data for 16 field and 11 cluster population II variables with periods between 10 and 20 days. This is by no means an exhaustive list, but includes most (if not all) of the best observed stars. The values of most of the parameters are taken from the study referenced in each case, this value considered to be probably the best available. In many cases the values are taken from graphs or curves and are therefore subject to a reading error, which is represented by the number of figures given. This error is probably far smaller than the actual error, which generally is not known.

| Star | P(days) | logP | $\langle V \rangle$ | $\langle M_V \rangle$ | $\langle B-V \rangle_0$ | $\log(L/L_\odot)$ | logTe | $\log(R/R_\odot)$ | ΔV | Asym(lum) | ϕ_b^1 | $\phi_b^1 - \phi_m^1$ | Type |
|---------------------|-------------------|-------|---------------------|-----------------------|-------------------------|-------------------|-------|-------------------|--------------------|--------------------|-------------------|-----------------------|-----------------|
| AL Vir | 10.3 ⁴ | 1.012 | 9.54 ⁴ | -1.35 ⁴ | 0.56 ⁴ | 2.50 | 3.736 | 1.300 | 0.82 ¹⁰ | 1.45 ¹⁰ | — | — | x ¹⁰ |
| AP Her ^a | 10.4 ⁹ | 1.017 | 10.78 ⁸ | -1.36 | 0.59 ⁸ | 2.52 | 3.728 | 1.326 | 0.75 ⁸ | 1.8 ⁷ | — | — | x ⁷ |
| V1077 Sgr | 13.4 ⁹ | 1.127 | 13.01 ⁸ | -2.26 | 0.54 ⁸ | 2.85 | 3.742 | 1.463 | 1.29 ⁸ | 2.3 ⁷ | 0.42 ⁷ | 0.30 ⁷ | c ⁷ |
| V802 Sgr | 13.5 ⁹ | 1.130 | 13.67 ⁸ | -1.76 | 0.59 ⁸ | 2.68 | 3.728 | 1.406 | 0.96 ⁸ | 1.25 ⁷ | — | — | f ⁷ |
| V410 Sgr | 13.8 ⁹ | 1.140 | 12.58 ⁸ | -2.29 | 0.53 ⁸ | 2.87 | 3.744 | 1.469 | 0.97 ⁸ | 1.9 ⁷ | 0.42 ⁷ | 0.27 ⁷ | c ⁷ |
| CS Cas | 14.7 ⁹ | 1.167 | 12.05 ⁸ | -2.38 | 0.56 ⁸ | 2.91 | 3.736 | 1.505 | 1.44 ⁸ | 2.0 ⁷ | 0.48 ⁷ | 0.25 ⁷ | c ⁷ |
| FI Sct | 14.9 ⁹ | 1.173 | 14.09 ⁸ | -2.41 | 0.53 ⁸ | 2.92 | 3.744 | 1.494 | 1.19 ⁸ | 1.8 ⁷ | 0.42 ⁷ | 0.29 ⁷ | c ⁷ |
| V1187 Sgr | 15.1 ⁹ | 1.179 | 13.85 ⁸ | -1.93 | 0.62 ⁸ | 2.75 | 3.724 | 1.449 | 1.18 ⁸ | 2.2 ⁷ | 0.35 ⁷ | 0.26 ⁷ | f ⁷ |
| V741 Sgr | 15.2 ⁹ | 1.182 | 12.72 ⁸ | -1.94 | 0.59 ⁸ | 2.75 | 3.728 | 1.441 | 0.98 ⁸ | 1.67 ⁷ | 0.31 ⁷ | 0.21 ⁷ | f ⁷ |
| CZ Sct | 15.4 ⁹ | 1.188 | 14.40 ⁸ | -1.96 | 0.61 ⁸ | 2.76 | 3.726 | 1.450 | 1.05 ⁸ | 1.25 ⁷ | — | — | f ⁷ |
| AL Sct | 15.6 ⁹ | 1.193 | 14.02 ⁸ | -1.97 | 0.62 ⁸ | 2.77 | 3.724 | 1.459 | 1.28 ⁸ | 1.11 ⁷ | — | — | f ⁷ |
| V377 Sgr | 16.2 ⁹ | 1.210 | 13.32 ⁸ | -2.03 | 0.60 ⁸ | 2.79 | 3.727 | 1.463 | 0.96 ⁸ | 1.0 ⁷ | — | — | f ⁷ |
| V478 Oph | 16.4 ⁹ | 1.215 | 12.94 ⁸ | -2.05 | 0.59 ⁸ | 2.80 | 3.728 | 1.466 | 0.93 ⁸ | 1.0 ⁷ | — | — | f ⁷ |
| CO Sct | 17.1 ⁹ | 1.233 | 14.17 ⁸ | -2.61 | 0.59 ⁸ | 3.03 | 3.728 | 1.581 | 1.45 ⁸ | 2.33 ⁷ | 0.47 ⁷ | 0.31 ⁷ | c ⁷ |
| W Vir ^b | 17.3 ⁹ | 1.238 | 9.93 ⁸ | -2.13 | 0.61 ⁸ | 2.83 | 3.726 | 1.485 | 1.18 ⁸ | 1.86 ⁷ | 0.30 ⁷ | 0.18 ⁷ | f ⁷ |
| V1303 Sgr | 18.5 ⁹ | 1.267 | 12.88 ⁸ | -2.73 | 0.57 ⁸ | 3.06 | 3.734 | 1.584 | 1.24 ⁸ | 3.03 ⁷ | 0.45 ⁷ | 0.31 ⁷ | c ⁷ |

Table 2.1a Observational details for 16 field variables

| Star | P(days) | logP | $\langle V \rangle$ | $\langle M_V \rangle$ | $\langle B-V \rangle_0$ | $\log(L/L_\odot)$ | $\log T_e$ | $\log(R/R_\odot)$ | ΔV | Asym(lum) | ϕ_b^1 | $\phi_b^1 - \phi_m^1$ | Type |
|---------------------------------|-------------------|-------|---------------------|-----------------------|-------------------------|-------------------|------------|-------------------|-------------------|-------------------|-------------------|-----------------------|-----------------|
| M14 No.17 | 12.1 ⁴ | 1.082 | 14.81 ⁴ | -1.52 ⁴ | 0.65 ⁴ | 2.60 | 3.718 | 1.386 | 0.62 ⁵ | 2.0 ⁵ | — | — | f ⁵ |
| M14 No.7 | 13.6 ⁴ | 1.134 | 14.80 ⁴ | -1.53 ⁴ | 0.69 ⁴ | 2.62 | 3.711 | 1.410 | 0.71 ⁵ | 1.35 ⁵ | — | — | x ⁵ |
| ω Cen No.29 ^c | 14.7 ⁴ | 1.167 | 11.82 ⁴ | -2.08 ⁴ | 0.85 ⁴ | 2.86 | 3.68 | 1.592 | 1.06 ¹ | 1.26 ¹ | — | — | f ¹ |
| M3 No.154 | 15.3 ⁴ | 1.185 | 12.32 ¹ | -2.71 ⁴ | 0.51 ⁴ | 3.04 | 3.745 | 1.552 | 1.33 ¹ | 1.9 ¹ | 0.46 ¹ | 0.38 ¹ | c ¹ |
| M12 No.1 ^d | 15.5 | 1.190 | | | | | | | | | | | |
| M2 No.1 | 15.6 ⁴ | 1.194 | 13.46 ⁴ | -1.99 ⁴ | 0.48 ⁴ | 2.74 | 3.752 | 1.388 | 1.1 ³ | 2.2 ³ | 0.39 ³ | 0.25 ³ | f ³ |
| M80 No.1 | 15.6 ⁴ | 1.194 | 13.42 ⁴ | -1.88 ⁴ | 0.59 ⁴ | 2.73 | 3.728 | 1.431 | 0.9 ⁶ | ? | ? | ? | f ⁸ |
| M2 No.5 | 17.6 ⁴ | 1.246 | 13.34 ⁴ | -2.11 ⁴ | 0.47 ⁴ | 2.78 | 3.754 | 1.404 | 1.05 ³ | 1.6 ³ | 0.34 ³ | 0.25 ³ | f ³ |
| M14 No.1 | 18.7 ⁴ | 1.272 | 14.06 ⁴ | -2.27 ⁴ | 0.75 ⁴ | 2.93 | 3.70 | 1.587 | 1.29 ⁵ | 1.5 ⁵ | 0.42 ⁵ | 0.22 ⁵ | xc ⁵ |
| M10 No.2 ^e | 18.8 ⁴ | 1.274 | 11.82 ⁴ | -2.29 ⁴ | 0.65 ⁴ | 2.90 | 3.720 | 1.532 | 1.2 ² | 3.0 ¹ | 0.38 ¹ | 0.24 ¹ | f ¹ |
| M2 No.6 | 19.3 ⁴ | 1.286 | 13.18 ⁴ | -2.27 ⁴ | 0.49 ⁴ | 2.85 | 3.750 | 1.447 | 1.1 ³ | 2.0 ³ | 0.34 ¹ | 0.19 ¹ | f ¹ |

Table 2.1b Observational details for 11 cluster variables

Notes for tables 2.1a and 2.1b are on the next page

References: 1 Arp (1955), 2 Bohm-Vitense et al (1974), 3 Demers (1969), 4 Demers & Harris (1974),
5 Demers & Wehlau (1971), 6 Eggen (1961), 7 Kwee (1967b), 8 Kwee (1968), 9 Kwee & Braun
(1967), 10 Michalowska-Smak & Smak (1965)

| | |
|-------------------------|---|
| P(days) | Period in days |
| log P | Logarithm of period in days |
| $\langle V \rangle$ | Mean apparent visual magnitude |
| $\langle M_v \rangle$ | Mean absolute visual magnitude |
| $\langle B-V \rangle_0$ | Mean intrinsic colour |
| log(L/L _☉) | Logarithm of luminosity in solar units |
| log T _e | Logarithm of effective temperature |
| log(R/R _☉) | Logarithm of radius in solar units (from log(L/L _☉) and logT _e) |
| ΔV | Range in visual magnitude |
| Asym(lum) | Asymmetry of light curve = (time spent on descending branch)/ (time spent on ascending branch) |
| ϕ_b^l | Phase of secondary bump on light curve from mean light ascending |
| $\phi_b^l - \phi_m^l$ | Phase of secondary bump from maximum light |
| Type | Crested (c), flat-topped (f) or neither (x). |

The values come from the study referenced in each case.

a Reference 10 gives $V = 0.95$ for AP Her

b For the (log(L/L_☉), logT_e) of W Vir reference 2 gives (2.89, 3.736) and reference 4 gives (2.86, 3.705)

c For ω Cen No. 29 the light curve in reference 1 is only photographic

d For M12 No. 1 Joy (1949) gives some velocity data (not sufficient to determine the curve), the amplitude is about 30 km/s

e Joy (1949) also gives velocity data for M10 No. 2, amplitude about 84 km/s, again not sufficient to determine the curve.

The values of $\log P$ and $\langle M_V \rangle$ for the cluster variables define a $P - \langle M_V \rangle$ relation for the period range 10 - 20 days. Kwee (1968) split his $P - \langle M_V \rangle$ relation for the cluster stars into two parallel relations, one for the flat-topped variables and one for the crested type. The available evidence for this is scarce (there being few c-type cluster stars) but not contradictory, and it seems that the theoretical models may also follow two relations (section 6.6).

Consequently, using the data in table 2.1, we arrived at the following relation for the f-type cluster variables with $10 < P < 20$ days.

$$\langle M_V \rangle = 2.17 - 3.48 \log P \quad (2.9)$$

For the c-type we assume a parallel relation, slightly higher in the $\langle M_V \rangle - \log P$ plane. Looking at the crested cluster variables M3, no. 154, and M5 nos. 42 and 84 (with $P > 20$ days), and comparing their actual $\langle M_V \rangle$ values with those they would have if they followed equation (2.9), it appears that a decrease of 0.5 in the $\langle M_V \rangle$ value is a reasonable one. So for the crested variables we get

$$\langle M_V \rangle = 1.67 - 3.48 \log P \quad (2.10)$$

The two relations (2.9) and (2.10) then allow us to find $\langle M_V \rangle$ values for the field variables. Then for all variables ($\log(L/L_\odot)$, $\log T_e$) pairs are found from the $(\langle M_V \rangle, \langle B-V \rangle_0)$ pairs using the tables of Bohm-Vitense (1973).

For the unclassified variables (not the unknown ones, i.e. ST Pup and RS Pav) relation (2.9) is used, since the unclassified cluster variables M14 nos. 1 and 7 seem to fall closer to this one than to (2.10).

Figure 2.3 shows the $\langle M_V \rangle$ -log P relations - in this and succeeding figures, circles are cluster stars, triangles are field stars, filled figures are f-type and open figures are c-type. The x-type stars have a cross inside an open symbol. As a note to these new estimations of $\log(L/L_\odot)$ and $\log T_e$, the result for W Vir seems to fall nicely between the values given by Demers and Harris (1974) and Bohm-Vitense et al. (1974).

From the determinations of $\log(L/L_\odot)$ and $\log T_e$ it is possible to find the stellar radius, from

$$L = 4\pi R^2 \sigma T_e^4$$

From these figures a Period-Radius relation can be found. In figure 2.4 log P is plotted against $\log(R/R_\odot)$. We see that because of the two distinct P- M_V relations we get two P-R relations. At the same period the crested variables have a larger mean radius. These relations are, for the crested variables,

$$P = 0.480(R/R_\odot)^{0.99} \quad (2.11)$$

and for the flat topped variables

$$P = 0.194(R/R_\odot)^{1.31} \quad (2.12)$$

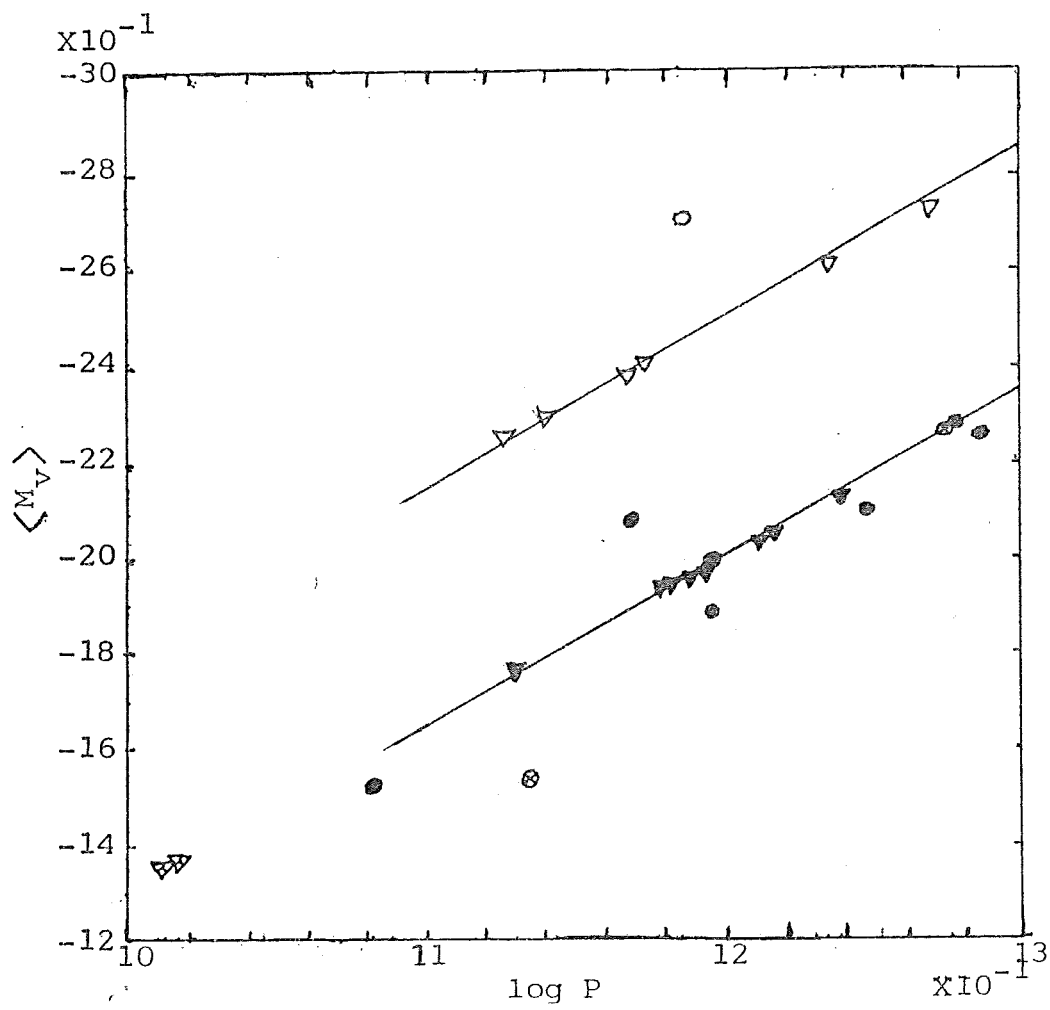


Figure 2.3 Observed M_V - P relationship

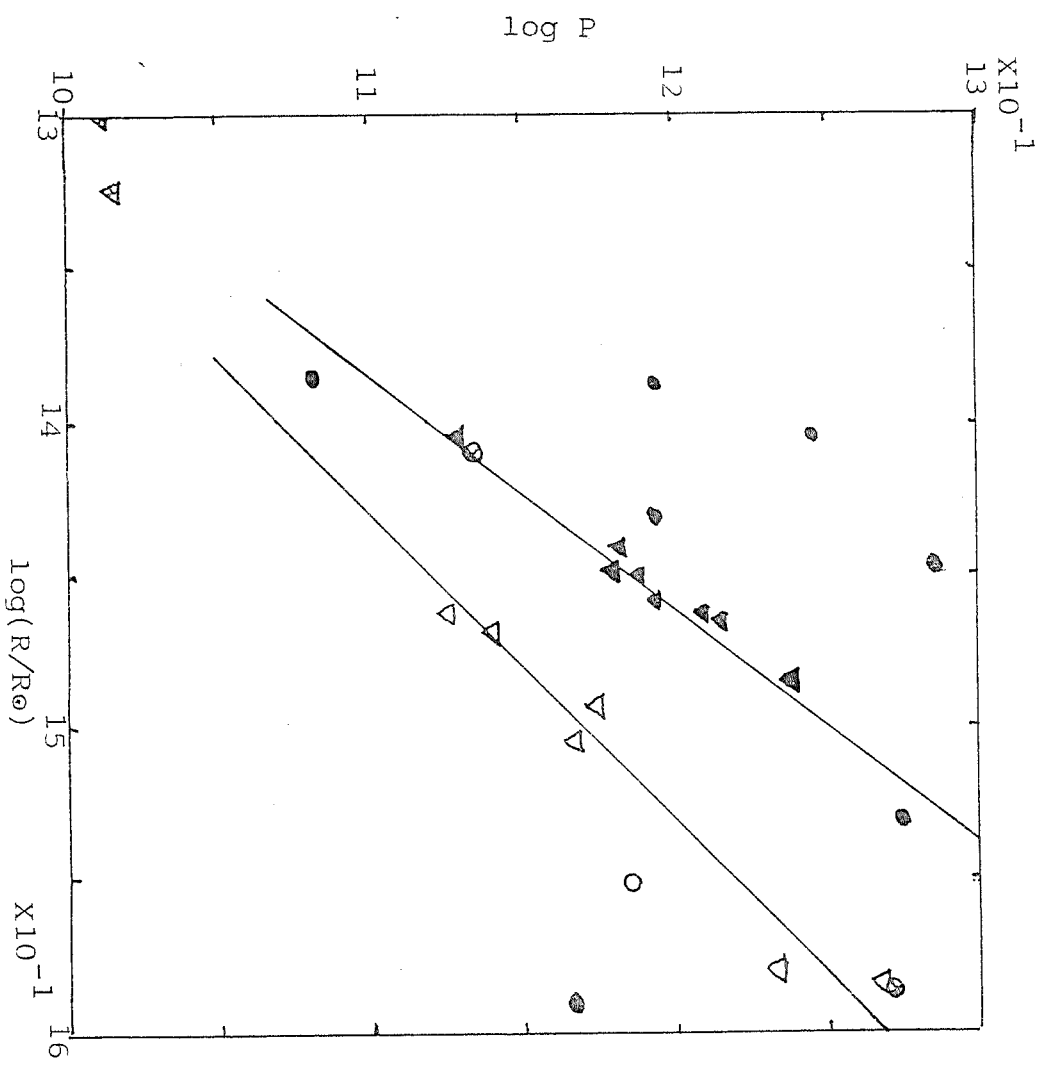


Figure 2.4 Observed $\log P$ - $\log R$ relation

These form two roughly parallel lines in the $\log P$ - $\log(R/R_\odot)$ plane. This compares with Bohm-Vitense et al.'s results for population II cepheids of all periods for a P-M-R relation.

$$P \propto R^{1.72} M^{-0.75} \quad (2.13)$$

The different P-R relations, the different P- M_V relations and maybe the suspicion of a trend in the light curve suggests a possible progression, which could be caused by a variation in the mass (which, as has been stated before, need only be small).

Figures 2.5a and 2.5b show a colour-magnitude diagram and an HR diagram for the variables listed, along with the observed instability strip given by Demers and Harris (1974). We see in both diagrams that the crested and flat-topped variables form two groups. The c-type variables appear at higher luminosities, while the f-type variables occur at lower $\log(L/L_\odot)$, and may be slightly cooler in general. The errors in these diagrams are probably quite large (viz. the disagreement over W Vir) but probably allow fairly general conclusions.

One of the most obvious features to look for when comparing observed light curves with theoretically obtained ones is the amplitude of the variation. The observational amplitude in the visual (ΔV) may not be accurately known since the maximum and minimum may not be well observed. This error is probably in general comparable to the error in the measurement of V itself. This varies from about ± 0.01 for 10th magnitude stars to ± 0.3 for 19th magnitude stars. The other

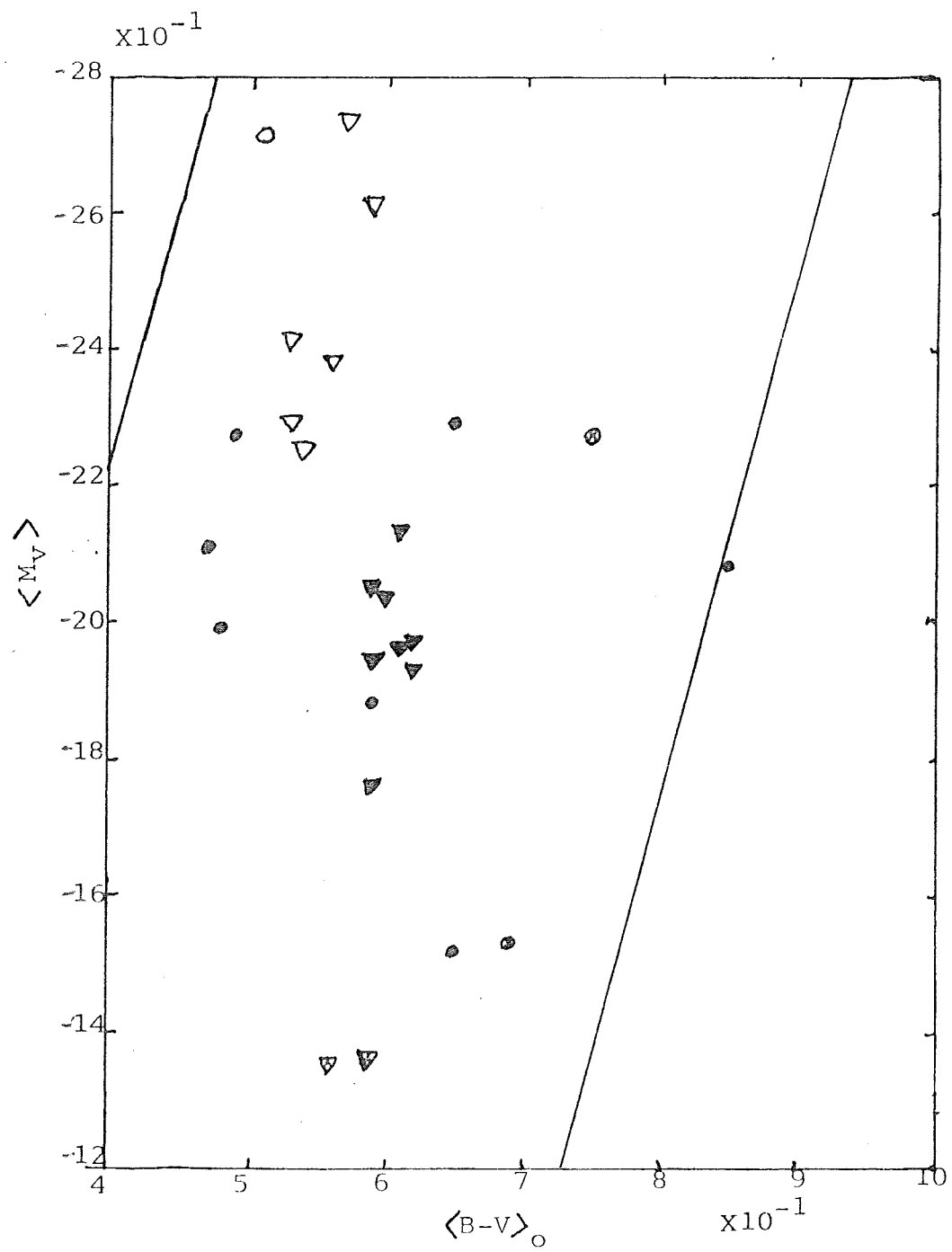


Figure 2.5a Observed colour-magnitude diagram

problem is knowing how to relate ΔV for the observed stars to ΔM_{bol} for the theoretical models. This is estimated in section 6.7.

From this we see that the other features of the light curve are very important. For the crested variables (and for some flat-topped ones) the phase on descending light can be measured, relative to mean light on the ascending branch (because this can usually be measured relatively accurately) and relative to maximum light. For the flat-topped variables the presence or absence of a bump may be significant (or possibly the presence of a dip in the "flat"-top). For both the asymmetry of the light curve (defined by [time spent on descending branch]/[time spend on ascending branch]) is an important feature.

The secondary bumps in the crested light curves appear to show no obvious progression with luminosity, effective temperature or period (figures 2.6a,b). Instead, the bump appears at an approximately constant phase $\phi'_b = 0.44 \pm 0.03$ after mean light on the rising branch. For the flat-topped variables that have secondary bumps (or maybe 'shoulders') ϕ'_b is also approximately constant, $\phi'_b \approx 0.34 \pm 0.05$.

In both cases the phase difference between maximum light and the bump, $\phi'_b - \phi'_m$, is still approximately constant, with smaller errors. For the crested variables $\phi'_b - \phi'_m \approx 0.29 \pm 0.02$, and for the flat-topped variables $\phi'_b - \phi'_m \approx 0.23 \pm 0.02$. It should be noted that this data is scarce and subject to large errors. It does not preclude the possibility of a continuous progression from c-type to f-type curves, and a decrease in ϕ'_b and $\phi'_b - \phi'_m$ as the luminosity and

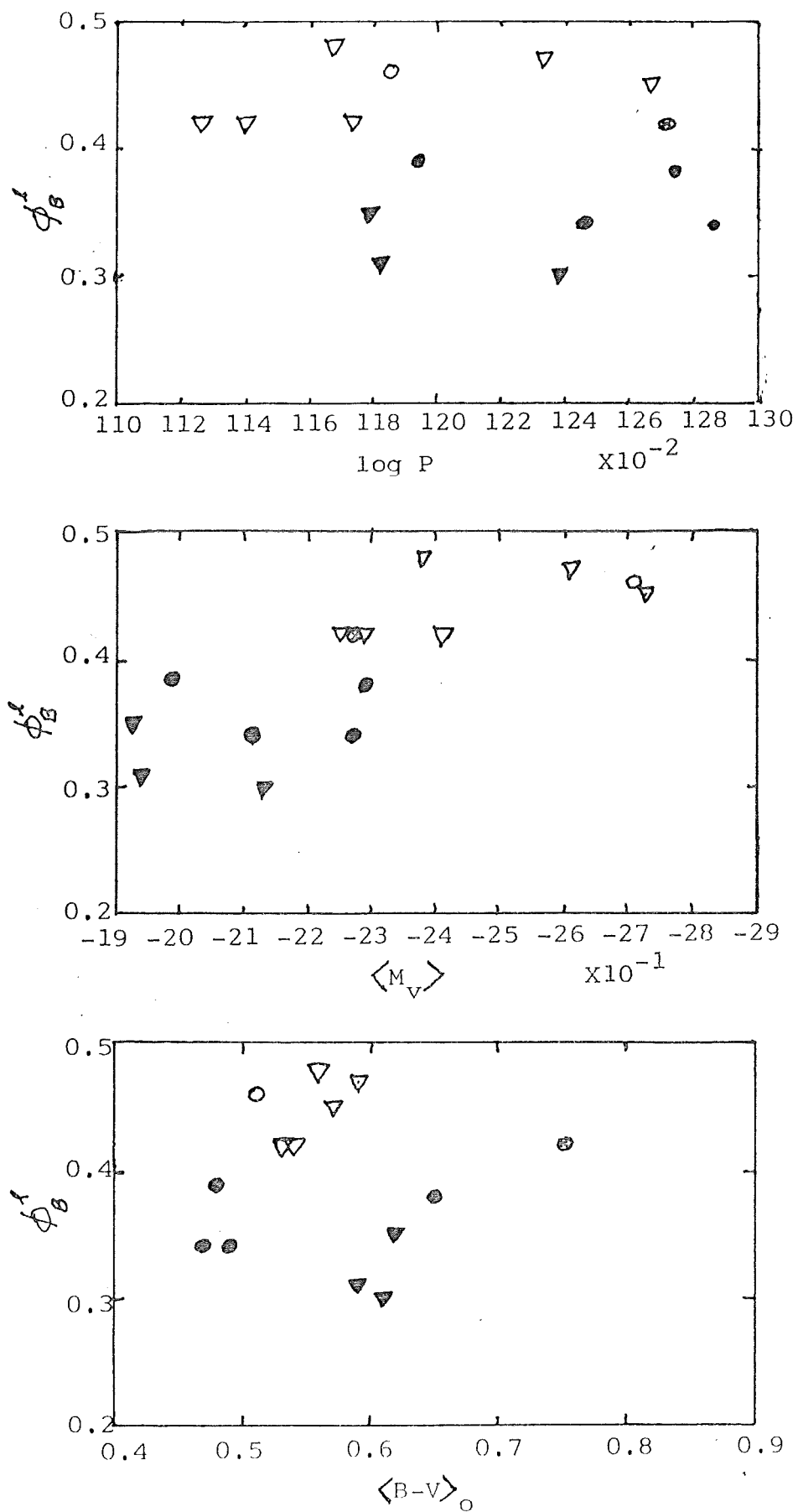


Figure 2.6a The variations of the phase of the secondary bump on the light curve with $\log P$, $\langle M_V \rangle$, and $\langle B-V \rangle_O$

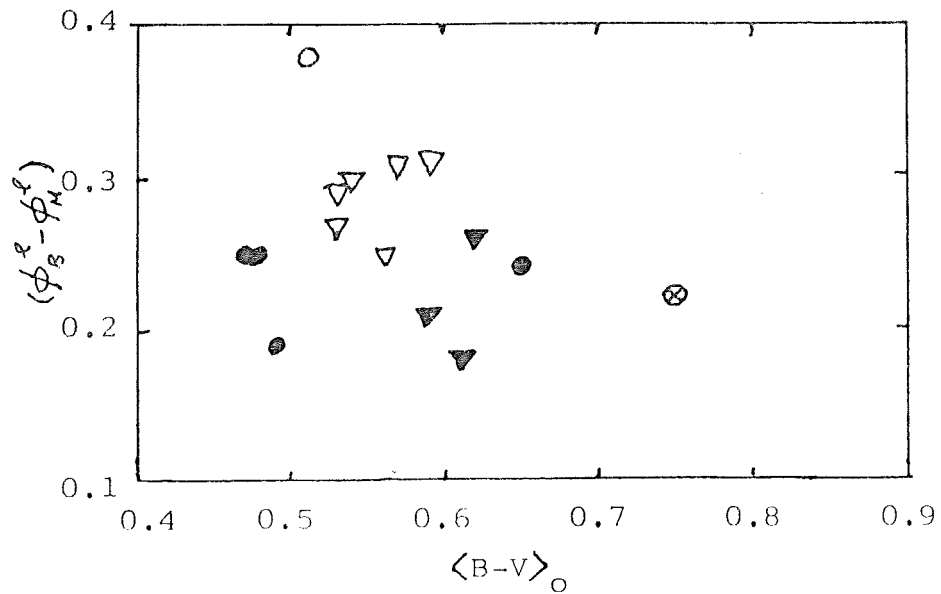
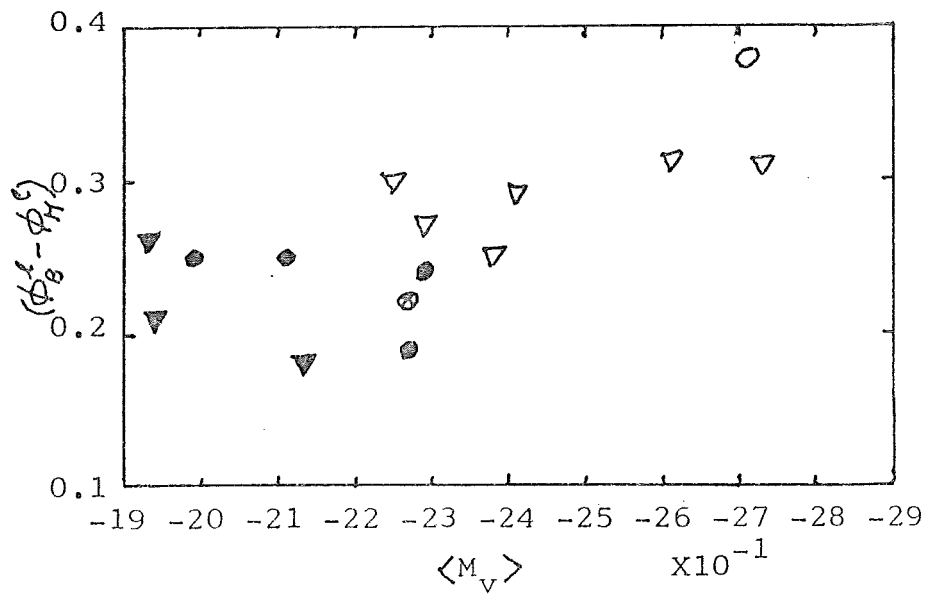
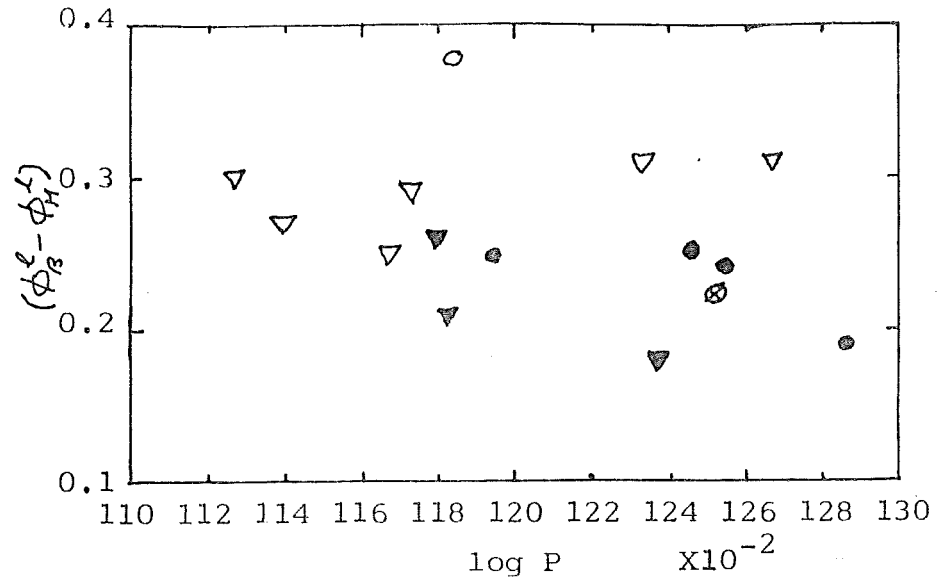


Figure 2.6b The variations of the phase difference $\phi_B^L - \phi_H^L$ with $\log P$, $\langle M_V \rangle$, and $\langle B-V \rangle_O$

effective temperature are decreased. Indeed figures 2.6a and b may indicate such a progression. In other words the crested and flat-topped variables need not be two distinct groups, merely extremes of a progression. If this is the case then it might be possible in the observations or the models to find an example of such a change at approximately constant periods. Unfortunately with the few light curves available it is difficult to make any firm conclusions, especially with the limited accuracy of the light curves, and the fact that many of these stars are subject to apparently random changes in period and light curves. An example of the problem is variable 6 in M2. The curve from Demers (1969) for the star is significantly different from that of Arp (1955). (Note that Arp's observations were given in photovisual and photographic magnitudes.) In an HR diagram, M2, no. 6, falls roughly in the gap between the c-type and f-type stars.

Turning our attention to the amplitudes of the light curves we find a range running from 0.6 in V up to 1.45 (the star RS Pav may have a greater range, but the available photometric details are not sufficient to produce a full light curve). There is a tendency for the flat-topped variables to have amplitudes of about 1mag, whilst the crested variables have amplitudes a little larger, maybe 1.25 mag. Otherwise there seem to be only two slight trends, firstly a general increase in ΔV as the period increases, secondly an increase in ΔV as the effective temperature decreases. This latter is more obvious in the flat-topped variables.

It may be useful to note here that those stars which do not fit into either classification generally have small amplitudes (< 1 mag.) and short periods (< 14 days).

Sadly no such conclusions can be made from the very scarce radial velocity data. W Virginis has a highly asymmetric (discontinuous) velocity curve with an amplitude of 55 km/s , and by taking Joy's (1949) data on M12 number 1 and M10 number 2 we find, by subtracting maximum and minimum values amplitudes of 30 km/s and 84 km/s respectively. In neither case is the data sufficient to properly define the velocity curve.

To conclude, it seems that one of the main features that a survey should reproduce is the two types of light curves, at the correct values of the stellar parameters; once this is done, perhaps the models can show if there is a progression between the two. Hopefully, some individual stars can also be modelled in detail, confirming the choice of composition and stellar parameters and the non-linear approach.

2.3 THEORETICAL ASPECTS OF POPULATION II CEPHEIDS

2.3.1 Introduction

Until 1980 no non-linear models of population II cepheids had been published in detail, except for some models of W Virginis itself. Then Carson, Stothers and Vemury (1981) and King, Cox and Hodson (1981) produced a series of non-linear models of the short period population II cepheids, commonly known as BL Herculis stars. In addition, many linear results

for these stars have been published, and some of the linear work stretches into the longer period region. Although the BL Herculis stars have different properties from the longer-period W Virginis variables, and they have different evolutionary origins (see section 2.2), they are probably very similar in composition and mass, so it is instructive to review the work done on these stars.

2.3.2 The BL Herculis Variables And Blue Edges

The linear work of Iben and Huchra (1971) primarily on RR Lyrae variables went up to a $\log(L/L_{\odot})$ value of 2.8, thus covering the region of the BL Herculis variables and part of the W Virginis region. Their blue edges, calculated using the Christy (1966a) approximation to the Cox and Stewart (1965) opacities show reasonable agreement with the Demers and Harris observed blue edge (1974), which was not known at the time. Iben and Huchra used a mass of $0.6M_{\odot}$, a hydrogen content $X = 0.7$ and two metallicities, $Z = 0.0001$ and $Z = 0.01$. This showed that the blue edge had only a minimal dependence on Z , the metal content, and also, for $\log(L/L_{\odot}) > \sim 2.0$, a first harmonic blue edge far to the redward of the fundamental blue edge, thus indicating that most population II cepheids are probably fundamental pulsators (this also seemed likely from the observations).

Tuggle and Iben (1972) repeated some of these calculations using spline interpolation in a set of Cox and Stewart opacity tables. Three mixes were used, the Massevitch mix ($X = 0.7$, $Z = 0.004$), the King Ia mix ($X = 0.7$, $Z = 0.001$), and the King

Ib mix ($X = 0.8$, $Z = 0.001$). The switch from Christy formula to spline interpolation caused a shift in the blue edge of up to about 0.008 in $\log T_e$. In all the Iben studies the "Castor-Iben" outer boundary condition is used. Iben (1971) points out that use of the "Baker-Kippenhahn" condition could shift the blue edge by up to about 0.03 to the red in $\log T_e$, maybe more at higher luminosities. The Tuggle-Iben blue edge, for $M/M_\odot = 0.6$, using the King Ia mix is plotted in Figure 2.7, along with the observed blue and red edges of Demers and Harris.

In the same figure is plotted the calculated blue edge of King, Cox and Hodson (1981, hereafter frequently referred to as KCH) for the same opacity mix, but merely estimated for $M/M_\odot = 0.6$, as KCH only calculated models at $M/M_\odot = 0.55$ and 0.75. These two edges agree fairly well, and indicate a helium content of about 30% for population II cepheids, maybe a little more, and a mass of about $0.6 M_\odot$, again maybe a little more. (Tuggle and Iben also noted that the blue edge in this region moves blueward as the mass increases. For example for $M/M_\odot = 0.8$, the blue edge is shifted about 0.015 blueward at $\log (L/L_\odot) = 2.0$ as compared with the result for $M/M_\odot = 0.7$.) These results are in agreement with the values derived from observational and evolutionary considerations of $0.47 < M/M_\odot < 0.8$, and $0.2 < Y < 0.3$. Moreover, the analysis of BL Herculis stars by Peterson (1980) indicates a mass of $0.6 M_\odot$.

The linear results from Carson, Stothers and Vemury (1981, hereafter CSV) for a mass of $0.6 M_\odot$ and $Y = 0.25$, $Z = 0.005$, using the Carson (1976) opacities, with the Christy

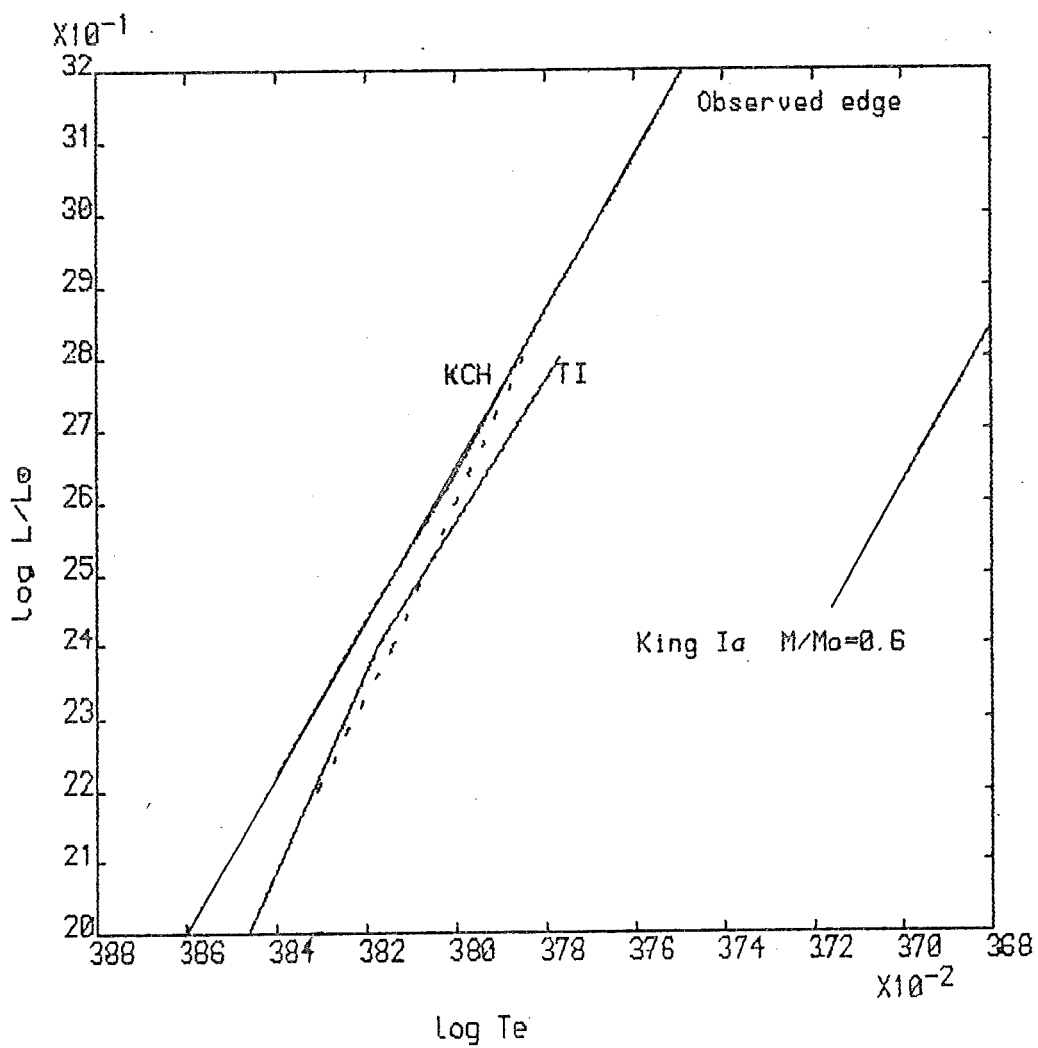


Figure 2.7 The Tuggle & Iben (1972) and King, Cox & Hodson (1981) blue edges compared with the observed edge

approximation to the Cox opacities used for $\log T < 3.85$ would seem to give blue edges in good agreement with those of KCH and Tuggle and Iben. However, CSV used the Baker-Kippenhahn outer boundary condition, which, it has already been stated, could make a large difference. KCH (based on the Castor [1971] theory) used the Castor-Iben condition. Also notable about the CSV work is the large dependence of the blue edge upon Z , a feature not seen before, and seemingly unique to the Carson opacities. These results have been checked by Worrell (1982a), who used the Castor-Iben condition. The results are plotted in figure 2.8, compared with the CSV results. We see that the Worrell blue edges are indeed very much to the blueward of the CSV edges. Also the dependence on Z has greatly diminished, though not to the minimal dependence revealed by other studies using the Cox opacities. As discussed, the first change is expected because of the differing external boundary condition. The change in the Z dependence seems to be dependent on how the switch-over from Carson opacities to the Christy approximation is made at low temperatures. CSV scaled the Christy opacities at $\log T < 3.85$ to make a smooth fit to the Carson opacities. Worrell used essentially the same treatment as is used in this study and described in section 5.2, an interpolation between the Christy value at $\log T = 3.8$ and the Carson values at $\log T = 3.9$. This seems to make the difference. Blue edges calculated by Worrell using the same scaling procedure as CSV also exhibit the large Z dependence.

Figure 2.9 shows the Worrell blue edges for the Carson opacities compared with edges calculated by Worrell for the same parameters, using the Stellingwerf (1975a) approximation to the Cox King Ia and King Ib opacities. The edges found

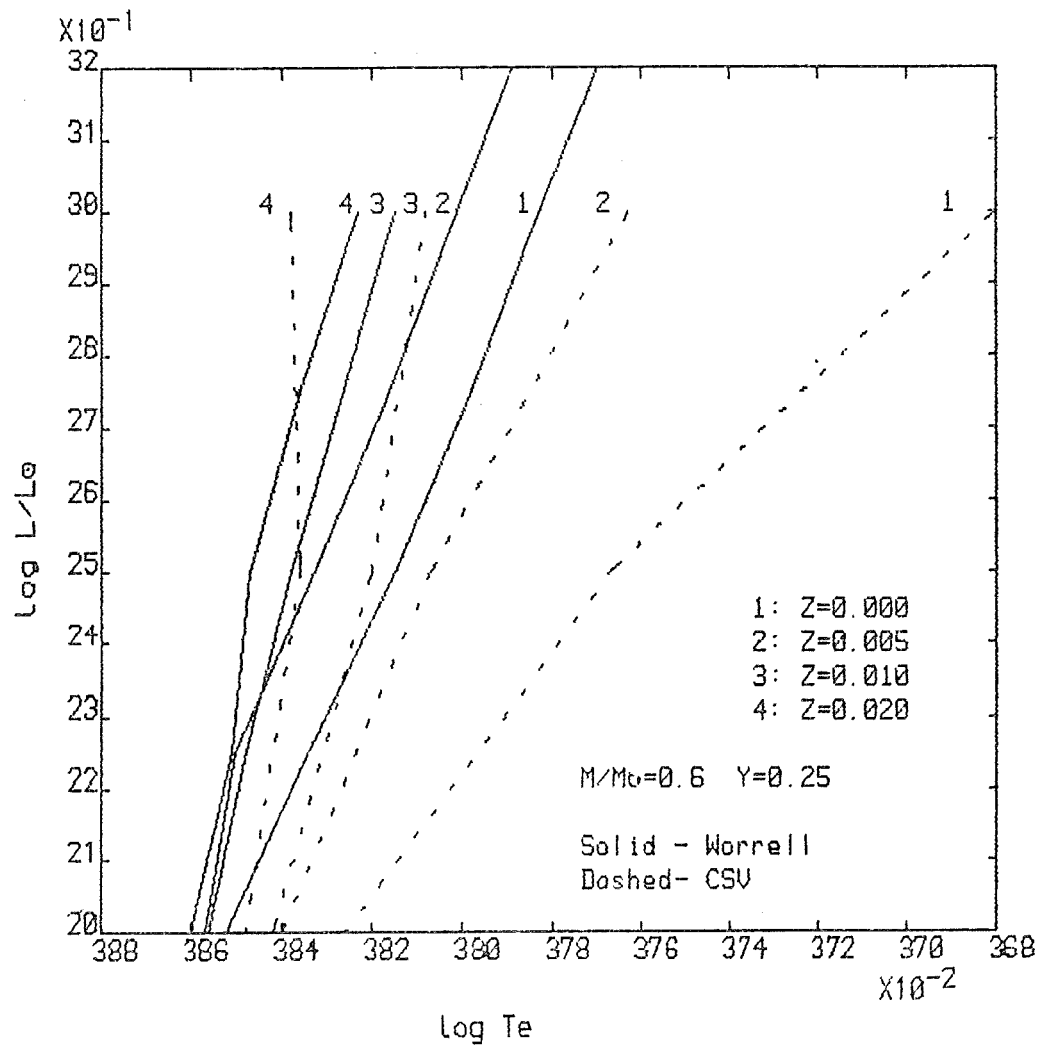


Figure 2.8 Comparison of the CSV and Worrell blue edges for different metal contents

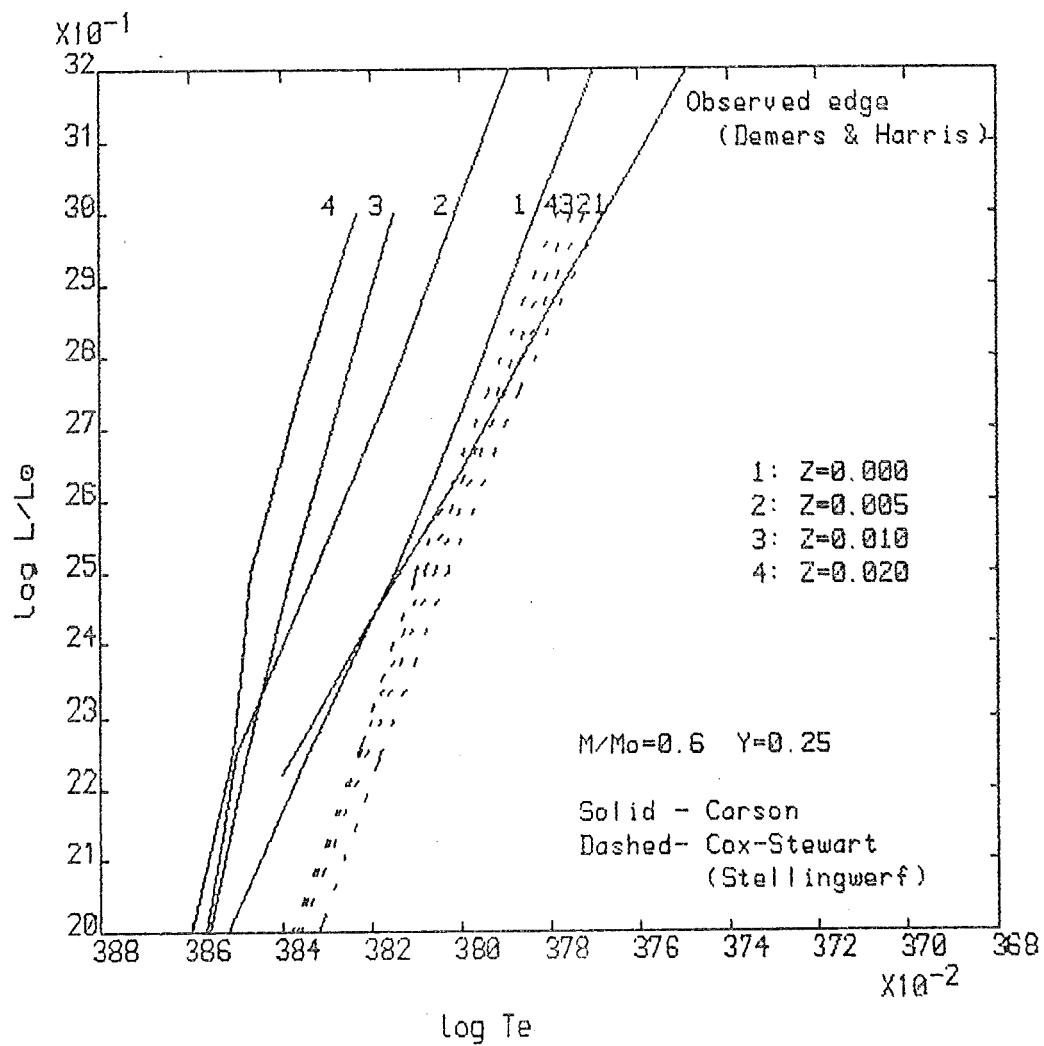


Figure 2.9 Worrell blue edges using the Carson opacities (solid) and the Cox-Stewart opacities in the Stellingwerf formulation (dashed)

using the Stellingwerf formula do show almost no dependence on Z , and lie near the Tuggle-Iben and KCH blue edges, which seems to validate the Worrell results.

In figure 2.10 three calculated blue edges are compared with the Demers and Harris observed edge. All are for 25% helium (estimated in one case) and $M/M_{\odot} = 0.6$, using the Castor-Iben boundary condition. As stated above, the Cox opacities seem to indicate (for $M/M_{\odot} = 0.6$) a helium content of about 30% for these stars, though 25% is also reasonable. If the Worrell results are accurate, the helium content would appear to be less than 25% for the same mass using the Carson opacities. These results cannot be too secure because of the large uncertainty in the observed edge, and also because the Worrell results with the Carson opacity still show some dependence on Z . A reduction of Z to 0.001 or less would move the edge towards the observed edge. A further problem associated with the Carson opacity is that the table used (section 5.2) is too coarse to allow accurate determination of the blue edge. (Note the crossover of the edges for two different Z values at $\log (L/L_{\odot}) \sim 2.2$.) However, the results are probably correct to 0.005 in $\log T_e$.

Several of the BL Herculis variable show bumps in their light and velocity curves, and there appears to be a progression rather like the Hertzsprung progression in classical cepheids (Stobie 1973). For classical cepheids this phenomenon has been explained by Christy (1968) and Stobie (1969a,b) as an echo of a pressure wave. The wave is generated in the second helium ionization zone, propagates down to the stellar centre, is reflected off it and arrives at the surface

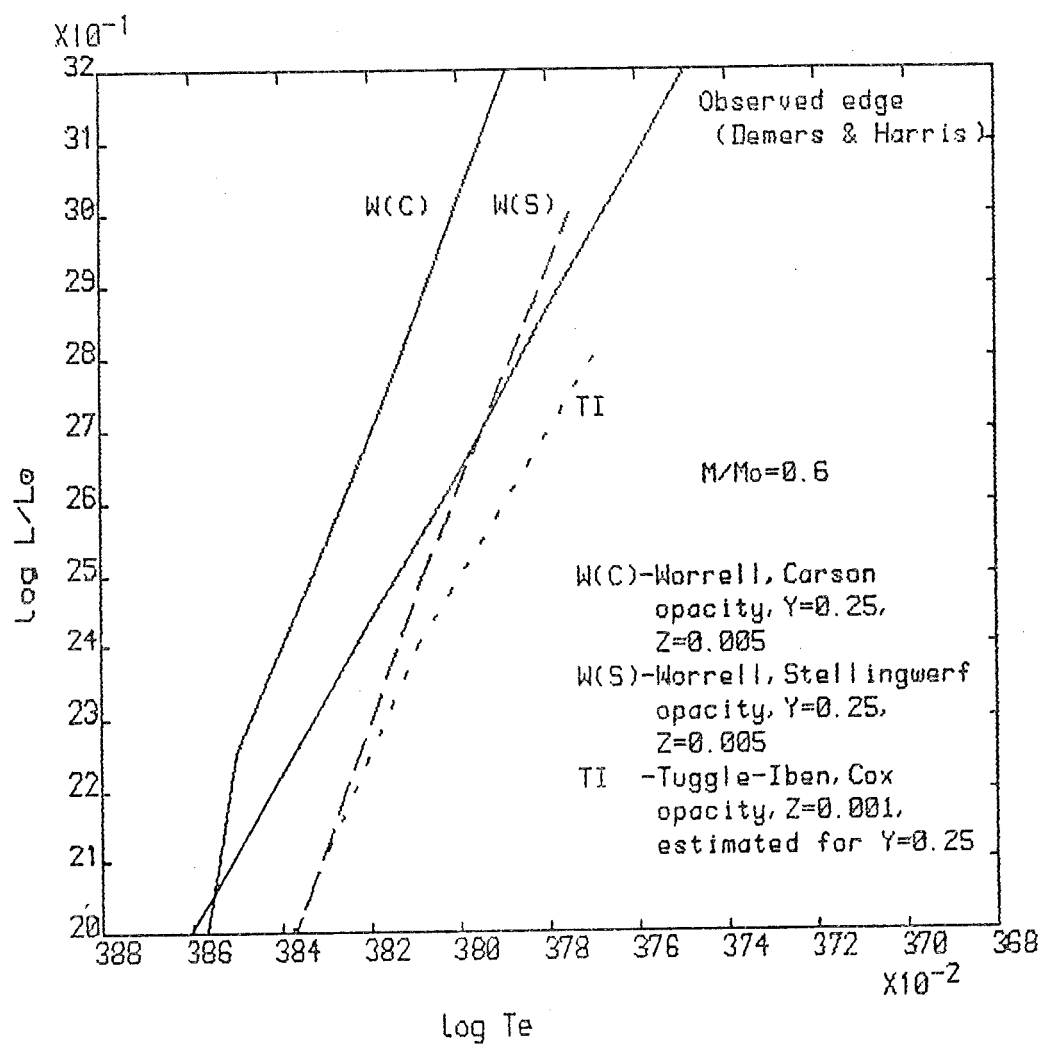


Figure 2.10 Blue edges for 25% helium using Carson, Stellingwerf and Cox opacities, compared with the observed edge

during the next period.

Simon and Schmidt (1976) suggested that the secondary bump is due to a close resonance of the second harmonic with the fundamental pulsation modes: $P_2/P_0 \approx 0.50$. Here variables with $0.46 \leq P_2/P_0 \leq 0.50$ show bumps on rising light and those with $0.50 \leq P_2/P_0 \leq 0.53$ show bumps on falling light.

The theoretical models of CSV, Carson and Stothers (1982), KCH, and Hodson, Cox and King (1980, 1982 - HCK I and II) confirm that the phase, ϕ , of the secondary bump is related to P_2/P_0 . However the linear work of KCH predicts a bump transition period (where the bump switches from the descending branch of the light curve to the ascending branch) that is too long (for $M/M_\odot = 0.55$), whilst the non-linear results of CSV (for $M/M_\odot = 0.6$) give about the correct transition period.

CSV (and also Vemury and Stothers 1978) express reservations about the significance of the resonance. They point out that for type II cepheids, there are resonances at $P_0 \sim 14$ days ($P_2/P_0 = 0.333$) and at $P_0 \sim 17$ days ($P_1/P_0 = 0.5$). Assuming a band width comparable to that for the $P_2/P_0 = 0.5$ resonance then the $P_1/P_0 = 0.5$ resonance should give an analog of the Hertzsprung progression for type II cepheids in the period range 10 - 25 days. However, such a progression is not observed (section 2.2). CSV and Carson and Stothers had as a main objective the reproduction of the wide variety of light curves observed for these stars. Their results are very successful in this respect. In their paper a model is produced of the prototype star, BL Herculis. This exhibits very good agreement with the observed star, probably the best model of an individual variable star to be published. The light curve and

bump phases are reproduced very well. In the second paper a variety of curves at constant periods are produced by adjusting the stellar parameters. A model constructed by CSV using the Cox-Stewart opacities in the Christy formulation did not produce results that were as good. Probably the major flaw in this series of non-linear models is that the amplitudes are frequently too large. For the redder models, this can perhaps be attributed to the omission of convection, which would be expected to restrict the amplitude.

For the KCH and HCK I and II non-linear models only 2 light curves have been published (HCK I), for $P = 1.55$ days and 3.82 days, and also one more for a reconstruction of CSV model 1 (the BL Herculis model). In this reconstruction their results differ somewhat from those of CSV. The bumps they get appear to be local phenomena; this does not seem to be the case for the CSV version, which reinforces the Christy "echo" idea. Also, no shoulder is observed following light maximum, a facet of the observations that CSV manage to reproduce. It is suggested that if KCH used the Carson opacity table given in CSV, without using the Christy formula for $\log T < 3.85$, then their results would not be in agreement with those of CSV, since as is discussed in section 5.2 the low temperature Carson opacities are probably in error. (see section 6.2.)

KCH suggest that the overlarge amplitudes of the CSV models are due to over-estimation of the bound-free helium opacity at about 40,000 K, which causes excessive driving. Also, their plot of the luminosity variations through their model using the Carson opacities shows an anomalous zone at a temperature of about 10^6 K. This strange behaviour is probably

caused by the carbon-oxygen "bump" in the Carson opacities (see section 5.2).

In the HCK II paper, the disagreement between the transition period in the calculated models and that observed in KCH is attributed to the use of linear methods. Results from non-linear models bring agreement with the observed transition period and the predicted transition period of the CSV non-linear work.

To summarise, it appears that non-linear models can give better results than linear models for certain aspects of the observed trends. Use of the Carson opacities supports the Christy "echo" phenomenon for the cause of secondary bumps, whilst the Cox opacities appear to give more weight to the P_2/P_0 resonance idea. Despite the over-estimated amplitudes of some of the CSV models, the light curves do seem to resemble those observed to a large degree. From the few light curves published using Cox opacities it seems that such good agreement is more difficult to obtain.

2.3.3 The W Virginis Variables

Considerably less work has been done on the longer period (> 10 days) population II cepheids. Apart from the already-mentioned linear determinations of the blue edge only four detailed non-linear models have been published, of the 17.3 day variable W Virginis (Christy 1966b; Davis 1972; Davis and Bunker 1975).

Christy's model was based on his non-linear method of 1964. It had the objective of trying to find a model with a mass near $1 M_{\odot}$ that could produce a period of about 17 days. The stellar parameters were based on Abt's (1954) study, and were $M/M_{\odot} = 0.88$, $\log(L/L_{\odot}) = 3.262$, $\log T_e = 3.740$. The composition was $Y = 0.45$, $Z = 0.002$, which has an improbably high helium content in the light of more recent results. The model was violently unstable with a growth rate of about 3 periods and a fundamental period of 18.5 days. Because Christy confused the surface radius with the photospheric radius this was later changed to 19.6 days to compare with Davis' 1972 model. The violence of the pulsation and the generation of strong photospheric shocks caused the eventual ejection of the outer layer. The model also showed alternations in pulsation amplitude from period to period, reminiscent of so called RV Tauri behaviour. The resulting light variation of the model was not very like that of W Virginis, nor indeed of population II cepheids in general. From the published graphs of the motion we can estimate the following amplitudes:

$$\Delta R/R \simeq 0.3 \text{ (full amplitude)}$$

$$\Delta V \simeq 60 - 80 \text{ km/s}$$

$$\Delta M_{bol} \simeq 1.5 - 2.0$$

In Davis' first model of W Virginis (1972), he improved the non-linear methods of Christy by replacing the diffusion treatment of the energy transfer with the variable Eddington method of radiation transfer. Radiative transfer is a much better way to treat optically thin zones, especially where strong shock waves are involved. The stellar parameters used by Davis were the same as those used for Christy's model with

the exception of the composition, which was changed to $Y = 0.296$, $Z = 0.004$ (the Mashevich I mixture). Cox and Stewart opacity tables were again used. This is a much more reasonable helium content. Davis also calculated a pure diffusion model to allow direct comparison of diffusion theory with radiative transfer. The model produced has a fundamental period of 20.0 days, again with a large growth rate and an RV Tauri effect in both the velocity and light curves. The outer zone did not escape, but did show a distorted path. The main differences between the light curves for diffusion theory and radiative transfer are that the latter gives a smaller amplitude and produces a slight shoulder after light maximum, slightly closer to the observed W Virginis light curves. The amplitudes could once again be established from the published curves to give:

$$\Delta R/R \simeq 0.3$$

$$\Delta V \simeq 60 - 75 \text{ km/s}$$

$$\Delta M_{bol} \simeq 1.9-2.2 \text{ (diffusion)}$$

$$\simeq 1.1-1.3 \text{ (radiative transfer)}$$

Even with radiative transfer, however, the light curves still look unlike those observed.

For a further improvement, Davis (1974) included relativistic velocity terms in the radiative transfer hydrodynamics, since the large shocks that occur could well need such a treatment. The major change Davis reported was a stronger coupling of the radiation field with the velocity field, resulting in a light curve looking more like the velocity curve. This time the RV Tauri alternation of periods was not observed, and the shoulder after light maximum was more

pronounced, more like the observed curve of W Virginis. The velocity amplitude ΔV , was about 55 km/s, and the light amplitude, ΔM_{bol} about 1.2. For comparison the observed amplitudes of W Virginis are $\Delta V = 55$ km/s, and $\Delta M_V = 1.2$ (see section 2.2), so this last model would seem to be quite reasonable.

The model of W Virginis published by Davis and Bunker (1975) was essentially the same as that of Davis (1972), except for the use of the Kippenhahn IA opacity tables. This paper emphasizes the differences between W Virginis models, and models of classical cepheids in the same period range. W Virginis stars have larger dynamic motion in the atmosphere because of a much stronger shock that develops. The radiative transfer hydrodynamics predicts hydrogen emission lines as the shock propagates. As pointed out in section 2.2 these emission lines are seen in the observations, along with a doubling of the absorption lines at about the correct phase.

The models of W Virginis stars so far presented still do not show light curves very like those observed; the dichotomy of light curve shapes mentioned by Kwee (1976b) has not been considered in these models. Those investigators have used a mass $M = 0.88 M_\odot$, since the mass of BL Herculis variables has been determined to be close to $0.6 M_\odot$, a similar mass is probably appropriate to W Virginis variables, which is somewhat smaller than the $0.88 M_\odot$, and so different values of $\log(L/L_\odot)$ and $\log T_e$ are needed. Similarly the determinations of $\log(L/L_\odot)$ and $\log T_e$ for W Virginis by Demers and Harris (1974) and Bohm-Vitense et al. (1974) indicate a different position in the HR diagram. The determination of the

instability strip by the authors provides an opportunity to construct a series of non-linear models surveying this region, to see if the observed light curves can be reproduced using the Carson opacities.

CHAPTER 3

THE EQUATIONS OF STELLAR PULSATION

3.1 THE BASIC EQUATIONS

The equations describing the dynamics of a model star are essentially those of static stellar structure (see, for example, Cox and Giuli 1968; Clayton 1968) with the time dependence of the variables included. Here these equations are solved by difference methods. (See section 3.3)

In a Lagrangian form the equations to be solved are:

Continuity of mass:

$$\frac{dr}{dM_r} = \frac{1}{4\pi r^2 \rho(r)} \quad (3.1)$$

Hydrodynamic Equilibrium:

$$\frac{\partial^2 r}{\partial t^2} = -\frac{GM_r}{r^2} - 4\pi r^2 \frac{\partial P}{\partial M_r} \quad (3.2)$$

Radiative Energy Transfer:

$$L_r = - (4\pi r^2)^2 \frac{4\sigma}{3\kappa(r)} \frac{d(T^4)}{dM_r} \quad (3.3)$$

where r is the space variable and t is the time variable. M_r is the mass contained within radius r , $\rho(r)$ is the matter

density at this radius, L_r the radiation flow (luminosity), P the total pressure, T the temperature and $\kappa(r)$ the opacity, all at the radius r . σ is the Stefan-Boltzmann constant.

Omitting energy generation we can write a heat flow equation:

$$T \frac{\partial S}{\partial t} = \frac{\partial Q}{\partial t} = - \frac{dL}{dM_r} \quad (3.4)$$

where E is the internal energy per unit mass, W is the PdV work done, S is the entropy and Q is the heat flow per gram. By the First Law of Thermodynamics we have,

$$\Delta E = Q - W$$

so

$$\frac{\partial E}{\partial t} = - \frac{dL}{dM_r} - P \frac{\partial V}{\partial t}$$

or

$$\frac{\partial E}{\partial t} + P \frac{\partial V}{\partial t} + \frac{dL}{dM_r} = 0 \quad (3.5)$$

For the dynamics we can write an energy conservation equation:

$$\frac{d}{dt} \left(\frac{1}{2} \dot{r}^2 - \frac{GM_r}{r} \right) = - 4\pi r^2 \dot{r} \frac{\partial P}{\partial M_r} \quad (3.6)$$

and then, using (3.1),

$$\frac{d}{dt} \left(\frac{1}{2} \dot{r}^2 - \frac{GM_r}{r} \right) = - \frac{d}{dM_r} (4\pi r^2 \dot{r} P) + P \frac{dV}{dt} \quad (3.7)$$

Finally by combining this with (3.5) we get the overall energy conservation equation:

$$\frac{d}{dt} \left(\frac{1}{2} \dot{r}^2 - \frac{GM_r}{r} + E \right) + \frac{d}{dM_r} (4\pi r^2 \dot{r} P + L) = 0 \quad (3.8)$$

In equation (3.3) convection is ignored as a possible energy transport mechanism, although parts of the envelopes of the stars considered will be unstable to convection (the hydrogen ionization region in particular). This should still be a fairly good approximation for most of the models, since the convection will be very inefficient in the tenuous envelopes of type II cepheids, because of the low matter density. Results from computed static model envelopes (section 6.1) confirm this for the blueward half of the instability strip, though it seems that the redder stars might have a significant convective flux (see section 6.1 for a further discussion). Ignoring convection also makes the non-linear pulsation problem far more tractable.

Only the stellar envelope appears to partake in the pulsation, and so energy generation is omitted. (See section 2.1)

3.2 THE BOUNDARY CONDITIONS

The inner boundary is defined by choosing a constant inner radius, $R_{inner} \sim 0.1R_*$, and inside this we assume there to be an adiabatic sphere radiating a constant luminosity, an approximation to the non-pulsating stellar core. So, at the inner boundary of the envelope:

$$\left(\frac{dr}{dt}\right)_{R_{inner}} = 0 \quad (3.9)$$

and

$$L(R_{inner}) = L_0 \quad (3.10)$$

The outer boundary condition for the dynamics is defined by Christy (1967) to be zero total pressure,

$$P_{tot}(\text{surface}) = 0 \quad (3.11a)$$

However, a better boundary condition would be zero gas pressure,

$$P_g(\text{surface}) = 0 \quad (3.11b)$$

or

$$P_{tot}(\text{surface}) = P_r(\text{surface}) \quad (3.11c)$$

This is a much better condition where radiation pressure is not insignificant at the surface of a star, which is the case with many type II cepheids. Both of these conditions are "standing wave" or total reflection boundary conditions.

Possibly a "running wave" boundary condition might be better for some of these stars (see section 2.1), but this would be more difficult to incorporate into a non-linear scheme.

Near the surface of the star the radiation flow should properly be described by a time-dependent transport equation. However, the transport equation provides a much harder numerical problem, since the temperature of any point depends on that of all neighbouring points within several mean free paths. In the diffusion theory it only depends on the two adjacent points, and so diffusion theory (although it is not a good description of the optically thin regions) provides a simpler problem. In classical cepheids and RR Lyrae stars the diffusion approximation seems to be sufficient, however it

might provide better results for some type II cepheids (again see section 2.1).

The radiative boundary condition is chosen to approximate the results of transport theory by using an "extrapolated boundary" (Christy 1967). In the Eddington approximation this can be expressed as:

$$\left. \frac{d(T^4)}{d\tau} \right|_{\text{surface}} = \frac{3}{4} T_e^4 = \frac{T_s^4}{2/3} \quad (3.12)$$

The equations (3.1), (3.2), (3.3) and (3.5) are considered as an initial value problem. As such they can be solved by putting them into difference form and integrating them forward in time starting from some given initial conditions, after the methods given in Richtmyer and Morton (1967). The initial conditions usually considered are a previously integrated static model envelope, and an initial velocity profile through the star, chosen to approximate the pulsational mode it is desired to excite.

3.3 THE DIFFERENCE EQUATIONS

The method used (following Christy 1967) is a semi-implicit one. The dynamical equations are integrated explicitly for each time step, while the thermodynamical equations are treated in an implicit manner.

The envelope of the star is divided into a number of zones, each containing a constant (with time) mass. The boundaries between each zone are represented by an integer I , where $I = 1$ is the inner boundary of the envelope and $I = N$

represents the surface of the star. Half integral values of I represent values of that quantity at the centre of the zone, so at each boundary we can give the mass contained within that boundary, M_I . Then the mass $\Delta M_{I-1/2}$, contained in the zone between $I-1$ and I , is given by

$$\Delta M_{I-1/2} = M_I - M_{I-1} \quad (3.13)$$

Also the mass associated with a boundary, i.e. contained between $I-1/2$ and $I+1/2$, is then given by

$$\Delta M_I = \frac{1}{2}(\Delta M_{I-1/2} + \Delta M_{I+1/2}) \quad (3.14)$$

The radius of each boundary, representing the variable $r(M,t)$, is given by R_I^n , where n represents the time t^n . So the specific volume of each mass zone is

$$V_{I-1/2}^n = \frac{4\pi(R_I^n)^3 - (R_{I-1}^n)^3}{3 \Delta M_{I-1/2}} \quad (3.15)$$

Similarly the mean temperature and pressure at time t^n of zone $I-1/2$ are represented by $T_{I-1/2}^n$ and $P_{I-1/2}^n$.

Since the radius is defined at t^n , it is best to time-centre the velocity at $t^{n+1/2} = t^n + 1/2\Delta t$, so that

$$R_I^{n+1} = R_I^n + \Delta t^{n+1/2} U_I^{n+1/2} \quad (3.16)$$

where,

$$\Delta t^{n+1/2} = t^{n+1} - t^n$$

Since a constant time step is not used (it is changed to satisfy various stability conditions) there is also another Δt , given by

$$\Delta t^n = t^{n+1/2} - t^{n-1/2}$$

So the time variable is defined in two ways;

$$t^{n+1} = t^n + \Delta t^{n+1/2} \quad (3.17a)$$

$$t^{n+1/2} = t^{n-1/2} + \Delta t^n \quad (3.17b)$$

and we also have

$$\Delta t^n = \frac{1}{2}(\Delta t^{n+1/2} + \Delta t^{n-1/2}) \quad (3.17c)$$

In pulsating stars a shock wave develops during the pulsation, causing rapid compression of some zones, particularly in the region of hydrogen ionization. These shock waves are treated by the Von Neumann-Richtmyer method (Richtmyer and Morton 1967), which introduces an artificial viscosity, acting like an extra pressure, the effect of which is to spread the shock front over several zones, thus improving the stability. The exact form of this viscosity has varied since Christy's work. Here the form used is that given by Stellingwerf (1975)

$$Q_{I-1/2}^{n-1/2} = C_Q P_{I-1/2}^{n-1/2} \left[\text{MIN} \left(\frac{(U_{I-1/2}^{n-1/2} - U_{I-1/2}^{n-1/2})}{(P_{I-1/2}^{n-1/2} V_{I-1/2}^{n-1/2})} + \alpha_v, 0 \right) \right]^2 \quad (3.18)$$

As in Christy C_Q is a constant chosen to achieve stability without losing too much accuracy. The usual values of C_Q range between 1.0 and 4.0. Stellingwerf introduced the parameter α_v , given in units of the sound speed, as a "turn-on" compression, providing a low level cut-off for the viscosity. Stellingwerf found that with $\alpha_v = 0$ (the original Christy formula) the artificial viscosity was producing a significant amount of damping in the lower regions of the envelope, thus affecting the limiting amplitude of the pulsation, an effect that had been noted by others. A small value of α_v , of the order of 0.1, is sufficient to eliminate most of the dissipative effects and still satisfy energy conservation.

From (3.2) we can write the equation of motion in difference form;

$$U_I^{n+1/2} = U_I^{n-1/2} - \Delta t \left[\frac{GM_I}{(R_I^n)^2} + \frac{4\pi(R_I^n)^2}{\Delta M_I} (P_{I+1/2}^n - P_{I-1/2}^n + Q_{I+1/2}^{n-1/2} - Q_{I-1/2}^{n-1/2}) \right] \quad (3.19)$$

At the inner boundary we have from (3.9)

$$U_1^{n+1/2} = 0$$

The outer boundary is treated by defining a fictitious pressure at $I = N+1/2$. For $P_{tot} = 0$ (3.11a), we require,

$$\frac{1}{2}(P_{N+1/2}^n + P_{N-1/2}^n) = 0$$

so

$$P_{N+1/2}^n = -P_{N-1/2}^n$$

and

$$P_{N+1/2}^n - P_{N-1/2}^n = -2P_{N-1/2}^n \quad (3.20a)$$

For $P_g = 0.0$ we require,

$$\frac{1}{2}(P_{N+1/2}^n + P_{N-1/2}^n) = P_{rN}^n$$

where P_{rN}^n is the radiation pressure at the surface. Since

the atmosphere is almost isothermal a good approximation to this (probably to within 1%) is,

$$P_{rN}^n \simeq \frac{1}{3}aW_{N-1/2}^n$$

thus

$$P_{N+1/2}^n = \frac{2}{3}aW_{N-1/2}^n - P_{N-1/2}^n$$

and

$$P_{N+1/2}^n - P_{N-1/2}^n = -2(P_{N-1/2}^n - \frac{a}{3}W_{N-1/2}^n) \quad (3.20b)$$

Equations (3.20a) and (3.20b) can be combined as

$$P_{N+1/2}^n - P_{N-1/2}^n = -2(P_{N-1/2}^n - \frac{B}{3}aW_{N-1/2}^n) \quad (3.20c)$$

where $B = 0$ for condition (3.11a) and $B = 1$ for condition (3.11b).

There is one further possible outer boundary condition.

If the star is considered to extend beyond the defined "surface" (see the discussion below about the mass associated with the surface boundary) then the pressures of zones $N-1/2$ and $N+1/2$ can be considered to be in proportion to the masses contained in these zones. So we have,

$$\frac{P_{N+1/2}}{P_{N-1/2}} = \frac{\Delta M_{N+1/2}}{\Delta M_{N-1/2}}$$

so

$$P_{N+1/2} = \frac{1}{\alpha} P_{N-1/2}$$

$$P_{N+1/2} - P_{N-1/2} = P_{N-1/2} (1/\alpha - 1) \quad (3.20d)$$

This condition might be useful as an outer boundary condition for stars of low effective temperature, acting to prevent the outer layers from escaping.

So at the outer boundary,

$$U_N^{\eta+1/2} = U_N^{\eta-1/2} - \Delta t^\eta \left[\frac{GM_N}{(R_N^\eta)^2} - \frac{4\pi(R_N^\eta)^2}{\Delta M_N} (2(P_{N-1/2}^\eta - B\alpha W_{N-1/2}^\eta) + Q_{N-1/2}^{\eta-1/2}) \right] \quad (3.21)$$

ΔM_N is an approximation to the mass associated with the outermost boundary. Christy put $\Delta M_N \simeq \Delta M_{N-1/2}$. It is usually assumed that some mass remains outside the defined stellar surface. The amount of mass remaining can be estimated in several ways, yielding a value for ΔM_N . If the mass zoning is continued beyond the boundary $I = N$, then the next zone out will contain a mass $\Delta M_{N+1/2} = 1/\alpha \Delta M_{N-1/2}$, where α is the mass ratio between successive zones (defined later). So ΔM_N can be estimated by

$$\begin{aligned} \Delta M_N &= \frac{1}{2}(\Delta M_{N+1/2} + \Delta M_{N-1/2}) \\ \Delta M_N &\simeq \frac{(1+\alpha)\Delta M_{N-1/2}}{2\alpha} \end{aligned} \quad (3.22)$$

This is the approximation used in most cases in this study. An alternative is to attempt to take account of all of the mass remaining outside the star. A possibility is to continue the zoning out to infinity, giving a total mass external to $I = N$,

$$M_{ext} \simeq \sum_{k=1}^{\infty} \frac{1}{\alpha^k} \Delta M_{N-1/2}$$

So that ΔM_N could be estimated as,

$$\begin{aligned} \Delta M_N &= \frac{1}{2} (\Delta M_{N-1/2} + \sum_{k=1}^{\infty} \frac{1}{\alpha^k} \Delta M_{N-1/2}) \\ &= \frac{1}{2} \Delta M_{N-1/2} \sum_{k=0}^{\infty} \frac{1}{\alpha^k} \\ \Delta M_N &= \frac{\alpha}{2(\alpha-1)} \Delta M_{N-1/2} \end{aligned} \quad (3.22)$$

(since $\alpha > 1$)

For a typical value of α , say $\alpha \sim 1.3$, formulae (3.22) and (3.23) can give quite different results.

As in Christy, $W \equiv T^4$ is used as the temperature variable, since it varies approximately linearly with mass over much of the envelope. From (3.3) a difference formula can be written for the luminosity at a boundary,

$$L_I^n = (4\pi(R_{\theta I}^n)^2)^2 (W_{I-1/2}^n - W_{I+1/2}^n) 2F_I^n \quad (3.24)$$

where $2F_I^n$ is a difference approximation to the quantity $4\sigma/3/(\kappa\Delta M)$. A suitable form for this is discussed later. Now the energy equation can be written down in difference form.

$$\begin{aligned} (E_{I+1/2}^{n+1} - E_{I+1/2}^n + (\frac{1}{2}(P_{I+1/2}^n + P_{I+1/2}^{n+1}) + Q_{I+1/2}^{n+1/2})(V_{I+1/2}^{n+1} - V_{I+1/2}^n))\Delta M_{I+1/2} \\ = \frac{\Delta t}{2} (L_I^{n+1} + L_I^n - L_{I+1}^{n+1} - L_{I+1}^n) \end{aligned} \quad (3.25)$$

This form of the energy equation is an implicit one, involving the new temperatures at three adjacent mass points. It is time centred at $n+1/2$ and space centred at $I+1/2$. As in Christy the equation is solved by a process of iteration at each time step. (Christy points out that another possibility would be to linearize the equation and solve it as a set of N coupled linear equations.)

The inner boundary condition, equation (3.10) is given by,

$$L_I^{n+1} = (4\pi(R_I^{n+1})^2)^2 (W_{1/2}^{n+1} - W_{3/2}^{n+1}) 2F_I^{n+1} = L_0 \quad (3.26)$$

where L_0 is the equilibrium luminosity of the star. This determines $W_{1/2}^{n+1}$.

At the outer boundary Christy (and others) used the relation,

$$L_S = 4\pi R_S^2 2\sigma T_S^4 \quad (3.27)$$

incorporated into equation (3.25) at $I = N-1$. The luminosity radiated by a star, assuming it to be a black body, is given by,

$$L = 4\pi (R_{phot})^2 \sigma T_e^4 \quad (3.28)$$

where R_{phot} is the photospheric radius, defined at $T = T_e$.

Replacing T_e^4 by $2T_S^4$ (from the Eddington approximation), we get

$$L = 4\pi (R_{phot})^2 2\sigma T_S^4 \quad (3.29)$$

Christy used R_{N-1} as his value for R_S , since the radius R_N is somewhat unreliable. Here equation (3.29) is used, using an approximation to R_{phot} . This treatment probably makes little physical difference, but it does seem to aid in overcoming some numerical problems (see section 3.9). Judging by the plots of velocity histories given in section 6.9, and inferring the radius variations, it seems that both R_N and R_{N-1} might be unreliable in some models. Use of R_{phot} seems to help. The value of R_{phot} is found by interpolation, estimating T_e^4 from $2(T_{N-1/2})^4$. The position of T_e is found, and R_{phot} interpolated, taking care to use the correct space centring.

So at the outer boundary, we have

$$\begin{aligned} (E_{N-1/2}^{n+1} - E_{N-1/2}^n + (\frac{1}{2}(P_{N-1/2}^{n+1} + P_{N-1/2}^n) + Q_{N-1/2}^{n+1/2})(V_{N-1/2}^{n+1} - V_{N-1/2}^n))\Delta M_{N-1/2} \quad (3.30) \\ = \frac{\Delta t}{2} (L_{N-1}^{n+1} + L_{N-1}^n - 2\sigma 4\pi (R_{phot}^n)^2 V_{N-1/2}^n + (R_{phot}^{n+1})^2 V_{N-1/2}^{n+1}) \end{aligned}$$

3.4 THE SOLUTION OF THE IMPLICIT FORM OF THE ENERGY EQUATION

Equation (3.25) is solved by a Newton-Raphson type iteration procedure, for the new temperatures $W_{I+1/2}^{n+1}$. The corrections to the temperatures at each iteration are defined by

$$i\Delta W_{I+1/2}^{n+1} = iW_{I+1/2}^{n+1} - iW_{I+1/2}^{n+1} \quad (3.31)$$

The $(i+1)$ th iterate is expressed as,

$$\begin{aligned} i+1 P_{I+1/2}^{n+1} &= iP_{I+1/2}^{n+1} + \frac{i\partial P}{\partial W_{I+1/2}} i\Delta W_{I+1/2}^{n+1} \\ i+1 E_{I+1/2}^{n+1} &= iE_{I+1/2}^{n+1} + \frac{i\partial E}{\partial W_{I+1/2}} i\Delta W_{I+1/2}^{n+1} \\ i+1 F_{I+1/2}^{n+1} &= iF_{I+1/2}^{n+1} + \frac{i\partial F_I}{\partial W_{I+1/2}} i\Delta W_{I+1/2}^{n+1} + \frac{i\partial F_I}{\partial W_{I-1/2}} i\Delta W_{I-1/2}^{n+1} \end{aligned} \quad (3.32)$$

and the luminosity, $i+1 L_I^{n+1}$ is given by (3.24).

Using equations (3.32) to linearize (3.25), the energy equation can be written in a simple form,

$$-\alpha_{I+1/2} i\Delta W_{I+3/2}^{n+1} + \beta_{I+1/2} i\Delta W_{I+1/2}^{n+1} - \gamma_{I+1/2} i\Delta W_{I-1/2}^{n+1} = \delta_{I+1/2} \quad (3.33)$$

where

$$\begin{aligned} \alpha_{I+1/2} &= \Delta t^{n+1/2} (A_{I+1}^{n+1})^2 (iF_{I+1}^{n+1} - \frac{i\partial F_{I+1}}{\partial W_{I+3/2}}^{n+1} (iW_{I+1/2}^{n+1} - iW_{I+3/2}^{n+1})) \\ \beta_{I+1/2} &= \frac{i\partial E_{I+1/2}^{n+1}}{\partial W_{I+1/2}} + \frac{1}{2} \frac{i\partial P_{I+1/2}^{n+1}}{\partial W_{I+1/2}} (V_{I+1/2}^{n+1} - V_{I+1/2}^n) \Delta M_{I+1/2} + \alpha_{I-1/2} + \gamma_{I+3/2} \\ \gamma_{I+1/2} &= \Delta t^{n+1/2} (A_I^{n+1})^2 (iF_I^{n+1} + \frac{i\partial F_I}{\partial W_{I-1/2}}^{n+1} (iW_{I-1/2}^{n+1} - iW_{I+1/2}^{n+1})) \\ \delta_{I+1/2} &= \frac{\Delta t}{2} (iL_I^{n+1} + L_I^n - iL_{I+1}^{n+1} - L_{I+1}^n) \\ &\quad - \Delta M_{I+1/2} (iE_{I+1/2}^{n+1} - E_{I+1/2}^n + (\frac{1}{2}(P_{I+1/2}^n + iP_{I+1/2}^{n+1}) + O_{I+1/2}^{n+1/2})(V_{I+1/2}^{n+1} - V_{I+1/2}^n)) \end{aligned} \quad (3.34)$$

and

$$A_I^{n+1} \equiv 4\pi(R_I^{n+1})^2$$

Note that in the definition of $\beta_{I+1/2}$ the inclusion of $\alpha_{I-1/2}$ and $\gamma_{I+3/2}$ refers to the functional form given here, not to the values of these quantities, as the values may be different at the boundaries from those that would be found using equations (3.34)

This set of equations, together with the boundary conditions as given in (3.26) and (3.30), form a matrix equation of the form $\underline{M}\underline{x} = \underline{d}$, where \underline{M} is a tridiagonal matrix containing the elements $\alpha_{I-1/2}$, $\beta_{I+1/2}$, $\gamma_{I+3/2}$ on the leading diagonal, \underline{d} is a vector containing the $\delta_{I+1/2}$ and \underline{x} is the solution vector containing the new $i^{n+1}\Delta W_{I+1/2}$. The matrix set up looks like this,

$$\begin{bmatrix} \beta_{1/2} & -\alpha_{1/2} & & & \\ -\gamma_{3/2} & \beta_{3/2} & -\alpha_{3/2} & & \\ & -\gamma_{5/2} & \beta_{5/2} & -\alpha_{5/2} & \\ & & & & \ddots \\ & & & & & -\gamma_{N-1/2} & \beta_{N-1/2} \end{bmatrix} \begin{bmatrix} i^{n+1}\Delta W_{1/2} \\ i^{n+1}\Delta W_{3/2} \\ \vdots \\ \vdots \\ \vdots \\ i^{n+1}\Delta W_{N-1/2} \end{bmatrix} = \begin{bmatrix} \delta_{1/2} \\ \delta_{3/2} \\ \vdots \\ \vdots \\ \vdots \\ \delta_{N-1/2} \end{bmatrix}$$

By linearizing (3.26) and comparing with (3.33) it is possible to write down the elements for the inner boundary.

$$\begin{aligned}
 \alpha_{1/2} &= 2(A_1^{n+1})^2 (i F_1^{n+1} - \frac{i \partial F_1^{n+1}}{\partial W_{3/2}^{n+1}} (i W_{1/2}^{n+1} - i W_{3/2}^{n+1})) \\
 \beta_{1/2} &= 2(A_1^{n+1})^2 (i F_1^{n+1} + \frac{i \partial F_1^{n+1}}{\partial W_{1/2}^{n+1}} (i W_{1/2}^{n+1} - i W_{3/2}^{n+1})) \\
 \gamma_{1/2} &= 0 \\
 \delta_{1/2} &= -2(A_1^{n+1})^2 i F_1^{n+1} (i W_{1/2}^{n+1} - i W_{3/2}^{n+1}) + L_0
 \end{aligned} \tag{3.35}$$

Similarly, by linearizing (3.30) and comparing with (3.33) the elements for the outer boundary can be written down,

$$\begin{aligned}
 \alpha_{N-1/2} &= 0 \\
 \beta_{N-1/2} &= \Delta t^{n+1/2} ((A_{N-1}^{n+1})^2 (i F_{N-1}^{n+1} - \frac{i \partial F_{N-1}^{n+1}}{\partial W_{N-3/2}^{n+1}} (i W_{N-3/2}^{n+1} - i W_{N-1/2}^{n+1})) + \sigma A_{phot}^{n+1} \\
 \gamma_{N-1/2} &= \Delta t^{n+1/2} ((A_{N-1}^{n+1})^2 (i F_{N-1}^{n+1} + \frac{i \partial F_{N-1}^{n+1}}{\partial W_{N-1/2}^{n+1}} (i W_{N-3/2}^{n+1} - i W_{N-1/2}^{n+1})) \\
 \delta_{N-1/2} &= \frac{\Delta t}{2} (L_{N-1}^n + i L_{N-1}^{n+1} - 2\sigma(A_{phot}^n W_{N-1/2}^n + i A_{phot}^{n+1} i W_{N-1/2}^{n+1})) \\
 &\quad - \Delta H_{N-1/2} (i E_{N-1/2}^{n+1} - E_{N-1/2}^n + (\frac{1}{2}(P_{N-1/2}^n + i P_{N-1/2}^{n+1}) + Q_{N-1/2}^{n+1/2}) (V_{N-1/2}^{n+1} - V_{N-1/2}^n))
 \end{aligned} \tag{3.36}$$

Equation (3.33) can now be solved by a conventional matrix method. The one used here is the same as that used by Christy, described by Richtmyer and Morton (1967).

To solve (3.33), we look for two sets of quantities, $X_{I+1/2}$ and $Y_{I+1/2}$, such that

$$\Delta W_{I+1/2}^{n+1} = X_{I+1/2} \Delta W_{I+3/2}^{n+1} + Y_{I+1/2} \tag{3.37}$$

Substituting (3.37) into (3.33) and dropping time superscripts,

$$\begin{aligned}
 -\alpha_{I+1/2} i \Delta W_{I+3/2} &= (\gamma_{I+1/2} X_{I+1/2} - \beta_{I+1/2}) i \Delta W_{I+1/2} + (\delta_{I+1/2} + \gamma_{I+1/2} Y_{I+1/2}) \\
 \text{or } i \Delta W_{I+1/2} &= \frac{\alpha_{I+1/2}}{(\beta_{I+1/2} - \gamma_{I+1/2} X_{I+1/2})} i \Delta W_{I+3/2} + \frac{(\delta_{I+1/2} + \gamma_{I+1/2} Y_{I+1/2})}{(\beta_{I+1/2} - \gamma_{I+1/2} X_{I+1/2})}
 \end{aligned}$$

So that

$$\begin{aligned} X_{I+1/2} &= \frac{\alpha_{I+1/2}}{(\beta_{I+1/2} - \gamma_{I+1/2} X_{I-1/2})} \\ Y_{I+1/2} &= \frac{(\delta_{I+1/2} + \gamma_{I+1/2} Y_{I-1/2})}{(\beta_{I+1/2} - \gamma_{I+1/2} X_{I-1/2})} \end{aligned} \quad (3.38)$$

Since $\gamma_{1/2} = 0$ (equation 3.35),

$$\begin{aligned} X_{1/2} &= \alpha_{1/2} / \beta_{1/2} \\ Y_{1/2} &= \delta_{1/2} / \beta_{1/2} \end{aligned}$$

So from these starting values at $I-1/2 = 1/2$, all of the $X_{I+1/2}$ and $Y_{I+1/2}$ can be calculated from equations (3.38). At the surface we know $\alpha_{N-1/2} = 0$, so $X_{N-1/2} = 0$, and therefore

$$\dot{\Delta} W_{N-1/2} = Y_{N-1/2}$$

and so all of the $\dot{\Delta} W_{I+1/2}$ can be found from (3.37). This gives the solution vector. The iterations proceed until the corrections $\dot{\Delta} W_{I+1/2}$ are reduced to a sufficiently small size (usually to five figures).

The gradients $\partial E / \partial W_{I+1/2}$ and $\partial P / \partial W_{I+1/2}$ can be found from the equation of state (see section 5.1). The F_I and gradients are discussed below.

3.5 THE LUMINOSITY INTERPOLATION

Christy at first used a very simple opacity average to find F_I ,

$$F_I^n = \frac{4\sigma/3}{(K_{I+1/2}^n \Delta M_{I+1/2} + K_{I-1/2}^n \Delta M_{I-1/2})} \quad (3.39)$$

where $K_{I+1/2}$ is the opacity in zone $I+1/2$, given by $T_{I+1/2}$ and $1/V_{I+1/2}$. However, this caused convergence problems in the

solution of the heat equation when the radiation front which develops in the hydrogen ionization zone is moving through the star at large amplitudes. This is because equation (3.39) cannot handle the large change in opacity across a zone that occurs in such cases. It gives too little weight to the larger opacity. Christy then developed the following difference expression for F_I (dropping time superscripts)

$$F = \frac{4\sigma}{3} \frac{(W_{I+1/2}/K_{I+1/2} + W_{I-1/2}/K_{I-1/2})}{(\Delta M_{I+1/2} + \Delta M_{I-1/2})(W_{I+1/2} + W_{I-1/2})} \quad (3.40)$$

This permitted the use of quite coarse zoning in the hydrogen ionization region without causing numerical difficulties. This is the treatment used here.

Stobie (1969a) considered several forms of the opacity mean, concluding that the form (3.40) used by Christy gave the best overall representation of the effective opacity.

Then Stellingwerf (1975) introduced a formula which appears to give better results than the Christy formula for areas slightly away from the main opacity peak. At the peak itself it produces much the same error.

In the formulation used here, Stellingwerf's formula can be written as

$$F = \frac{4\sigma}{3} \frac{\langle dW/K \rangle}{(\Delta M_{I+1/2} + \Delta M_{I-1/2})(W_{I+1/2} - W_{I-1/2})} \quad (3.41)$$

$$\text{where } \langle dW/K \rangle = \frac{(W_{I+1/2}/K_{I+1/2} - W_{I-1/2}/K_{I-1/2})}{(1 - (\log(K_{I+1/2}/K_{I-1/2})/\log(W_{I+1/2}/W_{I-1/2}))} \quad (3.42)$$

This expression is exact for all variations of the form $K \propto W^n$, $n \neq 1$, however, if

$n = \partial \log \kappa / \partial \log W \approx \log(\kappa_{I+1/2} / \kappa_{I-1/2}) / \log(W_{I+1/2} / W_{I-1/2})$ approaches unity then equation (3.41) can become very inaccurate. In this case the expression

$$\langle dW/\kappa \rangle \approx \frac{W_{I-1/2} \log(W_{I+1/2} / W_{I-1/2})}{K_{I-1/2}} \quad (3.43)$$

may be used.

The two derivatives of F_I , $\partial F_I / \partial W_{I-1/2}$ and $\partial F_I / \partial W_{I+1/2}$ are also required. Writing

$$S_I = \frac{4\sigma/3}{(\Delta M_{I+1/2} + \Delta M_{I-1/2})}$$

(3.40) can be expressed as

$$\begin{aligned} F_I &= S_I \frac{(W_{I+1/2} / K_{I+1/2} + W_{I-1/2} / K_{I-1/2})}{(W_{I+1/2} + W_{I-1/2})} \\ \text{So } \frac{\partial F_I}{\partial W_{I-1/2}} &= S_I \left[(W_{I+1/2} + W_{I-1/2})^{-1} \left(1/K_{I-1/2} - \frac{W_{I-1/2}}{(K_{I-1/2})^2} \frac{\partial K}{\partial W_{I-1/2}} \right) \right. \\ &\quad \left. - (W_{I+1/2} + W_{I-1/2})^{-2} (W_{I+1/2} / K_{I+1/2} + W_{I-1/2} / K_{I-1/2}) \right] \\ \Rightarrow \frac{\partial F_I}{\partial W_{I-1/2}} &= F_I \left[\left(1/K_{I-1/2} - \frac{W_{I-1/2}}{(K_{I-1/2})^2} \frac{\partial K}{\partial W_{I-1/2}} \right) \left(\frac{W_{I+1/2}}{K_{I+1/2}} + \frac{W_{I-1/2}}{K_{I-1/2}} \right) - \frac{1}{(W_{I+1/2} + W_{I-1/2})} \right] \\ \text{similarly} & \quad (3.44) \\ \frac{\partial F_I}{\partial W_{I+1/2}} &= F_I \left[\left(1/K_{I+1/2} - \frac{W_{I+1/2}}{(K_{I+1/2})^2} \frac{\partial K}{\partial W_{I+1/2}} \right) \left(\frac{W_{I+1/2}}{K_{I+1/2}} + \frac{W_{I-1/2}}{K_{I-1/2}} \right) - \frac{1}{(W_{I+1/2} + W_{I-1/2})} \right] \end{aligned}$$

The gradients of the Stellingwerf formula are a little more involved, but can be found in much the same manner. From equation (3.41)

$$\begin{aligned} F_I &= \frac{S_I \langle dW/\kappa \rangle}{(W_{I+1/2} - W_{I-1/2})} \\ \frac{\partial F_I}{\partial W_{I-1/2}} &= S_I \left[(W_{I+1/2} - W_{I-1/2})^{-1} \frac{\partial \langle dW/\kappa \rangle}{\partial W_{I-1/2}} + \langle dW/\kappa \rangle (W_{I+1/2} - W_{I-1/2})^{-2} \right] \quad (3.45) \end{aligned}$$

Then from (3.42)

$$\begin{aligned} \frac{\partial \langle dW/\kappa \rangle}{\partial W_{I-1/2}} &= \langle dW/\kappa \rangle \left[\left(\frac{1}{K_{I-1/2}} \frac{\partial K}{\partial W_{I-1/2}} - \frac{1}{W_{I-1/2}} \right) \left(\frac{W_{I-1/2} / K_{I-1/2}}{(W_{I+1/2} / K_{I+1/2} - W_{I-1/2} / K_{I-1/2})} \right) \right. \\ &\quad \left. - \left(\log(W_{I+1/2} / W_{I-1/2}) - \log(K_{I+1/2} / K_{I-1/2}) \right)^{-1} - 1 / (W_{I-1/2} \log(W_{I+1/2} / W_{I-1/2})) \right] \end{aligned}$$

Then substituting into (3.45) gives,

$$\frac{\partial F_I}{\partial W_{I-\frac{1}{2}}} = F_I \left[\left(\frac{1}{K_{I-\frac{1}{2}}} \frac{\partial K}{\partial W_{I-\frac{1}{2}}} - \frac{1}{W_{I-\frac{1}{2}}} \right) \left(\frac{W_{I-\frac{1}{2}}/K_{I-\frac{1}{2}}}{(W_{I+\frac{1}{2}}/K_{I+\frac{1}{2}} - W_{I-\frac{1}{2}}/K_{I-\frac{1}{2}})} \right) \right. \\ \left. - \frac{1}{(\log(W_{I+\frac{1}{2}}/W_{I-\frac{1}{2}}) - \log(K_{I+\frac{1}{2}}/K_{I-\frac{1}{2}}))} - \frac{1/W_{I-\frac{1}{2}}}{\log(W_{I+\frac{1}{2}}/W_{I-\frac{1}{2}})} - \frac{1}{(W_{I+\frac{1}{2}} - W_{I-\frac{1}{2}})} \right] \quad (3.46)$$

Similarly,

$$\frac{\partial F_I}{\partial W_{I+\frac{1}{2}}} = F_I \left[\left(\frac{1}{W_{I+\frac{1}{2}}} - \frac{1}{K_{I+\frac{1}{2}}} \frac{\partial K}{\partial W_{I+\frac{1}{2}}} \right) \left(\frac{W_{I+\frac{1}{2}}/K_{I+\frac{1}{2}}}{(W_{I+\frac{1}{2}}/K_{I+\frac{1}{2}} - W_{I-\frac{1}{2}}/K_{I-\frac{1}{2}})} \right) \right. \\ \left. - \frac{1}{(\log(W_{I+\frac{1}{2}}/W_{I-\frac{1}{2}}) - \log(K_{I+\frac{1}{2}}/K_{I-\frac{1}{2}}))} + \frac{1/W_{I+\frac{1}{2}}}{\log(W_{I+\frac{1}{2}}/W_{I-\frac{1}{2}})} - \frac{1}{(W_{I+\frac{1}{2}} - W_{I-\frac{1}{2}})} \right]$$

If expression (3.43) is used for $\langle dW/\kappa \rangle$ instead of (3.42) then

the derivatives of $\langle dW/\kappa \rangle$ are,

$$\frac{\partial \langle dW/\kappa \rangle}{\partial W_{I-\frac{1}{2}}} = \langle dW/\kappa \rangle \left(\frac{1}{W_{I-\frac{1}{2}}} - \frac{1}{K_{I-\frac{1}{2}}} \frac{\partial K}{\partial W_{I-\frac{1}{2}}} - \frac{1/W_{I-\frac{1}{2}}}{\log(W_{I+\frac{1}{2}}/W_{I-\frac{1}{2}})} \right) \\ \frac{\partial \langle dW/\kappa \rangle}{\partial W_{I+\frac{1}{2}}} = \frac{\langle dW/\kappa \rangle}{\log(W_{I+\frac{1}{2}}/W_{I-\frac{1}{2}})} \frac{1/W_{I+\frac{1}{2}}}{\log(W_{I+\frac{1}{2}}/W_{I-\frac{1}{2}})}$$

3.6 THE TIME STEP.

The time step to be found at each integration step is $\Delta t^{n+\frac{1}{2}}$. Having found this then Δt^n can be found from equation (3.17c). Two conditions are placed on $\Delta t^{n+\frac{1}{2}}$. The first and usually the most stringent is that the time step used must be less than the time taken for a sound wave to traverse a zone (see Christy 1964; Richtmyer and Morton 1967). Approximating the sound speed by $\sqrt{P_{I-\frac{1}{2}} V_{I-\frac{1}{2}}}$, then we have

$$\Delta t^{n+\frac{1}{2}} < \frac{\Delta R}{\sqrt{P_{I-\frac{1}{2}} V_{I-\frac{1}{2}}}} \quad (3.47)$$

where $\Delta R = R_I - R_{I-1}$

Secondly we must ensure that two zone boundaries cannot cross during a time step. This is given by,

$$\Delta t^{n+\frac{1}{2}} < -\Delta R/\Delta U \quad \text{for } \Delta U = U_I - U_{I-1} < 0 \quad (3.48)$$

This condition cannot be fully satisfied, since it is calculated from the velocities for the time step t^n . Those at t^{n+1} are still to be found. Thus in a rapidly accelerating compression this condition might be violated. Therefore a check still has to be made to prevent boundaries crossing, which would cause negative densities. To help with this problem, and to ensure that the missing factor of γ (the ratio of specific heats) in equation (3.47) is taken care of, only a fraction, about $1/2 - 2/3$, of the maximum time-step allowed by (3.47) and (3.48) is used.

3.7 THE INITIAL MODEL

The difference scheme described here requires as a starting point an initial model in hydrostatic and thermodynamic equilibrium. Thermodynamic equilibrium is required because the time scale for the thermal relaxation of stars is much greater than the pulsation period. A separately calculated stellar envelope (see section 4) divided into N mass zones is used for this purpose.

The envelope is divided into about 35 - 50 mass zones in such a way as to compromise between accuracy (more zones) and speed (fewer zones). The ratio α is defined as the ratio of the masses of two adjacent zones,

$$\alpha = \Delta M_{I-1/2} / \Delta M_{I+1/2} \quad (3.49)$$

so that the mass contained in each zone ⁱⁿ decreases geometrically as the zones move deeper into the star, coinciding with the rise in density. This keeps the sound travel time

approximately the same in all zones.

The static model from the differential equations has about 1000 - 1500 layers in it, allowing the mass division to proceed fairly accurately. Beginning at the surface, with $\Delta M_{N-\frac{1}{2}}$, the values of δM_r from the finely divided model are accumulated until $\Delta M_{N-\frac{1}{2}}$ is surpassed. The final value of δM_r is then split in two, one part to finish the sum at exactly $\Delta M_{N-\frac{1}{2}}$, the other to begin the accumulation for $\Delta M_{N-\frac{3}{2}}$. This is really hardly necessary, but since it is an overhead, performed once per model, the ensured accuracy is useful. This is continued through the star until the inner boundary is reached. The variables R_I , $T_{I-\frac{1}{2}}$ and $P_{I-\frac{1}{2}}$ are initially estimated from the boundaries of the zones (for R_I), or from mean values through the zone.

It still remains, however, to specify the values of α and $\Delta M_{N-\frac{1}{2}}$, the mass of the outermost zone. By specifying the total number of zones required, N_E , along with the number required in the atmosphere ($\mathcal{V} \leq 2/3$ or $T \leq T_E$), N_A , it is possible to define α and $\Delta M_{N-\frac{1}{2}}$. If M_E is the total mass of the envelope, and M_A is the mass of the atmosphere (measured from the finely zoned model) then,

$$\begin{aligned} M_A &= \sum_{I=N_E-N_A}^{N_E} \Delta M_I \\ &= \Delta M_{N-\frac{1}{2}} \sum_{n=1}^{N_A} \alpha^{n-1} = \Delta M_{N-\frac{1}{2}} \frac{(1 - \alpha^{N_A})}{(1 - \alpha)} \end{aligned}$$

Similarly

$$M_E = \Delta M_{N-\frac{1}{2}} \frac{(1 - \alpha^{N_E})}{(1 - \alpha)}$$

$$\Rightarrow \frac{M_A}{M_E} = \frac{(\alpha^{N_A} - 1)}{(\alpha^{N_E} - 1)} \quad (3.50)$$

This equation can be solved iteratively for α , and then,

$$\Delta M_{N-\frac{1}{2}} = \frac{M_E(\alpha - 1)}{(\alpha^{N_E} - 1)} = \frac{M_A(\alpha - 1)}{(\alpha^{N_A} - 1)}$$

Here we also follow Christy in increasing the size of the zones above a certain temperature (2×10^5 K and 10^5 K were both used), to satisfy the criterion that the time for a sound wave to traverse a zone should not decrease any further beyond this point. This is because the greater sound speed in the denser interior would cause the maximum allowable time-step to become quite small (see equation [3.47]). Since the pulsation amplitudes in this region are quite small these locally larger zones (larger values of α) should have little effect on the models. It does of course mean that the number of zones in the final model will in general be less than N_E , the number asked for.

A solution of the differential equations of stellar structure will not necessarily also be a solution to the difference equations used here, so it is usually necessary to relax the newly divided model into the difference scheme. The difference equations can be rewritten for the case of zero velocity, spatially constant luminosity and no time variations:

Hydrostatic Equilibrium

$$\frac{GM_I}{(R_I)^2} = - \frac{4\pi(R_I)^2}{\Delta M_I} (P_{I+1/2} - P_{I-1/2}) \quad (3.51)$$

Thermal Equilibrium

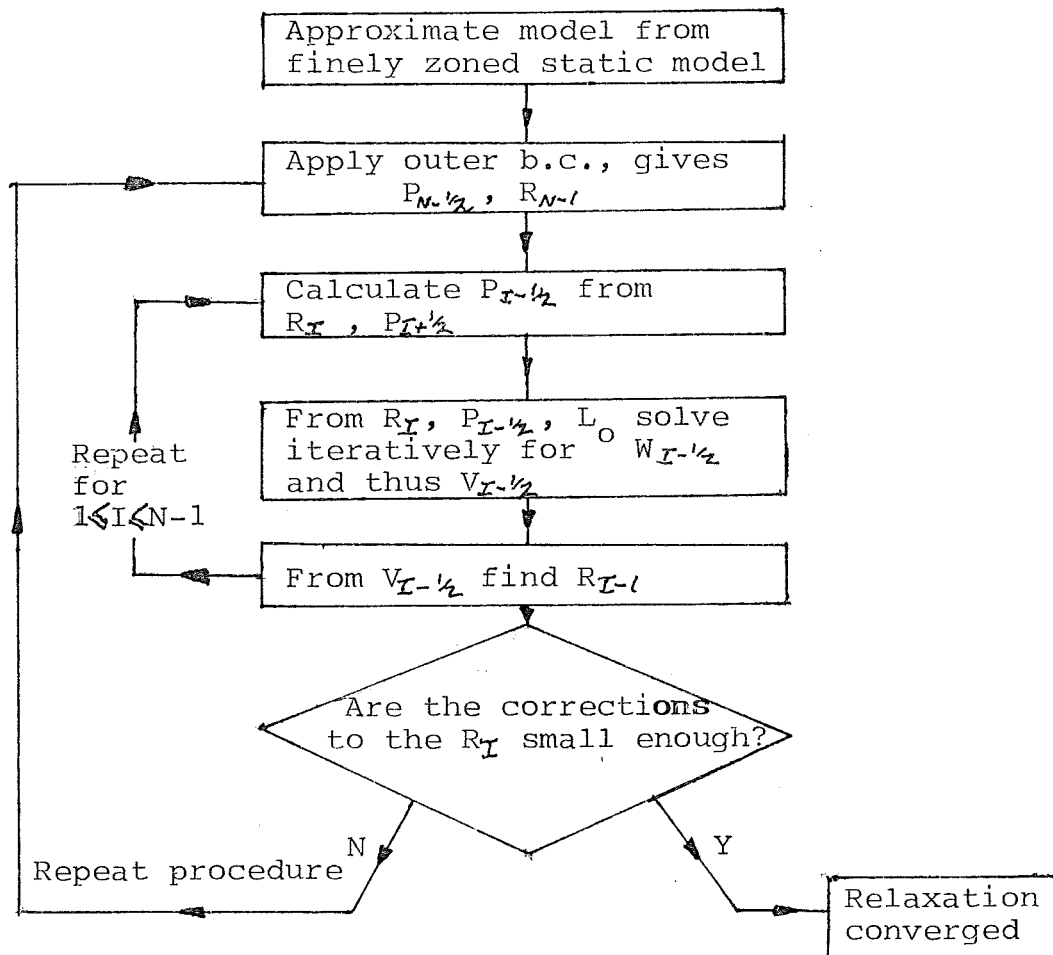
$$L_I = (4\pi(R_I)^2)^2 (W_{I-1/2} - W_{I+1/2}) 2F_I = L_0 \quad (3.52)$$

From (3.51) $P_{I-1/2}$ can be found, knowing R_I and $P_{I+1/2}$, then (3.52) can be solved iteratively for $W_{I-1/2}$. Thus $V_{I-1/2}$ can be found, and R_{I-1} calculated from (3.15).

At the surface, the outer boundary condition (3.11) can be applied to find $P_{N-1/2}$. So

$$P = \frac{GM_N \Delta M_N}{8\pi(R_N)^4} + \frac{B\omega N-1/2}{3} \quad (3.53)$$

where B is defined as before. Schematically the relaxation is shown below.



This is by no means the only method of relaxation, but it is the one adopted here. Normally only two or three grand iterations are required. Without such a relaxation it is found that the integration of the pulsation equations will frequently break down quite quickly. The final thing to be done to the initial model is to give it an initial velocity profile as a starting point for the pulsation. Occasionally it might be desirable to start with a zero velocity distribution, and start

the growth of the pulsation from computational "white noise". This procedure might be preferable for testing stable stars, or modelling only marginally unstable stars; for most cases the time taken for the oscillations to grow to full amplitude from noise is far too long for it to be useful. So most models are begun with a velocity distribution. One profile used is that of Christy,

$$U(r) = -13(r/R)^{10} - 7(r/R)^5 \text{ km/s} \quad (3.54)$$

Another is

$$U(r) = -18(r/R)^5 \text{ km/s} \quad (3.55)$$

which is based on formulae given in Stobie (1969a). In that paper Stobie gives power law distributions for the fundamental, and first and second harmonics (for classical cepheids), and he also discusses the effect of the choice of the initial distribution. For the type II cepheids (mostly fundamental pulsators) the possible contamination by other modes is not thought to be too much of a problem, partly because of the short e-folding times of these stars, and also because the first harmonic blue edge is considerably redder than the fundamental blue edge (section 2.3). Since the e-folding times are so short, it was decided not to use artificial amplification of the motion, also discussed by Stobie (1969a). Most of these stars are almost full grown after 10 periods or so in any case.

3.8 TESTING FOR A PERIOD

The beginning and ending of a period is defined here as being when a chosen radius, while decreasing, crosses its equilibrium value. Two possible radii are normally used, either the radius of the boundary of INT(N/2) (halfway through the zones of the envelope), or the radius of the boundary used as the observation point. The observation boundary is chosen as the one closest to $\tau = 0.2$ in the equilibrium model. This value is chosen following Carson, Stothers and Vemury (1981). CSV, however, chose the boundary nearest $T = 3 \times 10^5$ K in determining the period. During each period the following quantities are all taken from the zone nearest $\tau = 0.2$;

U_{in} - maximum inward velocity

U_{out} - maximum outward velocity

$\Delta U = U_{in} - U_{out}$

R_{max}, R_{min} - maximum and minimum radii

$\Delta R/R$ - full amplitude = $(R_{max} - R_{min})/R$

L_{max}, L_{min} - maximum and minimum luminosities

$\Delta M_{bol} = 2.5 \log(L_{max}/L_{min})$

The peak kinetic energy of the star for the period is also noted, the kinetic energy being found from

$$K.E. = \sum_{i=1}^N \Delta M_{i-\frac{1}{2}} (U_{i-\frac{1}{2}})^2$$

where

$$U_{i-\frac{1}{2}} = \frac{1}{2} (U_i + U_{i-1})$$

The work done in each cycle, for each zone, $\Delta M_{i-\frac{1}{2}} \oint dW$ is also calculated, where $dW = (P+Q)dV$. Q is included since it is a pressure and thus does work, even if it is artificial. Since (while the pulsation is growing, and later for numerical

reasons), the P-V loop will in general not close exactly, the value $1/2(P_{\text{initial}} - P_{\text{final}})(V_{\text{initial}} - V_{\text{final}})$ is added for each zone (Vemury and Stothers 1978). The integrated work function for the star then comes from
$$\sum_{I=1}^N \Delta M_{I-1/2} \oint (P + Q) dV$$

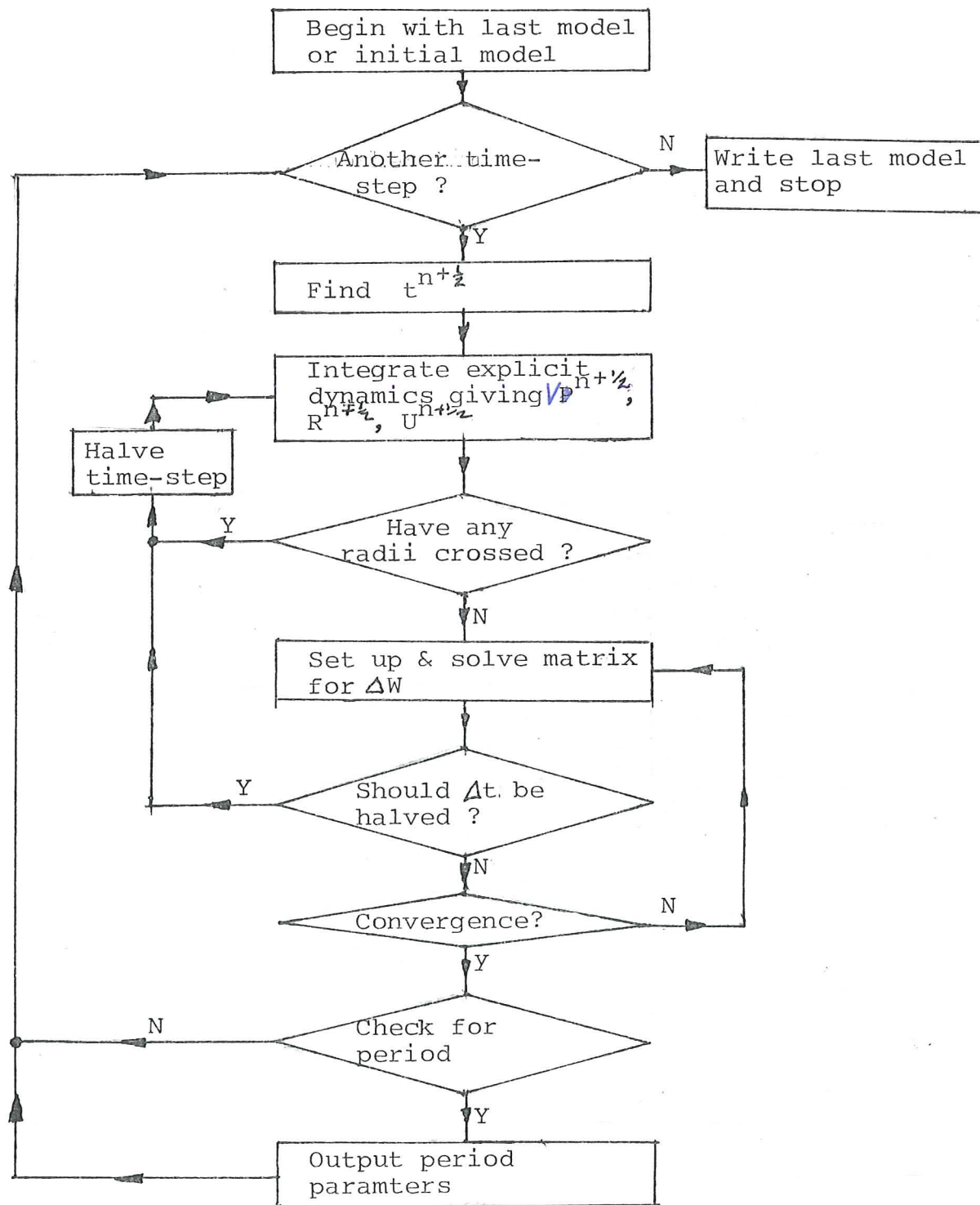
3.9 NUMERICAL PROBLEMS

To avoid problems of numerical overflow on the machine used, the luminosity, along with such things as the kinetic energy, the $\delta_{I+1/2}$ and the work done were scaled downwards by a factor of 10^{35} . Also the gradients $\partial F_I / \partial W_{I-1/2}$ and $\partial F_I / \partial W_{I+1/2}$ tended to be rather small, and were therefore scaled up. Other possible overflows were avoided by choosing the order of calculation carefully.

Several problems occur in the solution of the energy equation. These were usually overcome by halving the time-step. However, in the instance of having a fractional correction $\left| \frac{\Delta W_{I+1/2}}{W_{I+1/2}} \right|$ that is greater than (say) 0.8, rather than halving the time-step (which is time consuming) only some of the correction is applied, say a fraction $1/\eta$, where
$$\eta = 2 \left| \frac{\Delta W_{I+1/2}}{W_{I+1/2}} \right|$$
. So the correction applied to each temperature would be $\Delta W_{I+1/2} / \eta$. This avoids some convergence problems without the need to halve the time-step and recompute the integration step. A specific problem encountered in the modelling of type II cepheids was the occurrence of negative luminosities between zones, caused by the inner zone having a lower temperature than the one just outside it. So a further

restriction was placed on the corrections $\Delta W_{L+1/2}$, - that they must not cause this inversion. If it occurred then $\Delta t^{n+1/2}$ would be halved. This restriction was not totally successful. In many cases where the luminosity would have become negative, it simply meant that the time-step was halved over and over again until the program crashed because Δt was too small. The introduction of the boundary condition (3.29) has partially overcome this problem, though it still occasionally occurs. Another partial solution to this seems to be to decrease the number of zones, or increase α , the zone ratio. This probably helps just by separating the rogue zones a little more widely in temperature. Of course this can only be taken so far, too few zones or too large a value of α will mean a decrease in accuracy.

The integration of the pulsation is shown schematically here.



CHAPTER 4

THE STATIC MODEL

The starting point of the pulsation integrations is usually taken to be a model stellar envelope in hydrostatic equilibrium. This is found by solving the differential equations of stellar structure for the case of no motion (hydrostatic equilibrium), and constant luminosity (no energy generation). These equations are: (see, for example Cox and Giuli 1968; Clayton 1968).

Continuity of Mass

$$\frac{dM_r}{dr} = 4\pi r^2 \rho(r) \quad (4.1)$$

Hydrostatic Equilibrium

$$\frac{dP}{dr} = -\frac{GM_r}{r^2} \rho(r) \quad (4.2)$$

Radiative energy transport

$$\frac{dT}{dr} = -\frac{3\rho(r)\kappa(r)L_r}{4ac4\pi r^2 T^3} \quad (4.3)$$

Energy generation

$$\frac{dL_r}{dr} = 4\pi r^2 \rho(r) \epsilon(r) = 0 \text{ for the case of no energy generation} \quad (4.4)$$

In this case the luminosity gradient in (4.4) is set equal to zero since energy generation is ignored, because only the stellar envelope is considered (see section 3), and the

temperature will in general never reach a point where nuclear reactions can begin. In (4.3) convection is ignored because the equation used for the pulsation (section 3.1, equation [3.3]) does not include it, for reasons described there. Also ignored are the effects of rotation and magnetic fields.

So by taking three stellar parameters, L , M , and T_e (or R) and a set of boundary conditions, along with an equation of state, $P = P(\rho, T)$ an opacity for stellar material $\kappa = \kappa(\rho, T)$, and a given composition X , Y , Z (assumed to be constant) equations (4.1) - (4.4) can be solved to produce a stellar envelope in hydrostatic and thermal equilibrium.

It has already been mentioned (section 2.1) that only the stellar envelope participates in the pulsation for most stars, and so the equations only have to be solved down to a finite inner radius, $R_{inner} \sim R_*/10$. This is also why the luminosity and composition are assumed to be constant in the initial model. The equations are solved by using a numerical quadrature method to integrate from the photosphere inwards, until R_{inner} is reached. In this work $R_{inner} = R_*/12$, and a further criterion is applied, in that T_{inner} must be $\geq \sim 7 \times 10^5$ K. Insisting on a minimum value for the inner temperature ensures that the inner boundary is far away from the important driving and damping zones.

For the surface boundary condition the Eddington approximation is used to represent the atmosphere. So the photosphere, $T = T_e$, is defined at optical depth $\tau = 2/3$. The temperature distribution in the atmosphere is given by

$$T^4(\tau) = \frac{3}{4} T_e^4 (\tau + 2/3) \quad (4.5)$$

Other formulae for the temperature distribution are possible (see, for example, Bohm-Vitense 1958; Baker and Kippenhahn 1962; Gingerich 1971), and equation (4.5) can be written in the more general form (Mihalas 1978)

$$T^4(\tau) = \frac{3}{4} T_e^4 (\tau + q(\tau)) \quad (4.6)$$

where $q(\tau)$ is the Hopf function.

The Eddington approximation is used for simplicity and to agree with the treatment in section 3.

The boundary condition on pressure is chosen to approximate to $P_g = 0$, or $P_{tot} = P_r$ at the surface, i.e. at $\tau = 0$. By taking the definition of optical depth;

$$d\tau = -\kappa(r)\varrho(r)dr \quad (4.7)$$

and combining this with equations (4.1) and (4.2) we get, assuming M_r and r to be constant throughout the atmosphere,

$$\frac{dP}{d\tau} = \frac{GM}{\kappa(r)R^2} \quad (4.8)$$

So at the surface, to approximate to $P_g = 0$, we have

$$P \simeq \frac{1}{2} \left(\frac{dP}{d\tau} \right)_{\tau=\delta} + P_r(T(\delta)) \quad (4.9)$$

where $\delta \ll 1.0$. It is not possible to use $\tau = 0$, since at the surface $\varrho \rightarrow 0$, so by solving (4.9) by iteration for a small value of τ (finding $\frac{dP}{d\tau}$ from [4.8]) the "surface" ($\tau = \delta$) values of P and ϱ can be found.

Now equation (4.8) can be solved for $\delta < \tau \leq 2/3$ by numerical methods (for example a simple Runge-Kutta procedure), thus giving values of P and ϱ at $\tau = 2/3$. These values at the photosphere can be used as the starting point for the envelope integration.

To solve equations (4.1) - (4.3) for the stellar envelope it is best to change to a better set of variables than M_r , r , P and T . Before the advent of fast, digital computers it was common to use the Schwarzschild reduced variables q , x , p and t (Schwarzschild 1958), which simplified the equations. That is no longer necessary. It is still useful to use logarithmic variables, because of the wide range of these variables (as much as 15 orders of magnitude in the case of P , for example). Since the equations are not solved at the stellar centre it is not necessary to use a transformation of the r and M_r variables to avoid the singularity in their logarithms there. So we define

$$\begin{aligned}\eta &= \log r \\ \zeta &= \log P \\ \xi &= \log M \\ \theta &= \log T\end{aligned}\tag{4.10}$$

In the outer regions of the envelope r and M_r are very slow moving variables, and near the surface the temperature becomes almost constant. For integrating the envelope alone it was decided that the pressure would be a better independent variable than mass or radius. Applying the transformations (4.10) to equations (4.1) - (4.3), and using ζ as the independent variable, we find

$$\frac{d\xi}{d\zeta} = -\frac{4\pi\rho}{G} 10^{4\eta+\zeta-2\xi}\tag{4.12}$$

$$\frac{d\eta}{d\zeta} = -\frac{1}{G\rho} 10^{\eta+\zeta-\xi}\tag{4.13}$$

$$\frac{d\theta}{d\zeta} = \frac{3\kappa L}{16\pi acG} 10^{\zeta-\xi-4\theta}\tag{4.14}$$

Here common logarithms are used, since the real value of a variable is more easily estimated from them, but there is no reason why natural logarithms should not be used.

Equations (4.12) - (4.14) can be solved by, for example, Runge-Kutta integration (Ralston [1965] provides a good introduction to numerical quadrature). Fourth order Runge-Kutta integration is the method used here. For a system of differential equations,

$$y'_i = f_i(y_i, x) \quad (4.15)$$

where x is the independent variable, to integrate to the point $x_{n+1} = x_n + d$, beginning at a point x_n , we can write

$$\Delta y_{i,n} = \frac{d}{6} (k_1 + 2k_2 + 2k_3 + k_4) \quad (4.16)$$

where

$$\begin{aligned} k_1 &= f_i(y_{i,n}, x_n) \\ k_2 &= f_i(y_{i,n} + \frac{1}{2}dk_1, x_n + \frac{1}{2}d) \\ k_3 &= f_i(y_{i,n} + \frac{1}{2}dk_2, x_n + \frac{1}{2}d) \\ k_4 &= f_i(y_{i,n} + dk_3, x_n + d) \end{aligned} \quad (4.17)$$

Then

$$y_{i,n+1} = y_{i,n} + \Delta y_{i,n} \quad (4.18)$$

So for equations (4.12) - (4.14) we put $\zeta = x$, $\xi = y_1$, $\eta = y_2$ and $\theta = y_3$. Starting from the values at $\tau = 2/3$ (from the atmosphere integration), the envelope can be integrated into some desired value of R_{inner} .

We also required ~~is~~ the mass, δM_r , of each layer integrated, to be used in the division into mass zones (see section 3.7) Using the mass transformation given in (4.10), δM_r can be found from

$$\delta M_r = M_r (10^{\delta \xi} - 1) \quad (4.19)$$

where $\delta \xi$ is the change in ξ calculated from the Runge-Kutta integration step. Since $\delta M_r \ll M_r$, this section is calculated in double precision to attain sufficient accuracy.

Since the pulsation equations treat the atmosphere in the same way as the envelope, by assuming the diffusion approximation, it is necessary to integrate the static model of the atmosphere in the same way as the envelope. Having completed the envelope integration, the atmosphere is then integrated in the same way, beginning at $\tau = 2/3$ and ending at $P_{min} = P(\tau = \delta)$. It is found that this does give a surface temperature $T_\delta \approx T(\tau = \delta)$, to a good approximation. This reintegration of the atmosphere also allows r and M_r to vary, thus providing values of δM_r for $\tau < 2/3$.

This procedure provides a solution to the differential equations (4.1) - (4.3), describing the structure of a stellar envelope of homogeneous composition and constant luminosity. It should be noted that for a real stellar model only certain combinations of L , M , and T_e would give solutions, but since we are avoiding the central regions a wide range of values will provide solutions.

No particularly difficult problems are encountered in computing a model stellar envelope, so long as care is taken in the order of some calculations to avoid the occurrence of numerical underflows or overflows. It would also be a good idea to scale the mass and luminosity in the case of high mass or luminosity stars.

The envelope is covered in 1000 - 1500 steps, with about 50 in the atmosphere ($T < T_e$), to allow accurate division into mass zones.

CHAPTER 5

THE STELLAR PHYSICS

5.1 THE EQUATION OF STATE

In order to solve the equations of stellar structure it is necessary to have an equation of state representing the dependences $P = P(\rho, T)$ and $E = E(\rho, T)$, where P is the pressure of a gas/radiation mixture, E its internal energy per unit mass, ρ its density and T its temperature. The equation of state used here applies to a mixture of radiation and a non-degenerate gas consisting of hydrogen, helium and two metals. The Saha equations are solved simultaneously at every call for all the elements considered. Since the temperatures in the envelopes of the stars to be considered will probably not reach 10^6 degrees it was thought pointless to assume complete ionization for high temperatures. Similarly, these envelopes will never reach degenerate conditions, so degeneracy is ignored. However, radiation pressure can be very important, and is included. The partition functions of the various ionic configurations are considered to be constant, rather than including their variation with pressure and temperature. Trial runs on static models including varying partition functions showed the effect of their variation to be negligible.

One negative ion (H^-) is considered, since its effect in the low temperature atmospheres of these stars might be significant, as it soaks up some electrons. For the metals, some of the higher ionization states were completely ignored, on the justification that the temperature would never be high enough to remove the electrons. The two metals considered were nitrogen, representing the abundant group of elements carbon, nitrogen, oxygen, neon; and magnesium, representing the group of elements such as silicon and aluminium which have low first ionization energies, and thus act as electron donors in stellar atmospheres. The ratio (by mass) of these two metals was taken as nitrogen:magnesium = 4:1.

Molecules have not been included, and this might be an improvement for future work, since they may have some effect in the cooler stars modelled.

The total pressure, P , can be written as,

$$P = P_i + P_e + P_r \quad (5.1)$$

where P_r is the radiation pressure, given by,

$$P_r = \frac{aT^4}{3}$$

a is the radiation energy density constant.

$P_e = N_e kT$ is the electron pressure. N_e is the electron number density

$P_i = N_n kT$ is the ion pressure. N_n is the number density of nuclei

k is Boltzmann's constant

$N = N_n + N_e$ is the total number density of all particles

Usually the temperature of the gas will be known, along with either the density ρ , or the pressure P , and so either N or N_n must be found in order to calculate the third quantity. Either way N_e , the electron density, has to be calculated. The electron density is given by,

$$N_e = N_n \sum_k \alpha_k \sum_j j f_{jk} (N_e, T) \quad (5.2)$$

where α_k is the fraction by number of element k , f_{jk} is the fraction of element k in ionization state j (where $j = 0$ is the ground state), and a summation written without explicit limits means "sum over all values". Equation (5.2) is a non-linear equation in N_e which can be solved exactly in some simple cases (pure hydrogen, hydrogen plus one metal ion), but in general needs to be solved by some sort of iteration.

The α_k can be found from the fractions by mass, β_k , which are given as input (the usual X , Y , Z represent mass fractions for hydrogen, helium, and metals), and the atomic masses, A_k .

$$\alpha_k = \frac{\mu_n \beta_k}{A_k}$$

where

$$\mu_n = 1 / \sum_k \frac{\beta_k}{A_k}$$

The quantity N_n may or may not be known, depending on whether the pressure or density is known. If P is known then

$$N_n = N - N_e, \text{ and } P = P_g / kT$$

where $P_g = P_i + P_e$ is the gas pressure.

If the density is known then

$$N_n = N_0 e^{-\mu_n}$$

where N_0 is Avogadro's number.

So N_n is also known.

The f_{jk} are given by (number density of element k in state j) / (number density of element k) = N_{jk}/N_k

$$f_{jk} = \frac{(N_{j-1,k}/N_{j,k})(N_{j-2,k}/N_{j-1,k}) \dots (N_{j,k}/N_{j+1,k})}{1 + (N_{j-1,k}/N_{j,k}) + (N_{j-2,k}/N_{j,k})(N_{j-1,k}/N_{j,k}) + \dots + (N_{j-1,k}/N_{j,k}) \dots (N_{j,k}/N_{j+1,k})}$$

or

$$f_{jk} = \frac{\prod_{\ell=j}^{J_k-1} N_e \Phi_{\ell k}(T)}{\sum_{m=0}^{J_k} \prod_{\ell=m}^{J_k-1} N_e \Phi_{\ell k}(T)} \quad (5.3)$$

J_k is the maximum ionization state of element k.

$\Phi_{\ell k}(T) = N_{\ell k} / (N_{\ell+1,k} N_e)$ is given by Saha's equation;

$$\Phi_{\ell k}(T) = \frac{U_{\ell k}}{U_{\ell+1,k}} \frac{1}{2} \left(\frac{h^2}{2\pi m k} \right)^{3/2} T^{-3/2} e^{(\chi_{\ell k}/KT)} \quad (5.4)$$

$U_{\ell k}$ are the partition functions

$\chi_{\ell k}$ is the ionization energy ($l \rightarrow l+1$) of ionization state l

h is the Planck constant

m is the electron mass

So equation (5.2) is solved by direct substitution iteration, calculating N_e^{i+1} from N_e^i and substituting it directly into (5.2), until convergence is reached. Use of the geometric mean of the i and (i+1) values of N_e provides surer but slower convergence.

Newton-Raphson iteration could be used to solve (5.2), but since it depends on $\delta N_e^i / N_e^i$ being small it was not used since for a fast convergence the initial value of N_e must be a fairly good approximation. The method used here is more flexible and usually converges in 2 or 3 iterations (to five figures).

Having found N_e and the f_{jk} , then μ , the mean molecular weight can be found from

$$\mu = \frac{1}{\sum_k \frac{\bar{n}_k}{\beta_k}}$$

where $\bar{n}_k = 1/A_k(1 + \nu_e(k))$ is the number density per unit mass of particles and electron for element k and $\nu_e(k) = \sum_j j f_{jk}$ is the number of electrons provided by each state.

The major numerical problems encountered in the equation of state are caused by having very large or very small numbers for the values of some of the ratios. On the machines used the limits are $10^{\pm 38}$, and the products found in equation (5.4) would quickly underflow or overflow. To circumvent this problem logarithms are used in calculating the numerators (i.e. finding sums instead of products). Then the numerators are normalized, so that for each element the largest value of $\log(\prod_{l=1}^{J_k-1} N_e \Phi_{lk})$ is 1.0. Then to speed calculations, values below -10.0 are ignored. Antilogarithms are taken to find the scaled numerators. Since the denominators are sums of the numerators this is in fact a renormalization process, the scaling factor is divided out.

The internal energy per unit mass is found from the following equation (Cox and Giuli 1968, page 334).

$$E = N_n(1 + \bar{f}) \frac{3kT}{2} + \frac{M_0}{e} \sum_k \alpha_k \sum_{j=1}^{J_k} f_{jk} \sum_{m=1}^J \chi_{m-1,k} + \frac{aT^4}{e} \quad (5.5)$$

The first term is the thermal (kinetic) energy, where

$$\bar{f} = \sum_k \alpha_k \sum_j j f_{jk}$$

The third term is the energy density of the radiation field.

The second term is the summed contribution of the various

ionization states. For just positive ions this has the form given in (5.5); however, if negative ions are present they must be included separately;

$$E_{ion} = \sum_K \alpha_K \left(\sum_{d=1}^{J_K} f_{dk} \sum_{m=1}^d \chi_{m-k} - \sum_{d=-q}^{-1} f_{dk} \sum_{m=-q}^d \chi_{mk} \right)$$

where $-q$ is the most negatively charged ionized state. E_{ion} thus has its zero point at the ground state of the neutral atom.

Two other quantities are required from the equation of state; these are the gradients $(\partial P / \partial T)_e$ and $(\partial E / \partial T)_e$. From (5.1) P can be expressed as

$$P = \frac{N_0 k e T}{A n} + N_e k T + \frac{a T^4}{3}$$

then

$$\left(\frac{\partial P}{\partial T} \right)_e = P_2 / T + \left(\frac{\partial N_e}{\partial T} \right)_e k T + \frac{4 P_r}{P} \quad (5.6)$$

and from (5.5)

$$\left(\frac{\partial E}{\partial T} \right)_e = \frac{N_n (1 + \bar{f})}{e} \frac{3k}{2} + \frac{3k T N_n}{2e} \left(\frac{\partial \bar{f}}{\partial T} \right)_e + \frac{N_n}{e} \sum_K \alpha_K \sum_d \left(\frac{\partial f_{dk}}{\partial T} \right)_e \sum_{m=1}^d \chi_{m-k} + \frac{4a T^3}{e} \quad (5.7)$$

where

$$\left(\frac{\partial \bar{f}}{\partial T} \right)_e = \sum_K \alpha_K \sum_d j \left(\frac{\partial f_{dk}}{\partial T} \right)_e$$

$$\left(\frac{\partial f_{dk}}{\partial T} \right)_e = \frac{1}{N_e} \left(\frac{\partial N_e}{\partial T} \right)_e (f_{dk} (J_K - j) - f_{jk} \sum_d f_{dk} (J_K - j)) + f_{dk} \left(\left(\frac{\partial \ln \Pi_{dk}}{\partial T} \right)_e - \sum_d \left(\frac{\partial \ln \Pi_{dk}}{\partial T} \right)_e f_{dk} \right) \quad (5.8)$$

$$\left(\frac{\partial \ln \Pi_{dk}}{\partial T} \right)_e = - \frac{1}{k T^2} \sum_{l=j}^{J_K-1} \left(\frac{3}{2} k T + \chi_{lk} \right)$$

So to find both $(\partial P / \partial T)_e$ and $(\partial E / \partial T)_e$, the gradient $(\partial N_e / \partial T)_e$ is required. From (5.2)

$$\left(\frac{\partial N_e}{\partial T} \right)_e = N_n \sum_K \alpha_K \sum_d j \left(\frac{\partial f_{dk}}{\partial T} \right)_e \quad (5.9)$$

Then, from (5.8)

$$\sum_j j \left(\frac{\partial f_{jk}}{\partial T} \right)_e = \frac{1}{N_e} \left(\frac{\partial N_e}{\partial T} \right)_e \sum_k + \sum_k \tilde{\Sigma}_k$$

where

$$\begin{aligned} \Sigma_k &= \sum_j j f_{jk} (J_k - j - \sum_j f_{jk} (J_k - j)) \\ \tilde{\Sigma}_k &= \sum_j j f_{jk} \left(\left(\frac{\partial \ln T_{jk}}{\partial T} \right)_e - \sum_j f_{jk} \left(\frac{\partial \ln T_{jk}}{\partial T} \right)_e \right) \end{aligned}$$

then substituting into (5.9), and solving for $(\partial N_e / \partial T)_e$, gives

$$\left(\frac{\partial N_e}{\partial T} \right)_e = \frac{N_n \sum_k \alpha_k \tilde{\Sigma}_k}{(1 - N_n / N_e \sum_k \alpha_k \Sigma_k)} \quad (5.10)$$

Using (5.10) the required gradients can be found from (5.6) and (5.7). Analytic expressions are used for $(\partial P / \partial T)_e$ and $(\partial E / \partial T)_e$ since it seems likely that computing them will be quicker than using any numerical method, which would involve at least one further call to the equation of state.

The routine as used accepts X , Y , Z , the A_k 's, χ_{jk} 's and J_k 's as original input data. Then in a call to subroutine STATE T is required as input, along with either P or ρ . The major output is ρ or P , along with E , $(\partial P / \partial T)_e$ and $(\partial E / \partial T)_e$ if desired.

It should be noted that a routine is also available to carry out interpolation in tables to provide values of P , E and their gradients. This routine is not as accurate as using an on-line version, but is considerably faster, and was used for some test runs, also for checking such things as the possible stability or instability of a particular star. The tables used are constructed in a format similar to that of the Carson

opacity tables, but with more points. This allows the same interpolation routines to be used for all tables.

Some references that were generally useful here are Clayton (1968, Chapter 2), Cox and Giuli (1968, Chapters 9, 15) and Mihalas (1978, Chapter 5).

5.2 THE OPACITY

5.2.1 The Carson Opacities And Their Use

Until fairly recently most theoretical work on stellar pulsation has used the Cox-Stewart (1965) opacities, or some later modification of them, or an interpolation formula fitted to them. These opacities (also referred to as the Los Alamos opacities) are based on the early work of Stromgren (1932) and Keller and Meyerott (1955). The methods used are described mainly in the review by Cox (1965). These opacities use as an atomic model the "hydrogenic" approximation, treating the atom as having a hydrogen-like coulomb field, due to an effective nuclear charge, and dealing with perturbations from this field. Carson et al. have questioned the validity of this approximation. Carson and Hollingsworth (1968) used numerically exact methods on one electron model to check the hydrogenic approximation. They found that only if care is taken in the choice of the effective nuclear charges is the approximation a good one.

In 1968 Carson, Mayers and Stibbs applied non-hydrogenic methods to the problem, using the generalized (non-zero temperature or "hot") Thomas-Fermi model for the atom. The few results obtained showed that the Cox-Stewart values for the opacity could be increased by a factor of two or three using the new methods.

Carson (1976) went on to calculate a full series of stellar opacities. His methods involved a mixture of earlier procedures, plus several improvements. In the atomic opacities hydrogen and helium are treated "exactly", whilst for the heavier elements the generalized Thomas-Fermi statistical model is used. At the lower temperatures negative ions are included along with a few diatomic molecules. Conduction was treated using the code of Hubbard and Lampe (1968).

The main agreement between these new opacities and those of Cox and Stewart is quite good. However, there are differences of detail. The main H-He I peak shows an opacity that is up to two times lower, whilst beyond $\log T \sim 4.5$ the opacity is generally higher than the Cox-Stewart values. At $5.4 < \log T < 6.4$ there is a double bump feature not present in earlier work. These peaks are due to the final ionization of carbon and oxygen, with contributions from nitrogen. At higher values of $\log T$ the opacity reaches the normal scattering limit.

The Carson opacities are the ones used in this work. Opacity tables exist for a number of compositions, but only one is close to that of population II stars. This is for composition $X = 0.745$, $Y = 0.25$, $Z = 0.005$. The population II variables considered in this work have compositions of

$0.2 < Y < 0.3$ and $10^{-4} < Z < 10^{-2}$, so the composition used is not unreasonable. It seems that $Y = 0.25$ is an accepted value, while $Z = 0.001$ is a more usually accepted metallicity. Since no table was available for $Z = 0.001$, and as it was thought that interpolating between tables to produce one would introduce unwanted errors, the 0.005 value for Z was used.

Each table gives $\log \kappa$ for 38 values of $\log T$, with 9 or 10 values of $\log \rho$ for each temperature. The table for the population II mix is given in table 5.1. The opacity for this mixture is plotted in figure 5.1. Figure 5.2 shows the Cox-Stewart opacity for this mixture, computed from the Christy interpolation formula (1966). These two figures show the general differences in the opacity noted above. Also figure 5.1 shows that for low temperatures, $\log T \leq 3.8$, the Carson opacity almost stops decreasing as $\log T$ decreases, leveling off to a plateau, leaving the Carson opacity up to 4 or 5 orders of magnitude greater than the Cox-Stewart values. This has been interpreted as an error in the program or the use of it at these temperatures. The effect of this plateau is demonstrated in the test run on model 1 from CSV (see section 6.2). Consequently for $\log T < 3.85$ the Carson opacities are replaced by the Cox-Stewart ones, again in the Christy formulation. This also fits in with the work of Carson, Stothers and Vemury in various papers (Carson and Stothers 1976; Vemury and Stothers 1978; Carson, Stothers and Vemury 1981; Carson and Stothers 1982), who used the Christy opacity for $\log T < 3.85$, since at that time the Carson opacity values were not available for these lower temperatures. This mixed opacity is plotted in figure 5.3.

Opacity c74525 for composition : H=0.745, He=0.250, Z=0.005

| | | Log Opacity (cms ² /gm) | | | | | | | | |
|---------|-----|------------------------------------|---------|---------|---------|---------|---------|---------|---------|---------|
| Log Rho | | I | I+1 | I+2 | I+3 | I+4 | I+5 | I+6 | I+7 | I+8 |
| Log T | I | | | | | | | | | |
| 3.3 | -12 | -2.1626 | -2.2670 | -2.5636 | -2.9857 | -3.4170 | -3.4402 | -2.6316 | -1.6536 | -0.6564 |
| 3.4 | -12 | -2.1252 | -2.1246 | -2.1302 | -2.1796 | -2.3659 | -2.5405 | -2.1742 | -1.2419 | -0.1702 |
| 3.5 | -12 | -2.0992 | -2.0970 | -2.0916 | -2.0702 | -1.9928 | -1.8407 | -1.6063 | -0.8979 | 0.1293 |
| 3.6 | -11 | -2.0633 | -2.0566 | -2.0207 | -1.8626 | -1.4676 | -0.8303 | -0.1833 | 1.0931 | 1.3760 |
| 3.7 | -11 | -1.9779 | -1.9705 | -1.9013 | -1.7007 | -1.2560 | -0.5382 | 0.2443 | 2.3289 | 1.6082 |
| 3.8 | -11 | -1.3903 | -1.4450 | -1.2386 | -0.8230 | -0.3139 | 0.2392 | 0.8537 | 4.1703 | 2.0458 |
| 3.9 | -11 | -0.2225 | -0.1245 | 0.0269 | 0.2715 | 0.6000 | 1.1787 | 1.4831 | 2.0504 | 2.7664 |
| 4.0 | -11 | -0.1104 | 0.5225 | 1.1324 | 1.4191 | 1.6507 | 1.9257 | 2.2925 | 2.7358 | 3.3808 |
| 4.1 | -10 | 0.2267 | 1.1307 | 1.9500 | 2.4716 | 2.7803 | 3.0655 | 3.3787 | 3.9152 | 4.6178 |
| 4.2 | -10 | -0.0546 | 0.6911 | 1.6666 | 2.6372 | 3.3011 | 3.7073 | 3.9833 | 4.4218 | 3.4081 |
| 4.3 | -10 | -0.2298 | 0.3405 | 1.2726 | 2.3148 | 3.3148 | 4.1228 | 4.4683 | 4.8190 | 4.7931 |
| 4.4 | -10 | -0.2831 | 0.1263 | 0.9868 | 2.0444 | 3.1576 | 4.2636 | 4.9070 | 5.2222 | 5.0725 |
| 4.5 | -10 | -0.2294 | 0.0762 | 0.8292 | 1.8628 | 2.9966 | 4.1983 | 5.0334 | 5.3458 | 3.2087 |
| 4.6 | -9 | 0.1447 | 0.8299 | 1.7775 | 2.8392 | 3.9969 | 4.8806 | 5.4537 | 4.0504 | 5.6462 |
| 4.7 | -9 | -0.1331 | 0.7417 | 1.7168 | 2.6845 | 3.6669 | 4.5248 | 5.2311 | 4.6848 | 5.4636 |
| 4.8 | -9 | -0.2661 | 0.4521 | 1.1932 | 2.3241 | 3.2684 | 4.1628 | 4.8975 | 4.8619 | 5.2617 |
| 4.9 | -9 | -0.2356 | 0.1163 | 0.7641 | 1.8489 | 2.8130 | 3.8401 | 4.6103 | 4.8340 | 5.0676 |
| 5.0 | -9 | -0.3476 | -0.0991 | 0.5454 | 1.4797 | 2.4406 | 3.5172 | 4.3616 | 4.6592 | 4.8236 |
| 5.2 | -8 | -0.3505 | 0.0271 | 0.8073 | 1.6532 | 2.5486 | 3.5360 | 3.9812 | 4.0308 | 4.8078 |
| 5.4 | -8 | -0.2573 | -0.2081 | 0.0439 | 0.7513 | 1.5434 | 2.1922 | 2.9820 | 3.4460 | 3.8233 |
| 5.6 | -7 | 0.1734 | 0.1758 | 0.2105 | 0.7665 | 1.3160 | 2.0927 | 2.6762 | 3.3937 | 3.0072 |
| 5.8 | -7 | 0.3255 | 0.0443 | 0.0350 | 0.2994 | 0.7030 | 1.4115 | 1.9127 | 2.4752 | 2.9270 |
| 6.0 | -7 | -0.0223 | -0.0901 | -0.0387 | 0.0066 | 0.1053 | 0.7910 | 1.4902 | 2.0704 | 2.6780 |
| 6.2 | -6 | -0.2787 | -0.2690 | -0.2866 | 0.3108 | 0.1913 | 0.9931 | 1.5150 | 2.0422 | 2.3473 |
| 6.4 | -6 | -0.4189 | -0.4214 | -0.3855 | -0.0788 | -0.2093 | 0.3724 | 0.8439 | 1.1771 | 1.8913 |
| 6.6 | -5 | -0.4534 | -0.4509 | -0.4457 | -0.3908 | -0.1809 | 0.2603 | 0.6239 | 1.3040 | 1.2296 |
| 6.8 | -5 | -0.4624 | -0.4618 | -0.4610 | -0.4526 | -0.3944 | -0.1513 | 0.1200 | 0.6880 | 1.2531 |
| 7.0 | -5 | -0.4655 | -0.4650 | -0.4646 | -0.4643 | -0.4513 | -0.3720 | -0.1924 | 0.1764 | 0.8115 |
| 7.2 | -4 | -0.4701 | -0.4699 | -0.4692 | -0.4635 | -0.4420 | -0.3443 | -0.1038 | 0.3853 | 0.5232 |
| 7.4 | -4 | -0.4764 | -0.4764 | -0.4763 | -0.4761 | -0.4714 | -0.4390 | -0.3459 | -0.0799 | 0.2475 |
| 7.6 | -3 | -0.4859 | -0.4859 | -0.4860 | -0.4852 | -0.4793 | -0.4483 | -0.3271 | -0.0732 | -0.4518 |
| 7.8 | -3 | -0.5001 | -0.5001 | -0.5001 | -0.5001 | -0.4995 | -0.4930 | -0.4522 | -0.3304 | -0.3680 |
| 8.0 | -3 | -0.5210 | -0.5210 | -0.5210 | -0.5210 | -0.5211 | -0.5205 | -0.5114 | -0.4668 | -0.4720 |
| 8.2 | -2 | -0.5507 | -0.5507 | -0.5507 | -0.5508 | -0.5509 | -0.5499 | -0.5396 | -0.5484 | -1.0487 |
| 8.4 | -2 | -0.5911 | -0.5911 | -0.5911 | -0.5911 | -0.5913 | -0.5919 | -0.5925 | -0.6302 | -0.9487 |
| 8.6 | -1 | -0.6430 | -0.6430 | -0.6430 | -0.6431 | -0.6435 | -0.6455 | -0.6670 | -0.8586 | -0.7129 |
| 8.8 | -1 | -0.7064 | -0.7064 | -0.7064 | -0.7064 | -0.7066 | -0.7078 | -0.7179 | -0.9582 | -0.7927 |
| 9.0 | -1 | -0.7805 | -0.7805 | -0.7805 | -0.7805 | -0.7805 | -0.7811 | -0.7872 | -0.8944 | -0.8244 |

Table 5.1 Carson opacity for X=0.745, Y=0.25.

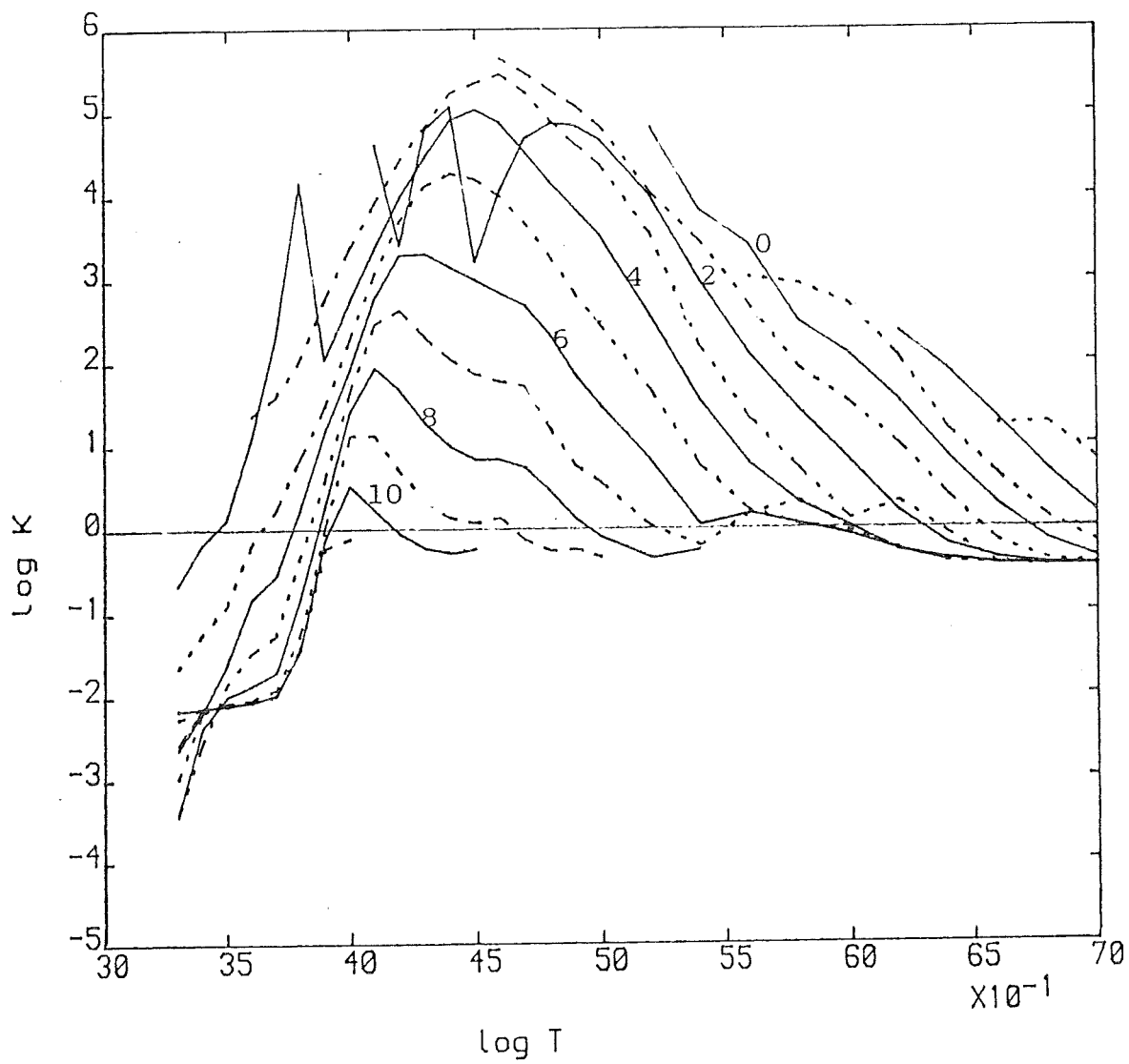


Figure 5.1 Carson opacity for $X=0.745$, $Y=0.25$.
Numbers on alternate curves show the values
of $\log(1/e)$

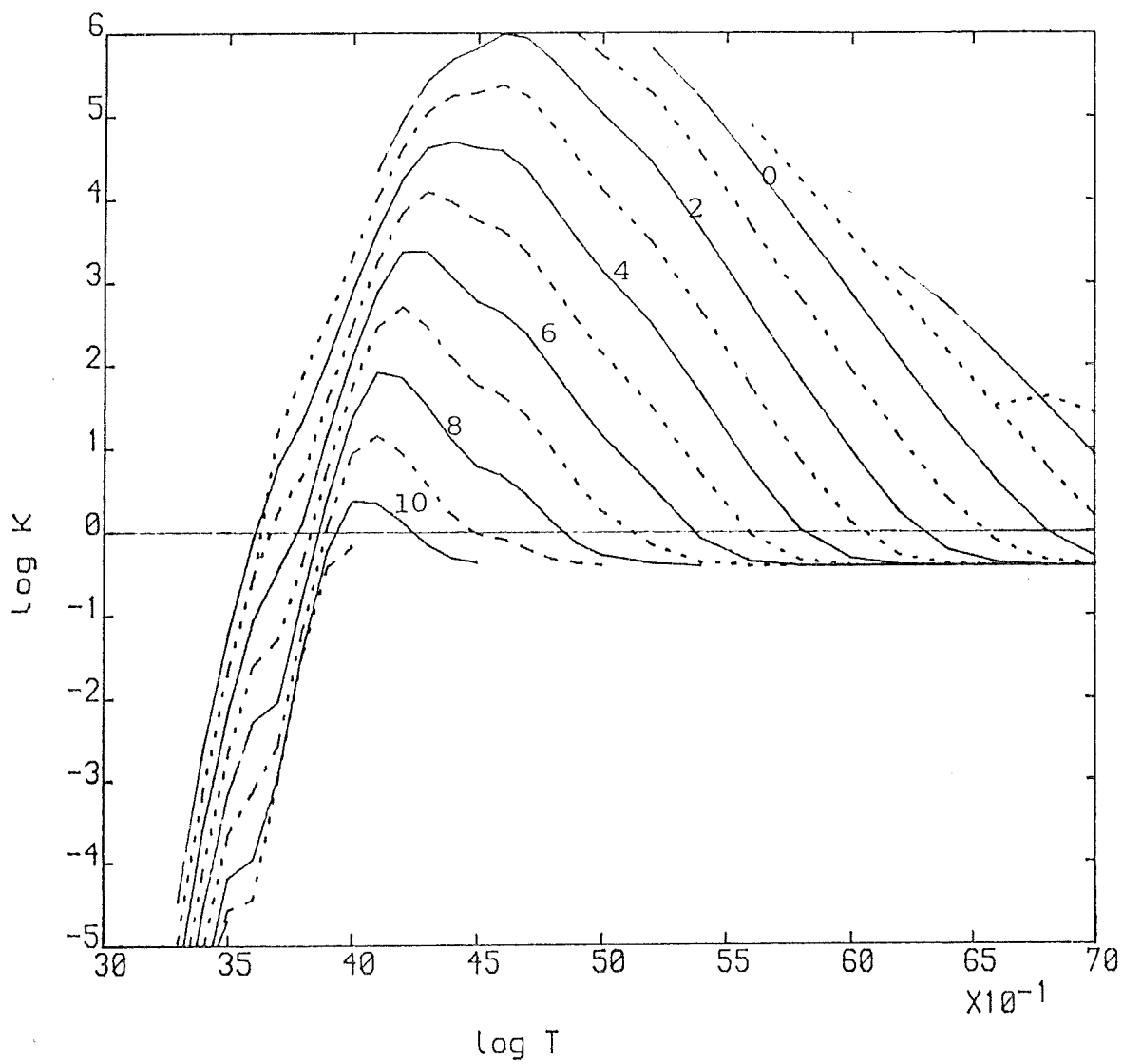


Figure 5.2 The Cox-Stewart opacity for $X=0.745$, $Y=0.25$, from the Christy formula

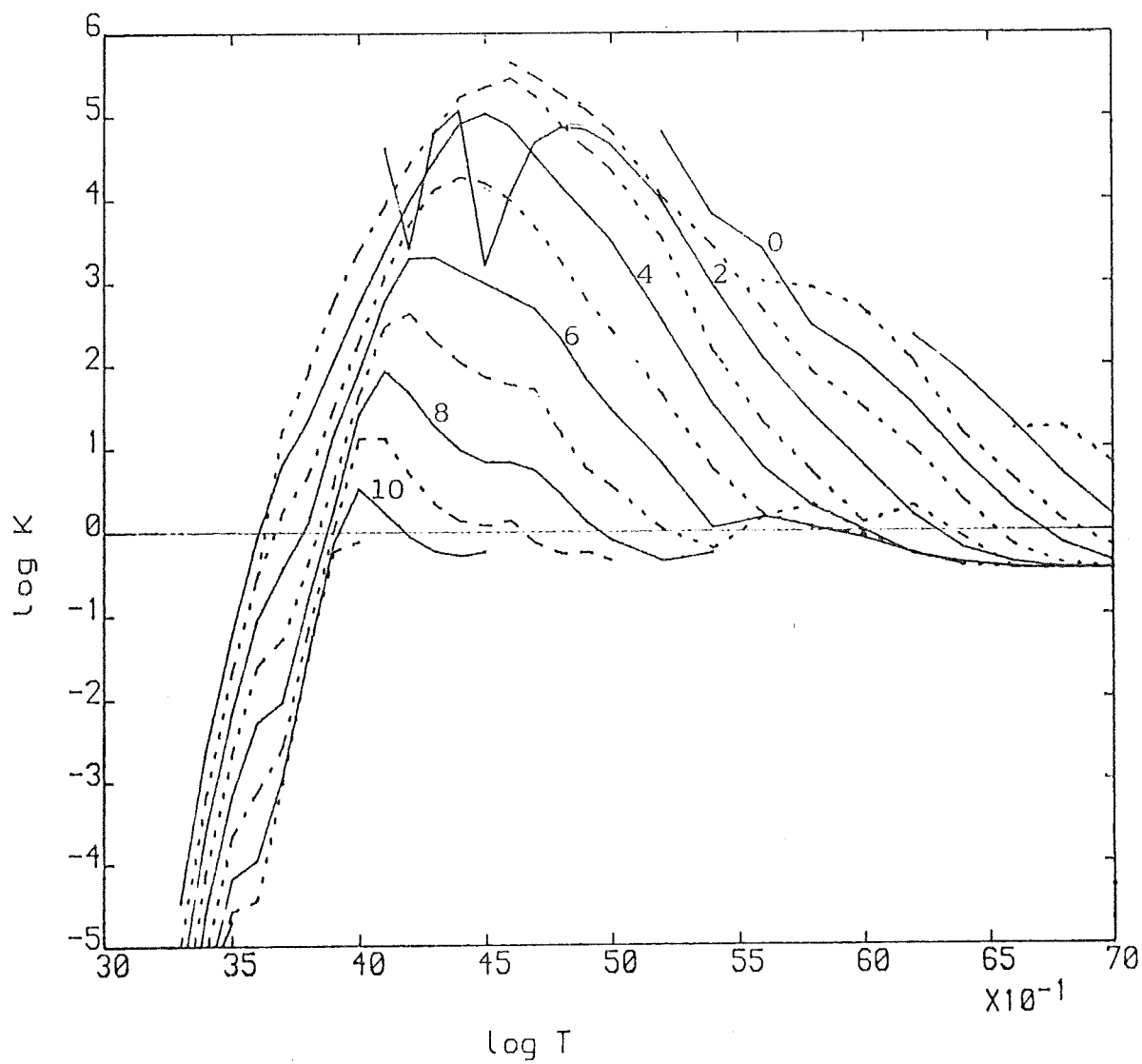


Figure 5.3 The combined Carson/Christy opacity for $X=0.745$, $Y=0.25$. Uses Christy formula for $\log T < 3.85$

This work uses linear or quadratic interpolation of the opacity tables, linear interpolation usually being preferred because simple quadratic interpolation can produce unreliable values of $(\partial\kappa/\partial T)_\rho$, which is also calculated numerically. However some test runs showed little difference between the results using the two forms of interpolation.

5.2.2 The Effect Of The Opacity

The Carson opacities have been used recently by Carson, Stothers and Vemury in several studies of stellar structure, evolution and pulsation.

Stothers (1974a) compared the Carson and Cox-Stewart opacities in a series of homogeneous stellar models in the mass range $1 \leq M/M_\odot \leq 120$. He found few differences in the models, except that the larger mass stars had slightly larger radii, and therefore lower effective temperatures, using the Carson opacities. The Carson opacities have also been used to reduce the discrepancy between theory and observation for the apsidal motion constant of binary systems (Stothers 1974b).

Carson and Stothers (1976) examined the effect of the new opacities on the evolution of giants and on classical cepheid pulsation. They found very little change in the evolutionary tracks for stars with masses $5 M_\odot$ and $7 M_\odot$. The theoretical mass-luminosity relation was changed by a small amount, and the inferred "evolutionary" masses for cepheids were increased only slightly. The theoretical blue edge for the cepheid instability strip was moved bluewards with the new opacities, in better agreement with the observations. The theoretical

"pulsational" masses were only increased by a small amount, thus failing to remove the discrepancy between pulsational and evolutionary masses. This discrepancy now seems to have been removed by a redetermination of the cepheid distance scale (for a review of the cepheid mass problem see A.N.Cox 1979, 1980). Vemury and Stothers (1977, 1978) extended the work on cepheids using the new opacities by studying the so-called "bump" cepheids. It had been found that to correctly reproduce this feature, the mass of the star had to be only about one-half the mass expected from evolutionary theory. The use of the Carson opacities seems to remove most of this discrepancy.

Stothers (1976) has also found that in hot massive stars the CNO opacity bump, present only in the Carson opacities, can act as a source of pulsational instability.

Recently Carson, Stothers and Vemury (1981) and Carson and Stothers (1982) have used the Carson opacities in modelling the BL Herculis variables (type II cepheids, with periods from 1 - 3 days). This work, along with that of A.N.Cox et al. in several papers, is reviewed elsewhere (section 2.3). Briefly, the Carson opacities seem to produce results in more general agreement with those observed, in particular for the shape of the light and velocity ~~light~~ curves. However, the higher opacity near the He II driving zone may give light and velocity amplitudes considerably larger than those observed.

CHAPTER 6

RESULTS

6.1 THE RED EDGE OF THE INSTABILITY STRIP

Before presenting the non-linear pulsation results, it may be instructive to look at the amount of convection in these stars. Convection is not included in the pulsation equations, and is therefore also ignored in the static model calculations. However, a routine to construct static model envelopes including the effects of convection was available, courtesy of C.S. Jeffery. Local Mixing Length theory (Bohm-Vitense 1958) is used, including the more recent modifications to this theory. A mixing length/pressure scale height ratio of 1.0 was used. The results presented are for models with $M/M_{\odot} = 0.6$ and using the Carson population II opacity, composition $X = 0.745$, $Y = 0.25$, $Z = 0.005$. In the envelopes, the amount of convection in the hydrogen and helium II ionization zones was looked at. In figure 6.1 is plotted the observed instability strip of Demers and Harris, along with the Worrell blue edge for $M/M_{\odot} = 0.6$, and the above composition. Line a represents the region where convection carries approximately 50% of the flux in the hydrogen ionization zone. This can be compared with line b, which represents the same amount of convection,

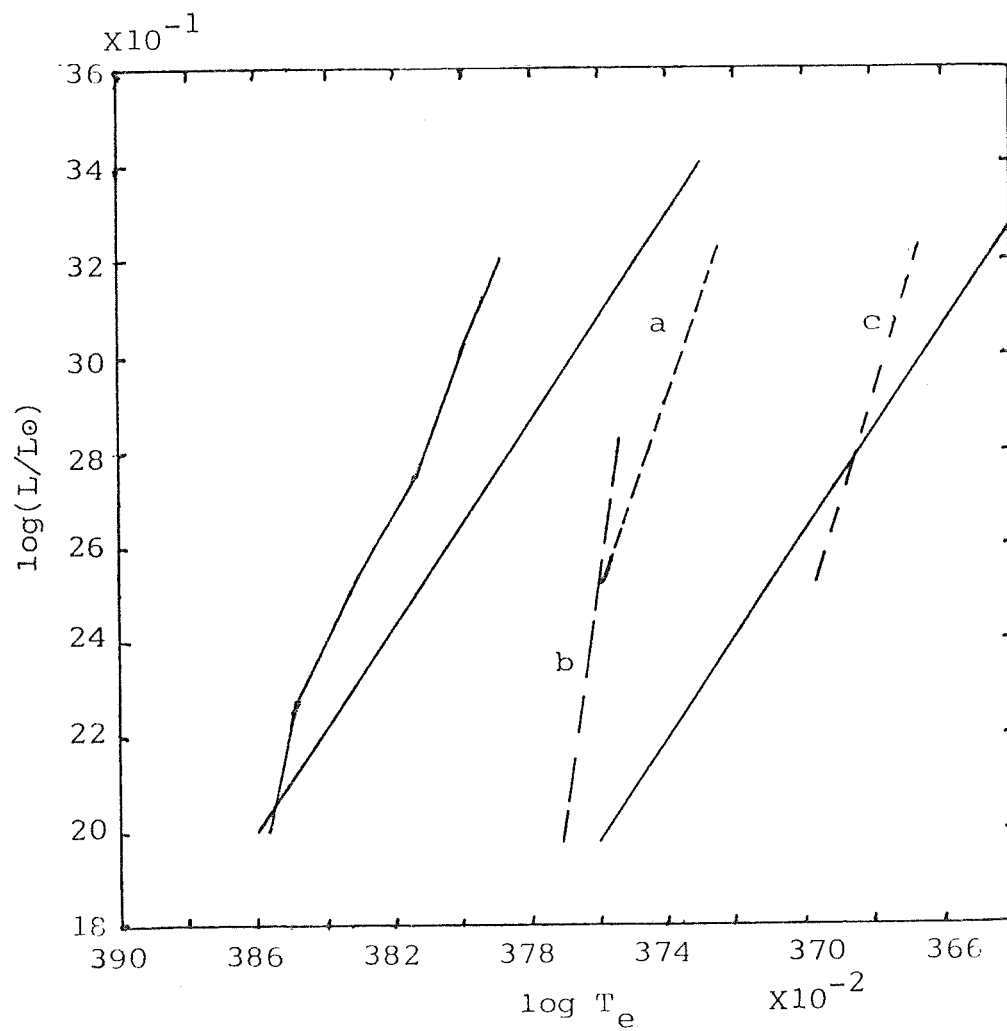


Figure 6.1 Possible red edges for the Instability Strip

but comes from King, Cox and Hodson (1981) and uses the Cox opacities, being their estimated red edge. The two are close enough to suggest that the only main difference is the use of different opacities. Neither line is close to the observed red edge. However, for these stars, even when convection accounts for half the flux in the hydrogen ionization zone, the amount in the helium II ionization zone is still negligible. This is because of the high L/M ratio of these stars. Deupree (1977a) concludes that if convection carries just a few percent of the flux in the helium II convection zone, it will quench the pulsation. Line c represents the region in which convection has this approximate level of significance for the envelopes calculated using the Carson opacity. Line c is very much closer to the observed red edge, and can be regarded as an estimated red edge for this work. For this line the convection in the hydrogen zone is 90-100%.

From these results we can see that convection plays little part in the pulsation near the blue edge, and is probably responsible for the red edge by suppressing the helium II driving zone. Also, from the middle of the instability strip to the red edge, convection in the hydrogen ionization zone is very significant, and is probably diminishing or suppressing any hydrogen driving. This may play a part in determining the amplitudes of these stars, and may even alter their light curves. Deupree (1977a), however, suggests that the shape of light curves is not altered greatly by convection. So whilst ignoring convection in the pulsational models, it must be remembered that it could be very significant for the redder models.

6.2 THE TEST MODEL

To test the independently written programs described in sections 3-5, model 1 of Carson, Stothers and Vemury (1981) was repeated. Hereafter the original model is referred to as CSV1. This model is characterized by the following parameters:

$$M/M_{\odot} = 0.6$$

$$\log(L/L_{\odot}) = 2.0$$

$$\log T_e = 3.81$$

$$\text{Composition (X,Y,Z)} = (0.745, 0.250, 0.005)$$

Following CSV, the "surface" of the star is taken to be the zone having optical depth closest to 0.2 in the equilibrium model. This is taken to be roughly comparable to the observed surface of a real star. The following quantities are also defined:

| | |
|--------------------|---|
| Peak K.E. | Peak kinetic energy of the pulsation |
| $\Delta R/R$ | Full radius amplitude/equilibrium radius |
| V_{out}, V_{in} | Maximum outward (positive) and inward (negative) surface velocities |
| ΔV | Full surface velocity amplitude |
| L_{max}, L_{min} | Maximum and minimum surface luminosities |
| ΔM_{bol} | Full amplitude of bolometric magnitude variation ($= 2.5 \log L_{max}/L_{min}$). |
| | (Note: Since L_{max} and L_{min} are sometimes subject to computer generated noise or spikes, it is usually better to measure this from the surface light curve). |

Asymmetry (vel. Asymmetry of the light or velocity curve.

$$\text{or lum.)} = (\text{Time to go from maximum to minimum}) /$$
$$(\text{Time to go from minimum to maximum})$$

ϕ_b^v

Phase of the secondary bump on the velocity curve after the phase of zero velocity on the ascending branch, plus unity.

 ϕ_b^l

Phase of the secondary bump on the light curve after the phase of mean light on the ascending branch, plus unity.

Firstly the model was constructed using the full Carson opacity at all temperatures, taken from table 5.1. Though the period obtained was approximately correct, the result was obviously in disagreement with CSV1, as is demonstrated by the curves plotted in figure 6.2. A large pre-maximum shock or bump is present in the light curve, essentially a much larger version of the smaller pre-maximum shock present in CSV's light curve. This problem was found to be caused by the opacity. The only feature of the input different from that used by CSV was that the Carson opacity was used for the lower temperatures. So the model was repeated, now following CSV precisely, the Christy formulation of the Cox opacities used for $\log T < 3.85$. The results for this are presented in table 6.1 (compared with CSV1) and figure 6.3. These results show very good agreement with CSV1, validating the program, confirming CSV's results, and also indicating that the Carson opacities are probably incorrect at low temperatures. The test run was repeated once more (after some minor program improvements, and after transferring the code to another computer), and the same result was obtained (to within reasonable limits).

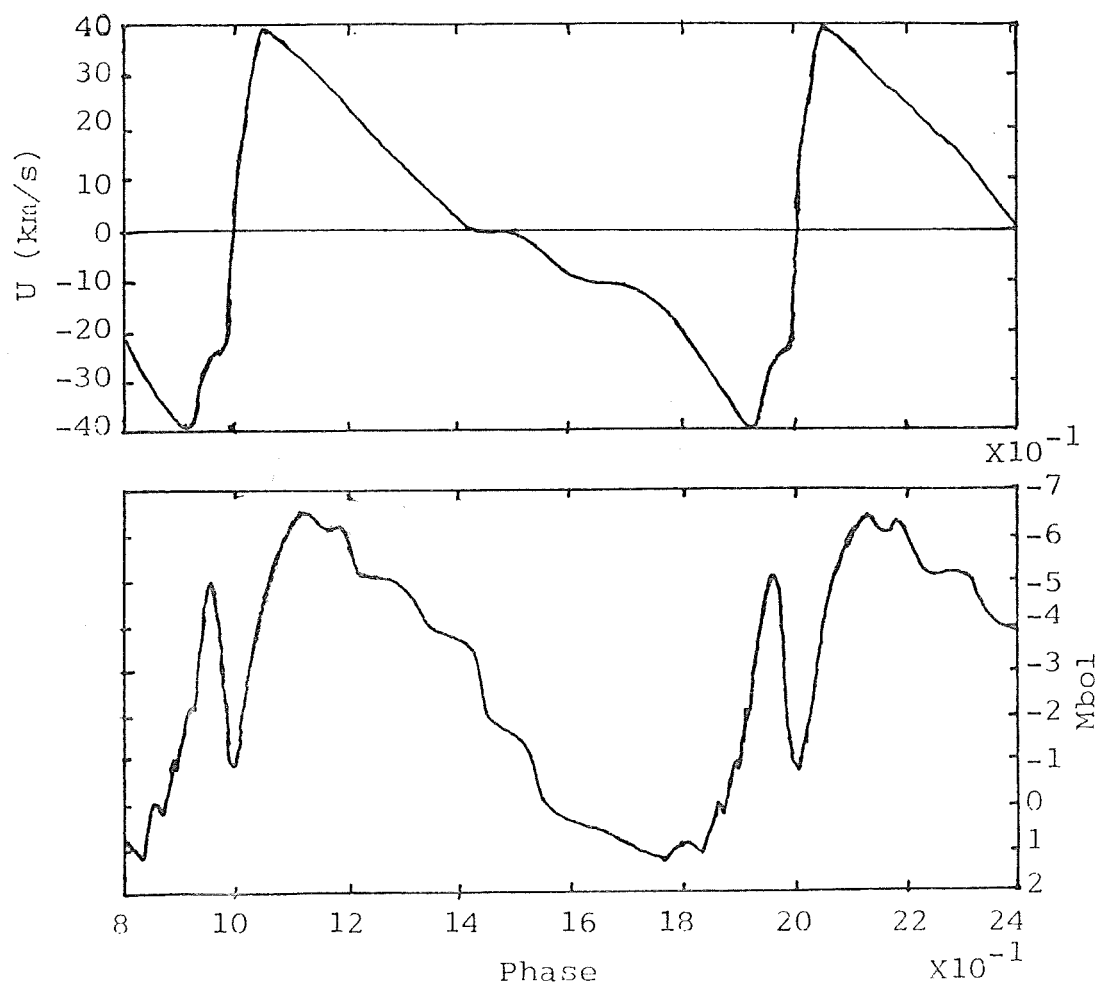


Figure 6.2 First attempt at CSV model 1. Light and velocity curves

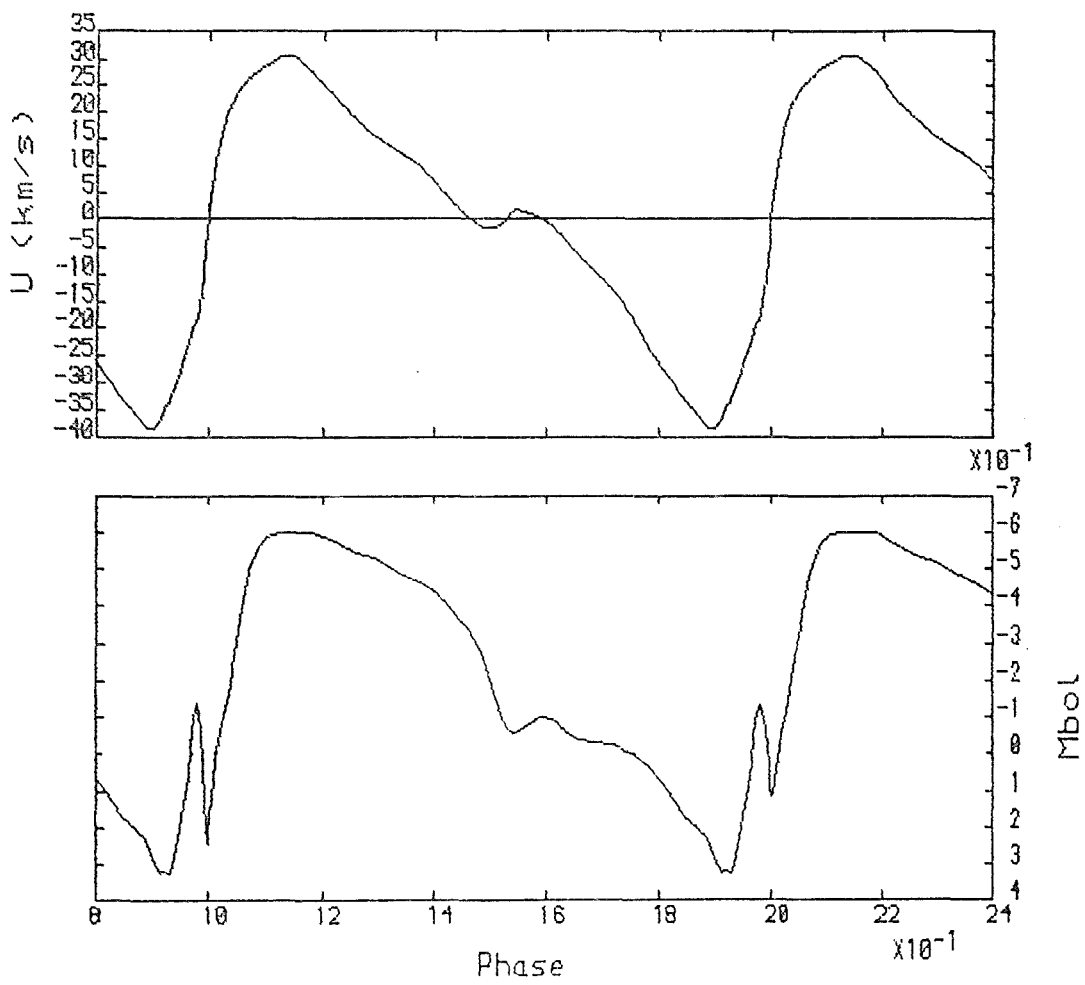


Figure 6.3 Second ("correct") attempt at CSV model 1. Light and velocity curves

| Parameter | CSV1* | Test model |
|--|-------|------------|
| M/M _⊙ | 0.6 | 0.6 |
| log(L/L _⊙) | 2.0 | 2.0 |
| log T _{eff} | 3.81 | 3.81 |
| R/R _⊙ | 8.13 | 8.0 |
| P (days) | 1.23 | 1.21 |
| Peak K.E. (10 ⁴⁰ ergs) | 1.4 | 1.3 |
| ΔR/R | 0.16 | 0.16 |
| V _{out} (km/s) | 31 | 33 |
| V _{in} (km/s) | -42 | -39 |
| ΔV (km/s) | 74 | 72 |
| L _{max} (ergs/s) | 5.3 | 5.4 |
| L _{min} (ergs/s) | 2.4 | 2.2 |
| ΔM _{bol} | 0.9 | 0.9 |
| Asymmetry (vel.) ... | 3.6 | 3.2 |
| Asymmetry (lum.) ... | 4.1 | 4.0 |
| ϕ _b ^v | 1.57 | 1.57 |
| ϕ _b ^l | 1.61 | 1.57 |
| Bump | D | D |
| Opacity used | CCH | CCH |
| Dynamic B.C. | ? | 2 |
| C _Q | 1.0 | 1.0 |
| α _v | 0.1 | 0.1 |
| No. of zones | ? | 44/5 |
| R _{inner} /R _* | ? | 0.18 |
| M _{env} /M _* | ? | 0.01 |

Table 6.1 Comparison of test model and CSV model 1

* Values taken from Carson, Stothers & Vemury (1981), model 1

Having discovered that the low temperature Carson opacities were unreliable, only a few models were run with the full Carson opacity to get periods in the range 10 - 20 days. These also showed a large pre-maximum shock, distorting the light curves so as to make them unlike either of the types seen in the observations (crested or flat-topped). It was then decided to use the combined Carson/Christy opacity in the future.

6.3 THE INSTABILITY STRIP SURVEY

A series of 25 models was constructed to cover the instability strip from the Worrell blue edge for $Y = 0.25$, $Z = 0.005$, to the observed red edge, for a mass of $0.6 M_{\odot}$. The luminosities and effective temperatures were chosen so as to obtain periods approximately in the range 10 - 20 days. The mass of $0.6 M_{\odot}$ seems to be appropriate in the light of observations, and of the bump mass determinations for BL Herculis stars. Later some models for $0.8 M_{\odot}$ and $0.5 M_{\odot}$ were constructed to look at the effect of varying the mass, and a few models were run using the Cox opacities, for comparison.

The models calculated for $0.6 M_{\odot}$ are shown on an HR diagram in figure 6.39. The luminosity and temperature ranges used were $2.6 \leq \log(L/L_{\odot}) \leq 3.2$ and $3.71 \leq \log T_e \leq 3.79$. Difficulties were encountered in constructing cool models at $\log(L/L_{\odot})$ values of 2.7 and 2.8, largely because of the excessive driving encountered here. This is in the region where it has been suggested that convection is very important in the driving zones. It is also where we expect to find the

flat-topped variables, thus unfortunately it has proved difficult to model this type. However, some of the models gave reasonable facsimilies of the flat-topped curves.

In addition, five models are presented using $M/M_{\odot} = 0.8$, one with $M/M_{\odot} = 0.5$, two using the Cox opacities in the Christy formulation and the above composition, and finally one model using the Cox and Tabor (1976) opacity table for the King Ia mix ($Y = 0.299$, $Z = 0.001$). The static and dynamic results for these three models are presented in tables 6.2 a and b and 6.3 a and b.

In most cases, the equations have been integrated forward in time until periodic repetition is achieved and/or the ratio $\frac{\sum \Delta M_{T-1/2} \oint dw}{\sum \Delta M_{T-1/2} |\oint dw|}$ is very small. Exact repetition is rarely achieved, both for numerical reasons, and (sometimes) because of real physical causes.

For some models, full growth was not achieved, or was doubtful, usually for reasons of time. These models are indicated by footnotes.

Most of the various quantities listed in tables 6.2 and 6.3 are the same as are defined for the test model. An exception is that ϕ_b^v and ϕ_b^l do not have unity added to them. Once again, the surface is taken to be that zone which in the equilibrium model was closest to $\gamma = 0.2$. In addition, a classification is added suggesting which class (crested or flat-topped) the light curve belongs to, an X indicating neither. Here upper-case letters are used for the classification (to aid in distinguishing models from observed stars in later discussion), and an X preceding the

classification indicates some doubt. The surface light and velocity curves are plotted in figures 6.4 - 6.37. In each, zero phase is taken at minimum radius. For the plotting, about one in four calculated points were used per period, and these were smoothed by taking a two-point running mean twice in succession (the same procedure used by CSV). Since observed light curves are smoothed, and subject to large errors and variations, smoothing of the modelled light and velocity curves is quite reasonable.

In tables 6.2 and 6.3 the following abbreviations are used:

$R_{0.2}/R_{\odot}$ R at the observed zone (nearest to $\tau = 0.2$)/ R_{\odot}

O.B.C Outer Boundary Condition 1 means $P_{\text{bot}} = 0$

2 means $P_g = 0$

3 means $P_{N+1/2} = P_{N-1/2} \frac{\Delta M_{N+1/2}}{\Delta M_{N-1/2}}$

For the opacity used:

CCH Carson table with Christy formula for $\log T < 3.85$

CHR Full Christy formula

KIN Cox and Tabor King Ia mix table, $Y = 0.299$, $Z = 0.001$

For number of zones: N_E/N_A = Number in envelope/Number in atmosphere

$R_{\text{inner}}/R_{\star}$ R_1/R_N for equilibrium model

M_{env}/M_{\star} $\sum \Delta M_{I-1/2}/M_N$

The Christy luminosity interpolation, on-line equation of state, and linear interpolation in the opacity tables are used throughout. Test runs with the Stellingwerf luminosity interpolation or with quadratic interpolation showed no significant changes. However, interpolation of the equation of state would have introduced significant errors.

| Model | M/M_{\odot} | $\log(L/L_{\odot})$ | $\log T_e$ | $R_{0.2}/R_{\odot}$ | $\log(R/R_{\odot})$ | OBC | Opac. | C_Q | α_v | N_e/N_a | α | M_{env}/M_* | R_{inner}/R_* |
|-------|---------------|---------------------|------------|---------------------|---------------------|-----|-------|-------|------------|-----------|----------|---------------|-----------------|
| 1 | 0.6 | 2.6 | 3.71 | 25.1 | 1.402 | 2 | CCH | 2.0 | 0.02 | 30/7 | 1.30 | 0.0033 | 0.09 |
| 2 | 0.6 | 2.7 | 3.75 | 23.5 | 1.372 | 2 | CCH | 1.0 | 0.1 | 36/5 | 1.18 | 0.0022 | 0.11 |
| 3 | 0.6 | 2.7 | 3.74 | 24.5 | 1.392 | 2 | CCH | 2.0 | 0.1 | 32/7 | 1.26 | 0.0026 | 0.13 |
| 4 | 0.6 | 2.7 | 3.73 | 25.7 | 1.412 | 2 | CCH | 2.0 | 0.02 | 32/7 | 1.26 | 0.0027 | 0.12 |
| 5 | 0.6 | 2.8 | 3.76 | 25.1 | 1.402 | 2 | CCH | 2.0 | 0.1 | 35/7 | 1.24 | 0.0023 | 0.03 |
| 6 | 0.6 | 2.8 | 3.75 | 26.2 | 1.422 | 2 | CCH | 2.0 | 0.1 | 39/5 | 1.17 | 0.0020 | 0.08 |
| 7 | 0.6 | 2.8 | 3.74 | 27.5 | 1.442 | 2 | CCH | 2.0 | 0.1 | 41/5 | 1.15 | 0.0018 | 0.09 |
| 8 | 0.6 | 2.8 | 3.73 | 29.6 | 1.462 | 3 | CCH | 2.0 | 0.1 | 30/7 | 1.25 | 0.0023 | 0.10 |
| 9 | 0.6 | 2.9 | 3.79 | 24.4 | 1.392 | 2 | CCH | 2.0 | 0.1 | 43/6 | 1.18 | 0.0013 | 0.10 |
| 10 | 0.6 | 2.9 | 3.78 | 25.6 | 1.412 | 2 | CCH | 2.0 | 0.1 | 39/5 | 1.18 | 0.0013 | 0.12 |
| 11 | 0.6 | 2.9 | 3.77 | 26.8 | 1.432 | 2 | CCH | 2.0 | 0.1 | 39/5 | 1.17 | 0.0013 | 0.11 |
| 12 | 0.6 | 2.9 | 3.76 | 28.1 | 1.452 | 2 | CCH | 2.0 | 0.1 | 43/5 | 1.14 | 0.0012 | 0.09 |
| 13 | 0.6 | 2.9 | 3.75 | 29.4 | 1.472 | 2 | CCH | 2.0 | 0.1 | 41/5 | 1.15 | 0.0020 | 0.07 |
| 14 | 0.6 | 2.9 | 3.74 | 30.8 | 1.492 | 2 | CCH | 4.0 | 0.1 | 42/5 | 1.14 | 0.0015 | 0.07 |
| 15 | 0.6 | 2.9 | 3.73 | 32.5 | 1.512 | 2 | CCH | 2.0 | 0.1 | 34/5 | 1.17 | 0.0034 | 0.06 |
| 16 | 0.6 | 3.0 | 3.78 | 28.7 | 1.462 | 2 | CCH | 2.0 | 0.1 | 41/5 | 1.15 | 0.0011 | 0.10 |
| 17 | 0.6 | 3.0 | 3.77 | 30.0 | 1.482 | 2 | CCH | 2.0 | 0.1 | 41/5 | 1.15 | 0.0011 | 0.07 |
| 18 | 0.6 | 3.0 | 3.76 | 31.4 | 1.502 | 2 | CCH | 2.0 | 0.1 | 41/5 | 1.14 | 0.0012 | 0.06 |
| 19 | 0.6 | 3.0 | 3.75 | 32.9 | 1.522 | 2 | CCH | 2.0 | 0.1 | 40/5 | 1.13 | 0.0012 | 0.09 |
| 20 | 0.6 | 3.0 | 3.74 | 34.8 | 1.542 | 2 | CCH | 2.0 | 0.1 | 41/5 | 1.12 | 0.0013 | 0.05 |
| 21 | 0.6 | 3.1 | 3.78 | 32.1 | 1.512 | 2 | CCH | 2.0 | 0.1 | 41/5 | 1.14 | 0.0009 | 0.08 |
| 22 | 0.6 | 3.1 | 3.77 | 33.5 | 1.532 | 2 | CCH | 2.0 | 0.1 | 43/6 | 1.13 | 0.0009 | 0.08 |
| 23 | 0.6 | 3.1 | 3.76 | 35.2 | 1.552 | 2 | CCH | 2.0 | 0.1 | 40/5 | 1.12 | 0.0010 | 0.08 |
| 24 | 0.6 | 3.1 | 3.75 | 36.8 | 1.572 | 2 | CCH | 2.0 | 0.1 | 42/6 | 1.11 | 0.0010 | 0.08 |
| 25 | 0.6 | 3.2 | 3.77 | 37.7 | 1.582 | 2 | CCH | 2.0 | 0.1 | 41/5 | 1.11 | 0.0008 | 0.11 |

Table 6.2a The Survey Models - static details

| Model | P (d) | PKE | $\Delta R/R$ | V_{out} | V_{in} | ΔV | L_{max} | L_{min} | ΔM_{bol} | Asym(vel) | Asym(lum) | ϕ_b^V | ϕ_b^1 | $\phi_b^1 - \phi_m^1$ | Type |
|-----------------|-------|------|--------------|-----------|----------|------------|-----------|-----------|------------------|-----------|-----------|------------|------------|-----------------------|------|
| 1 | 11.1 | 12.0 | 0.362 | 16 | -42 | 58 | 25 | 3 | 2.3 | 2.2 | 1.4 | — | 0.54 | 0.25 | F |
| 2 | 9.18 | 9.63 | 0.336 | 22 | -27 | 49 | 28 | 10 | 1.15 | 2.8 | 2.4 | — | — | — | X |
| 3 | 10.1 | 12.0 | 0.357 | 20 | -33 | 53 | 29 | 7 | 1.5 | 2.6 | 2.0 | — | — | — | X |
| 4 | 11.6 | 15.2 | 0.429 | 20 | -49 | 69 | 31 | 3 | 2.2 | 3.3 | 1.6 | — | — | — | F |
| 5 | 10.6 | 11.9 | 0.378 | 24 | -30 | 54 | 34 | 13 | 1.0 | 2.7 | 2.8 | — | 0.60 | 0.35 | XC |
| 6 | 12.6 | 17.0 | 0.508 | 23 | -52 | 75 | 42 | 4 | 2.0 | 4.3 | 3.0 | 0.50 | 0.49 | 0.30 | C |
| 7 | 13.4 | 20.2 | 0.606 | 29 | -52 | 81 | 41 | 6 | 1.9 | 4.3 | 4.9 | 0.29 | 0.36 | 0.25 | C/F |
| 8 ^a | 15.2 | 26.0 | 0.7 | 39 | -53 | 92 | 44 | 11 | 1.55 | 7.3 | 2.7 | — | — | — | F |
| 9 | 9.06 | 3.02 | 0.234 | 20 | -20 | 40 | 39 | 25 | 0.49 | 9.0 | 0.7 | 0.62 | — | — | X |
| 10 | 10.2 | 5.95 | 0.304 | 22 | -19 | 41 | 42 | 24 | 0.6 | 6.7 | 1.8 | 0.58 | — | — | X |
| 11 | 11.4 | 10.3 | 0.367 | 25 | -30 | 55 | 45 | 20 | 0.9 | 3.0 | 1.8 | 0.57 | 0.61 | 0.40 | XC |
| 12 | 13.0 | 16.1 | 0.453 | 23 | -46 | 69 | 48 | 13 | 1.4 | 4.3 | 2.6 | 0.54 | 0.58 | 0.37 | C |
| 13 | 14.6 | 20.7 | 0.568 | 25 | -51 | 76 | 53 | 12 | 1.5 | 4.0 | 3.2 | 0.35 | 0.40 | 0.27 | C |
| 14 ^b | 16.0 | 26 | 0.62 | 30 | -48 | 78 | 48 | 13 | 1.4 | 5.7 | 5.3 | — | 0.31 | 0.23 | F |
| 15 | 17.4 | 32.1 | 0.75 | 31 | -44 | 75 | 52 | 12 | 1.6 | 4.3 | 8.5 | — | 0.30 | 0.23 | F |
| 16 | 12.5 | 7.58 | 0.327 | 23 | -21 | 44 | 55 | 28 | 0.68 | 2.4 | 1.7 | 0.53 | 0.56 | 0.39 | XC |
| 17 | 14.2 | 13.3 | 0.422 | 22 | -37 | 59 | 60 | 22 | 1.05 | 2.7 | 4.0 | 0.53 | 0.51 | 0.35 | C |
| 18 | 15.9 | 19.1 | 0.524 | 24 | -47 | 71 | 65 | 15 | 1.5 | 4.3 | 2.6 | 0.40 | 0.47 | 0.31 | C |
| 19 | 17.3 | 24.1 | 0.60 | 26 | -46 | 72 | 67 | 15 | 1.6 | 6.8 | 3.2 | 0.22 | 0.35 | 0.26 | C/F |
| 20 ^c | 19.3 | 32.4 | 0.61 | 30 | -41 | 71 | 81 | 15 | 1.65 | 3.8 | 2.8 | — | 0.32 | 0.23 | C/F |
| 21 | 15.4 | 8.34 | 0.359 | 22 | -26 | 48 | 71 | 35 | 0.70 | 2.0 | 1.7 | 0.48 | 0.50 | 0.35 | C |
| 22 | 17.1 | 14.8 | 0.475 | 24 | -39 | 63 | 76 | 28 | 1.05 | 2.4 | 4.3 | 0.46 | 0.49 | 0.32 | C |
| 23 | 18.8 | 20.5 | 0.545 | 23 | -43 | 66 | 83 | 20 | 1.45 | 5.3 | 3.2 | 0.31 | 0.40 | 0.30 | C |
| 24 | 20.6 | 30.1 | 0.62 | 26 | -44 | 70 | 86 | 20 | 1.6 | 8.0 | 3.3 | — | 0.34 | 0.24 | C |
| 25 | 20.6 | 13.6 | 0.485 | 26 | -29 | 55 | 91 | 39 | 0.9 | 2.1 | 1.5 | 0.36 | 0.38 | 0.29 | C |

Table 6.2b The Survey models - dynamic details

a Stopped after 12 periods

b Showed 2 states,
data given for the "steadier" (non-RV Tauri) state

c Lost outer zone

| Model | M/M_{\odot} | $\log(L/L_{\odot})$ | $\log T_e$ | $R_{0.2}/R_{\odot}$ | $\log(R/R_{\odot})$ | OBC | Opac. | C_Q | α_v | N_e/N_a | α | M_{env}/M_* | R_{inner}/R_* |
|-------|---------------|---------------------|------------|---------------------|---------------------|-----|-------|-------|------------|-----------|----------|----------------------|------------------------|
| 51 | 0.5 | 3.0 | 3.76 | 31.4 | 1.502 | 2 | CCH | 2.0 | 0.1 | 29/7 | 1.21 | 0.0009 | 0.09 |
| 81 | 0.8 | 2.7 | 3.70 | 30.1 | 1.472 | 3 | CCH | 2.0 | 0.1 | 33/6 | 1.26 | 0.0056 | 0.11 |
| 82 | 0.8 | 2.8 | 3.72 | 30.9 | 1.482 | 3 | CCH | 2.0 | 0.1 | 33/6 | 1.25 | 0.0046 | 0.10 |
| 83 | 0.8 | 2.8 | 3.71 | 32.3 | 1.502 | 3 | CCH | 2.0 | 0.1 | 33/6 | 1.24 | 0.0048 | 0.09 |
| 84 | 0.8 | 2.9 | 3.72 | 34.8 | 1.532 | 3 | CCH | 2.0 | 0.1 | 36/6 | 1.20 | 0.0040 | 0.12 |
| 85 | 0.8 | 3.0 | 3.76 | 31.5 | 1.502 | 2 | CCH | 2.0 | 0.1 | 30/7 | 1.31 | 0.0029 | 0.09 |
| C1 | 0.6 | 2.8 | 3.73 | 29.5 | 1.462 | 3 | CHR | 2.0 | 0.1 | 30/7 | 1.28 | 0.0037 | 0.10 |
| C2 | 0.6 | 2.9 | 3.75 | 29.5 | 1.472 | 2 | CHR | 2.0 | 0.1 | 32/6 | 1.23 | 0.0030 | 0.12 |
| K1 | 0.6 | 3.0 | 3.76 | 31.5 | 1.502 | 2 | KIN | 2.0 | 0.1 | 29/7 | 1.28 | 0.0031 | 0.07 |

Table 6.3a The Comparison Models - static details

| Model | P (d) | PKE | $\Delta R/R$ | V_{out} | V_{in} | ΔV | L_{max} | L_{min} | ΔM_{bol} | Asym(vel) | Asym(lum) | ϕ_D^V | ϕ_D^I | $\phi_D^I - \phi_m^I$ | Type |
|-------|-------|------|--------------|------------------|-----------------|------------|------------------|------------------|-------------------------|-----------|-----------|------------|------------|-----------------------|------|
| 51 | 17.8 | 17.3 | 0.613 | 23 | -44 | 67 | 67 | 15 | 1.5 | 6.7 | 3.8 | — | 0.38 | 0.29 | C |
| 81 | 11.3 | 11.9 | 0.225 | 12 | -24 | 36 | 27 | 7.8 | 1.35 | 3.3 | 1.3 | — | — | — | X |
| 82 | 12.0 | 15.1 | 0.267 | 14 | -25 | 39 | 34 | 8.6 | 1.5 | 2.0 | 1.3 | — | — | — | X |
| 83 | 13.7 | 22.3 | 0.32 | 15 | -32 | 47 | 37 | 6.8 | 1.8 | 2.0 | 1.2 | — | — | — | X |
| 84 | 17.0 | 45.0 | 0.71 | 38 | -58 | 96 | 56 | 3.5 | 3.0 | 4.3 | 2.6 | — | — | — | F |
| 85 | 12.7 | 19.2 | 0.350 | 25 | -25 | 50 | 55 | 25 | 0.9 | 3.0 | 1.8 | — | — | — | X |
| C1 | 13.9 | 18.1 | 0.381 | 18 | -35 | 53 | 37 | 8.1 | 1.65 | 3.3 | 2.3 | — | 0.59 | 0.34 | C |
| C2 | 13.4 | 11.8 | 0.325 | 20 | -22 | 42 | 45 | 19 | 0.95 | 2.3 | 1.9 | 0.50 | 0.57 | 0.43 | XC |
| K1 | 16.0 | 33.3 | 0.610 | 33 | -53 | 86 | 68 | 14 | 1.7 | 4.6 | 5.7 | 0.40 | 0.43 | 0.39 | C |

Table 6.3b The Comparison Models - dynamic details

Figures 6.4 to 6.37 show the light and velocity curves all of the models, plotted against phase from minimum radius

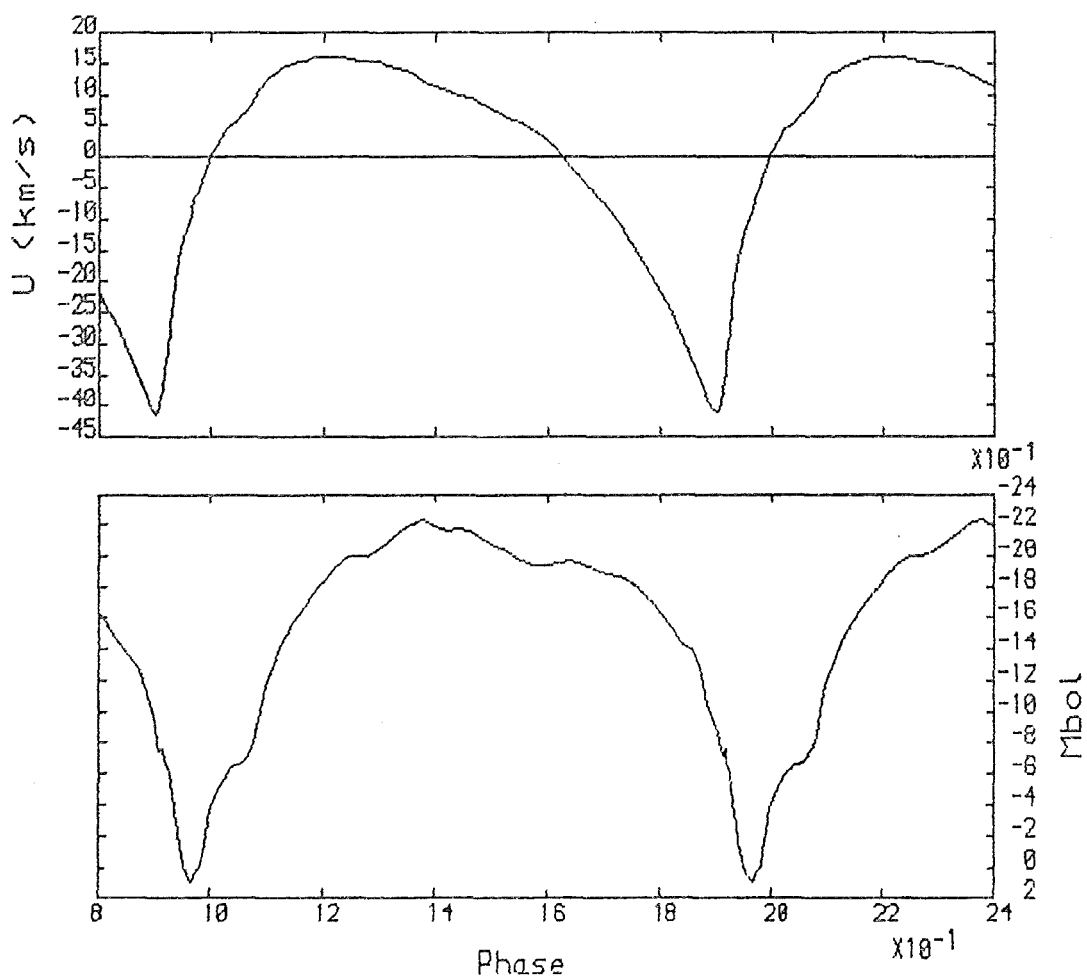


Figure 6.4 Model 1 $P \approx 11.1$ days

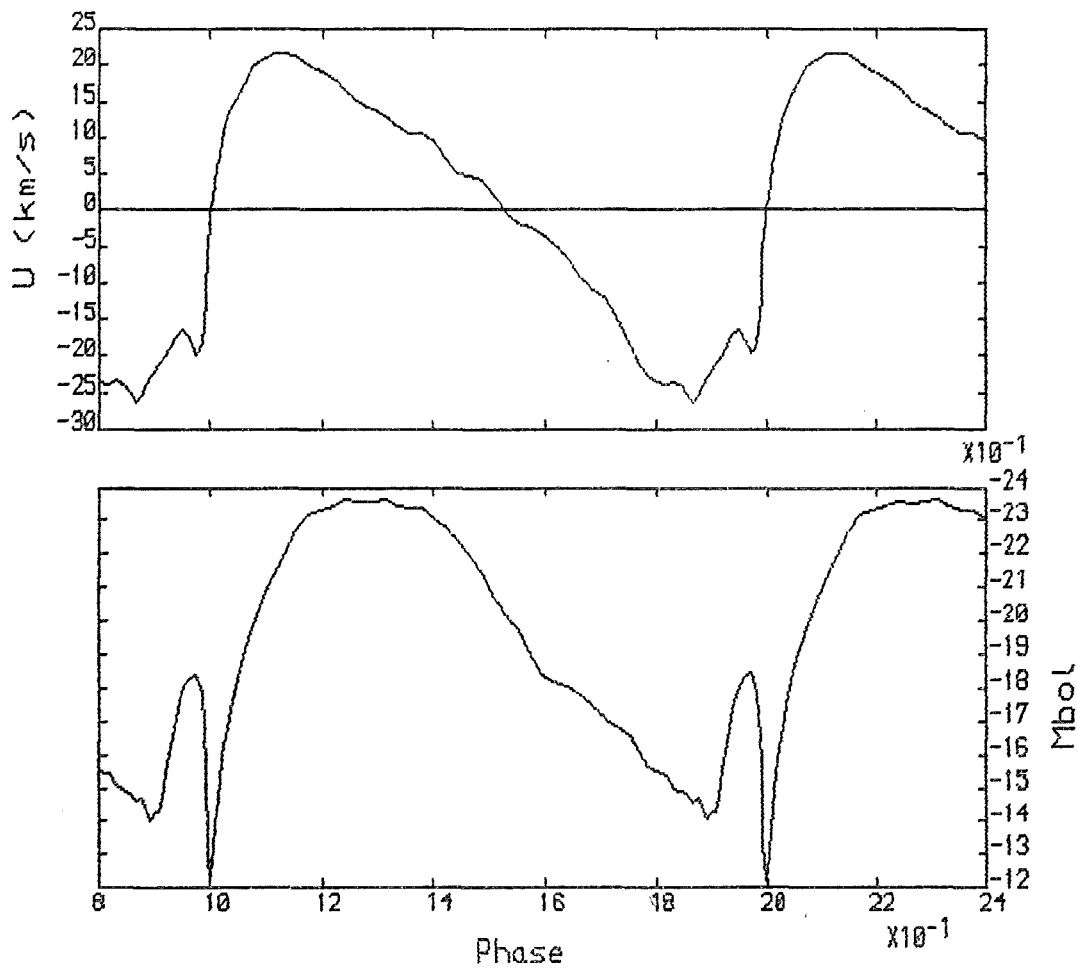


Figure 6.5 Model 2 $P = 9.2$ days

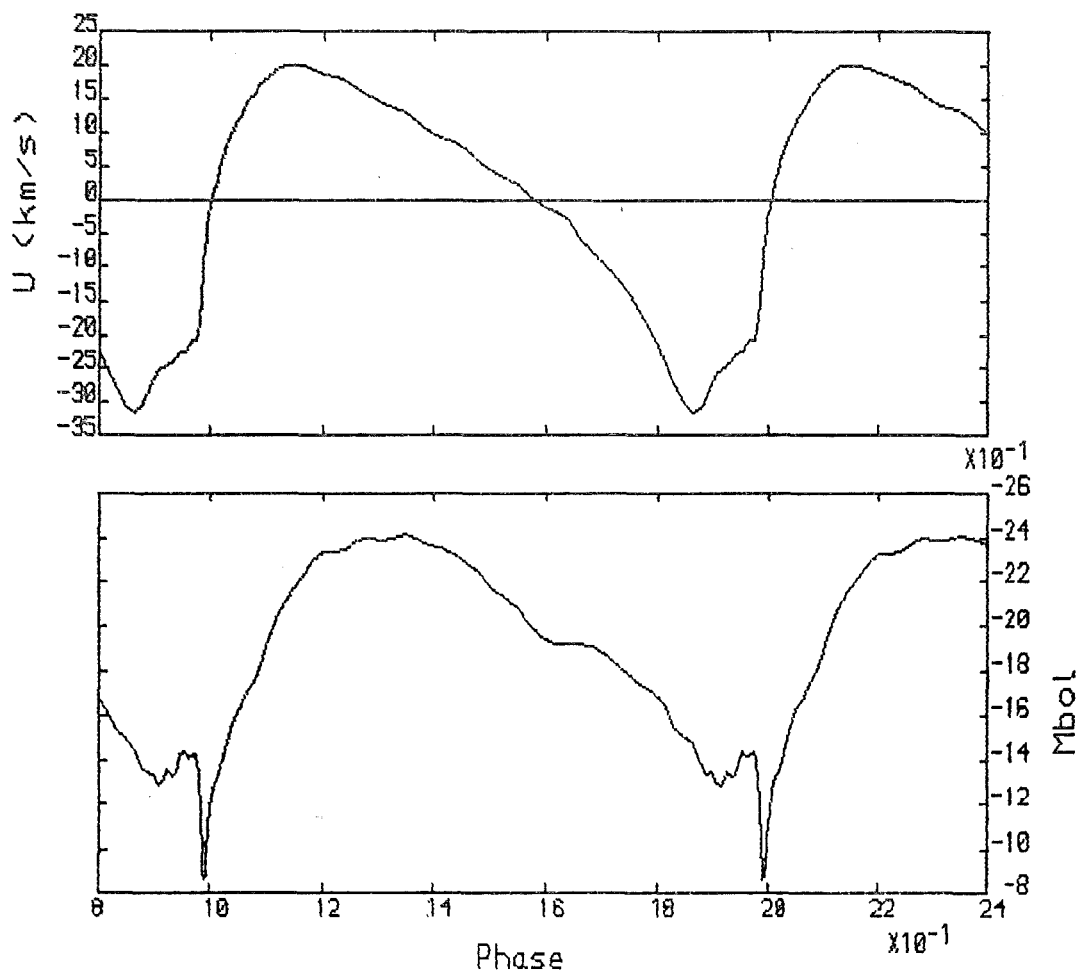


Figure 6.6 Model 3 $P = 10.1$ days

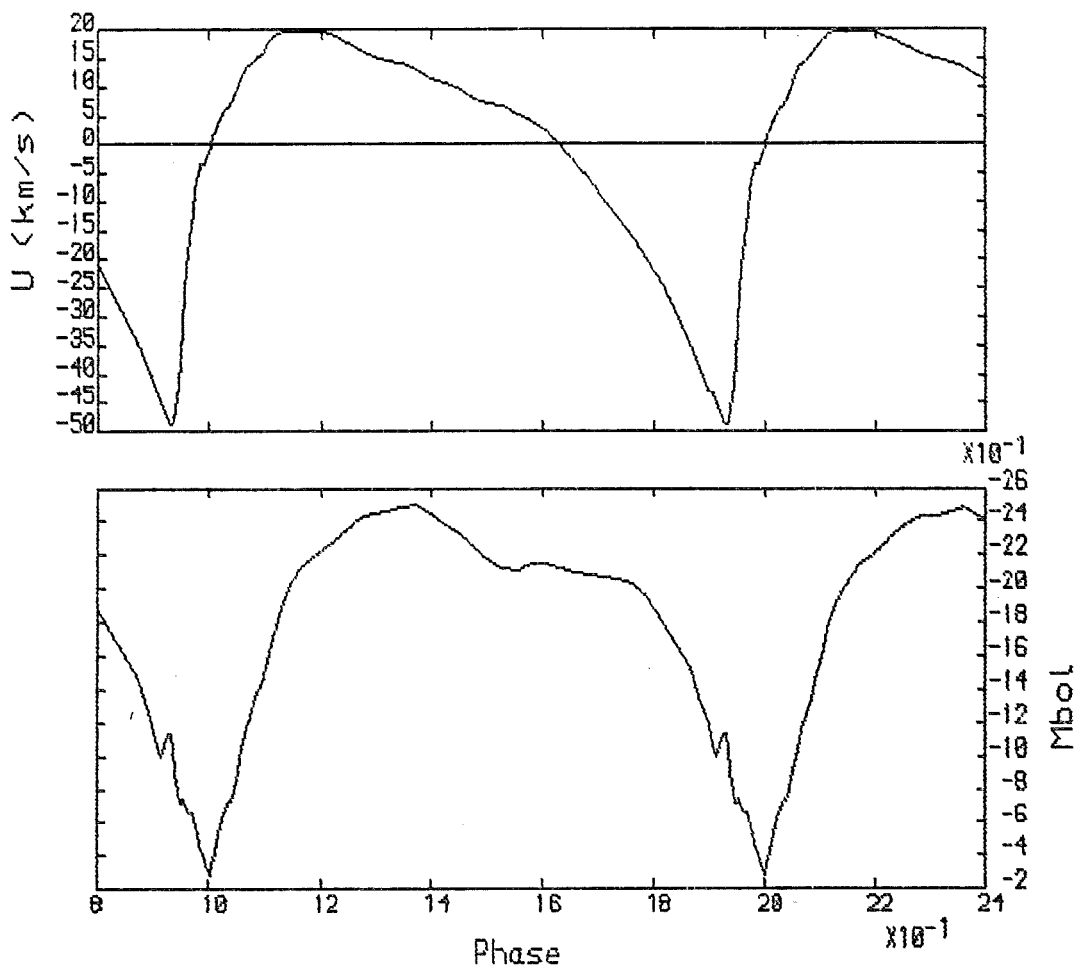


Figure 6.7 Model 4 $P = 11.6$ days

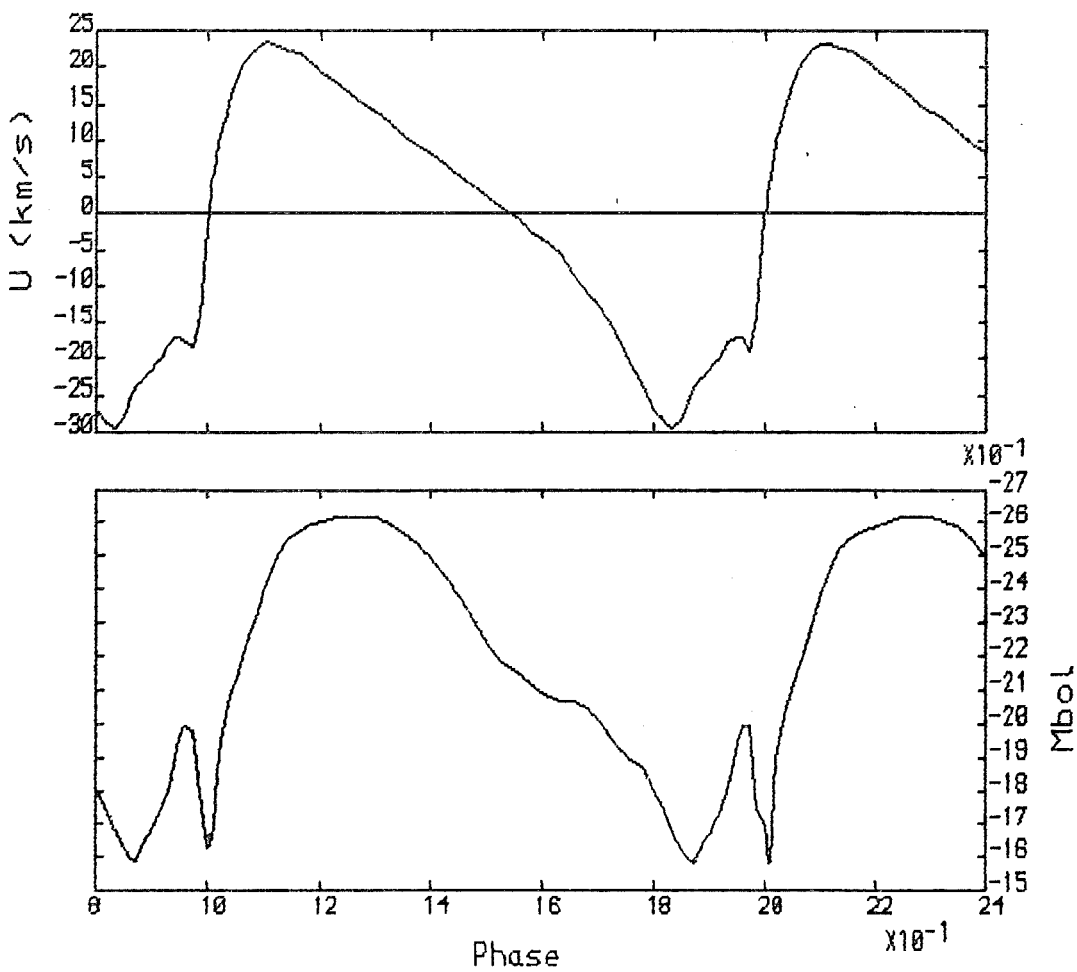


Figure 6.8 Model 5 $P = 10.6$ days

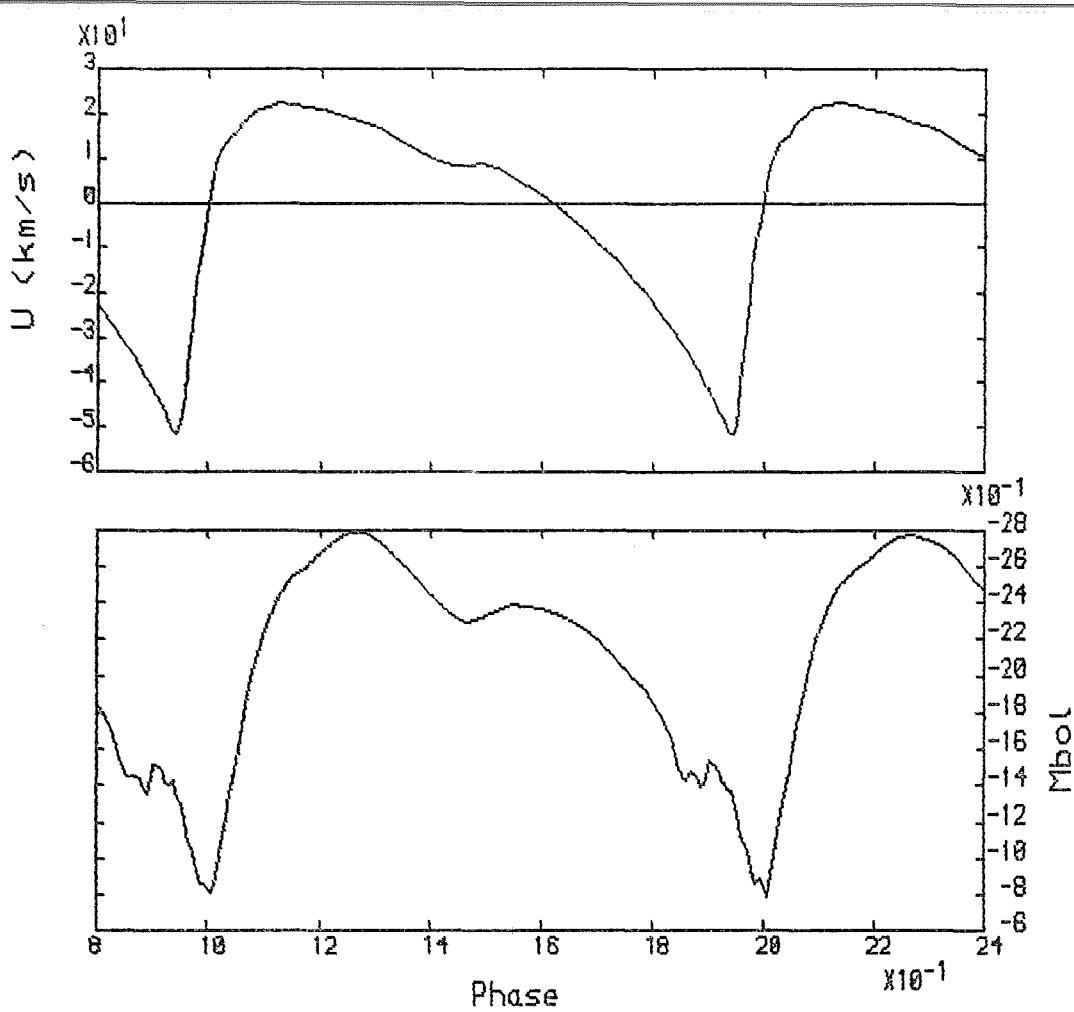


Figure 6.9 Model 6 $P = 12.6$ days

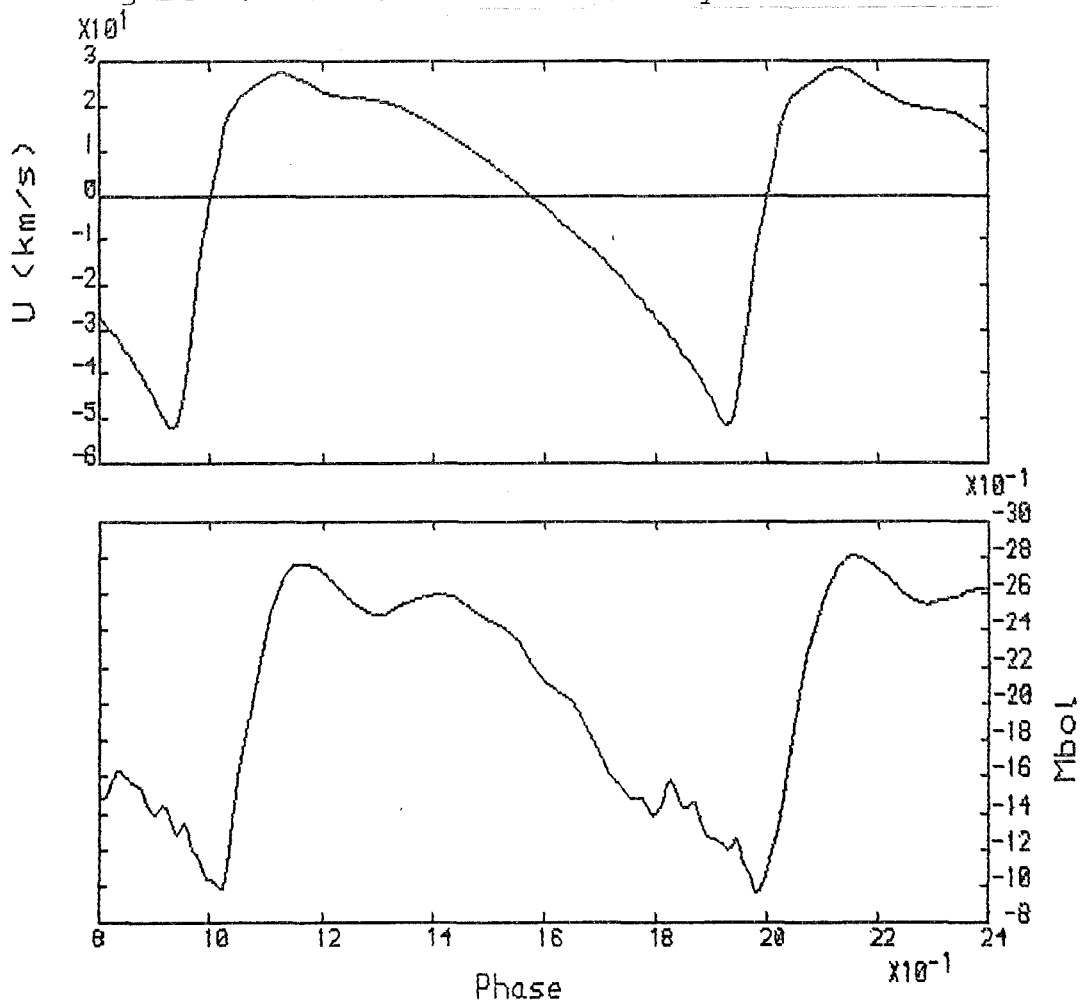


Figure 6.10 Model 7 $P = 13.4$ days

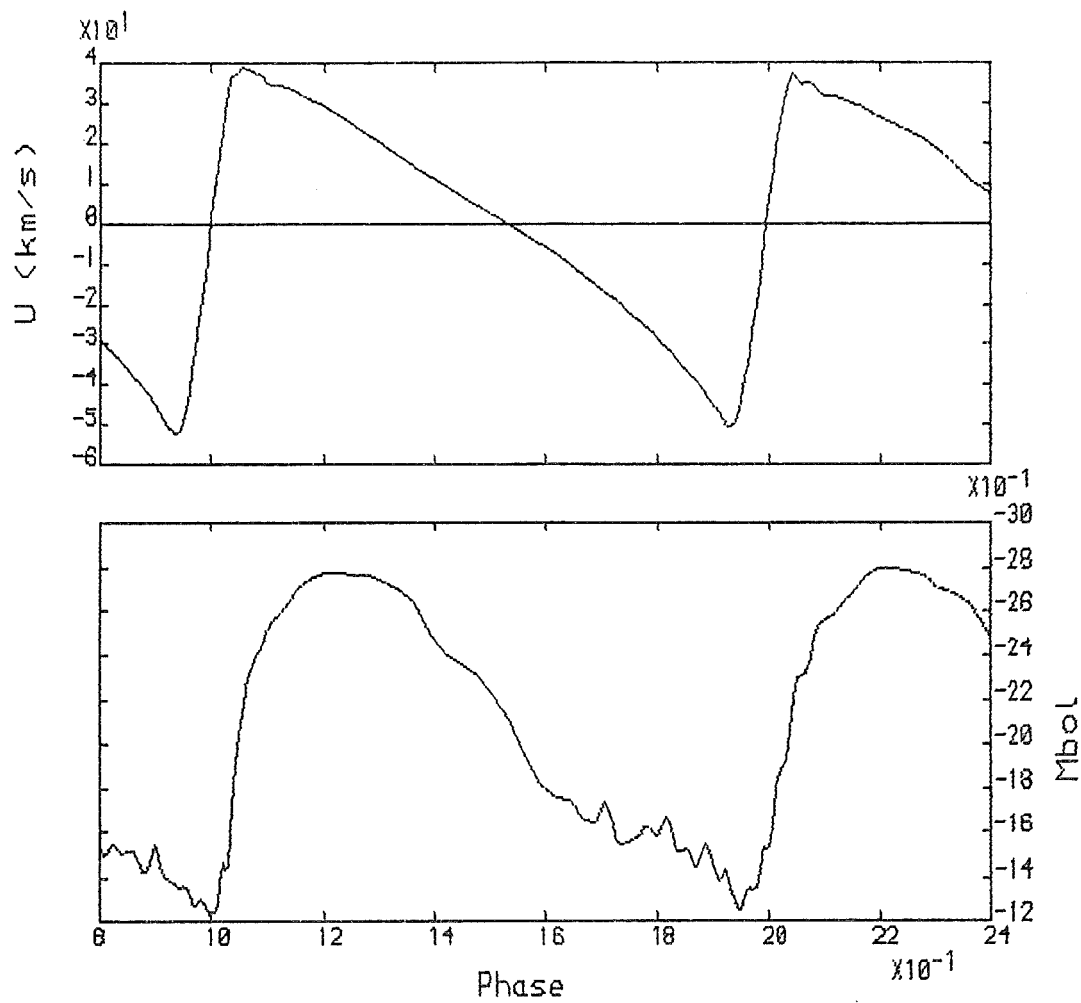


Figure 6.11 Model 8 $P = 15.2$ days

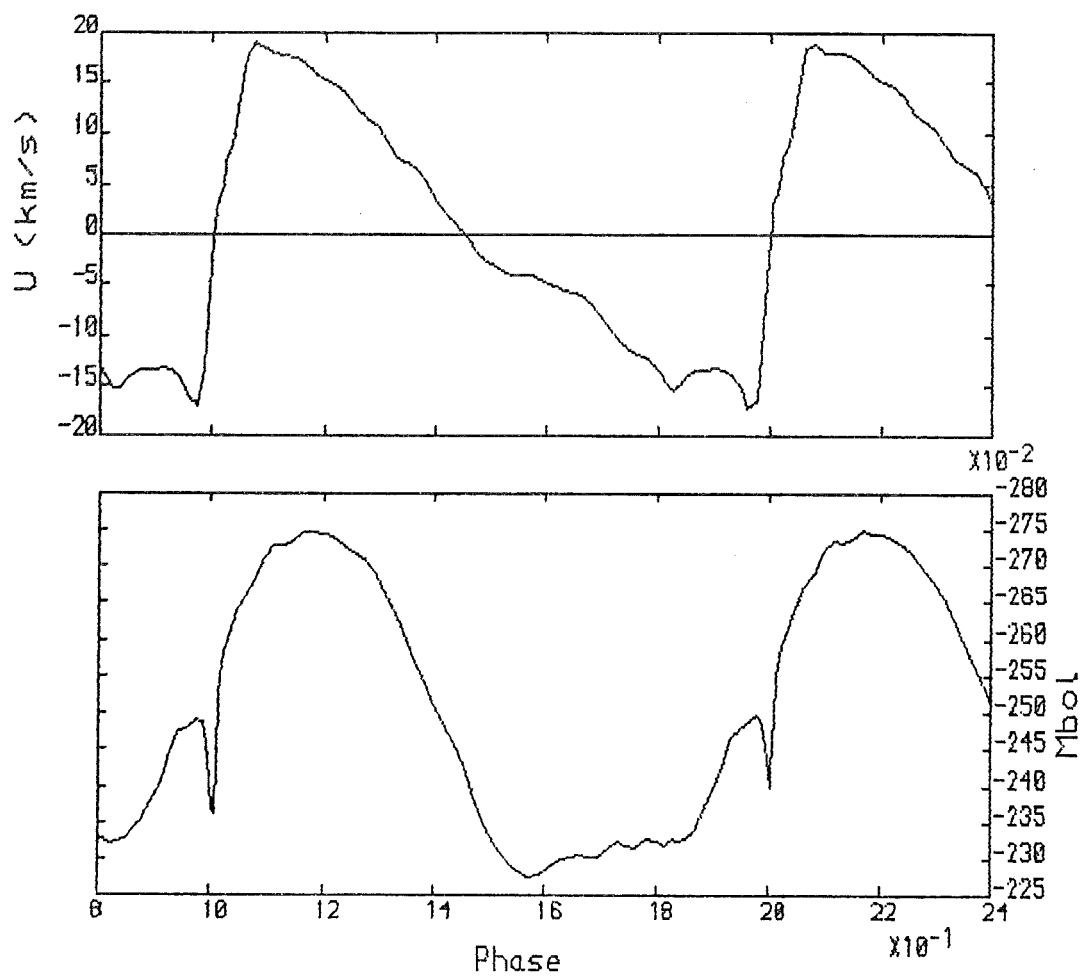


Figure 6.12 Model 9 $P = 9.1$ days

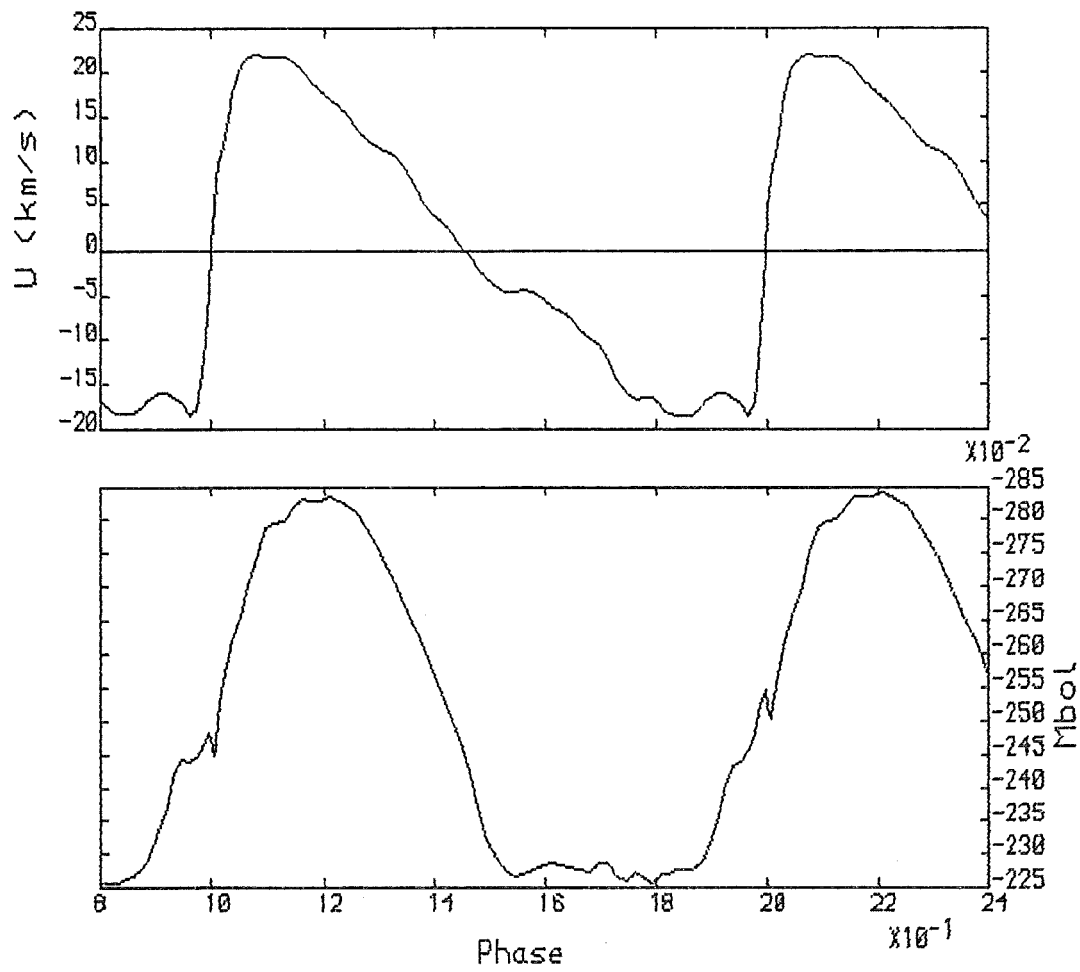


Figure 6.13 Model 10 $P = 10.2$ days

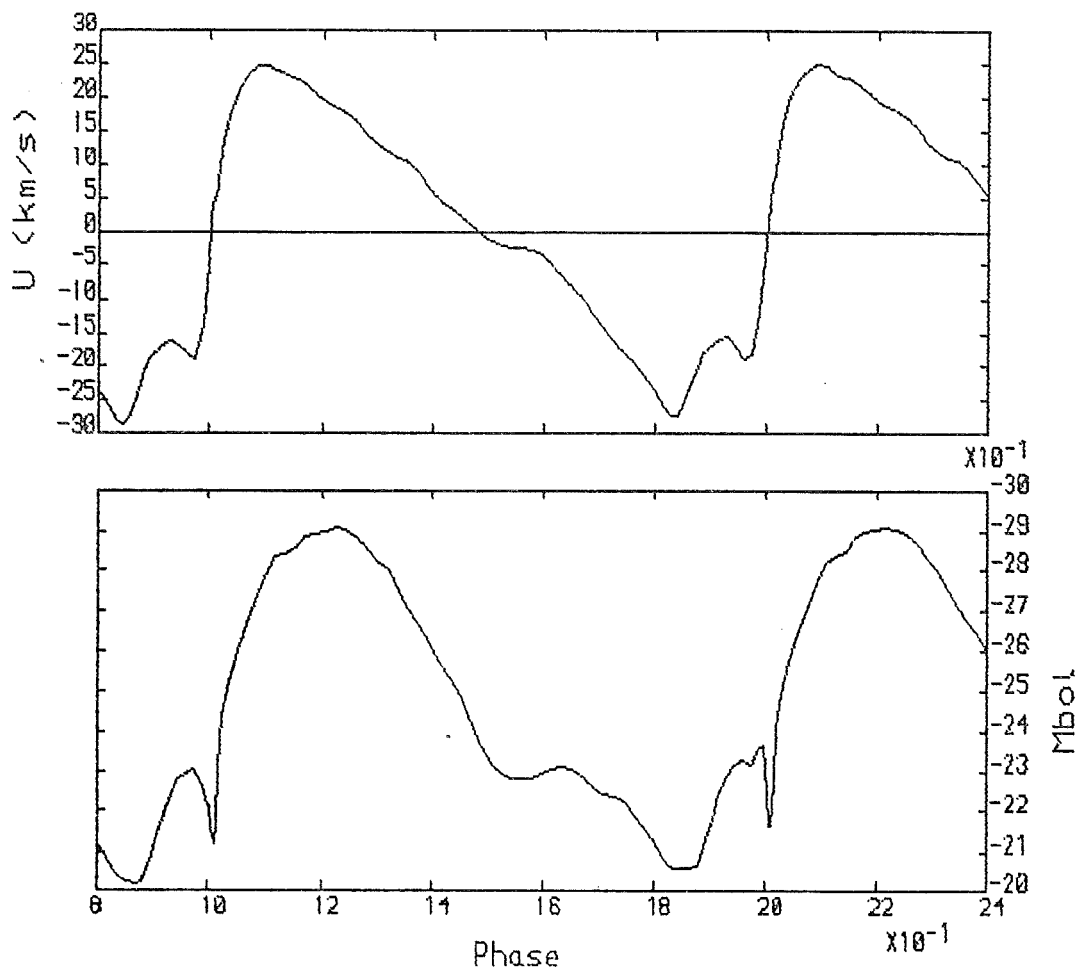


Figure 6.14 Model 11 $P = 11.4$ days

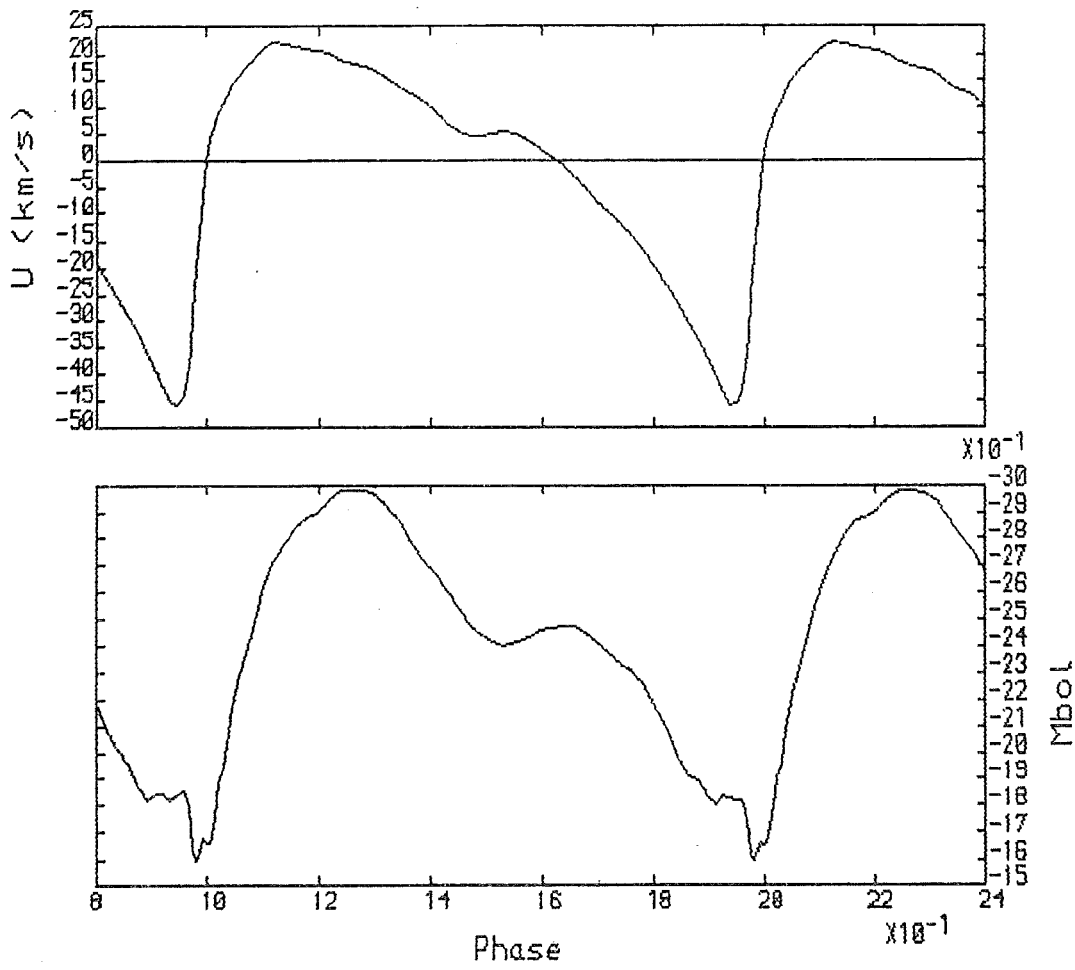


Figure 6.15 Model 12 $P = 13.0$ days

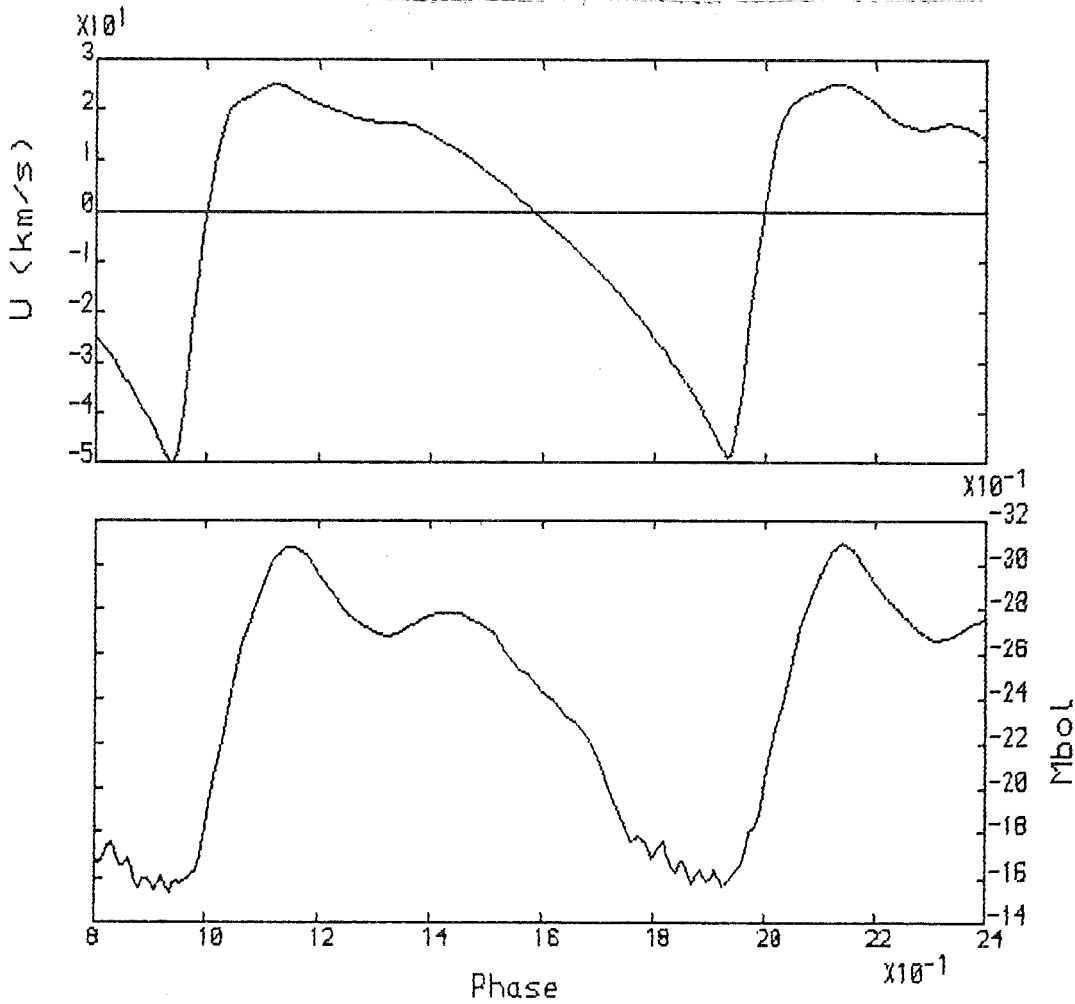


Figure 6.16 Model 13 $P = 14.5$ days

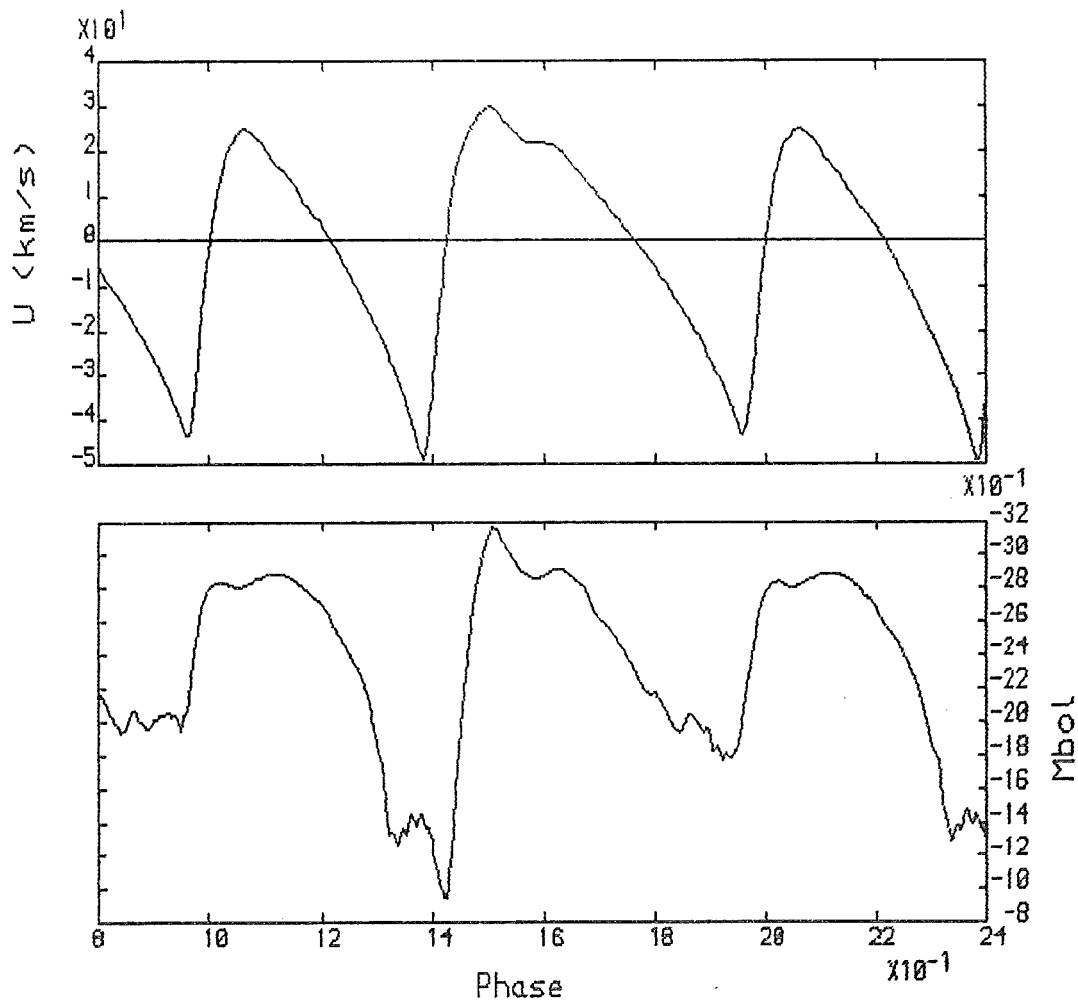


Figure 6.17a Model 14 $P = 32.0$ days, first state

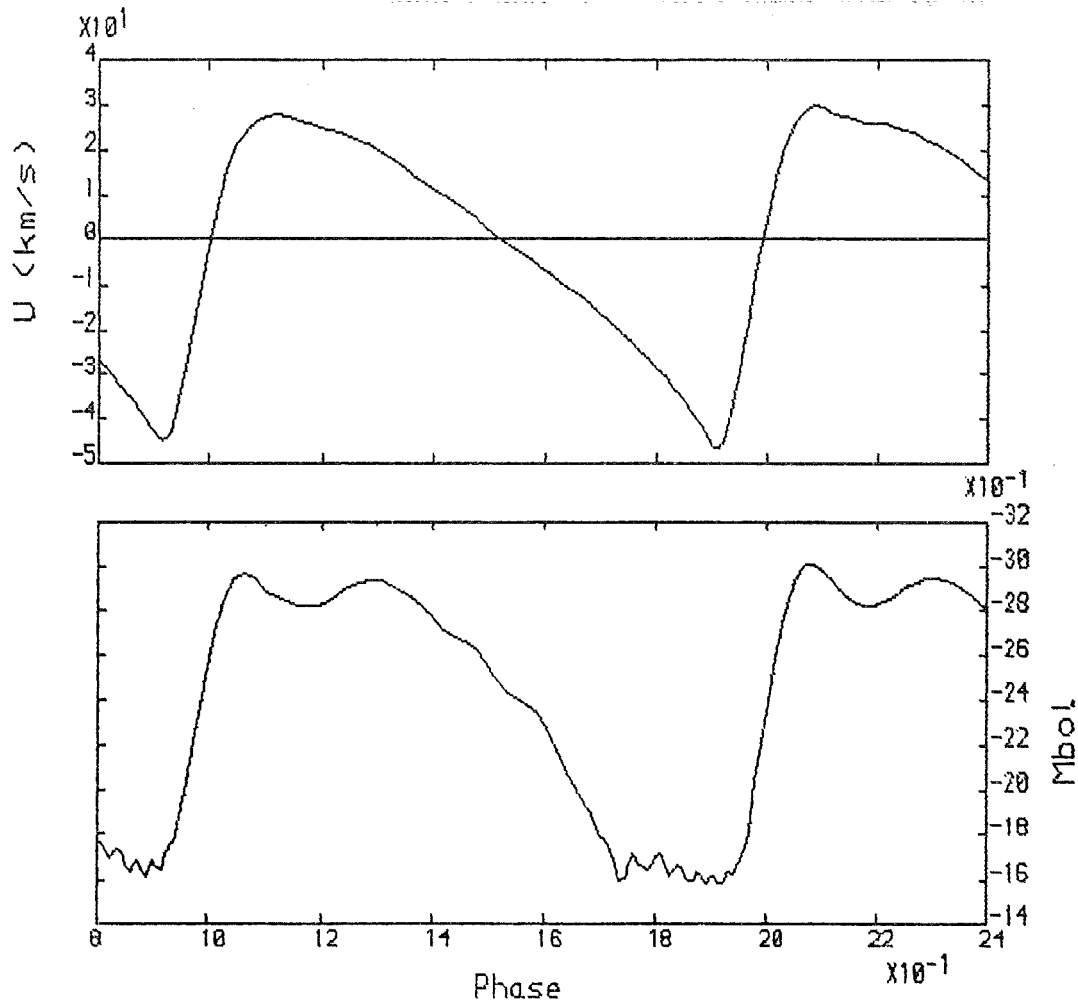


Figure 6.17b Model 14 $P = 16.0$ days, second state

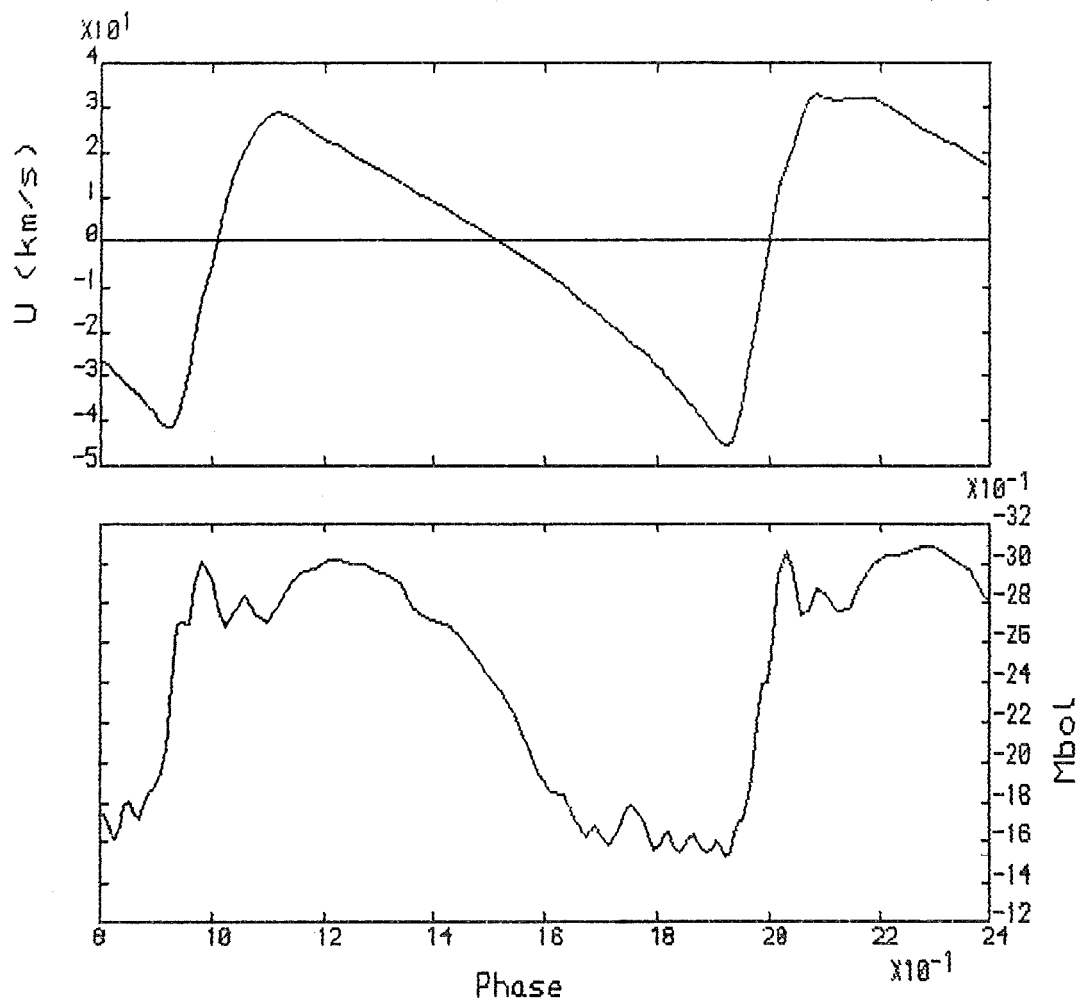


Figure 6.18 Model 15 $P = 17.4$ days

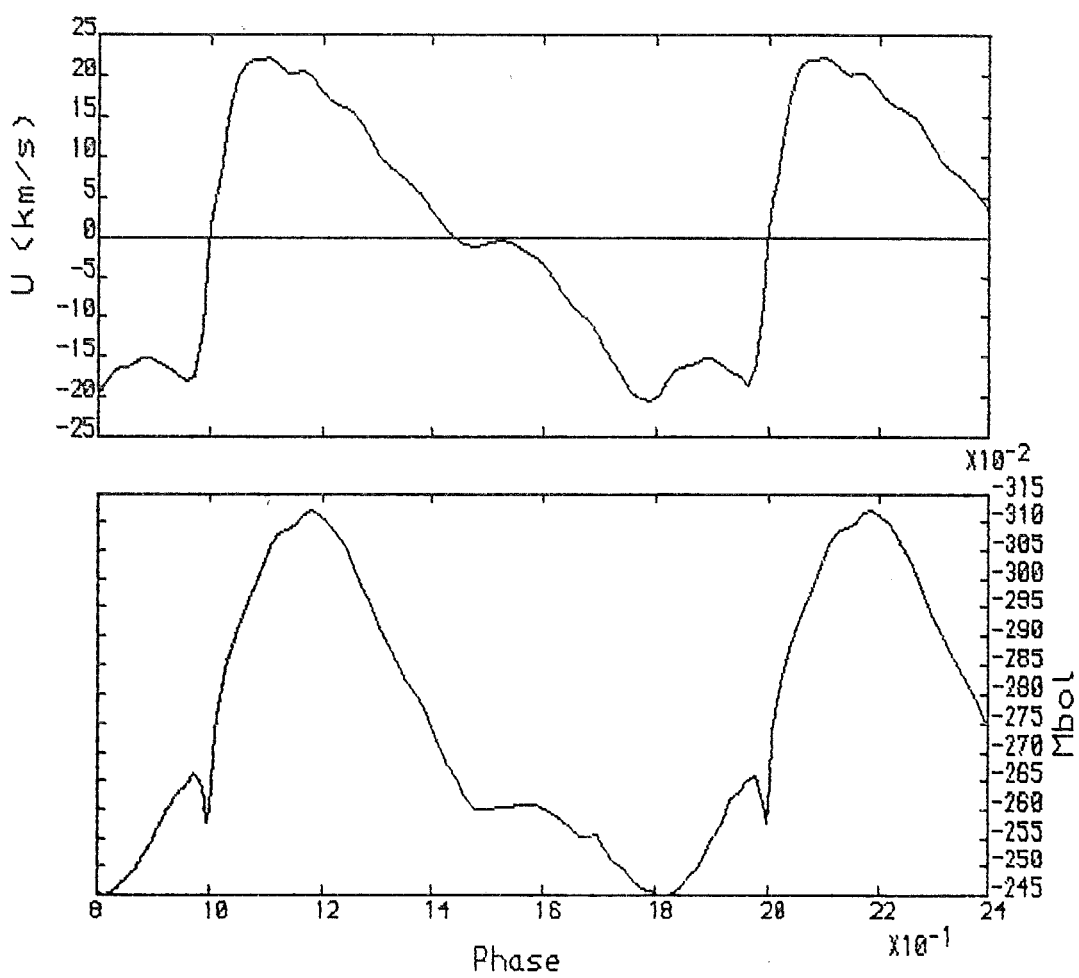


Figure 6.19 Model 16 $P = 12.5$ days

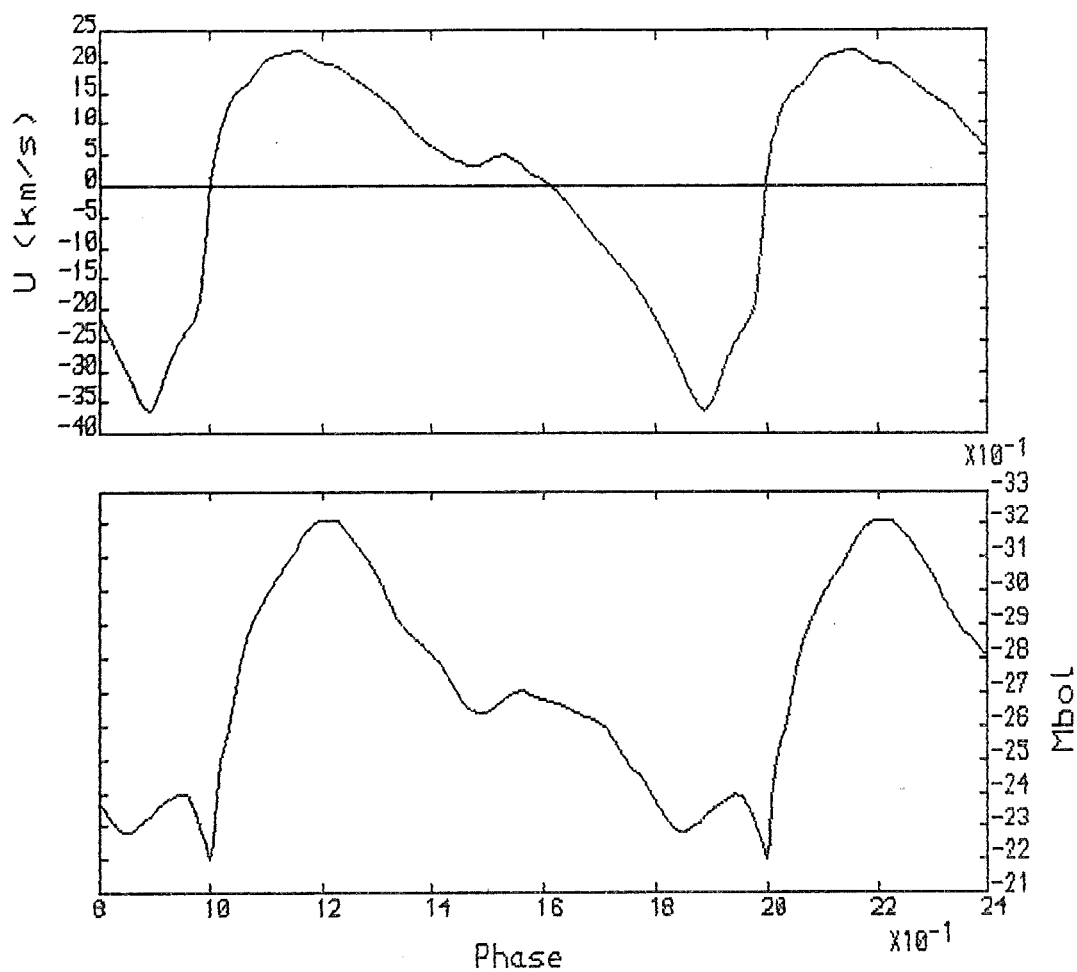


Figure 6.20 Model 17 $P = 14.2$ days

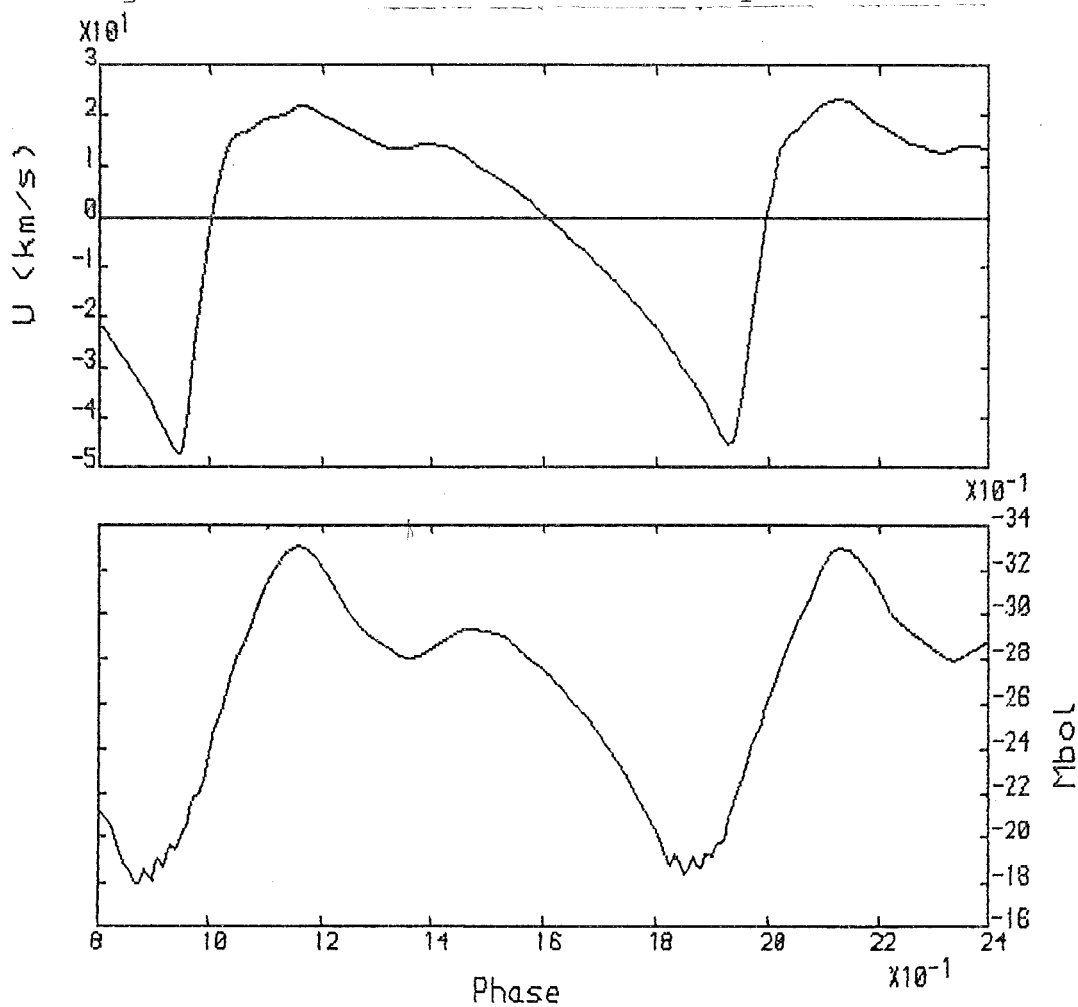


Figure 6.21 Model 18 $P = 15.9$ days

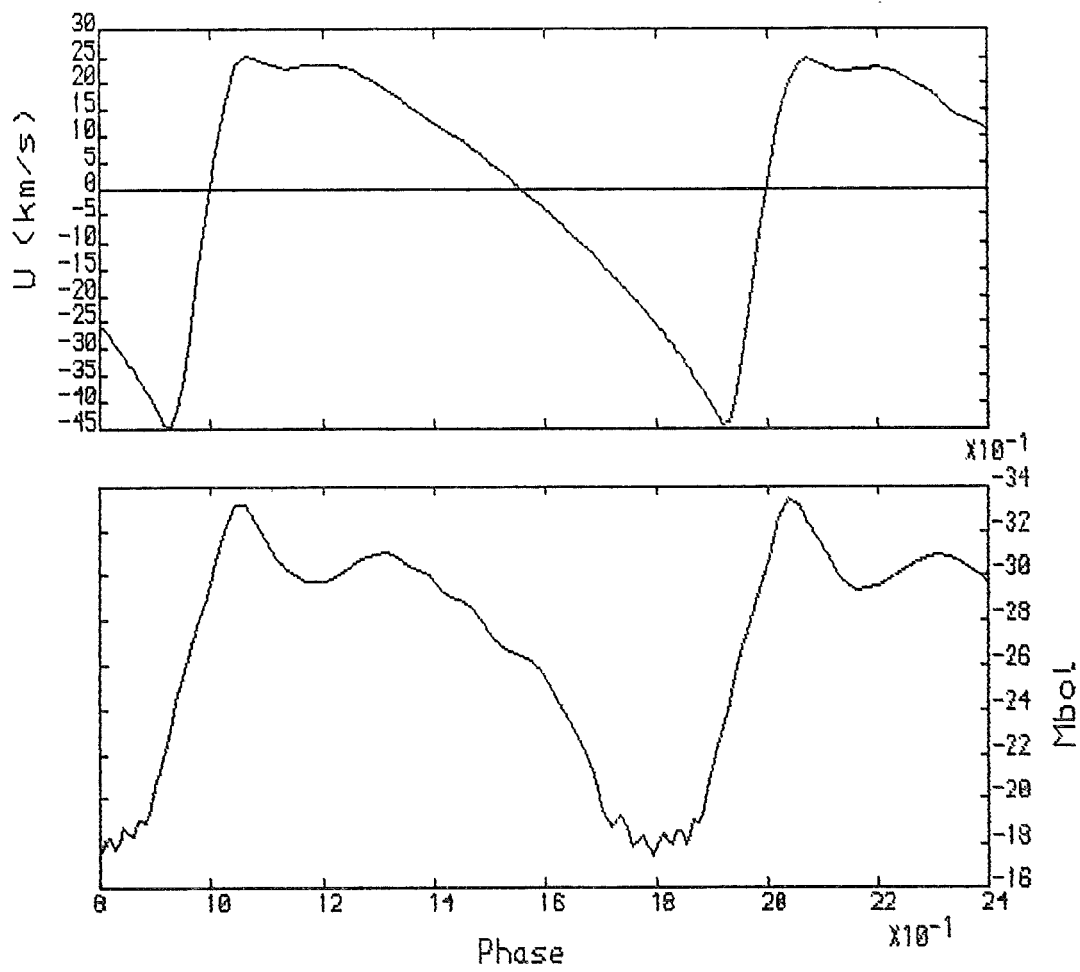


Figure 6.22 Model 19 $P = 17.3$ days

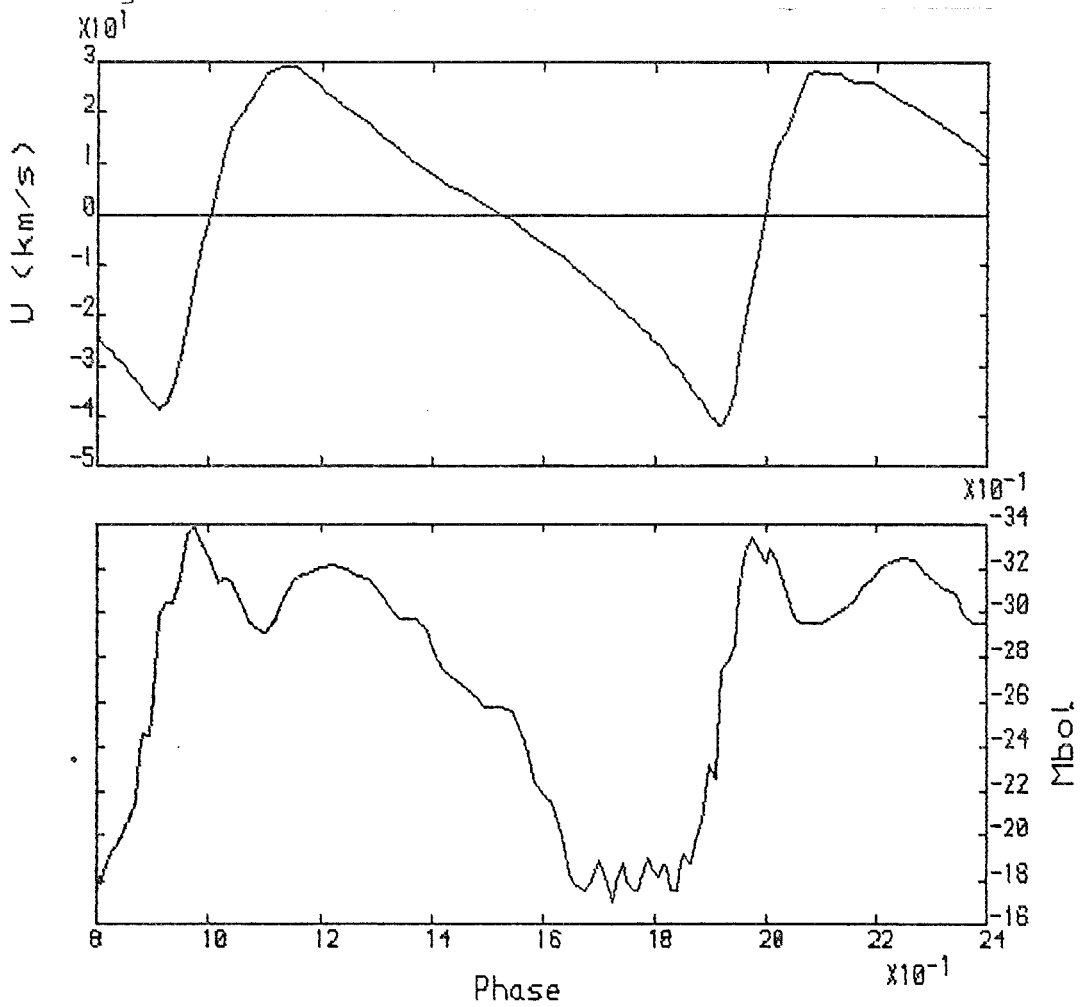


Figure 6.23 Model 20 $P = 19.3$ days

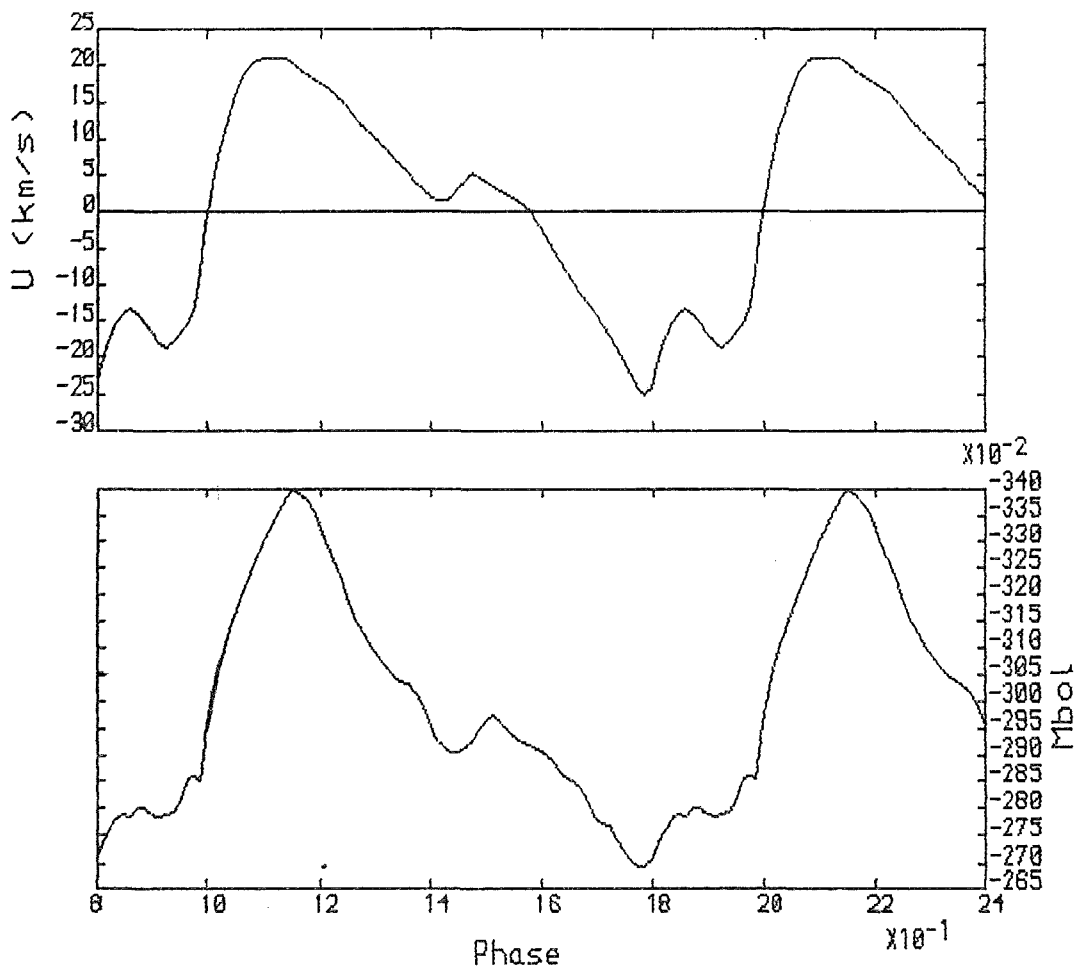


Figure 6.24 Model 21 $P = 15.4$ days

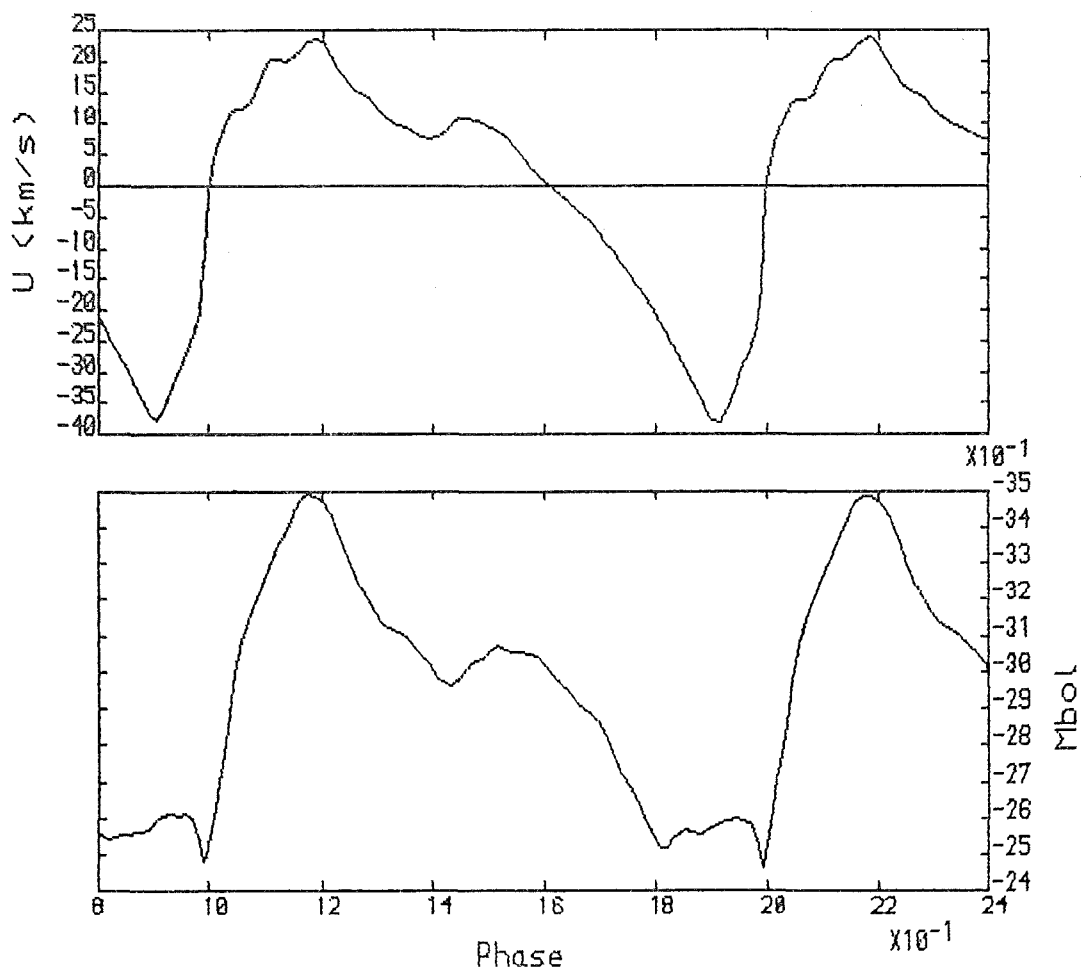


Figure 6.25 Model 22 $P = 17.1$ days

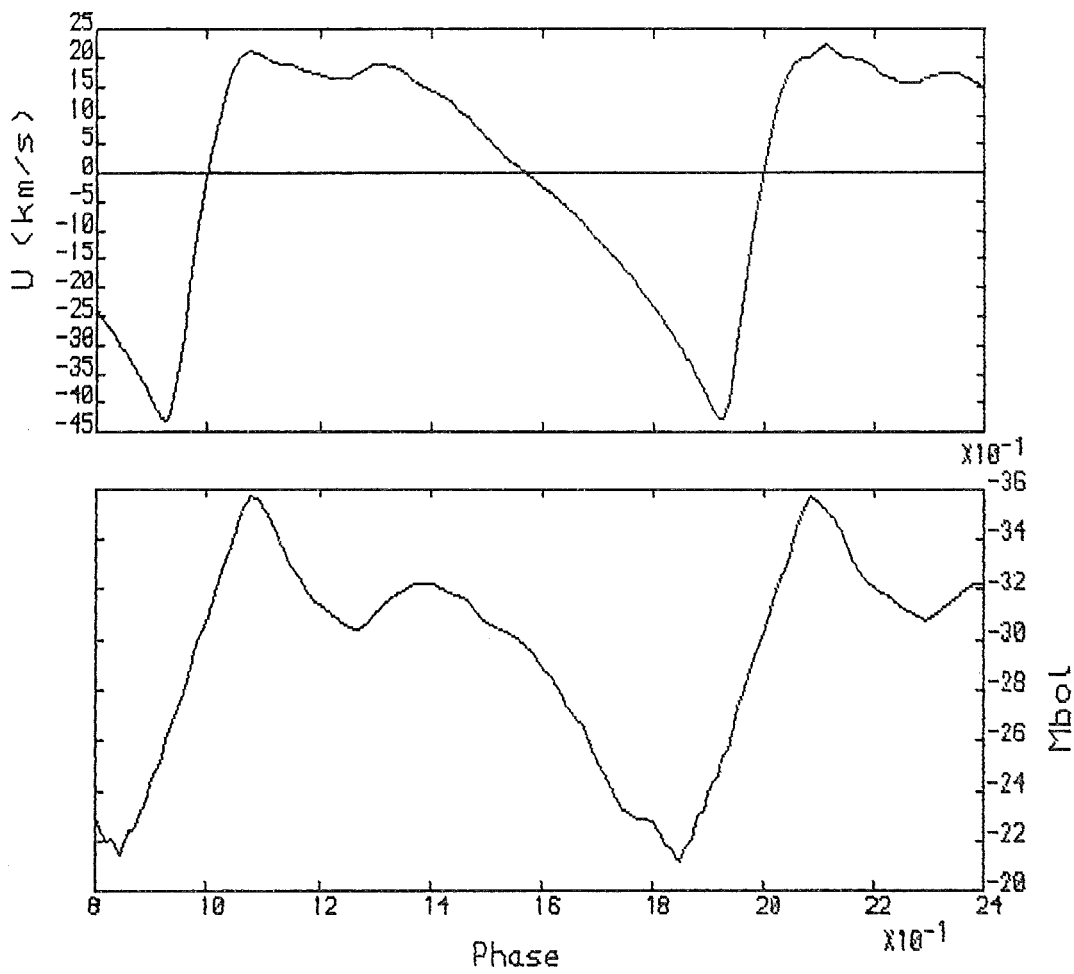


Figure 6.26 Model 23 $P = 18.8$ days

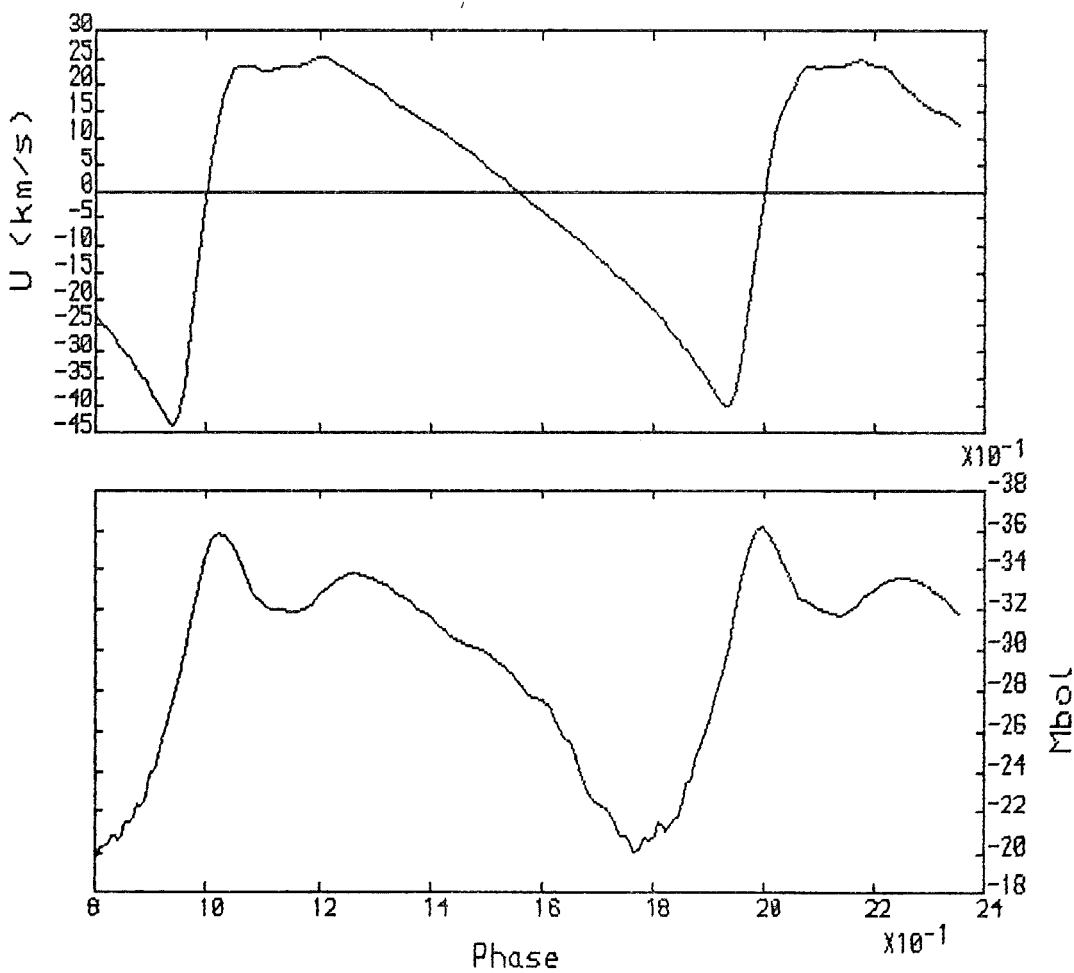


Figure 6.27 Model 24 $P = 20.6$ days

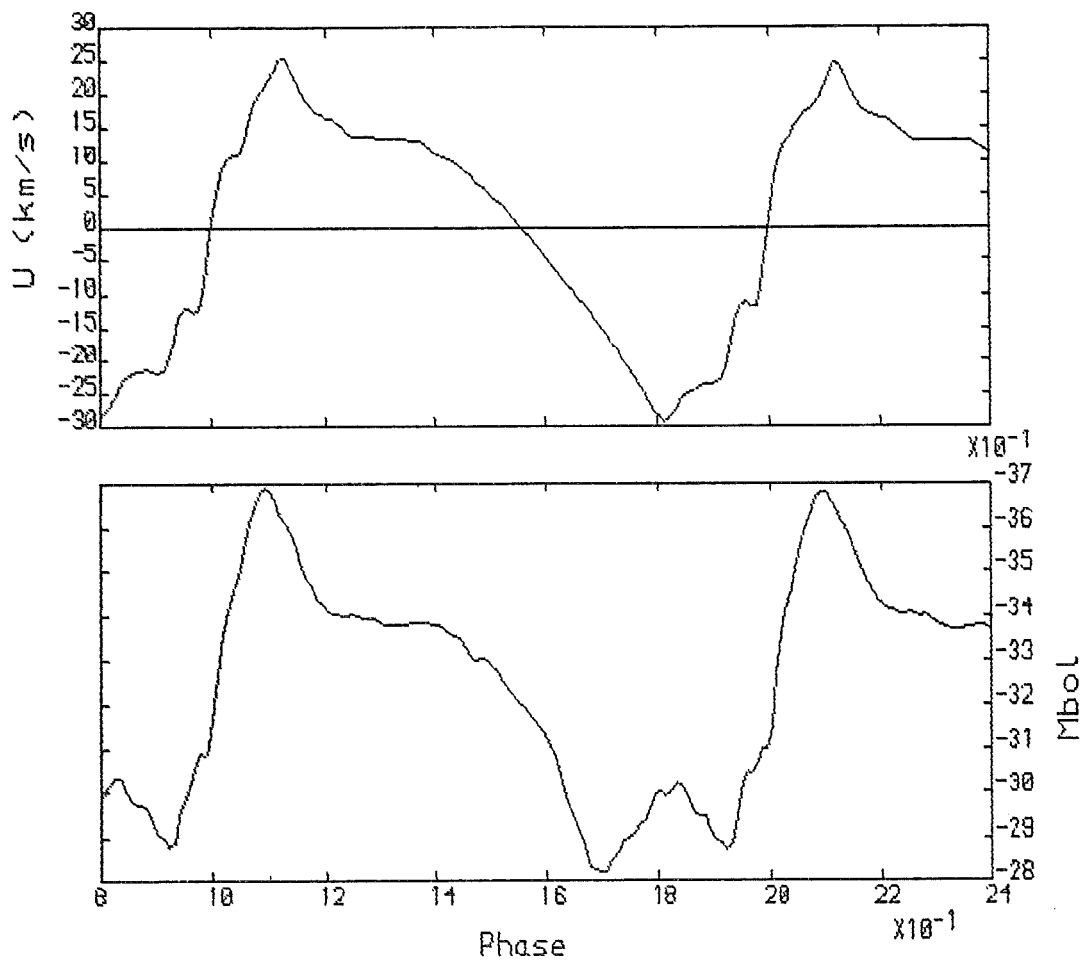


Figure 6.28 Model 25 $P = 20.6$ days

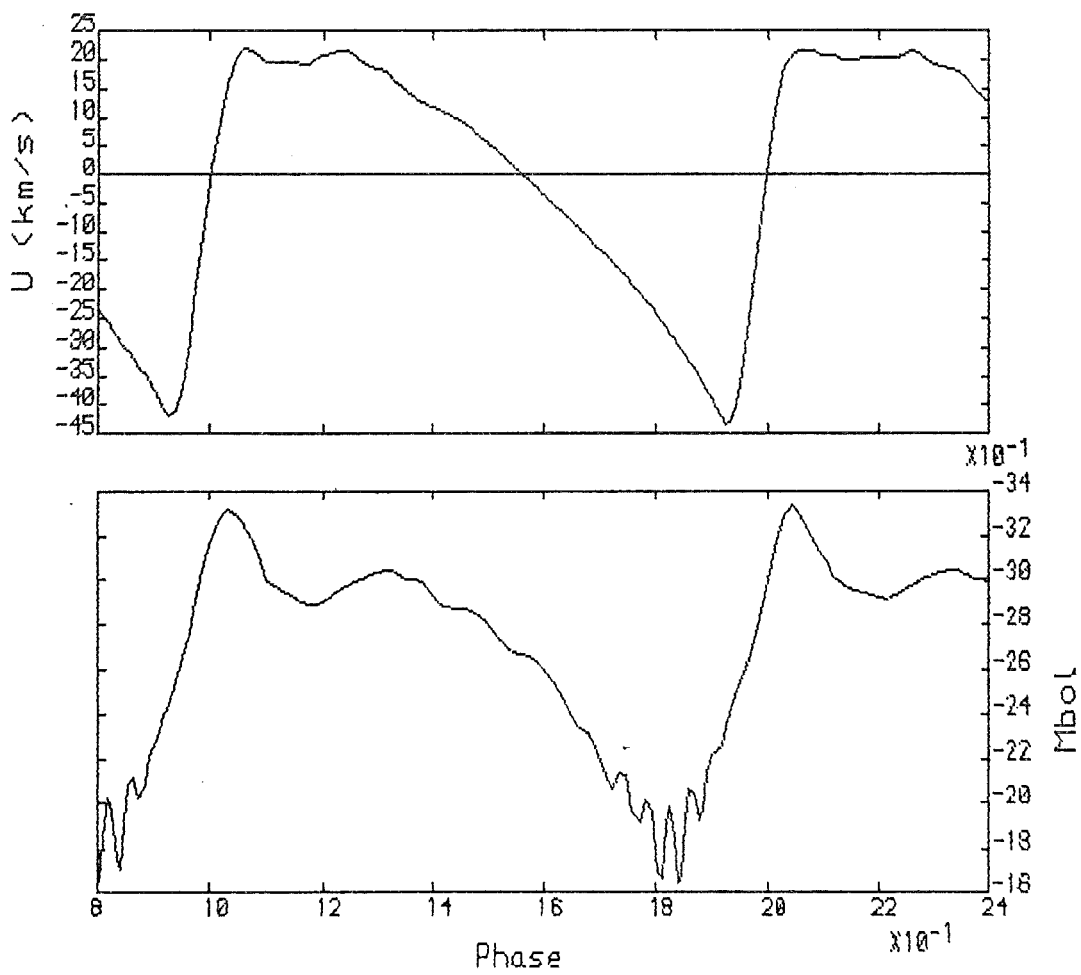


Figure 6.29 Model 51 $P = 17.8$ days

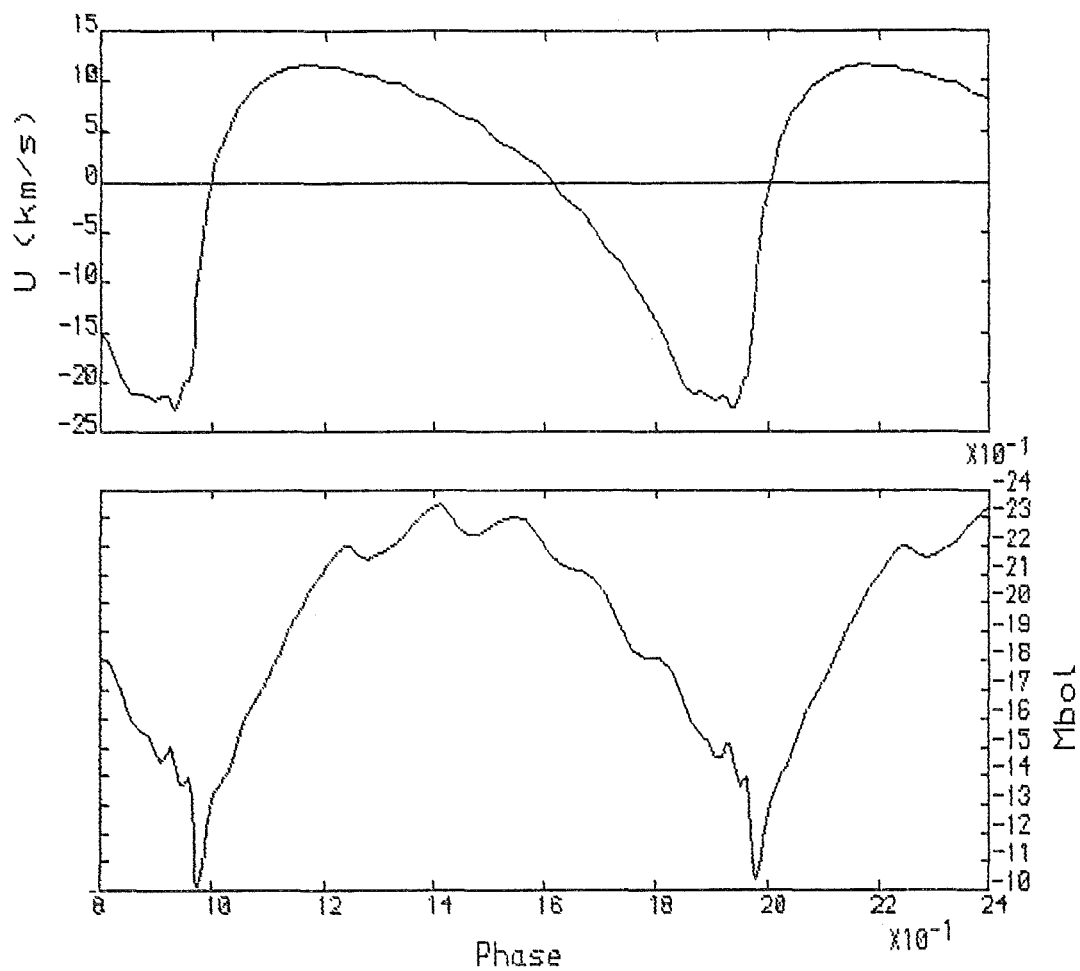


Figure 6.30 Model 81 $P = 11.3$ days

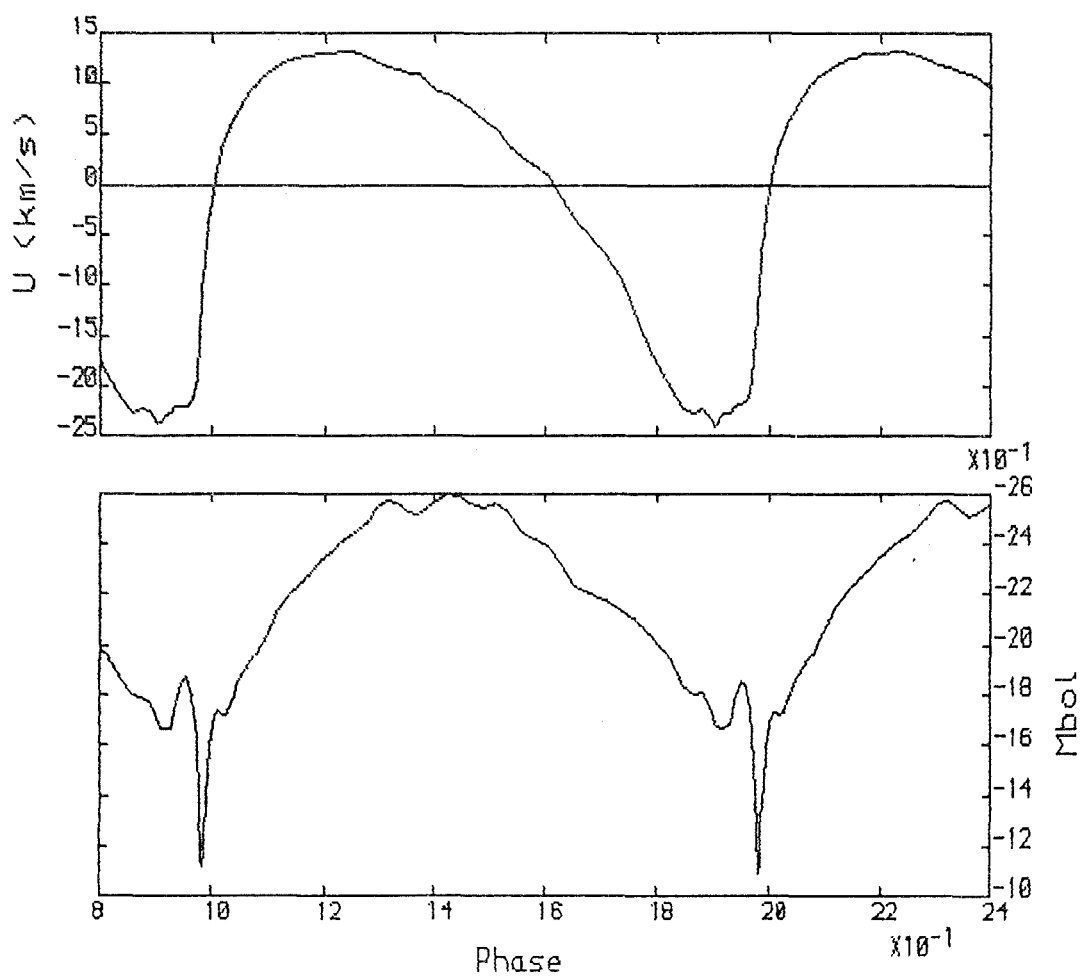


Figure 6.31 Model 82 $P = 12.0$ days

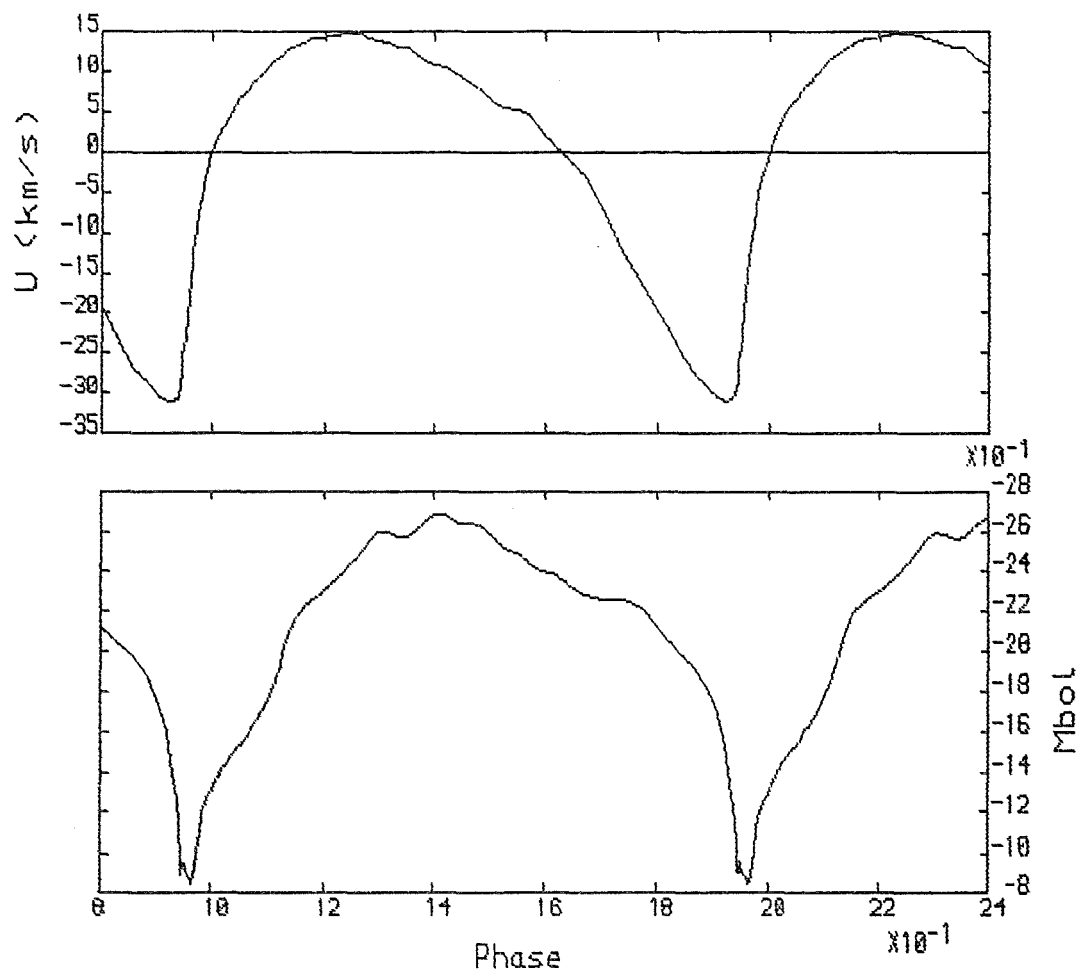


Figure 6.32 Model 83 $P = 13.7$ days

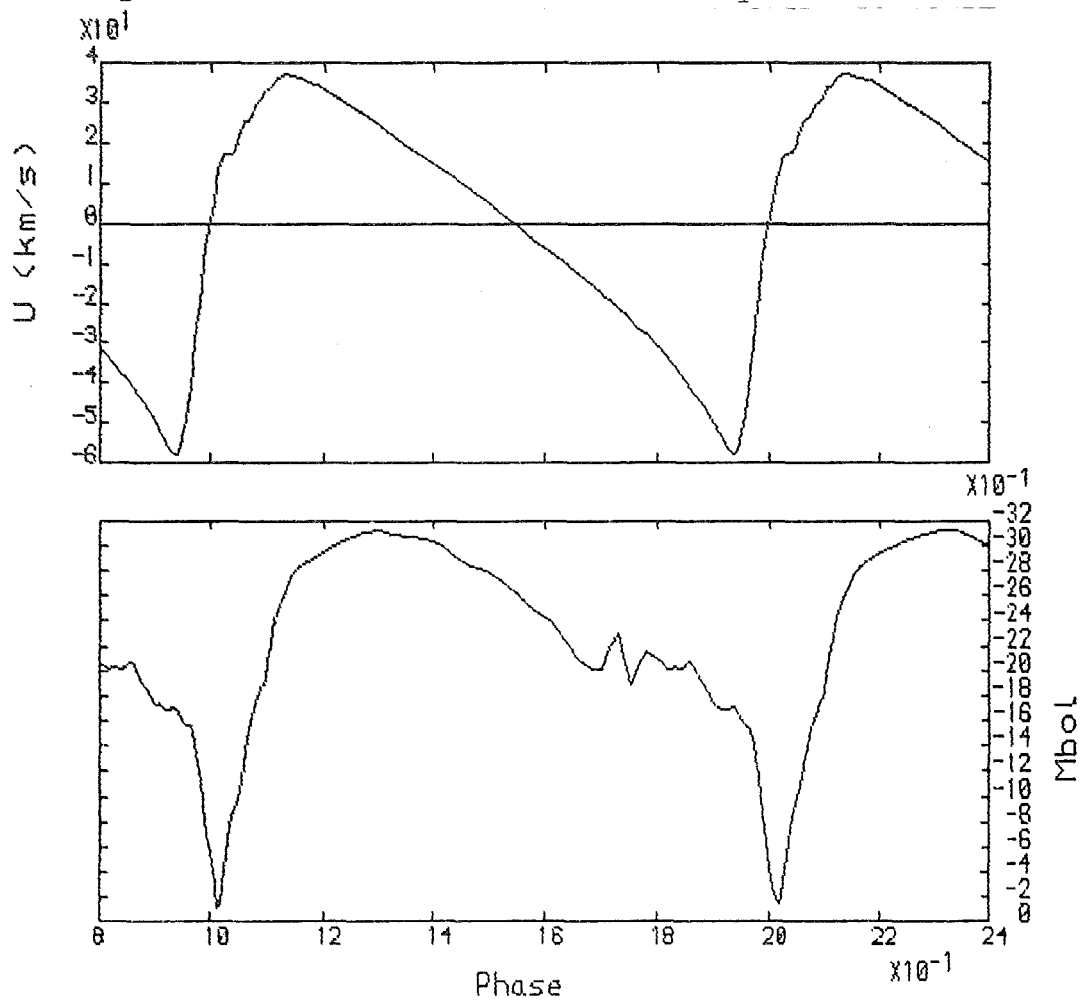


Figure 6.33 Model 84 $P = 17.0$ days

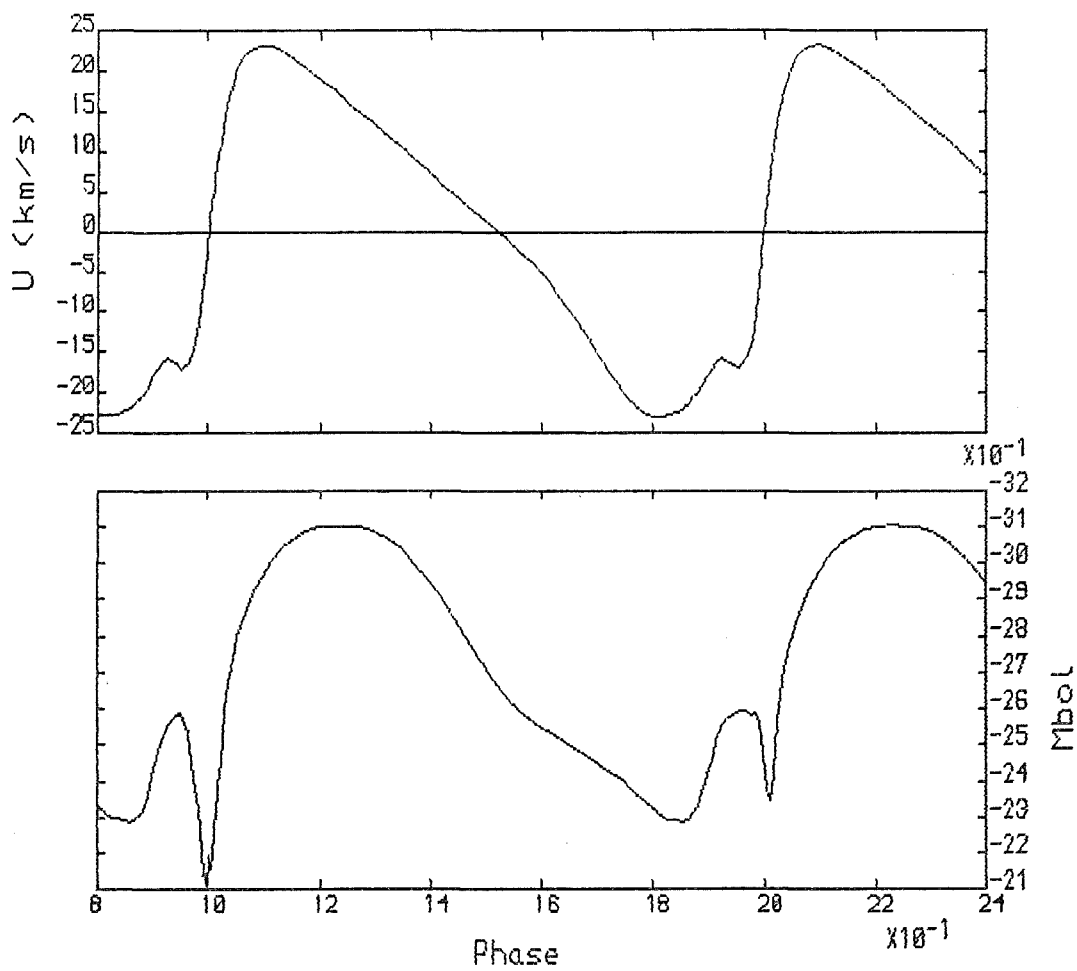


Figure 6.34 Model 85 $P = 12.7$ days

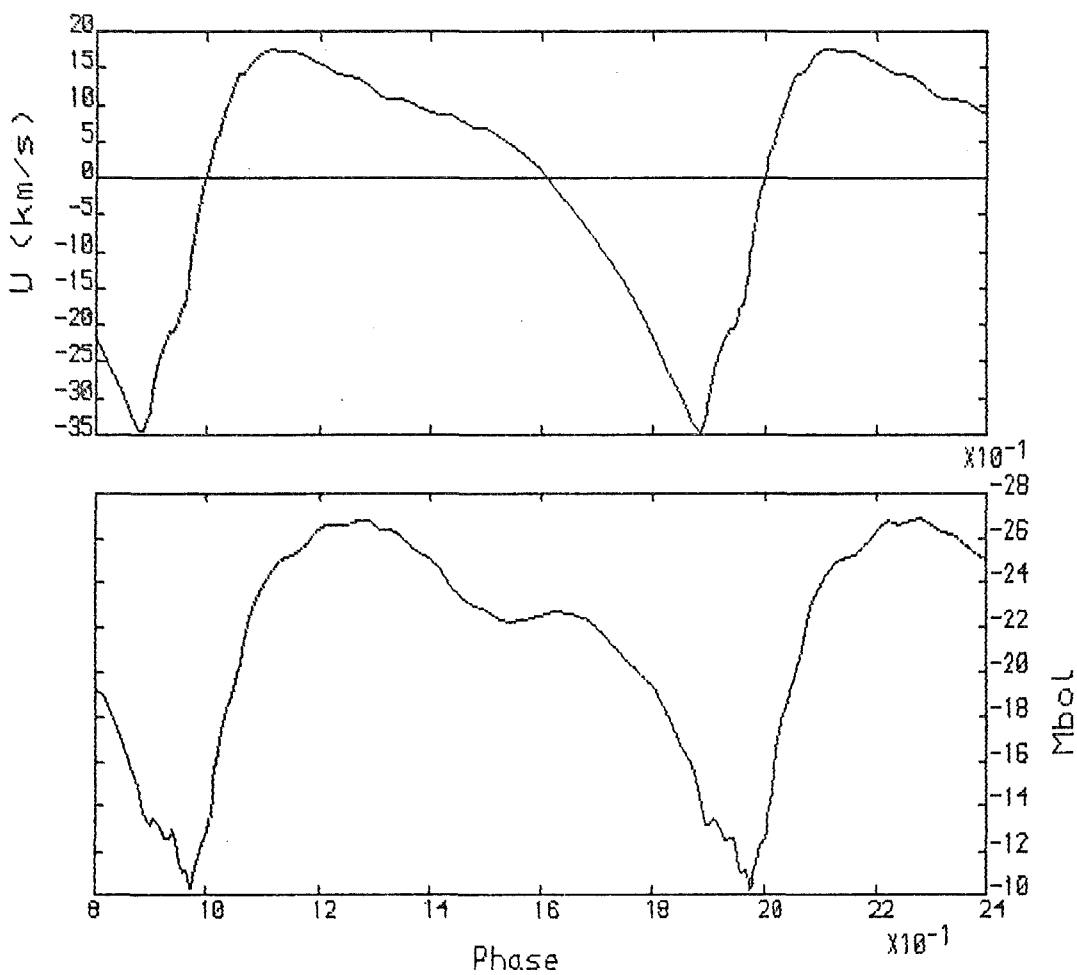


Figure 6.35 Model C1 $P = 13.9$ days

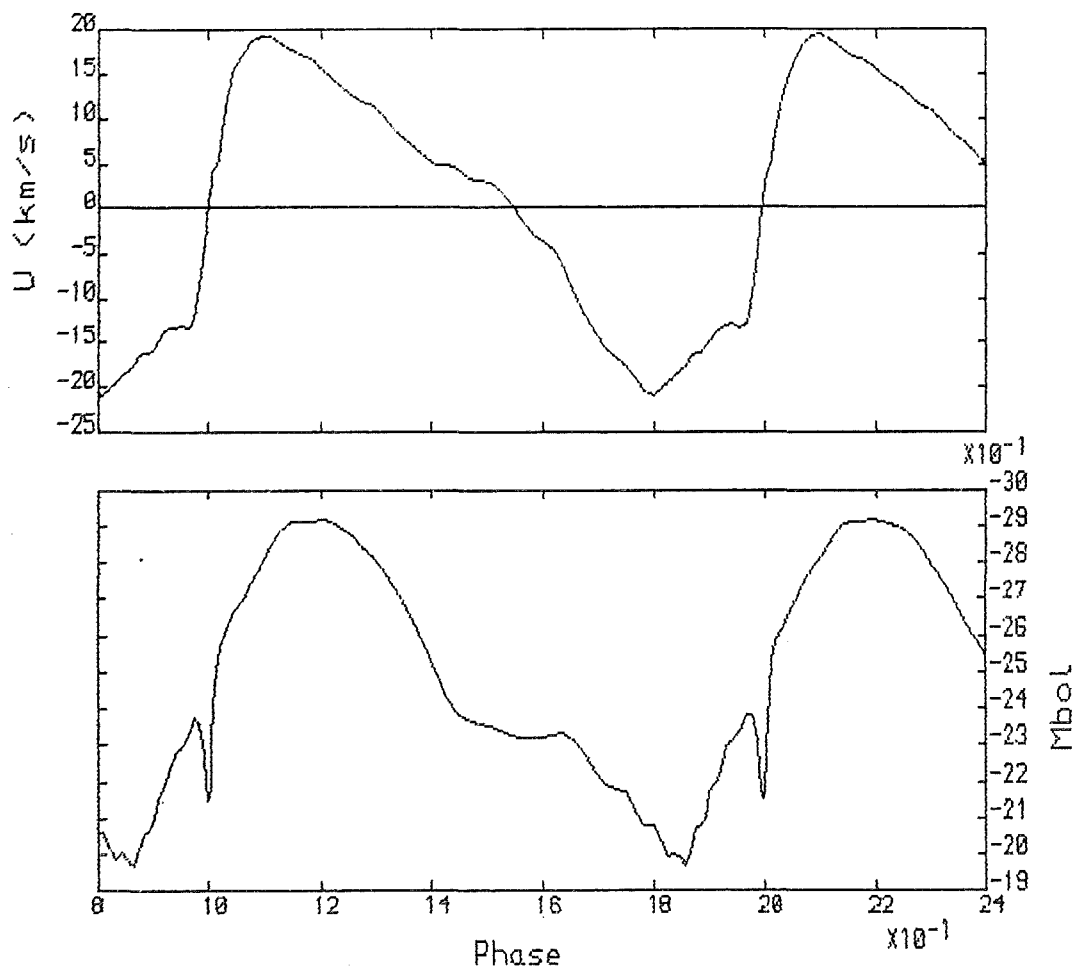


Figure 6.36 Model C2 $P = 13.4$ days

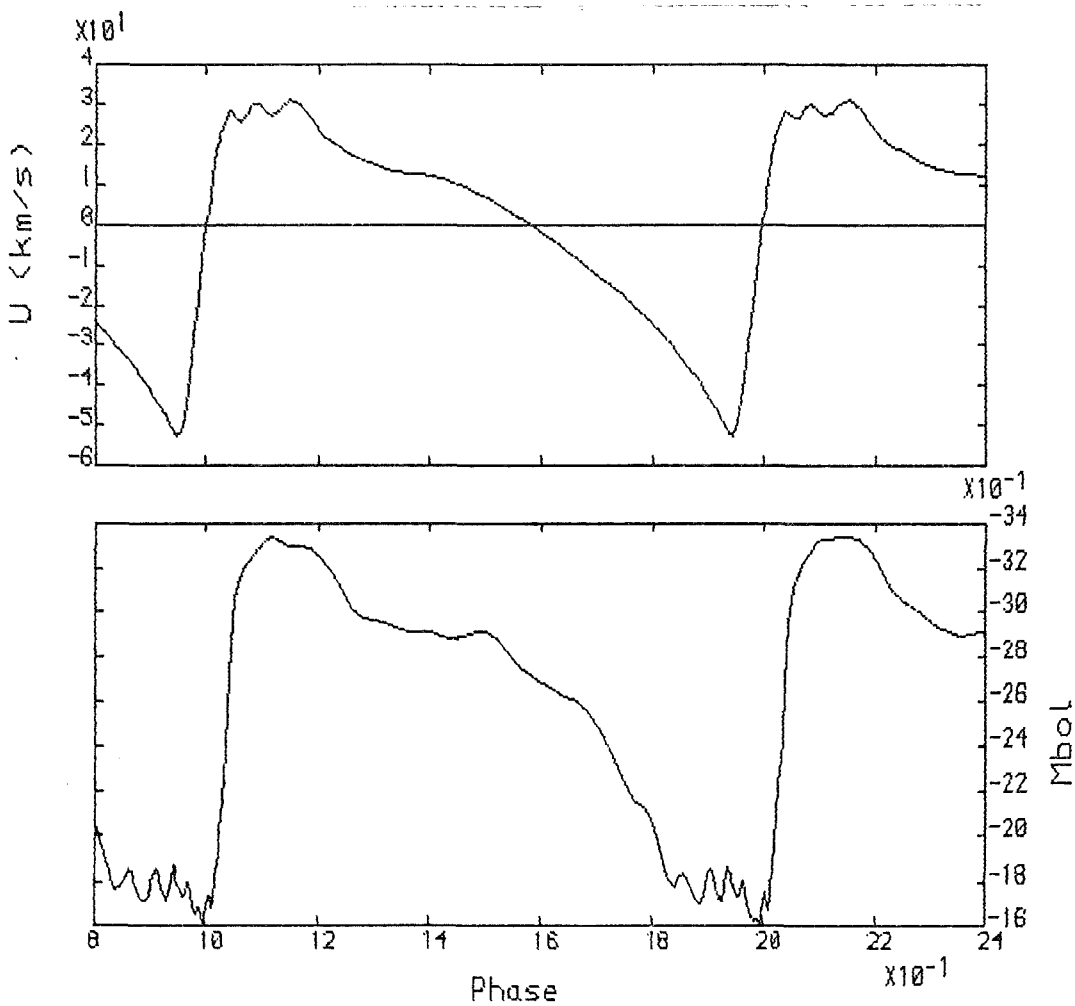


Figure 6.37 Model K1 $P = 16.0$ days

6.4 THE STATIC MODELS

For some of the models, the total number of zones used was surprisingly small, ~ 30 . Despite this small number of zones, the accuracy would seem to be good, since α , the mass ratio between zones, is still quite small, $1.1 < \alpha < 1.3$, and a repeat run for one model showed no improvement in accuracy when using 50 zones. This is a result of the low envelope mass of these stars. For all the models, there were about 1 - 3 zones in the hydrogen ionization region. An example of the relaxed equilibrium zoning is shown in figure 6.38. The hydrogen ionization region is the only region not well covered, but, with the artificial viscosity, 1 - 3 zones is usually sufficient. In only a few models were bumps due to the zoning apparent (generated as the hydrogen ionization front slips from one zone to another during the pulsation). These bumps were more apparent in the $0.8 M_{\odot}$ models.

In the plot of opacity through the star there is a bump at $\log T \sim 5.6$, at the base of the envelope. This is due to the C-O bump described in section 5. In the models using the Cox opacities this feature does not appear.

6.5 GENERAL FEATURES OF THE SURVEY MODELS

In discussing these results there are several features to look at: Trends and individual features in the calculated models, including a P-R or P-L- T_e relation, and the comparison of these with observations. Do we find similar periods, light curves, and amplitudes? For W Virginis stars in particular, do

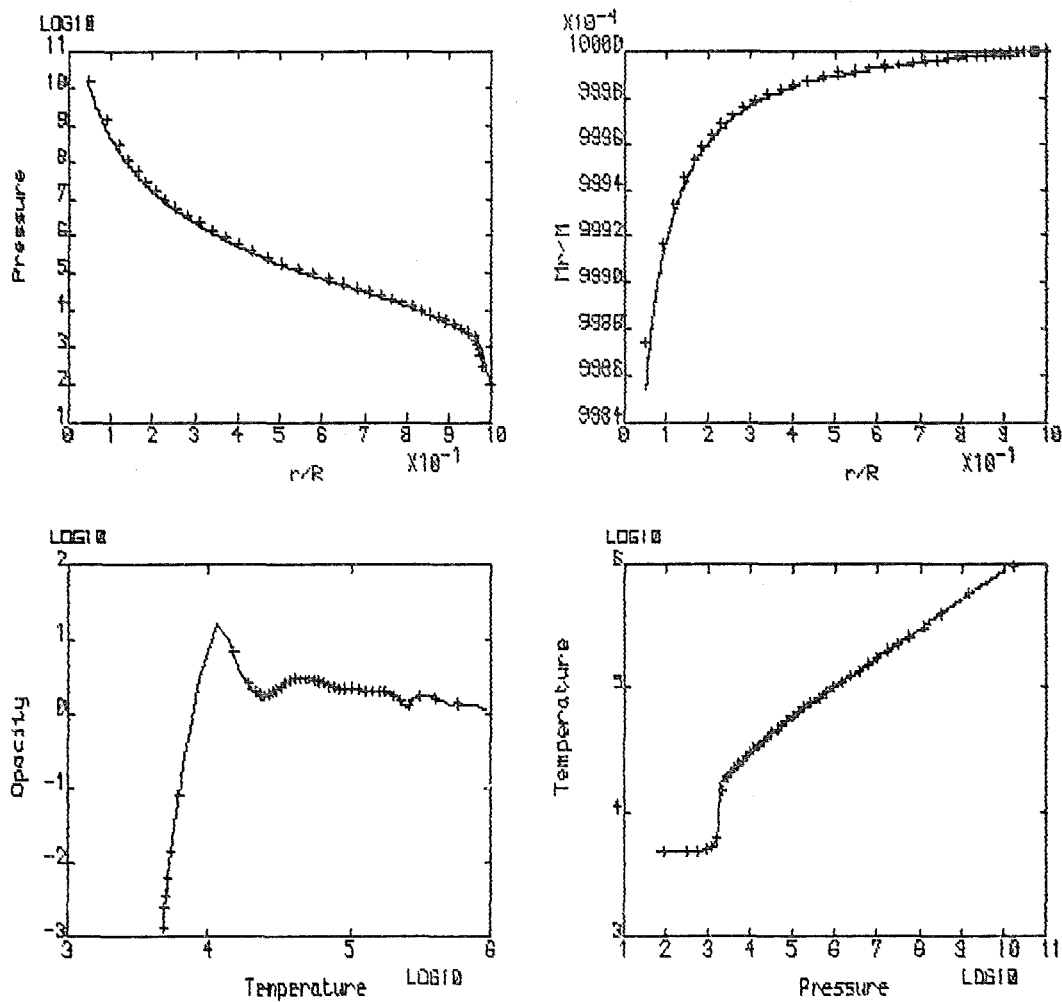


Figure 6.38 Relaxed static envelope for model 18
The line shows the integrated envelope,
and the crosses show the relaxed zones

the modelled light curves show the same dichotomy of crested and flat-topped, with a few looking like neither or possibly as if they were halfway between? Finally, is it possible to model individual stars with accuracy?

In addition to making comparisons with observations, we can look at the effect of changing the mass, and do some comparison with models made using the Christy opacity formula and the Cox-Tabor King Ia mix.

Classifying the modelled light curves is sometimes as difficult as classifying the observed ones. Although many are obviously crested, or flat-topped, or neither, a few seem to present a halfway state. For example, although the curve for model 15 has a pronounced dip following the first maximum, the following bump or shoulder is at the same height as the maximum; thus it might easily be classified as flat-topped. Similar arguments apply to a few curves. Also, for some curves which might be classified as X-type, there is a suggestion of a secondary bump, thus they might be almost of the crested variety.

Remaining with the general features of the light curves, many of the models show a pre-maximum shock, like that seen in the CSV1 test model curve. Some of the observed curves (particularly V741 Sgr, CZ Sct, AL Sct) show some evidence of such a shock, and it may be that the observations are in general insufficient to detect this feature should it be present, since it only lasts for a small fraction of the period. These shocks are frequently present in the X-type, or unclassified curves. In addition these curves only occur for $P < 13$ days, very much in agreement with the observations.

Displaying the models on an HR diagram (figure 6.39) we see grouping into crested and flat-topped types in general agreement with the observations, though slightly brighter and cooler. This is within the range of likely observational errors, and in any case may be corrected by an acceptable change in mass and/or composition. (In this diagram, and others following, the same procedure was adopted as in describing the observed stars. Open circles are C-type, filled are F-type, those half-filled are C/F and circles with crosses represent either X-types or XC-types.)

Lower luminosity X-curves also seem to lie in the right place, but there is no observational equivalent of the X-curves at high $\log T_e$ and $\log(L/L_\odot) = 2.9 - 3.0$.

It can be seen that there are unstable models to the blue side of the observed blue edge. Given the possible errors associated with the observed edges, as mentioned in section 2.2, this should not be cause for concern. Reduction of M/M_\odot and/or the helium abundance could provide much better agreement without altering the pulsational properties too significantly (For example see model 51, with $M/M_\odot = 0.5$). The approximate non-linear blue edge would seem to be in agreement with the Worrell linear blue edge for the same mass and composition, as presented in section 2.3.

The growth rates of the models were generally quite fast. For some of the redder models the e-folding time was only 3 or 4 periods, though more generally the e-folding time was about 10 - 20 periods. Near the blue edge, where the models are less unstable, this increased to about 40 - 50 periods. For a few

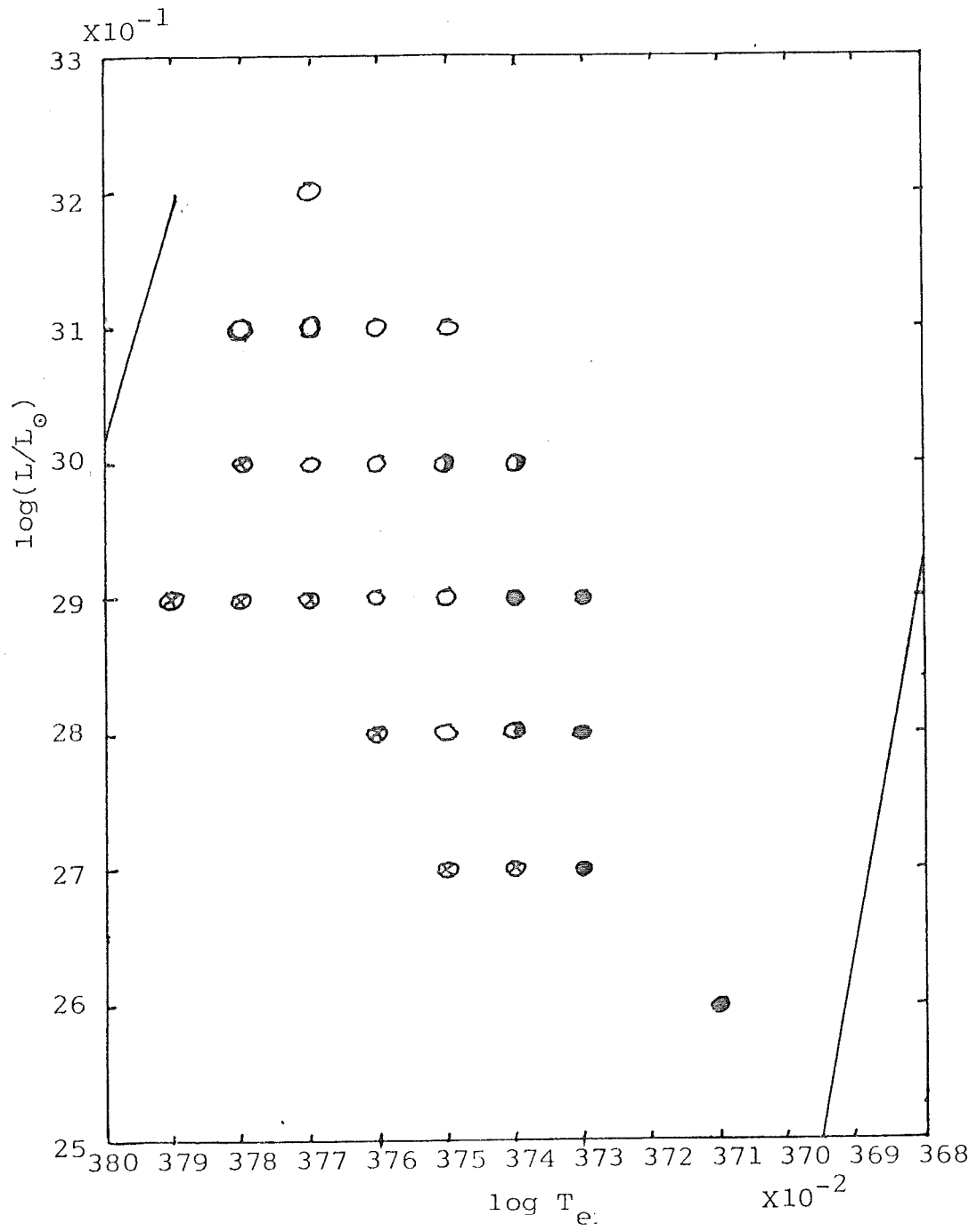


Figure 6.39 The survey models on an HR diagram

models, although the growth rate was large and the model reached full growth in about 10 - 20 periods, there followed a number of periods when the star had not settled into its final state. During this time, the amplitudes and periods alternated high and low, generally only by approximately $\pm 5\%$. For most such models, this behaviour died down, but for a few it persisted. In particular, model 14 exhibited very strange behaviour. These cases are discussed later. In the case of model 20, the star only settled into a good repetitive state after the outer boundary radius had escaped, having reached escape velocity. This interesting case is also discussed later, in connection with possible RV Tauri behaviour (see section 6.12). This loss of the outer zone brings up the question of the effect of the outer boundary condition. The majority of the models were run with the approximation to $P_g = 0$ as the outer dynamic boundary condition (equation [3.20b]). Model 8 and some of the comparison models were run with the third choice, equation (3.20d). In the case of model 8, use of this boundary condition allowed the model to run; previous attempts with the second choice had failed. The outer zone had almost escaped, causing the run to halt because of numerical difficulties caused by low densities. (These numerical problems did not occur in the case of model 20 mentioned above, allowing it to run to completion). Use of the new boundary condition solved the problem, although the model was still the same in behaviour and so presumably only just avoided failure. All attempts to model a star at $\log(L/L_\odot) = 2.8$, $\log T_e = 3.72$ failed.

Use of a larger value of α , the mass ratio between zones, also helped here. Although this caused the model to have fewer zones, it probably did not affect the results significantly. A test run of another model (number 13) was made with about 10 fewer zones to see what effect this might have (this model originally had 41 zones). No significant changes from the original model could be seen.

We also consider the effects of changing the parameters C_Q and α_V . the value of C_Q most used was 2.0, although values between 1.0 and 4.0 seemed to have much the same effect. Below 1.0 a noticeable loss in stability of the light and velocity curves could be seen. Above 4.0 the hydrogen ionization front becomes much too spread out. Similarly, the exact value of α_V had little effect, as long as $\alpha_V \leq 0.1$ times the local sound speed. Larger values caused the viscosity to be cut-off by too great an extent.

6.6 THE PERIOD-MASS-RADIUS RELATION

The log P-log R diagram for the models with $M/M_\odot = 0.6$ is plotted in figure 6.40. The values of $\log(R/R_\odot)$ used were calculated from $\log(L/L_\odot)$ and $\log T_e$, to follow the method used for calculating the observed P-R relation. For all types the P-R relation turns out to be:

$$P = 0.041(R/R_\odot)^{1.72} \quad (6.1)$$

which lies above and to the left of the P-R relations for $M/M_\odot = 0.6$ of CSV and Pohn-Vitense et al. (1974). This is explained by the larger amount of non-linearity in the

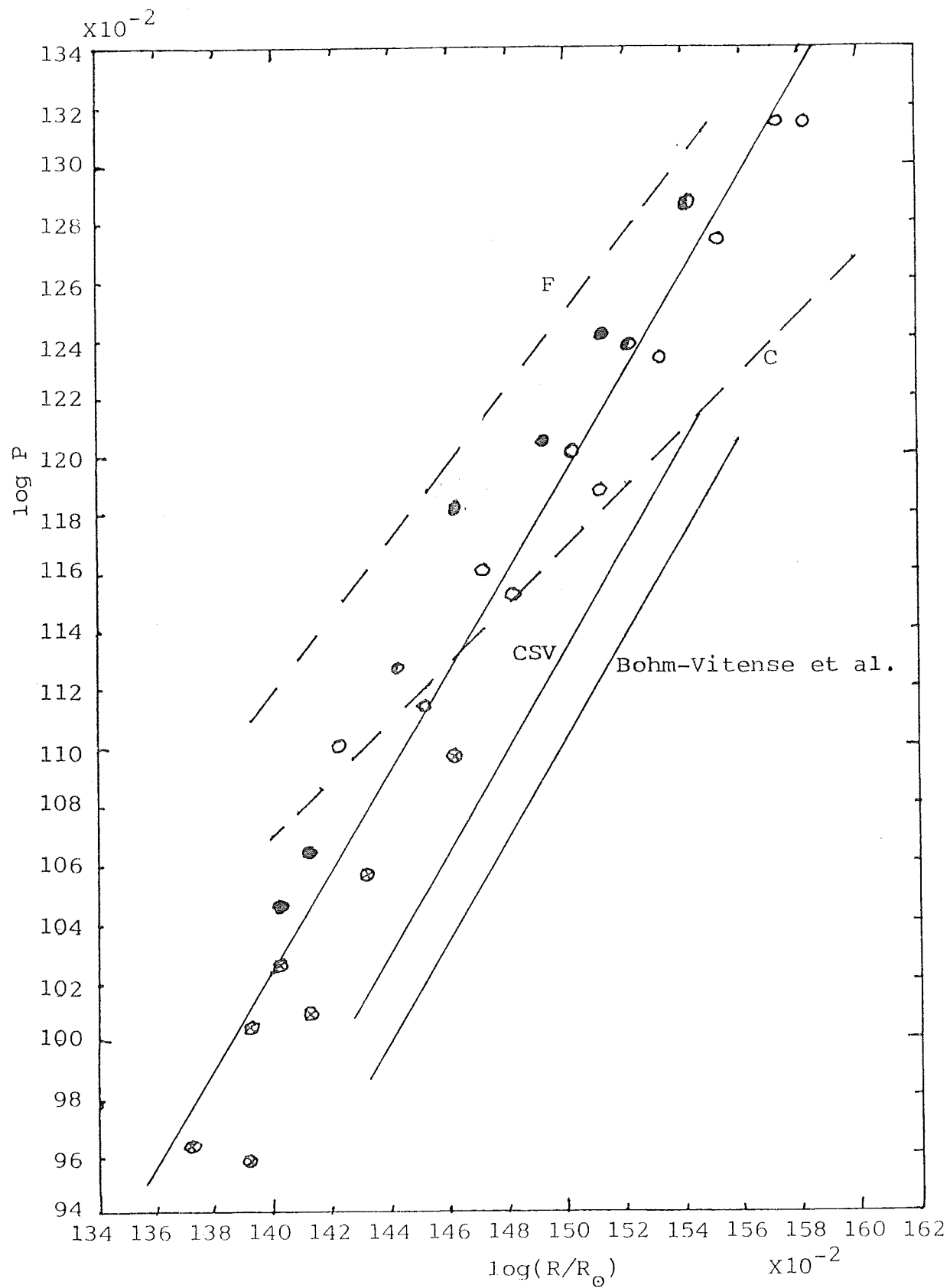


Figure 6.40 The $\log P$ - $\log R$ relation for the survey models

pulsations of these stars. This causes longer periods than would be predicted by linear methods, and hence a P-R relation higher in the P-R plane.

The high non-linearity and large amplitudes probably also account for the models not following the P-R relation exactly. The different models will have different amounts of deviation from linearity, and thus form a strip in the P-R plane rather than a line.

By also using the results for $M/M_{\odot} = 0.5$ and $M/M_{\odot} = 0.8$, we find a theoretical P-M-R relation of:

$$P = 0.029(R/R_{\odot})^{1.72} (M/M_{\odot})^{-0.72} \quad (6.2)$$

The powers agree well with Bohm-Vitense's result. The difference in the multiplying constant (and the position of the P-R relation) is probably due to the fact that both CSV and Bohm-Vitense et al. used all or mostly BL Herculis variables, those with $P < 3$ days, in their calculations. Here we have restricted ourselves to stars with $10 < P < 20$ days.

Bohm-Vitense et al.'s relation was:

$$P = 0.023(R/R_{\odot})^{1.72} (M/M_{\odot})^{-0.72} \quad (6.3)$$

and CSV's theoretical P-M-R relation:

$$P = 0.022(R/R_{\odot})^{1.75} (M/M_{\odot})^{-0.75} \quad (6.4)$$

Whilst admitting the scarcity of the observational data, it is clear that the results for the models calculated here agree with the observed P-R relation(s) (also plotted in figure 6.40) to well within any estimated errors. In the theoretical

P-R relation, it is possible to see a difference between the crested and flat-topped types, a split into two relations, but only by a small amount. The lack of clearly flat-topped modelled light-curves also make it difficult to be sure of a differentiation in the P-R plane. However, such distinction as exists is in the correct direction.

It is worth pointing out that the theoretical P-R relation found here is based on models of constant mass. The separation of the observed c and f classes could be due to a difference in mass, even a slight difference sufficing to separate the relations by a significant amount. If for the purpose of this discussion we assume that the crested and flat-topped variables follow identical P-M-R relations and that their $\log P - \log R$ relations are parallel, differing only by virtue of having different masses, then we may estimate the ratio M_C/M_F , where M_C is the mass of a crested variable and M_F is the mass of a flat-topped variable. We obtain a relation (for constant radius, R/R_\odot) of the form,

$$P_C/P_F = (M_C/M_F)^\gamma \quad (6.5)$$

where P_C is the period of the crested variable of a given radius and P_F is the period of a flat-topped variable of the same radius. Taking γ (the power of the mass variable in equations [6.2] - [6.4]) to be -0.72 we obtain an average result for the two observed P-R relations of

$$M_C/M_F \approx 1.3$$

So, for instance, if the mass of a flat-topped variable is approximately $0.55 M_\odot$, then the mass of a crested variable would be about $0.7 M_\odot$. This agrees very well with the

currently accepted average mass of these variables and also very well with the approximate range of possible masses as defined by evolutionary ideas (see section 2.2). A likely conclusion here is that the mass of a population II star ascending the Red-Giant branch determines when (and, on the HR diagram, where) it will undergo a "blue-loop", taking it into the instability strip. This in turn determines what type of type II cepheid it becomes, crested or flat-topped in the Kwee definition. Of course, we are not dealing here with a strict dichotomy but rather with a range of possibilities, governed by the limiting masses of stars undergoing blue-loops that take them into the instability region, say those with masses $0.5 \leq M/M_{\odot} \leq 0.75$. At the lower end of this range the star leaves the giant branch rather early and gives rise to a low-luminosity flat-topped type II cepheid. At the other end of the range the higher mass stars leave the giant branch later and produce the higher luminosity crested variables. In between these extremes it is possible to get the stars of doubtful classification, having slight characteristics of both kinds.

Now looking again at the theoretical models we have to bear in mind the fact that those plotted are all of the same mass, $0.6 M_{\odot}$. It is easy to imagine a wider spreading of the C- and F-types if a lower mass had been used to obtain F-type models and a higher mass to obtain C-types. The only result obtained for a lower mass ($0.5 M_{\odot}$, model 51) in fact turns out to be crested, but that is because the luminosity and effective temperature were deliberately chosen to compare with model 18 (i.e. with a C-type light curve). The higher mass stars are all of $0.8 M_{\odot}$, at the edge of the acceptable mass range, and

possibly outside it. It is significant that most of the light curves for these models do not really resemble either C- or F-types. It may be that they are of an unrealistically high mass, and so in this period range do not produce light curves that are observed.

6.7 THE LIGHT AND VELOCITY CURVES

Turning our attention to the features of the light and velocity curves we first look at their amplitudes. In order to compare the computed light amplitudes with observed ones it is necessary to translate the bolometric magnitude amplitudes (ΔM_{bol}) into visual magnitude amplitudes (ΔM_V). This relation is not easy to define, being dependent upon the variation of $\langle B-V \rangle_0$ during the pulsation. An approximate idea can be obtained if we assume limits to the $\langle B-V \rangle_0$ variations of these stars of about 0.4 to 0.9. This would give, for most of these stars, a correction to ΔM_{bol} of about +0.2 to +0.4. So we can say

$$\Delta M_V \simeq \Delta M_{bol} + (0.2 \longleftrightarrow 0.4) \quad (6.6)$$

For the $0.6 M_\odot$ models the range of values of ΔM_{bol} is from 0.49 to 2.6. With the adjustment above we would get a likely range for ΔM_V of about 0.7 to 3.0. The lowest amplitudes (which are for classless curves of stars near the blue edge) agree well with the lowest observed visual amplitudes, which are also for classless light curves. Amplitudes as large as 3.0 are not observed in the 10 - 20 day types II cepheids, the largest being ~ 1.5 mag. Those models with large light amplitudes frequently show a pronounced "dip" in the light

curves, just before the rise to maximum. The cause of this dip is unknown, and may or may not be a "real" feature. However it does increase the amplitude of the light curve by considerable amounts (maybe even doubling it) and is sometimes quite sensitive to the smoothing of the light curves, indicating variation on quite a small time scale. However, whether or not this dip is ignored, there is still a discrepancy between theory and observation here. A similar dip also occurs in model C2, although it is not large enough here to affect the amplitude. This may indicate that it is not an effect of the opacity, but more models using the Los Alamos opacities would be required to check this.

The probable cause of the difference in amplitudes of the theoretical and observed models is the assumption of no convection used in the modelling. The models that show large light amplitudes are those at the long period end of the range, also lying to the red side of the instability strip. This is exactly where convection would have most effect (see section 6.1) and we are almost certainly seeing the effects of ignoring it for some of these stars. What effect convection might have on the aforementioned dip in the light curves is not known, but it might calm the oscillations of some of these redder models, which were very difficult to build because the amplitudes grew to be so large.

There are two major trends in the amplitudes of the light curves, increasing ΔM_{bol} with period, and increasing ΔM_{bol} as the effective temperature decreases. The latter is to be expected because of the increased driving as the red edge of the instability strip is approached. Since period increases

this way as well the former trend follows. There is no particularly obvious trend with respect to changing luminosity.

The range of velocity amplitudes lies between about 40 and 90 km/s. The previous arguments about the lack of convection still apply in the case of the velocity amplitudes, so some overestimation of the amplitudes may have occurred. There is also the multiplying factor of 24/17 to be applied to the observed velocity curves to correct for line of sight and limb-darkening effects. This is almost academic because of the paucity of observed velocity curves. In the case of W Virginis this gives an amplitude of 78 km/s, and for M12 No. 1 and M10 No. 2 we get 42 km/s and 119 km/s respectively (note that these two curves are rather poor). The velocity amplitudes therefore lie in the correct range, but no firm conclusions can be made. Like the light curves, there is a tendency towards greater amplitudes at longer periods and cooler effective temperatures.

As expressed in section 2.2 the most important features of the observed light curves are the shapes, and the bump and phase details. These details can also be measured for the calculated models, more easily than for the observed curves. In figures 6.41a and b the phases ϕ_b^l and $\phi_b^l - \phi_m^l$ are plotted against period, luminosity and effective temperature for the survey models. For C-type models we find a mean $\phi_b^l = 0.49 \pm 0.04$ and for the F or C/F curves the mean ϕ_b^l is about 0.36 ± 0.04 (comparing with 0.44 ± 0.03 and 0.34 ± 0.05 respectively for the observed light curves).

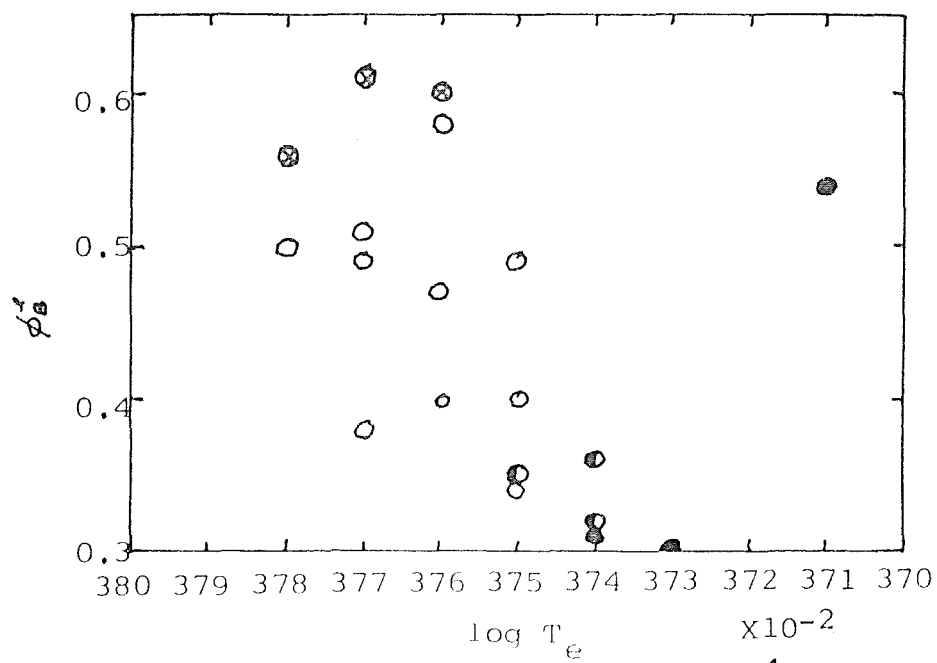
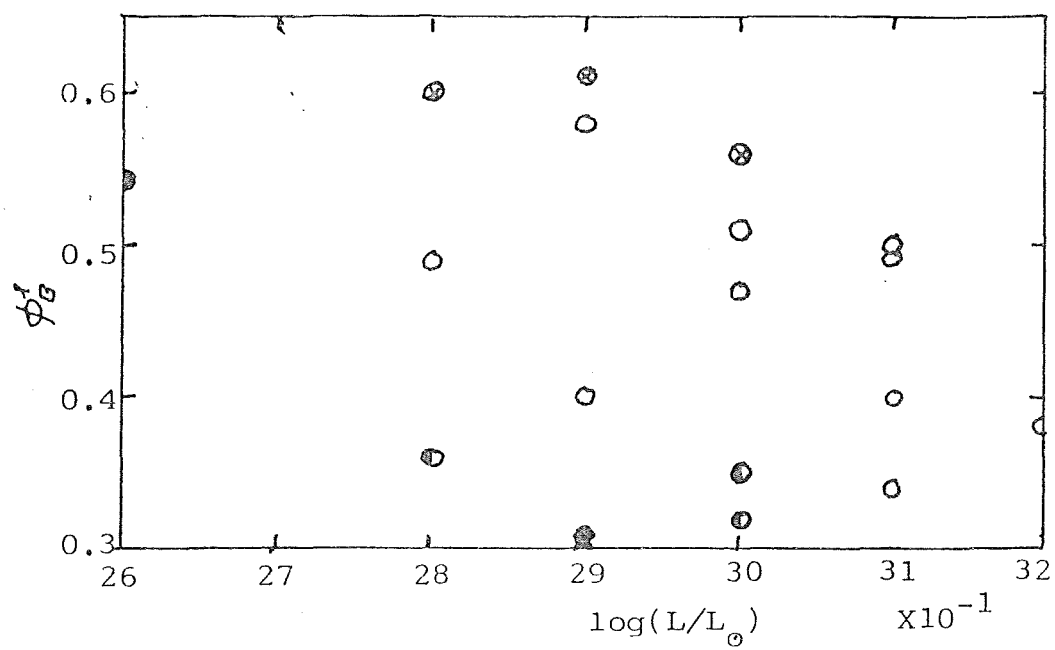
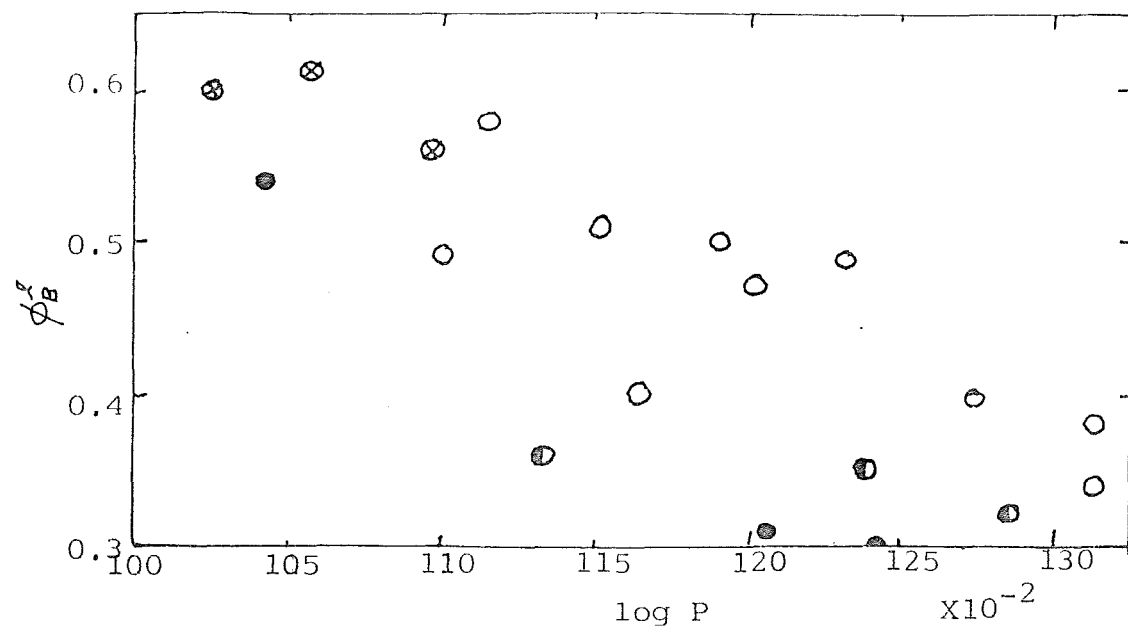


Figure 6.41a The variations of ϕ_B^l for the models

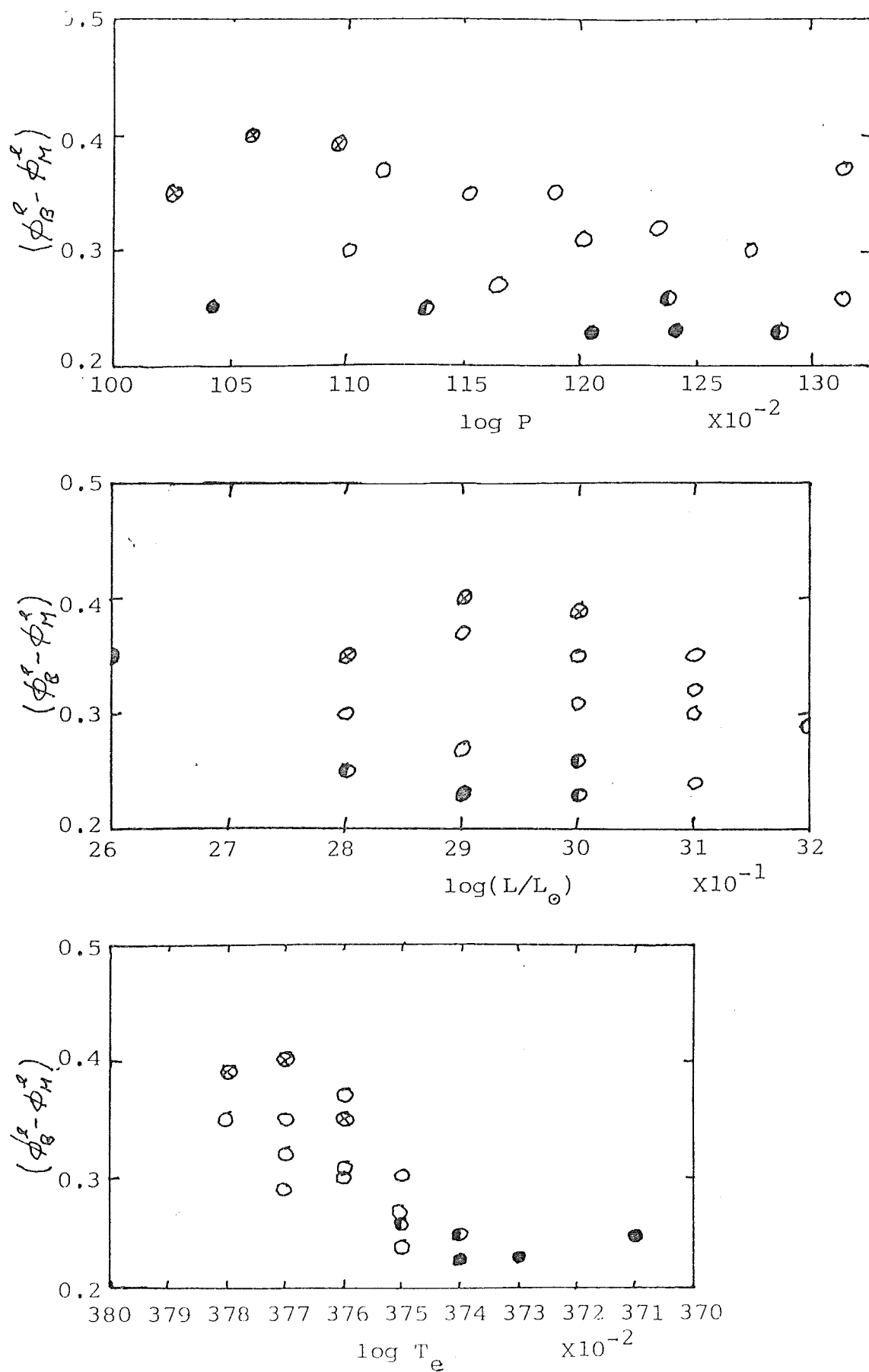


Figure 6.41b The variations of $\phi_B^p - \phi_M^p$ for the models

The best phase difference to measure is probably $\phi_b^l - \phi_m^l$, the phase of the secondary bump on the light curve minus the phase of maximum light. For the C-type curves an average value for $\phi_b^l - \phi_m^l$ of 0.33 ± 0.04 is obtained. For the F and C/F-types $\phi_b^l - \phi_m^l = 0.24 \pm 0.02$ (for just the F-types this might be slightly lower, ≈ 0.23). For the observed curves we found $\phi_b^l - \phi_m^l = 0.29 \pm 0.02$ for the crested curves and $\phi_b^l - \phi_m^l = 0.23 \pm 0.02$ for the flat-topped curves that have discernable secondary bumps. This is really very good agreement with observation, within either the estimated theoretical or observed error limits. It was decided to use $\phi_b^l - \phi_m^l$ as a measure of the bump because ϕ_o^l (phase of mean light on the ascending branch) can be very difficult to determine from observational data, since it is very susceptible to subjective decisions and errors in the observations (compare light curves for the same star produced by different observers). ϕ_m^l is also susceptible to these errors, but to a lesser extent. As for the general shapes of the light curves, it looks as though the crested types observed curves can be reproduced very well, and in the variety observed, by the C-type theoretical curves. The flat-topped curves cannot be reproduced as well, but curves in between, the c/f-type curves seem also to be well represented in the modelling.

The inability to faithfully reproduce well the f-types curves is probably due to the omission of convection as a method of energy transport, discussed elsewhere. At the stellar parameters likely to produce good F-type curves the models begin to fail for the reasons given previously (section 6.3).

The calculated velocity curves can be looked at in the same way as the light curves, with the exception of the comparison with observation. For the observed velocity curves that exist the general conclusion (section 2.2) is that the curves are highly asymmetric (discontinuous). This feature is generally found in the calculated curves as well. Secondary bumps are present, but there is not always a clear velocity bump when there is a light bump. This usually occurs when $\phi_b^v - \phi_m^l$ is small, for a C/F or F-type curve, and any secondary velocity bump is likely to coincide with the velocity maximum.

The difference $\phi_b^v - \phi_b^l$ is a varying quantity with an average value of ~ 0.03 . In their work on BL Herculis variables, CSV found $\phi_b^v - \phi_b^l \simeq 0.0$, so there would seem to be a significant difference here. It is probably too simple to treat these stars as merely long period extensions of the BL Herculis variables.

The causes of the secondary bumps on the light and velocity curves are discussed in section 6.9

6.8 TRENDS IN THE LIGHT AND VELOCITY CURVES

The trends of some aspects of the light curves with changing luminosity and effective temperature are discussed under the section dealing with that aspect. Here we discuss the trends in the shapes of the light curves, which include the secondary bumps and bump phases.

In the observational data we saw the dichotomy of F and C-type light curves and contended that there might be a continuous, though possibly sudden, progression between these types as $\log(L/L_{\odot})$ and $\log T_e$ were altered. In the theoretically modelled light curves we see a much firmer case for this contention.

Figures 6.42 - 6.52 show the trends in light curve for various constant values of $\log(L/L_{\odot})$ and $\log T_e$. If we take a line of constant luminosity (for instance the $\log(L/L_{\odot}) = 2.9$ series) and reduce $\log T_e$ we may be seeing a change from X-type light curves, through XC, C, and C/F all the way to F-type. For extremes in luminosity this may not be the case. For $\log(L/L_{\odot}) < \sim 2.8$ the luminosity is too low to produce crested curves, and for $\log(L/L_{\odot}) > \sim 3.1$ it maybe too high to produce flat-topped curves. We also see here a tendency for $\phi_b^f - \phi_m^f$ to decrease, suggesting that the merging of the light maximum and the secondary bump may produce the flat-top in the F-type curves.

When looking at lines of constant effective temperature, similar trends are seen. For low $\log T_e$ ($\sim 3.73 - 3.74$) as $\log(L/L_{\odot})$ increases the light curve retains the features of an F-type curve, though it may develop a slight crest at the highest value of $\log(L/L_{\odot})$. At higher luminosity the curves may well become crested, but here the periods stretch beyond the range studied, and the models become harder to produce. These stars (maybe the RV Tauri variables) could be the subject of a later study.

Figures 6.42 to 6.52 show the trends in the light curves for various constant values of $\log L/L_{\odot}$ and $\log T_e$. Phase is measured from minimum radius

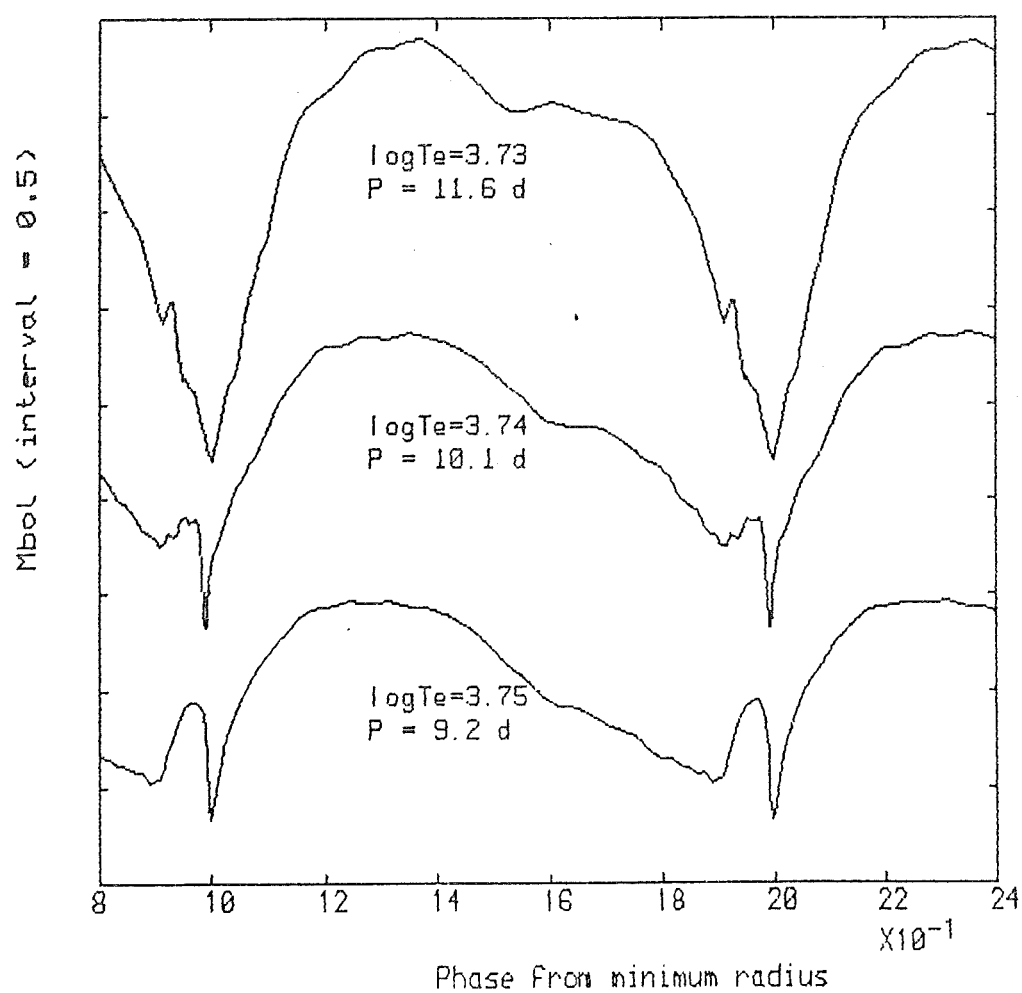


Figure 6.42 Light curves for $\log L/L_{\odot} = 2.7$

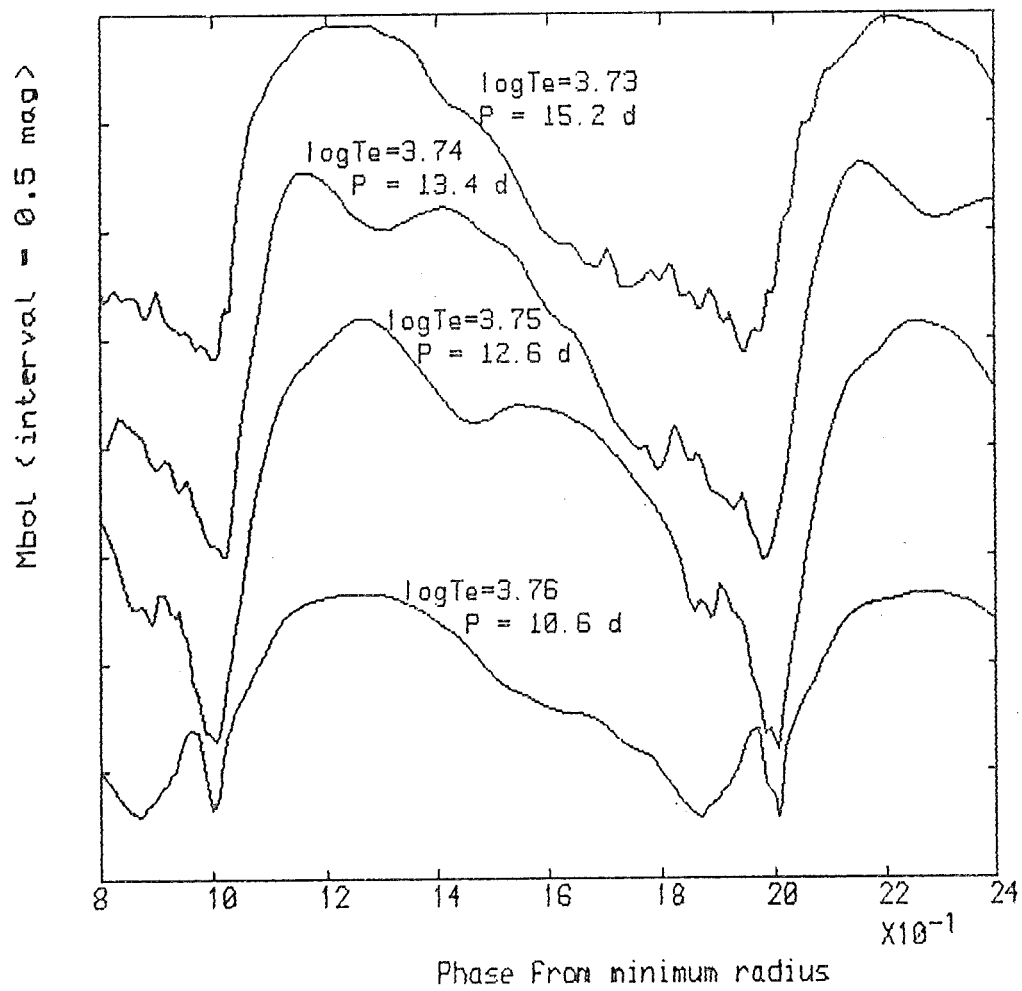


Figure 6.43 Light curves for $\log L/L_{\odot} = 2.8$

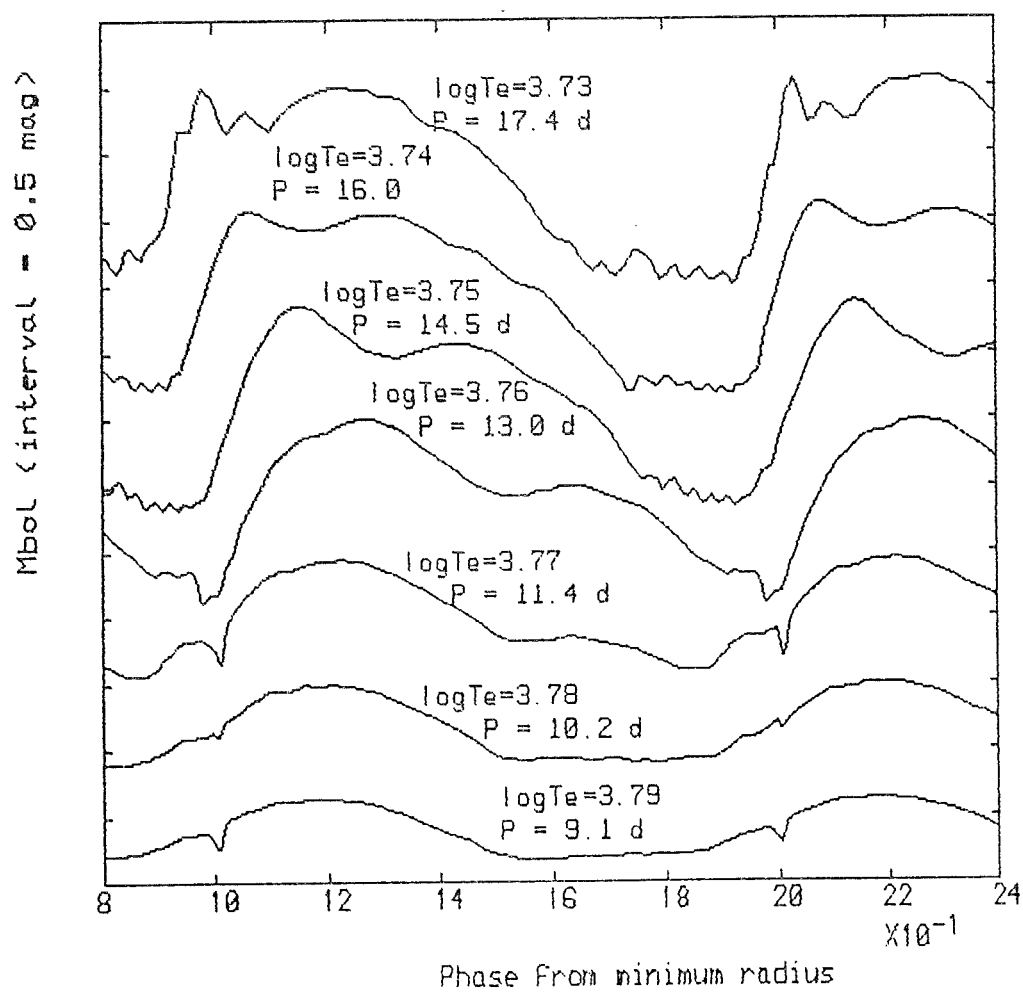


Figure 6.44 Light curves for $\log L/L_{\odot} = 2.9$

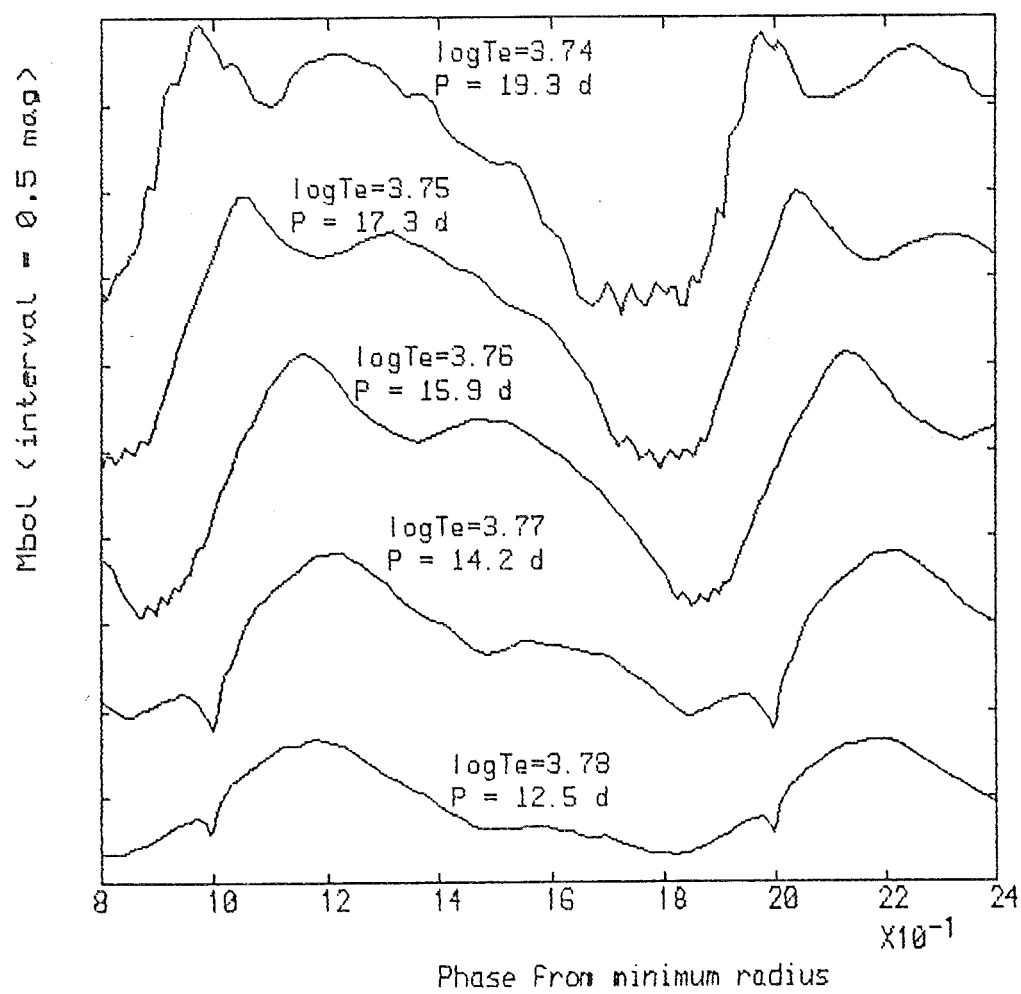


Figure 6.45 Light curves for $\log L/L_{\odot} = 3.0$

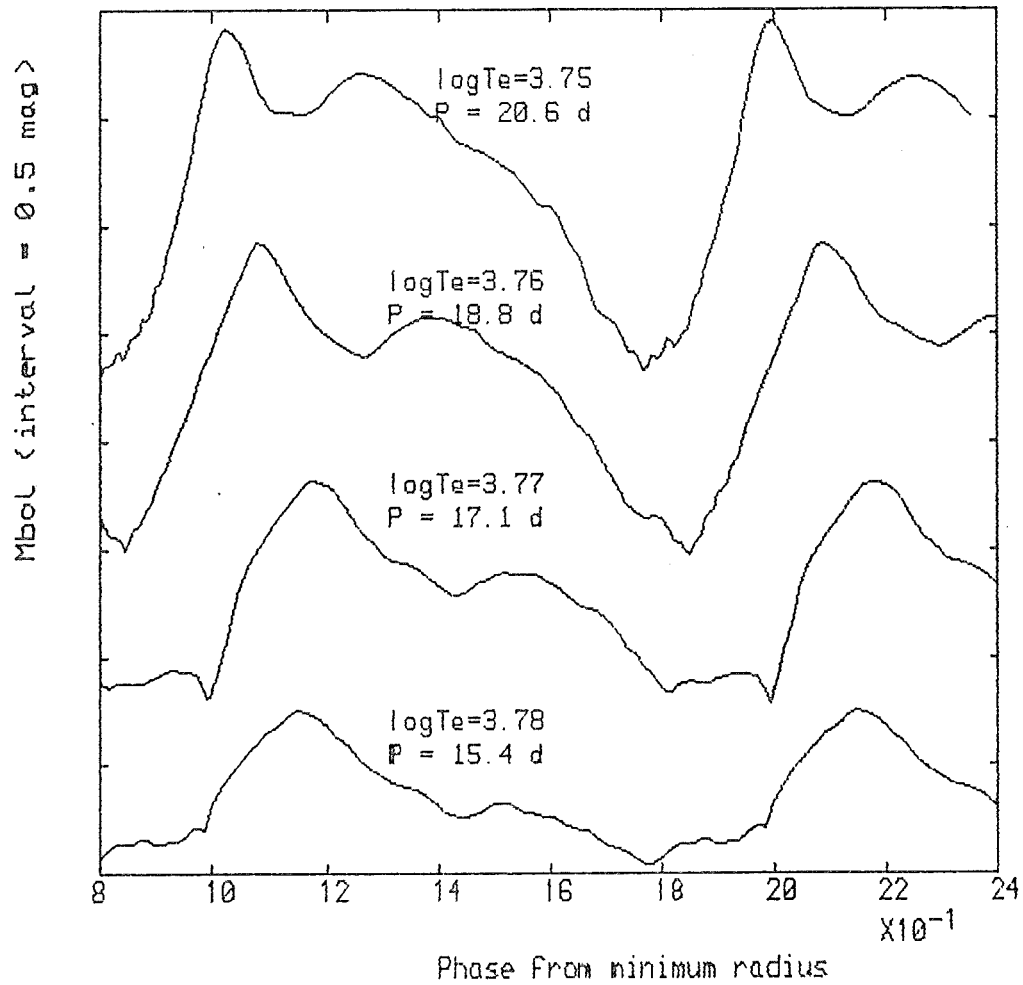


Figure 6.46 Light curves for $\log L/L_{\odot} = 3.1$

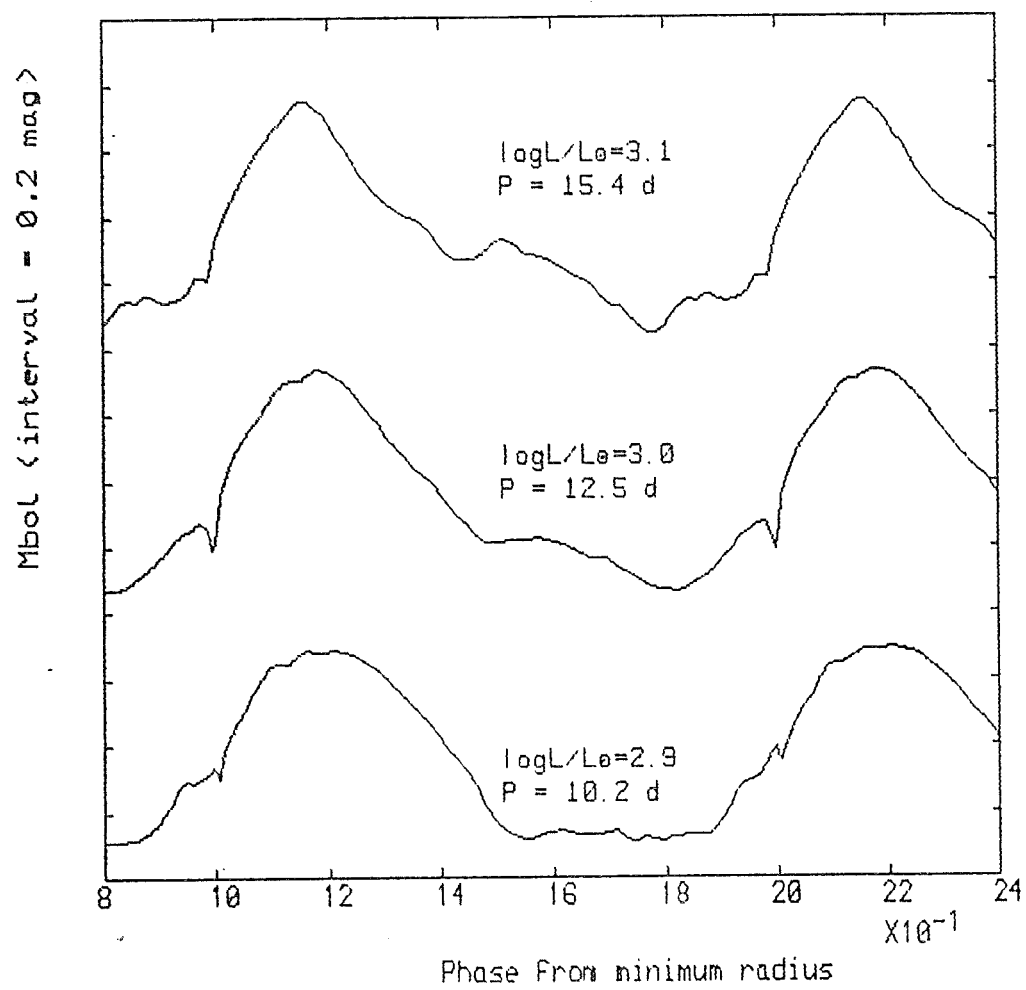


Figure 6.47 Light curves for $\log T_e = 3.78$

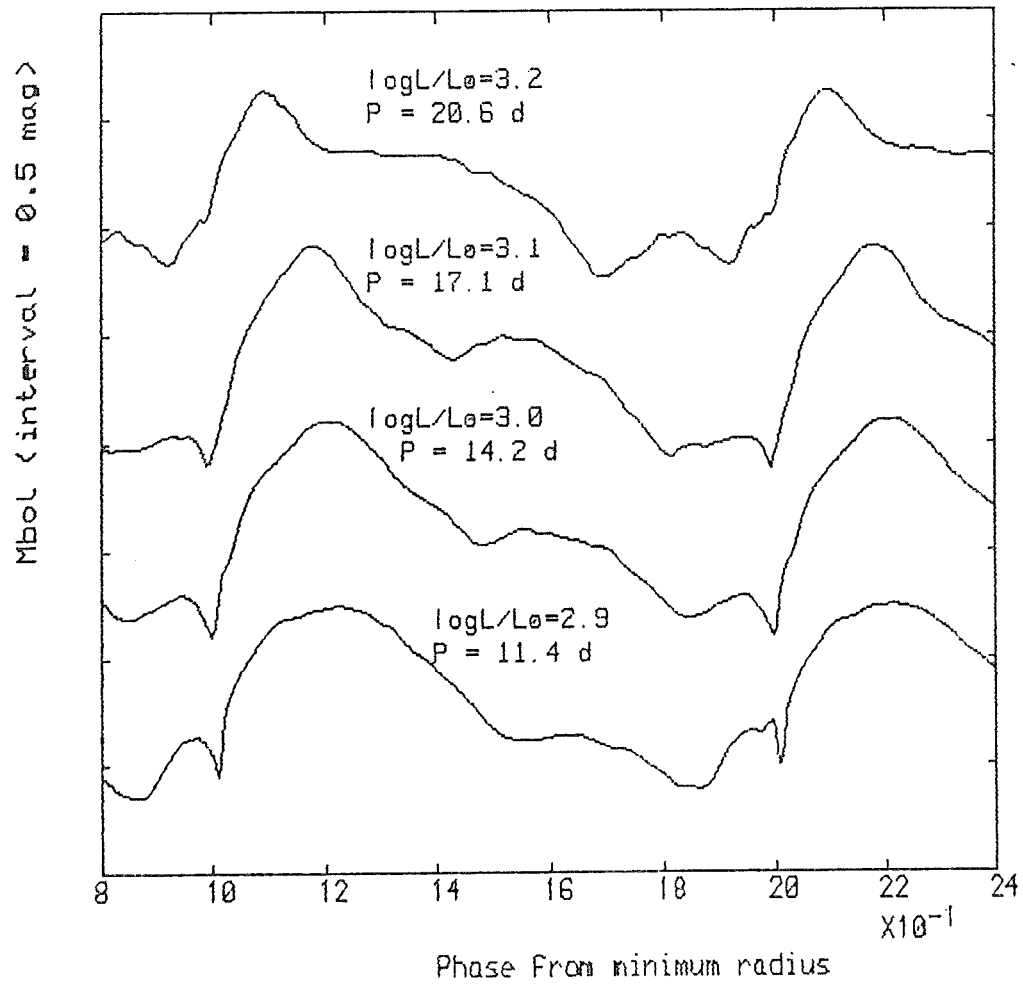


Figure 6.48 Light curves for $\log T_{\text{e}} = 3.77$

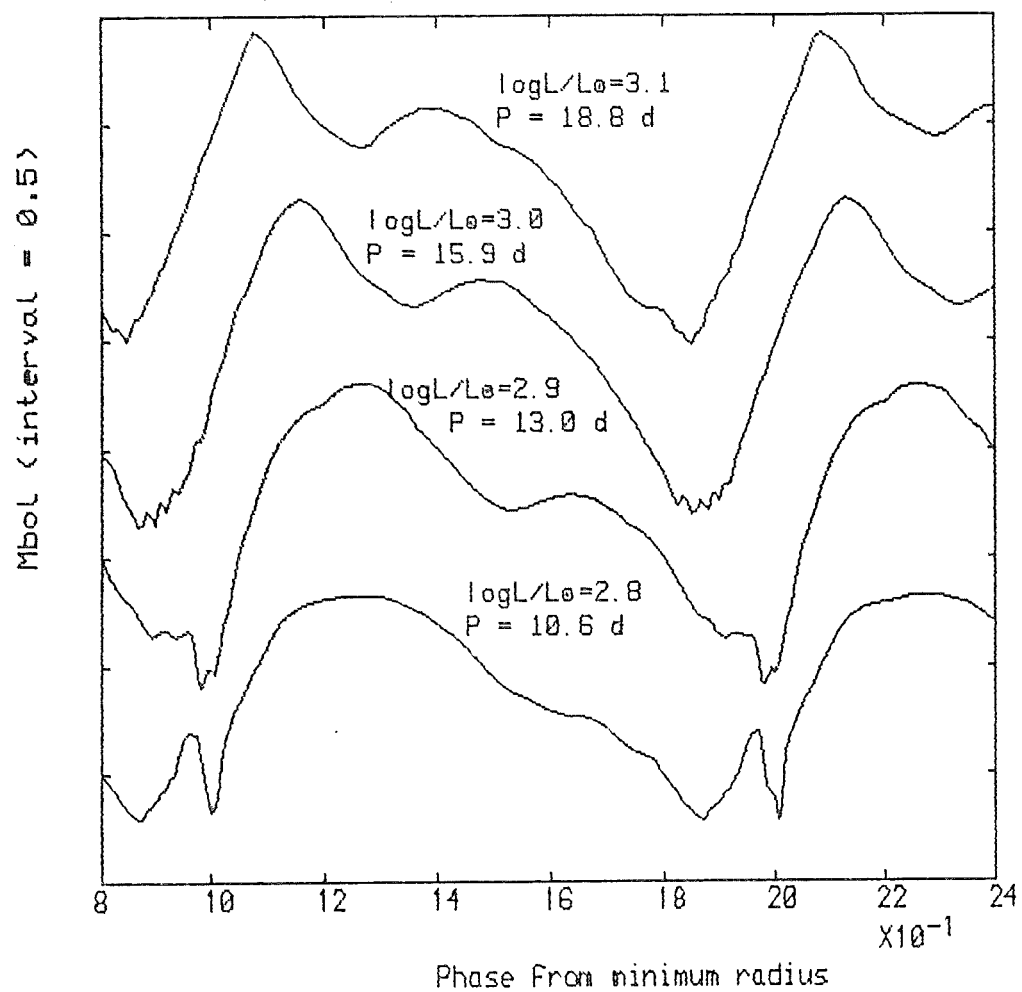


Figure 6.49 Light curves for $\log T_e = 3.76$

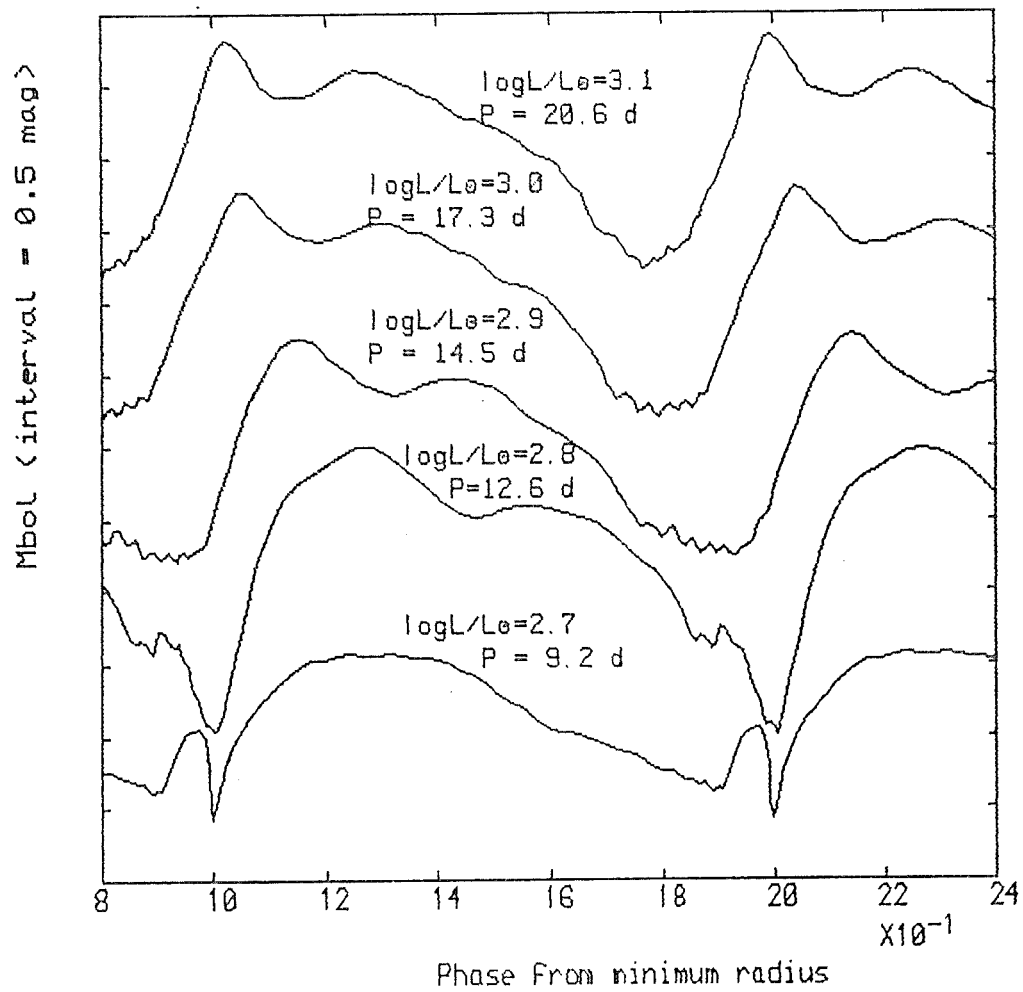


Figure 6.50 Light curves for $\log T_{\text{e}} = 3.75$

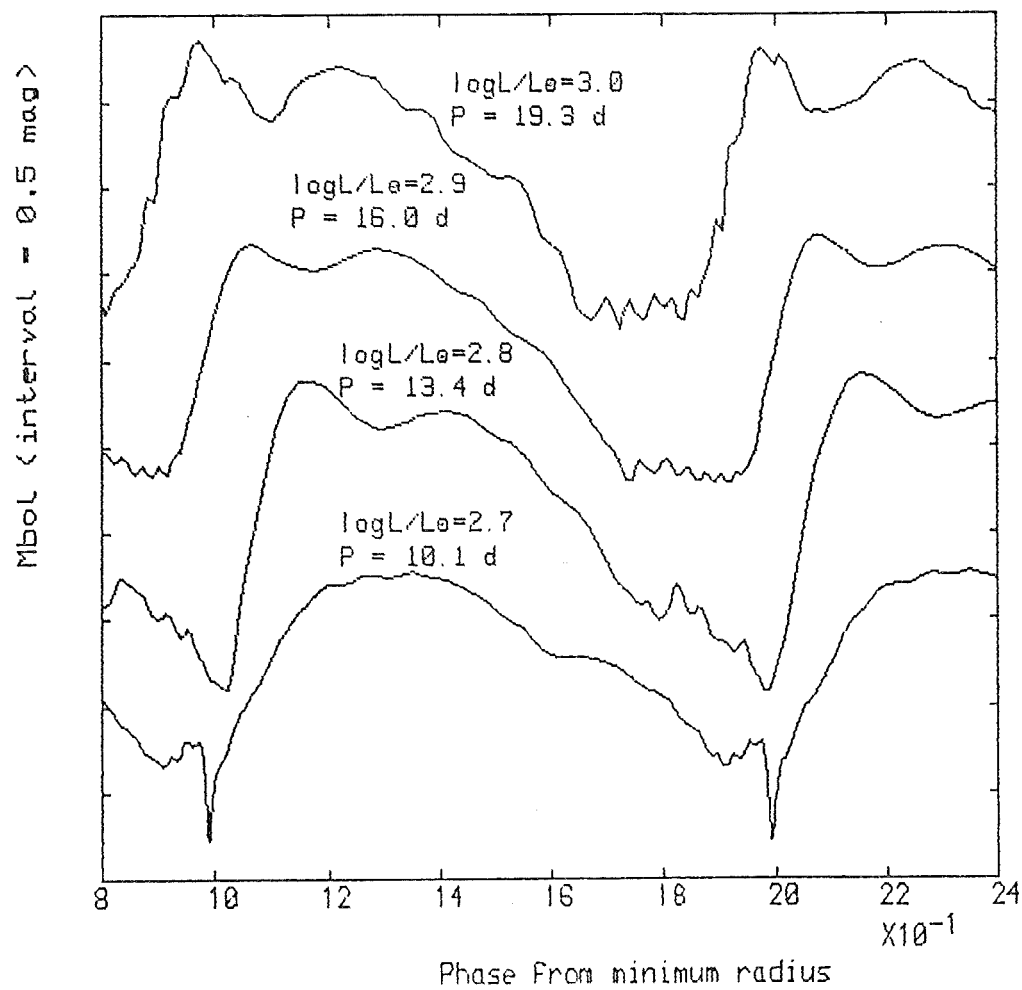


Figure 6.51 Light curves for $\log T_e = 3.74$

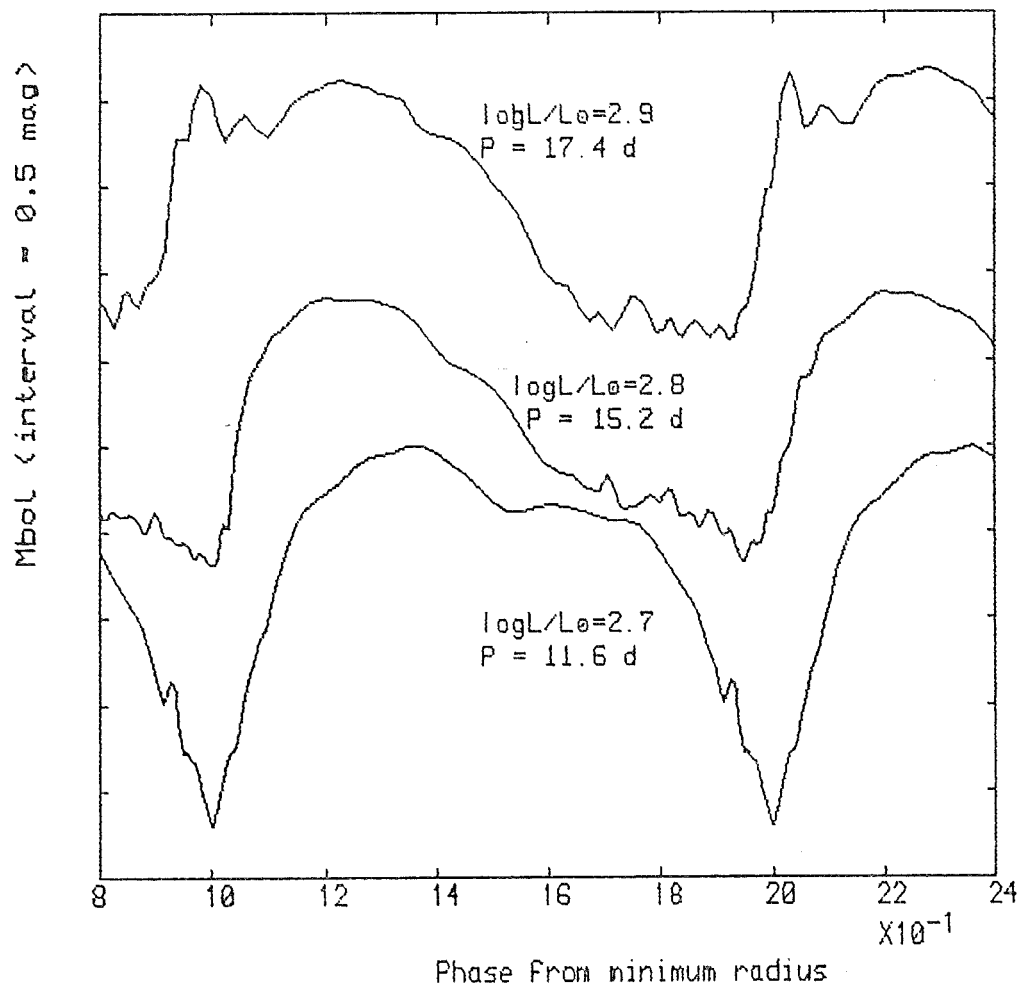


Figure 6.52 Light curves for $\log T_e = 3.73$

For higher values of $\log T_e (\geq 3.75)$ it is not clear that F-type light curves exist at all, the trend as $\log(L/L_\odot)$ increases may be from X or XC-type to C-type. Certainly at high luminosity ($\log(L/L_\odot) > \sim 2.9$) these models produce light curves that are very clearly crested. In fact, for model 25 there is a very clear crest but the secondary bump has become an extended shoulder.

The phases (from minimum radius) of the maximum and secondary bump (ϕ'_m and ϕ'_b) both generally decrease as $\log(L/L_\odot)$ increases (at constant $\log T_e$), while the difference $\phi'_b - \phi'_m$ decreases.

Looking at the overall trends (see figures 6.41a and b) we see that at higher $\log(L/L_\odot)$ the curves are more likely to be crested, this being caused by the higher luminosity which creates a greater driving and a higher asymmetry. Also at higher $\log(L/L_\odot)$ $\phi'_b - \phi'_m$ is slightly smaller, and the secondary bump follows sooner after primary maximum. Superimposed on this is the more obvious trend for $\phi'_b - \phi'_m$ to decrease as $\log T_e$ decreases, creating F-type curves if the luminosity is not too great. If the luminosity is high, the crest is simply too high for the secondary bump to be of sufficient height to merge with it and create the flat top. So we see no F-type curves at the higher luminosity range of the area considered. This is borne out by observations.

The phase ϕ'_b decreases with increasing period, but $\phi'_b - \phi'_m$ only shows this tendency slightly. Something definitely not seen here is the secondary bump travelling backwards in phase as the period increases and crossing the maximum to end up on the ascending branch of the light curve, an effect seen very

clearly in the PL Herculis variables. In other words the models, like the observed stars, do not follow a Hertzsprung progression (as is seen in classical cepheids).

6.9 THE DRIVING REGIONS

The driving in most types of variable stars studied up to now has been almost entirely in the helium II ionization region, caused by one of the methods described in section 2.1, or by a combination of them. In the models presented here we begin to see the hydrogen-helium I region taking a significant, if not dominant, role in the driving of the pulsation. Looking at the general trends we see that as luminosity increases and effective temperature decreases the driving from both regions increases. As $\log T_e$ decreases, the driving from both regions increases quite rapidly, probably without limit because of the neglect of convection. As $\log(L/L_\odot)$ increases both regions produce more driving, but the hydrogen/helium I driving region increases in strength faster than the helium II region, which appears to level off in power after about $\log(L/L_\odot) = 3.0$. For example, in model 23 ($\log(L/L_\odot) = 3.1$, $\log T_e = 3.76$) the H/He I driving region's peak is about three times that of the He II driving region (figure 6.54) Figure 6.53 shows more normal He II driving. Note that the large width of the H region is mainly due to spreading of the shock front by the artificial viscosity.

These results seem to indicate that the hydrogen/helium I ionization region may contribute a significant if not major portion of the driving. However, the inclusion of convection

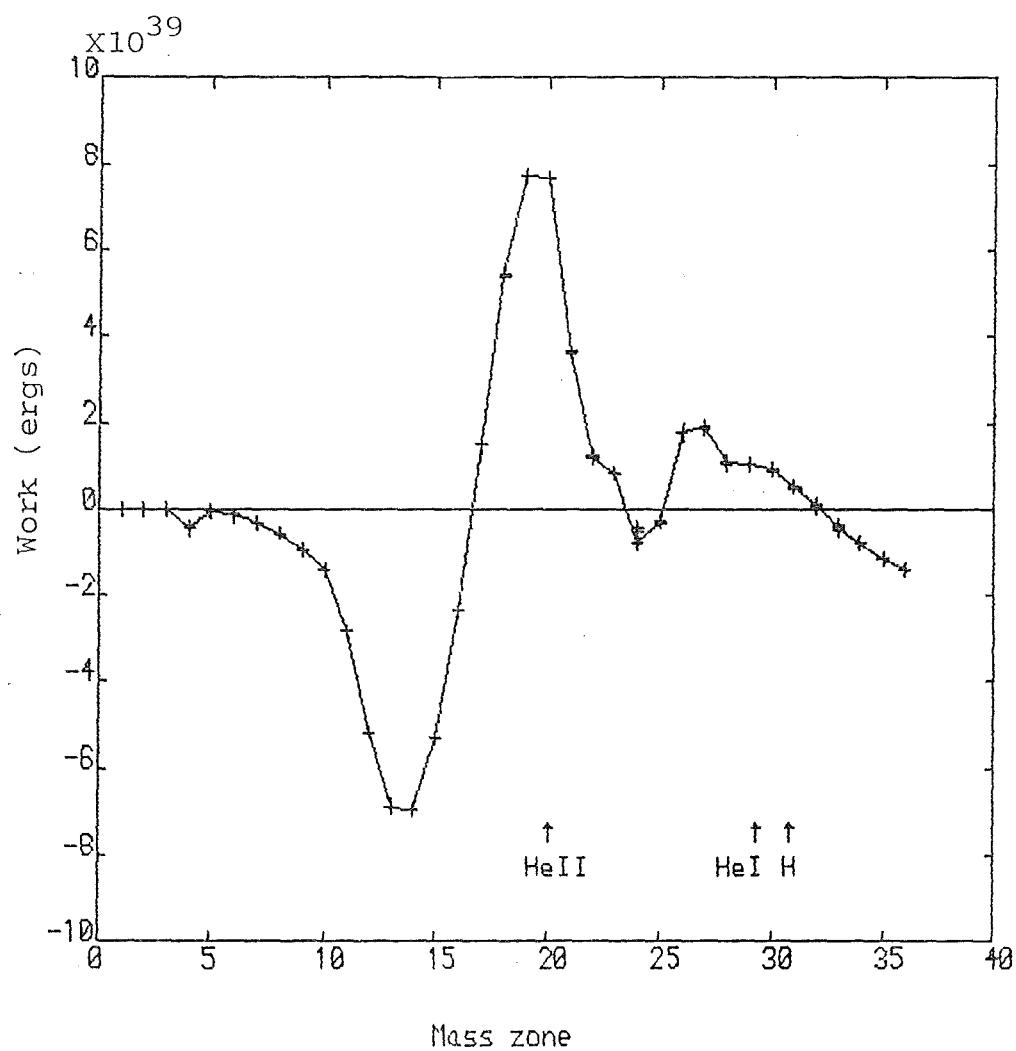


Figure 6.53 Work done in model 2

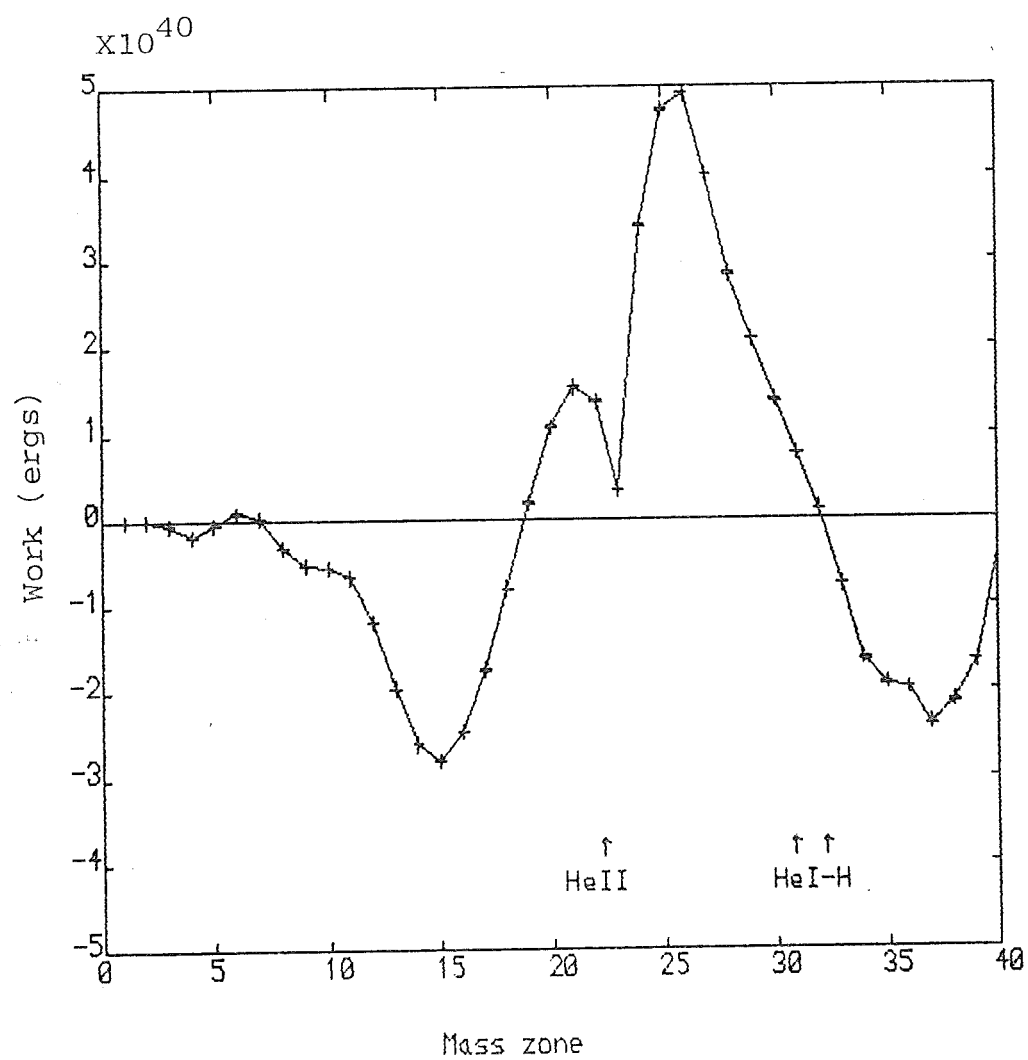


Figure 6.54 Work done in model 23

as a possible means of energy transport might reduce the amount of H/He I driving considerably, especially for the redder stars. The brief investigations of convection in static stellar envelopes carried out in section 6.1 indicates that, for instance in model 23, convection probably carries about 30% of the flux in the H/He I ionization region. Convection of this order will certainly reduce the driving, and may well eliminate it entirely. However, H/He I driving is probably very significant in some of these stars, and undoubtedly grows in importance as the effective temperature drops and the luminosity rises. RV Tauri and Mira-type variables are the likely places to look for stars truly driven by the H/He I ionization region. So the driving region in these stars still appears to be the He II ionization region, though in some cases with additional driving from the H/He I ionization region. What is the mechanism behind the driving? Section 2.1 discusses three main driving mechanisms, but which applies here? The mechanism seems likely to be the same for both He II and H/He I driving. In both cases the driving peak usually lies just inside the ionization peak, at a slightly higher temperature. The probable mechanism at work here is the κ -mechanism, as evidenced by the large temperature variations.

Some results were obtained on the driving of models, using variations in mass and in the Cox-Stewart opacities. Comparisons with these results are presented in section 6.13.

6.10 ANALYSIS OF THE MODELS - THE CAUSES OF THE SECONDARY BUMPS

In this section the history of the pulsation in the stellar envelopes is considered in an attempt to find out the causes of various features of the light and velocity curves, in particular the cause of the secondary bump. It is the C-type light curves that most obviously show this bump similar to the secondary bumps in BL Herculis variables (section 2.2 and references therein), though not precisely the same.

The secondary bumps in the BL Herculis light curves have been explained in two ways, which may be equivalent; the "echo" model of Christy (1968) and the resonance model of Simon and Schmidt (1976) (see section 2.3). The results of CSV and others confirm that the phase of the secondary bump is related to the value of P_2/P_0 , around the resonance $P_2/P_0 = 0.5$, however CSV point out that if the resonance idea is correct, then there should be similar progressions for two other resonances of type II cepheids, $P_2/P_0 = 0.33$ at $P_0 \simeq 14^d$ and $P_1/P_0 = 0.5$ at $P_0 \simeq 17^d$, and there is no evidence for such progressions in the observations.

In the calculated models described here there is some evidence of a progression in the secondary bumps, although it is not as pronounced as the Hertzsprung progression in the classical cepheids or the progression in the BL Herculis variables. Also, no bumps are seen on the ascending branches of the light curves, the extent of the bumps being from about 0.2 after light maximum to about 0.4 after light maximum. So though a progression does exist, it is not convincing evidence

for the resonance idea.

Another way to ascertain the cause of the secondary bumps is to examine the light and velocity histories of the models. Here evidence of the Christy "echo" phenomenon can be looked for, and this also provides a test of the Carson opacities. The CSV models clearly support the Christy idea for the origin of their bump; however, using the Carson opacities KCH found the bump to be a local phenomenon (see section 2.2), confined to the surface layers of the star. For the C-type light curves produced in this study, examples of light and velocity histories are plotted in figures 6.55 to 6.59.

Model 18 shows the reflection phenomenon most clearly, along with model 22. In both of these, and to a lesser extent in the other models of this type, a pressure wave seems to be generated in the He II ionization zone. This wave travels inwards, reflects off the (adiabatic) core and arrives at the surface during the next period, creating the secondary light and velocity bumps. The velocity bump precedes the light bump in phase, except for the very topmost surface layers (caused by the "freezing-in" of the luminosity variations in the atmosphere); that is, the luminosity variation of the outer layer is the same as that a few zones deep (it travels at the speed of light), but the velocity variation lags in time (it travels at approximately sound speed). However, the velocity variation in the outermost layers of real stars is probably not usually observed. In these cases the bump does not seem to be atmospheric, and the Christy echo phenomenon is its cause. However, this does not rule out the resonance idea of Simon and Schmidt, which may be equivalent. Linear study of these models

in conjunction with this work should answer this question.

What of the models that do not show a secondary bump? Model 16 is one of these (figure 6.60), although its classification as XC-type indicates that there is an incipient bump on its light curve. It is one of the shorter period (12.5 days) models that are neither C nor F-type. In the velocity history we see a weak bump generated by the Christy echo, but this only generates a late shoulder in the light curve rather than a bump. Incidentally, this model also demonstrates another occasional feature of models built with the Carson opacities. A low-lying zone (in this case the second from the bottom) shows a reversed luminosity behaviour, which seems to be caused by the C-O bump of the Carson opacities (see section 5.2). This does not invalidate the opacities, as its overall effect on the model seems to be negligible.

Model 16 is an example of the first appearance of the secondary bump at short periods. As the period increases the bump generally moves backward in phase, forming first the C-type models.

In these models the bump is present in both the light and velocity curves, but there are models for which there is a clear secondary light bump, but apparently no secondary bump in the velocity curve. Models 19 and 24 are examples of this. Closer examination of the velocity histories (figures 6.56, 6.58) show that the Christy echo does indeed give rise to a bump or potential bump, but it is very close to the velocity maximum, and is almost "swallowed". This seems to be caused more by a later maximum than an earlier bump. The rise to velocity maximum is less steep than normal, causing this

effect.

Turning our attention to the F-type models, the problems are different. Here we seek to support the idea that the secondary bump may still exist, but has merged with the maximum to produce the flat-top observed. Also the flat-topped curves were very difficult to produce. A detailed study of the models might aid understanding of why this is the case.

Model 8 is probably the best example of this idea. Unfortunately it is not a very stable model. It was difficult to produce, needing gentle "coaxing" to reach anything like a stable condition. Even then only 12 periods were obtained. It may also show RV Tauri behaviour, increasing its problems (see section 6.11). In figure 6.61 we see that the Christy reflection fades out, not appearing to produce a bump. However, if it had managed to produce one it seems likely that it would have been close to the velocity peak. The suspicion of RV Tauri behaviour is evidenced by the next period shown, which does not have much of a wave travelling down to be reflected. This behaviour was maintained for several periods. In the luminosity behaviour for this star we see considerable evidence of the problems associated with modelling this star. In the first period we see a spike on the downward side of the curve, which is probably caused by numerical problems. This spike repeated at irregular intervals, always in the same position. There is some evidence in this history of a secondary bump on the light curve, and if it does exist it is very close to peak light, almost completely merged with it.

Model 8 is probably the closest to a flat-topped curve as observed. However, in model 14 there is another possible example. This model (see section 6.12) seemed to pulsate in two separate states. The state shown in figure 6.62 is the non-alternating, perfectly repeatable state. In the velocity history we again see that the Christy "echo", if it results in a bump at all, gives one very close to the maximum velocity, creating a broader velocity peak rather than a secondary bump. This star was a little easier to model and shows the reflection of the pressure wave very clearly. Although this model's light curve is not a true F-type, its secondary bump is very near maximum light and is of approximately the same height.

Continuing the detailed look at some features of the models there is another particular feature to be examined. Some of the models (notably numbers 9, 11, 16) show a pre-maximum shock in the light (and velocity) curves. Some observed light curves also appear to have this shock in some form. It is the longer period analogue of the pre-maximum shock seen in CSV's BL Herculis model. The shock seems to be generated in the helium II ionization zone, maybe as a reflection of the pressure wave that has travelled inwards, after being reflected from the stellar surface at velocity maximum.

Model 20 proved to be an interesting model. It was not repeatable in its pulsations (having an almost RV Tauri-like alternation) until it threw off its outer shell; the rest of the model then settled into a regular, stable, repeatable pulsation, rather like that of model 14 (state 2). In figure 6.53 we see the outside zone with an almost constant

(increasing slightly) surface velocity, which is greater than the escape velocity of the star. The problems with the model prior to this escape seemed to be caused by the irregular "returns" of the outer zone to the rest of the star. When these returns were biperiodic the alternating RV Tauri-like behaviour was obtained. The velocity history of this model is another example in which the Christy echo returns to the surface very close to the velocity maximum.

Another oddity appears in model 1, and also to a considerably smaller degree in some others. In and near the He II ionization zone both the velocity and luminosity variations are rather strange. At one point here, the light and velocity variations are oscillating twice in one period (figure 6.64). this might be some sort of "almost harmonic" behaviour, an idea that would need further work (with some linear studies) to confirm. In fact, the linear studies of Worrell (1982b) have suggested that some higher luminosity stars show a decrease in $\delta R/R$ at one point (going out through the star in mass) though a true node is not present. This might in some way be connected with the behaviour seen here.

Detailed histories for the models with different masses or different opacities were also obtained. The differences between these and the standard survey models are presented in section 6.12.

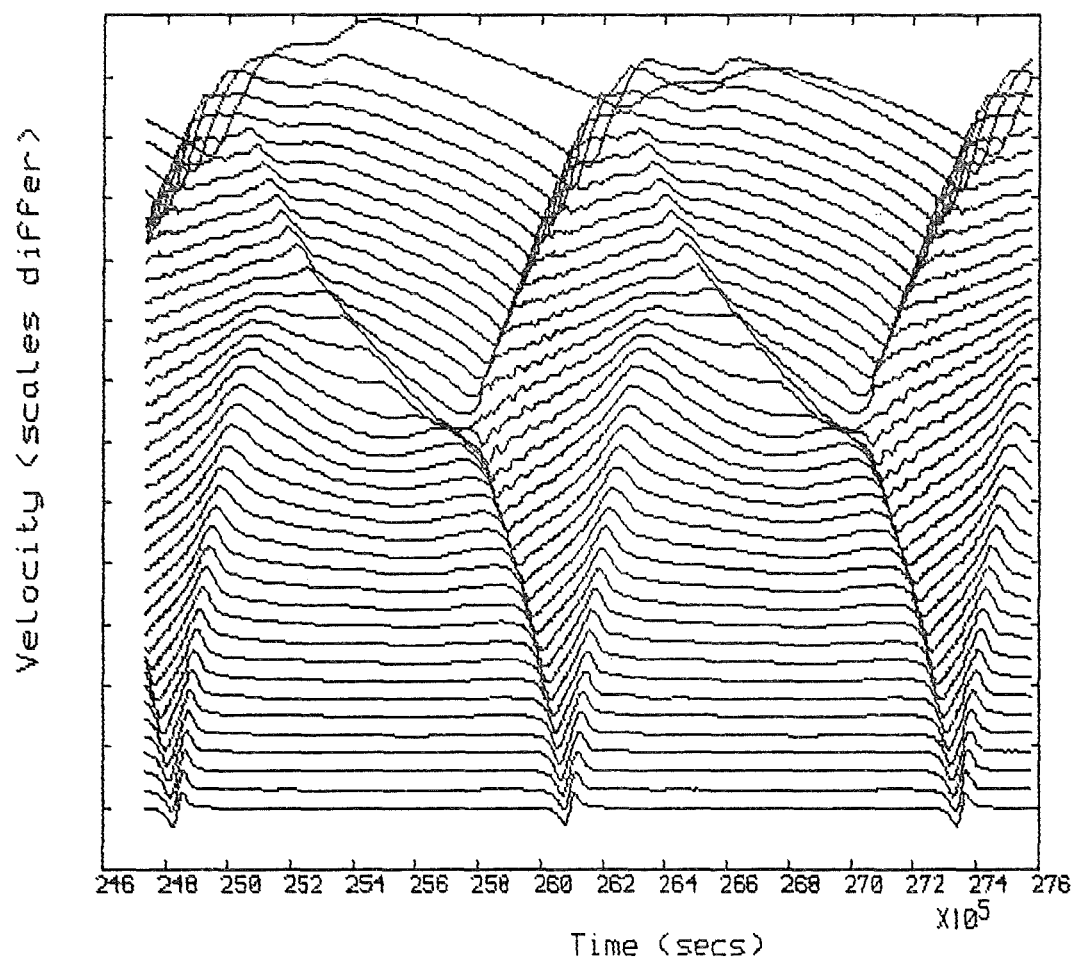


Figure 6.55 Velocity history for model 13

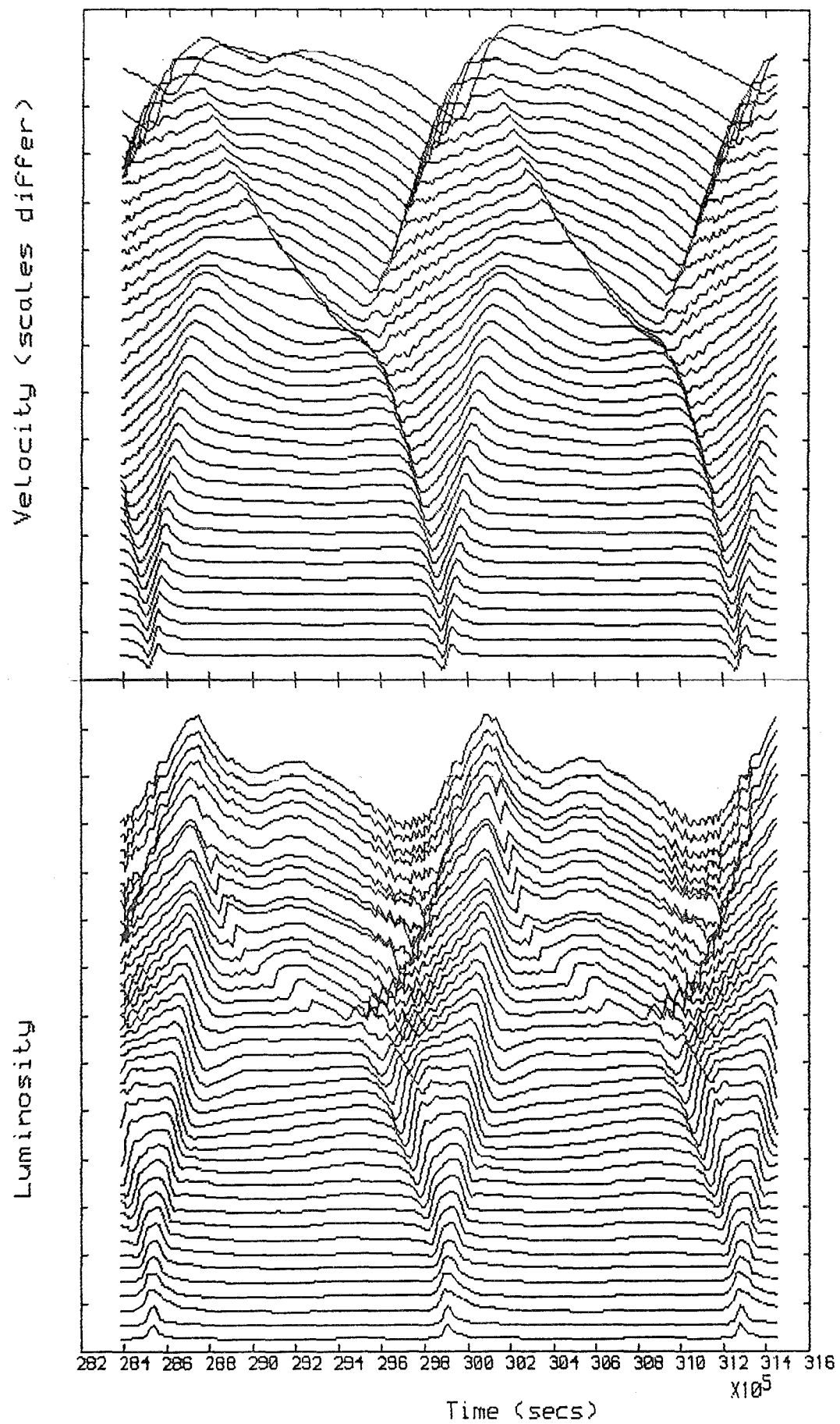


Figure 6.56 Velocity and luminosity histories for model 18

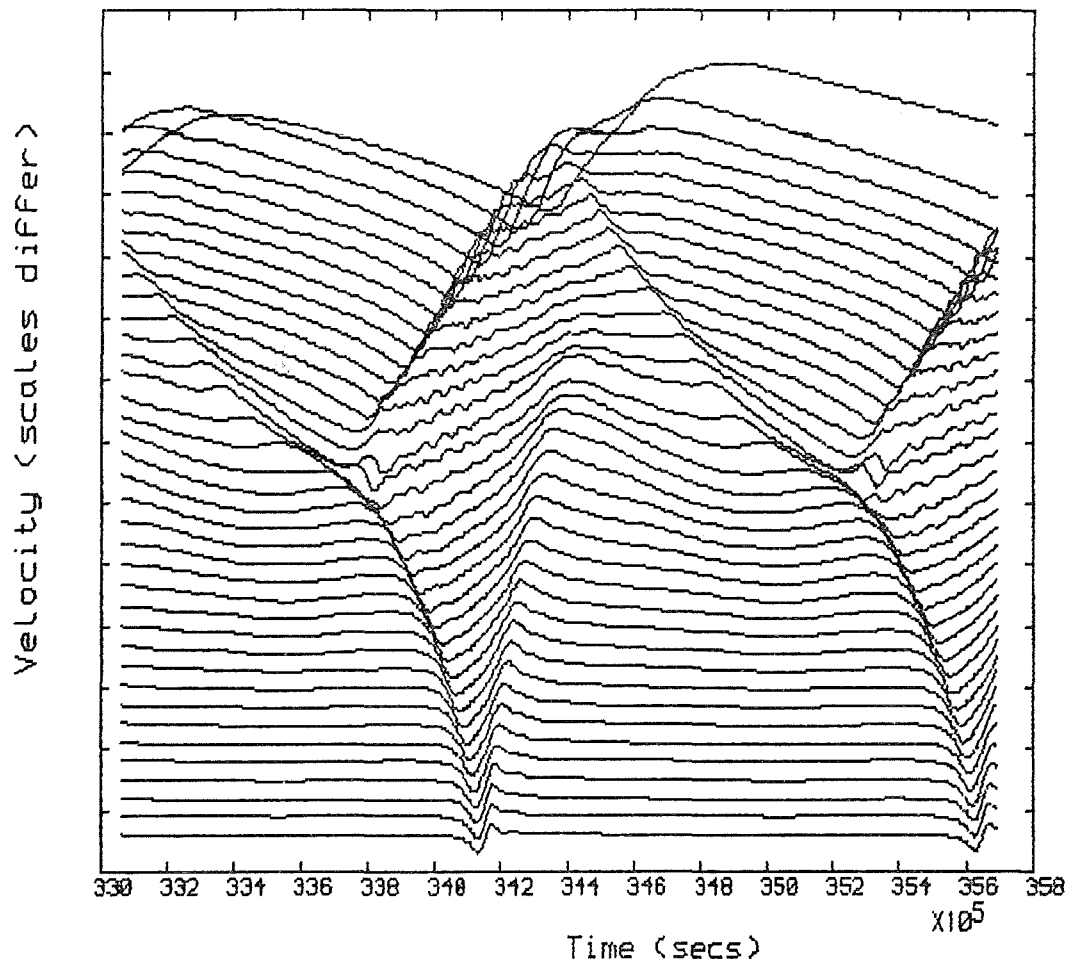


Figure 6.57 Velocity history for model 19

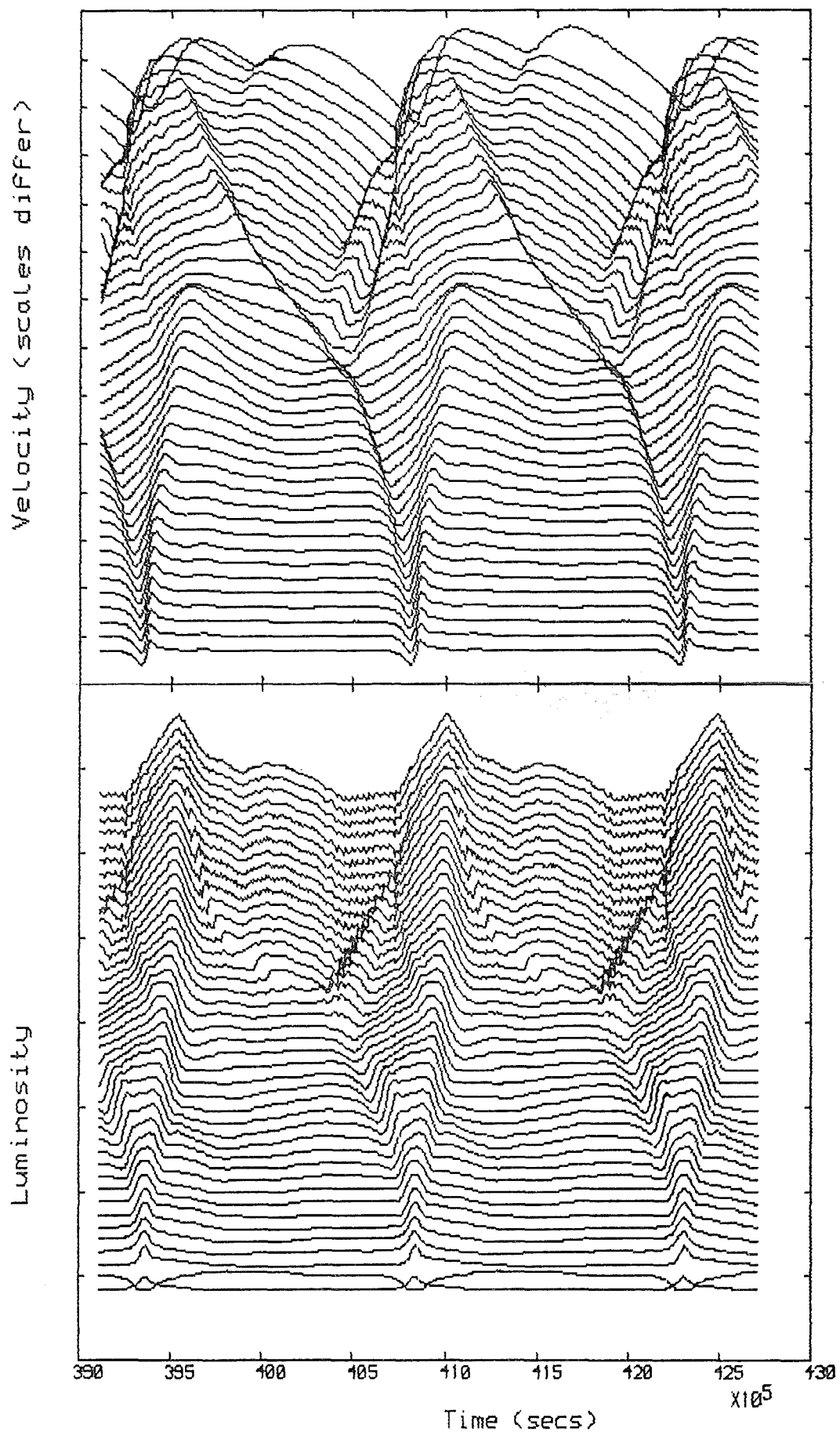


Figure 6-58 Velocity and luminosity histories for model 22

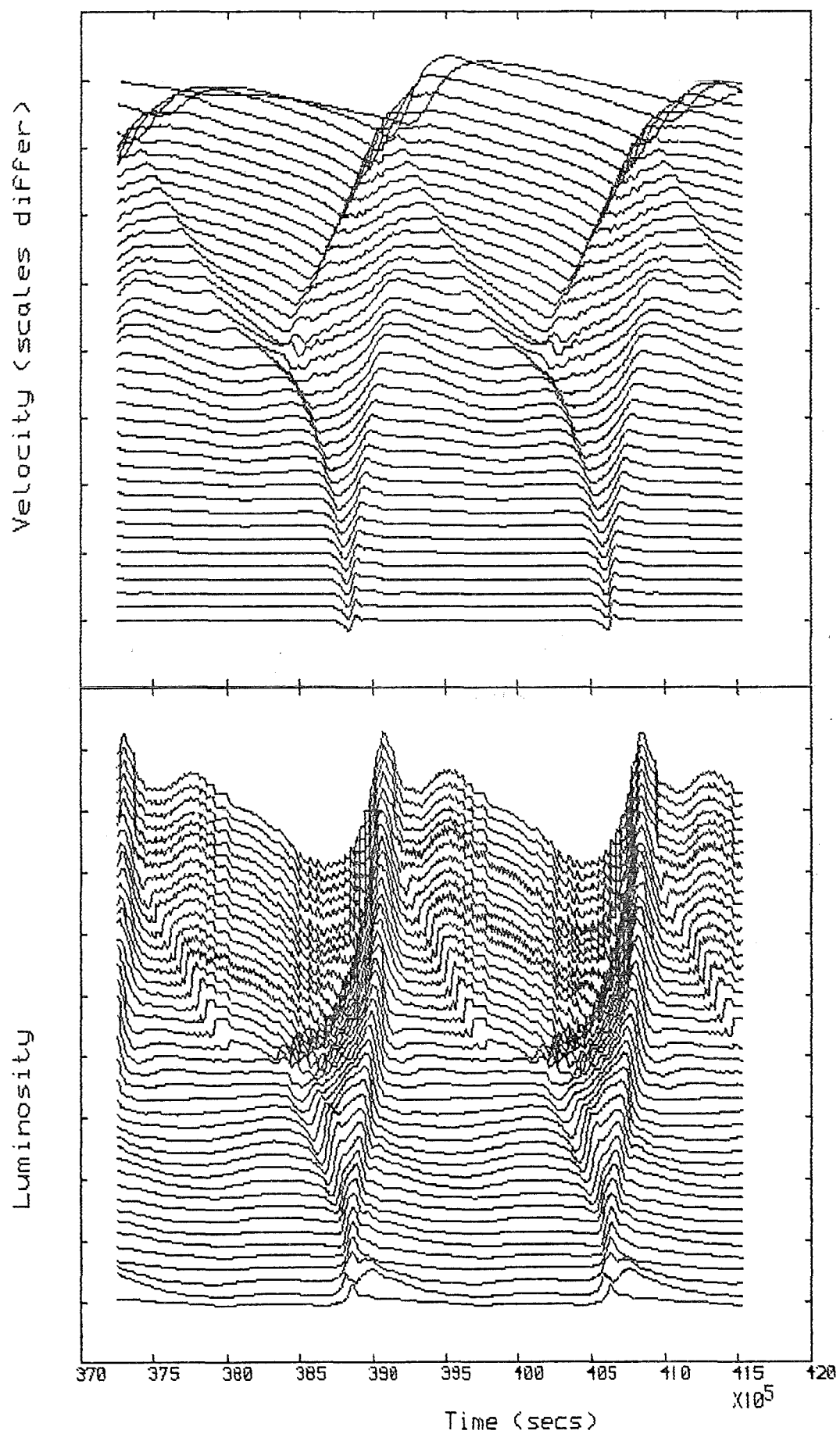


Figure 6.59 Velocity and luminosity histories for model 24

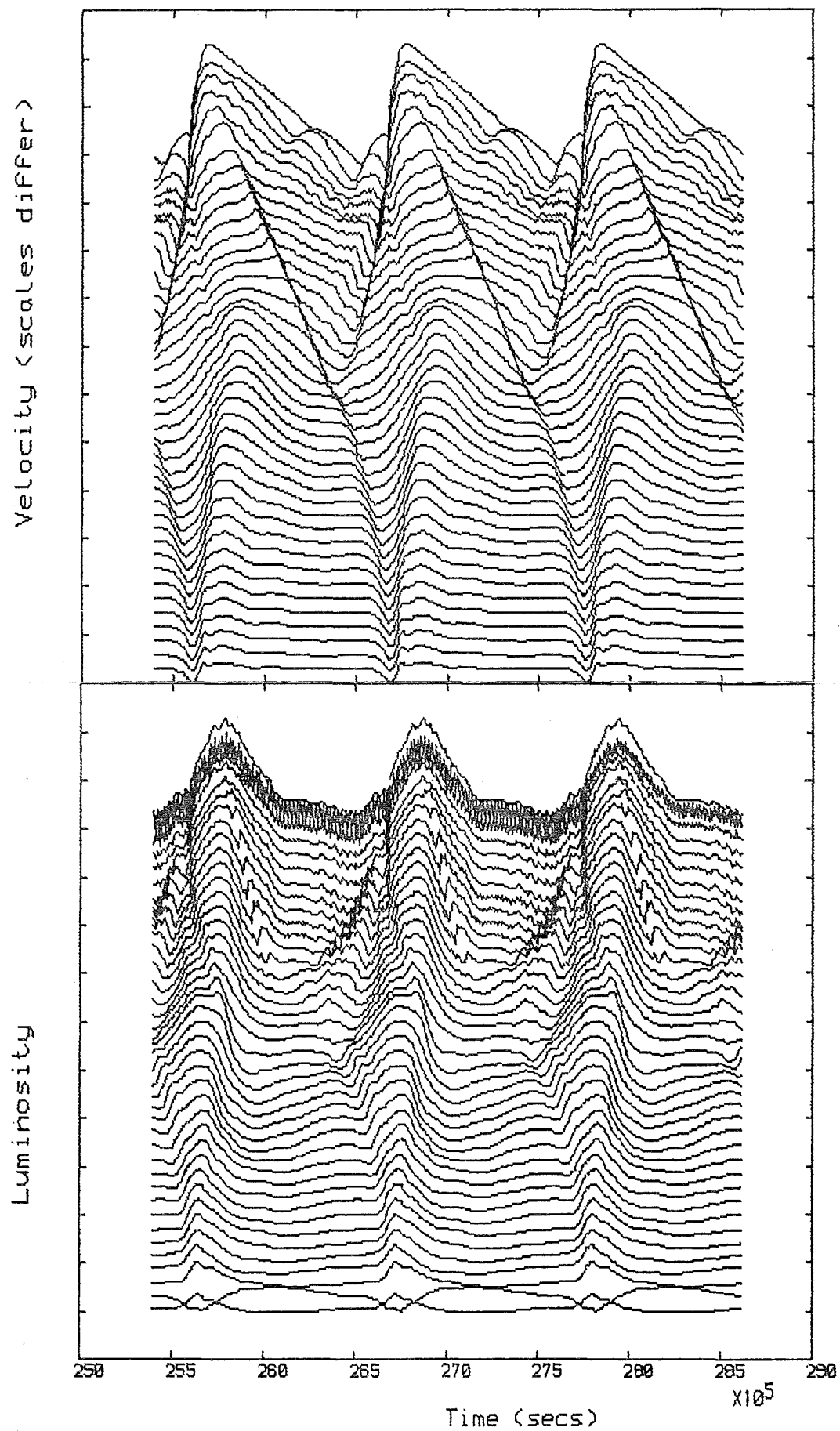


Figure 6.60 Velocity and luminosity histories for model 16

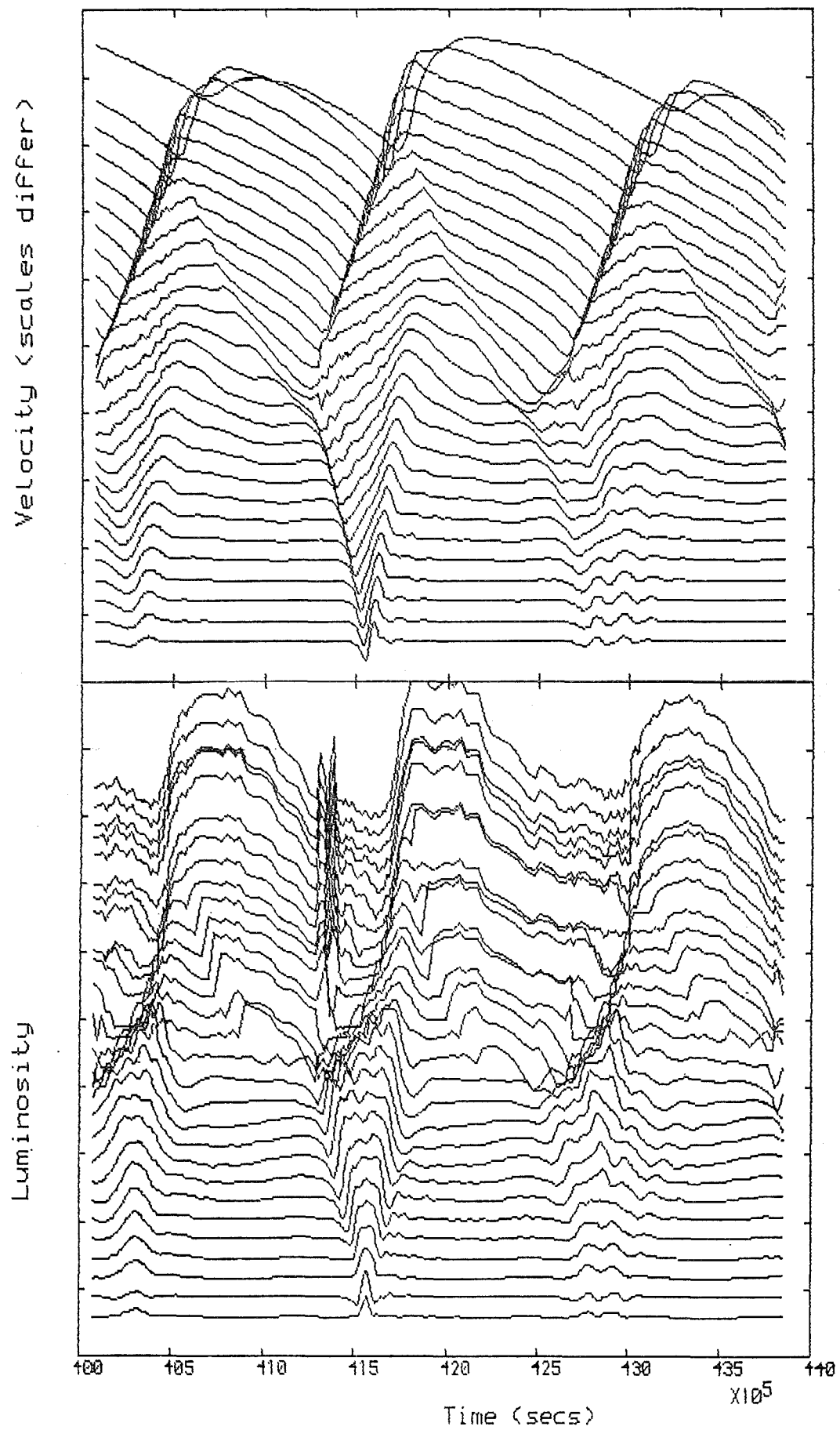


Figure 6.61 Velocity and luminosity histories for model 8

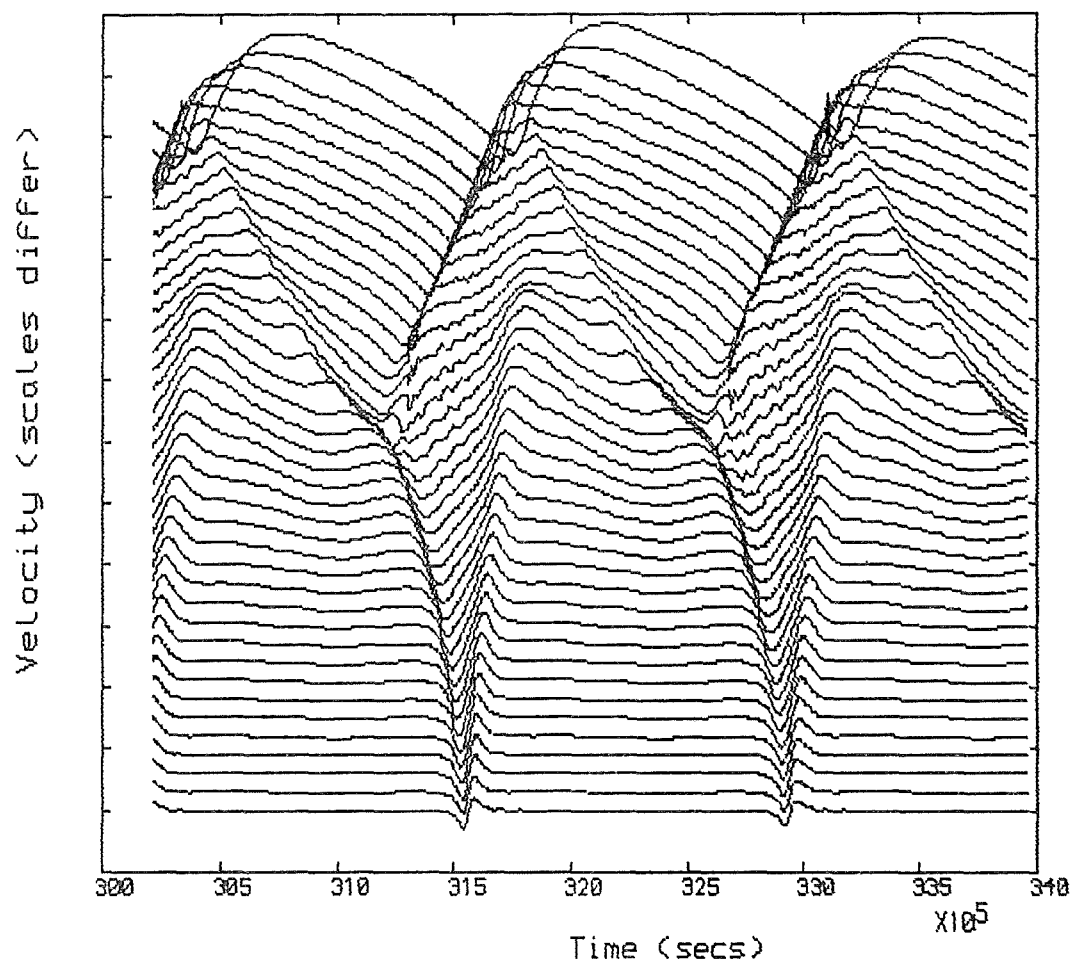


Figure 6.62 Velocity history for model 14

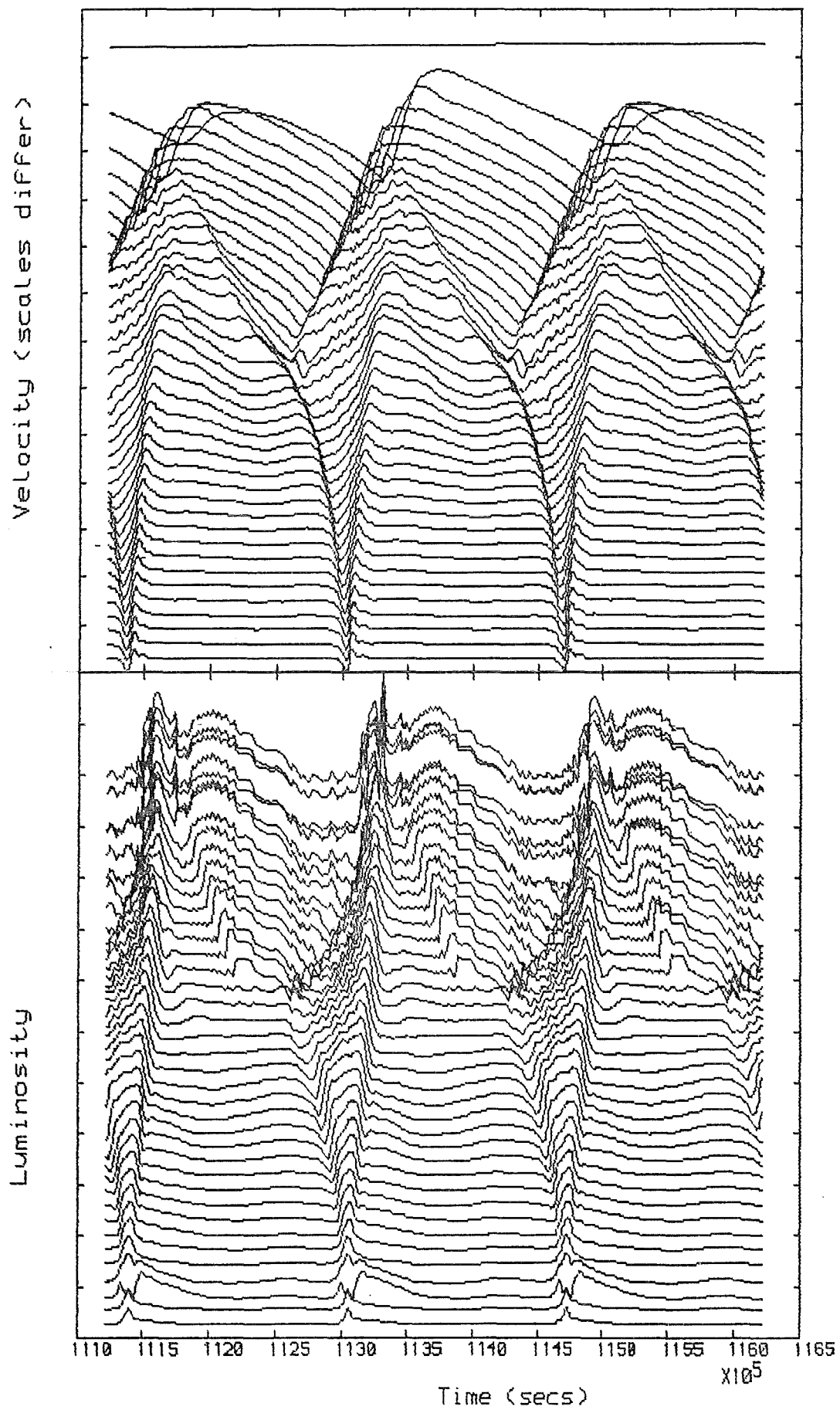


Figure 6.63 Velocity and luminosity histories for model 20

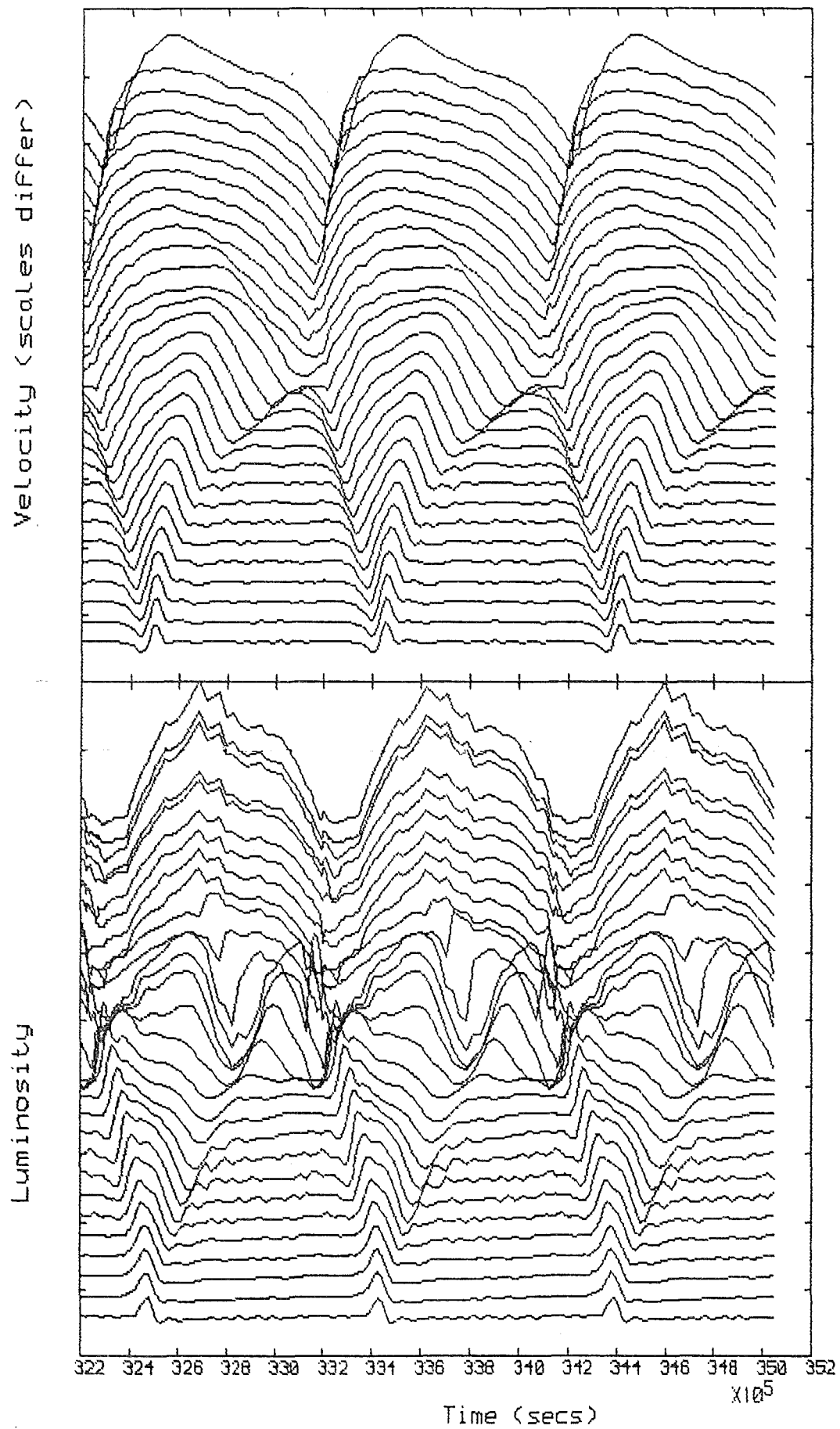


Figure 6.64 Velocity and luminosity histories for model 1

In their 1981 paper, CSV produced a series of models of type II variables with periods less than 10 days, but they also produced a model of an individual star, BL Herculis. This model was very successful in imitating the light and velocity curves of the observed star. Are any of the models produced in this survey good candidates for models of particular observed stars?

In general the survey models seem to have produced a good selection of C-type light curves, covering the variations seen in the observations. One of these models, number 13, seems to be a good candidate for a model of CS Cas, one of the field variables observed by Kwee, and classified as crested. The parameters known for both the model and the star are listed in table 6.4, and their light curves are plotted in figure 6.65. In table 6.4 the visual light amplitude (ΔM_V) quoted for model 13 is estimated from Δm_{bol} by adding 0.2 mag.

The discrepancies in the quantities $Asym(lum)$ and ϕ'_b can easily be ascribed to the difficulties in measuring these quantities, especially from the observed curve of CS Cas. The light curve may seem to be well defined but this is not so, and small errors can create large changes, especially in $Asym(lum)$.

What is impressive about this correspondence of model and star is the overall similarity of the light curves in conjunction with the closeness of periods and positions on the HR diagram.

| Parameter | Model 13 | CS Cas |
|-----------------------|----------|--------|
| $\log(L/L_0)$ | 2.9 | 2.91 |
| $\log T_{\text{eff}}$ | 3.75 | 3.74 |
| P (days) | 14.6 | 14.7 |
| ΔM_V | 1.8 | 1.44 |
| Asymmetry (lum.) | 3.2 | 2.0 |
| ϕ_b^1 | 0.40 | 0.48 |
| $\phi_b^1 - \phi_m^1$ | 0.27 | 0.25 |

Table 6.4 Comparison of Model 13 and CS Cas

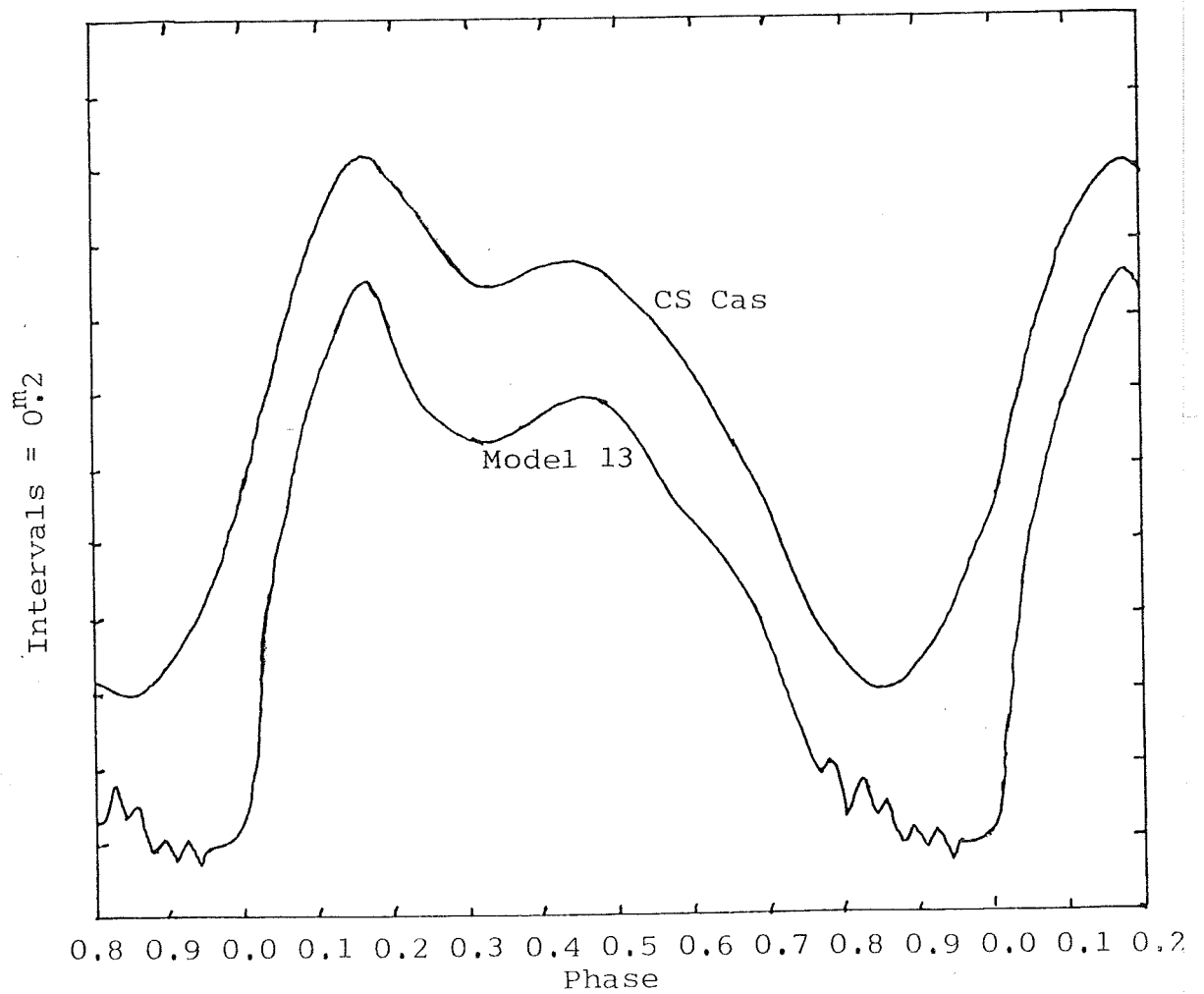


Figure 6.65 The light curves of model 13 and CS Cas

Another good C-type model to star correspondence is that between model 18 and FI Sct. The comparable parameters are given in table 6.5, and their light curves are plotted in figure 6.66.

Here the correspondence is not as good as that between CS Cas and model 13, in particular the periods and visual light amplitudes show greater disparity; still, the overall similarity of model and observed star is very impressive.

The similarity of C-type model light curves and crested observed light curves is in general close and impressive. Unfortunately, the same cannot be said for the F-type models and flat-topped variables. Probably the best correspondence here is between model 14 and AL Sct. The correspondence is nowhere near as good as that for the C-type curves.

The survey models have also shown that it is possible to model those stars at the low period end of the range (10 to 13 days) where light curves show no secondary bumps and are not flat-topped. A few modelled light curves show this lack of features, but model 10 shows best the similarity to the observed star AL Vir. The light curves are plotted in figure 6.67. The comparable features of model and star are given in table 6.6. Unfortunately, since AL Vir is not a C or F-type star, it is difficult to be sure of the estimates for $\log(L/L_0)$ (see section 2.2).

The models representing Kwee's crested variables (along with those representing the featureless light curve stars) show an excellent modelling of the light curves, seemingly as good as CSV's model of BL Herculis. The attempts to model the

| Parameter | Model 18 | FI Sct |
|-----------------------|----------|--------|
| $\log(L/L_0)$ | 3.0 | 2.92 |
| $\log T_{\text{eff}}$ | 3.76 | 3.744 |
| P (days) | 15.9 | 14.9 |
| ΔM_V | 1.8 | 1.19 |
| Asymmetry (lum.) | 2.6 | 1.8 |
| ϕ_b^1 | 0.47 | 0.42 |
| $\phi_b^1 - \phi_m^1$ | 0.31 | 0.29 |

Table 6.5 Comparison of model 18 and FI Sct

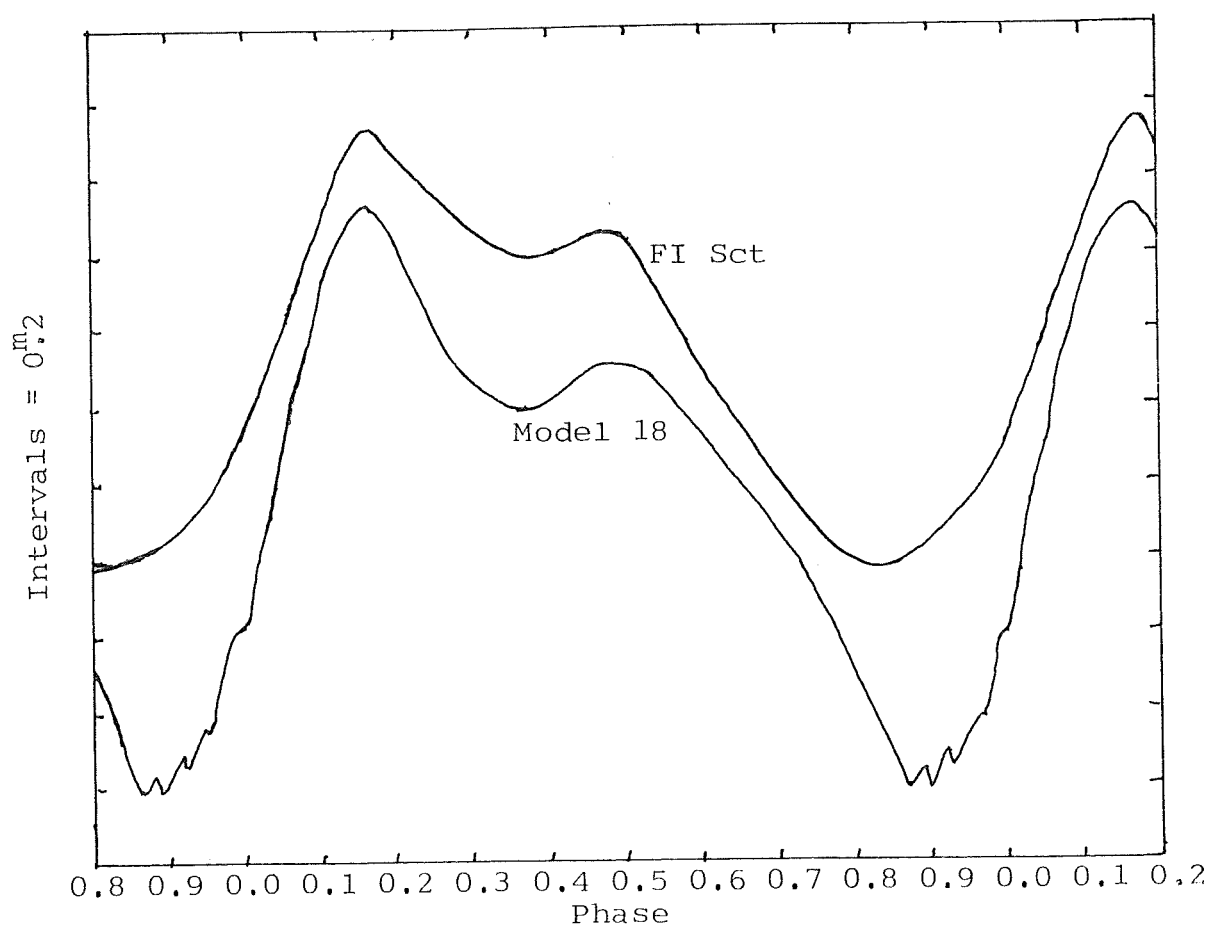


Figure 6.66 The light curves of model 18 and FI Sct

| Parameter | Model 10 | AL Vir |
|-----------------------|----------|--------|
| $\log(L/L_0)$ | 2.9 | 2.5 |
| $\log T_{\text{eff}}$ | 3.78 | 3.74 |
| P (days) | 10.2 | 10.3 |
| ΔM_V | 0.8 | 0.82 |
| Asymmetry (lum.) | 1.8 | 1.45 |

Table 6.6 Comparison of model 10 and AL Vir

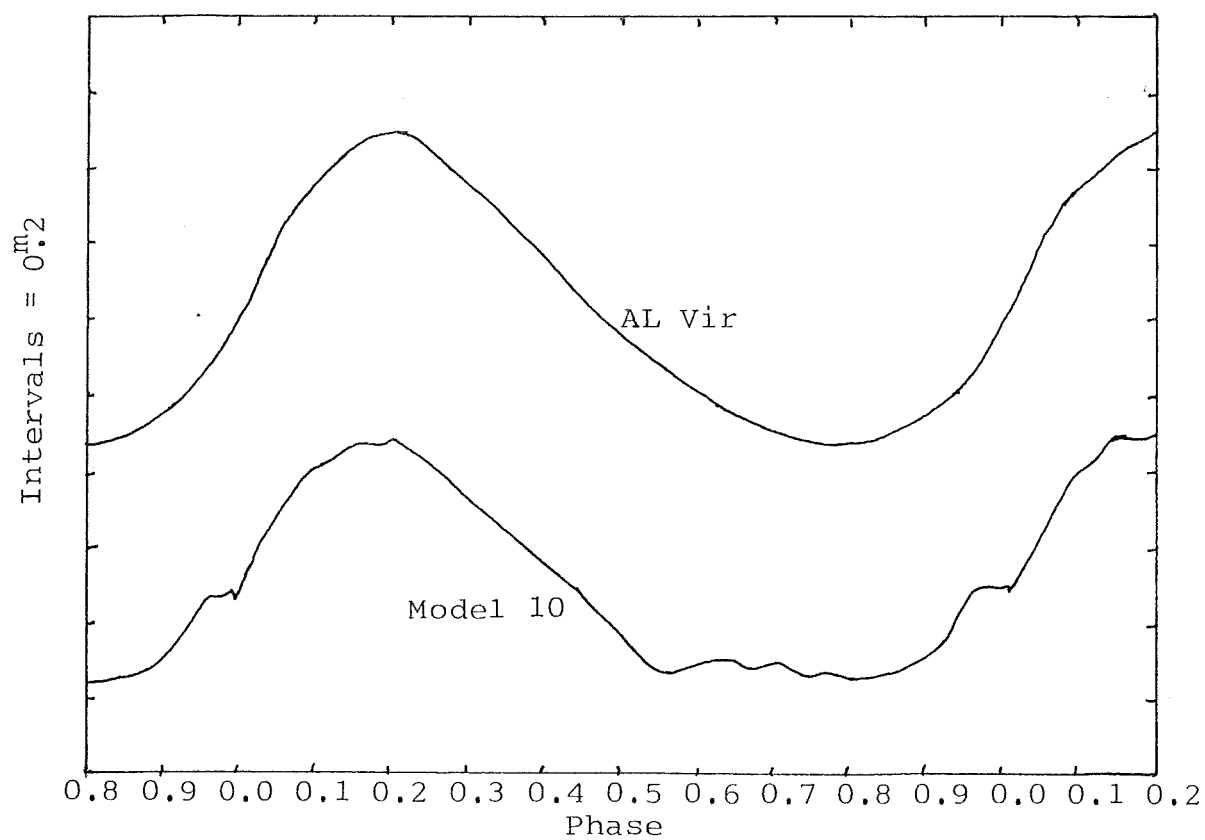


Figure 6.67 The light curves of model 10 and AL Vir

flat-topped light curves were less successful, but showed promise, and could probably be improved by the inclusion of convection and (perhaps) by using an improved external boundary condition.

Because of the lack of observed velocity curves, it has not been possible to compare those produced by the models with observations. In general terms the high asymmetry of the model velocity curves does seem to be what is needed, but more observations are required here.

6.12 RV TAURI AND OTHER "PECULIAR" BEHAVIOUR

In carrying out this survey of the population II instability strip some "peculiar" behaviour might be expected in a few models, whether it be numerical instabilities or a real physical effect. For these stars in particular we might expect to see some signs of so-called RV Tauri behaviour, or behaviour similar to that seen in the RV Tauri variables. RV Tauri stars show "period-doubling", caused by the alternation in the light and/or velocity curves of larger and smaller amplitudes, and possibly longer and shorter periods. The cause of this behaviour in these stars is not known.

In the W Virginis variables we do see small changes in the periods and amplitudes that seem to be more or less random in time. In the models produced for the survey are either of these features seen?

Of the 25 survey models it seems that numbers 14, 15, 22 and 24 best exhibit some sort of RV Tauri behaviour. In the latter three it is really only incipient and most easily seen in the velocity curves. In model 14 we see a clear demonstration of the alternation of periods. But this model also provides another puzzle. During the time the model was studied (approximately 50 periods) it changed from the RV Tauri behaviour to a more normal "single period" behaviour for about 8 - 10 periods, and then back again. This switching occurred roughly every 8 - 10 periods, the switch from one mode to the other taking just 3 - 4 periods. Figure 6.68 illustrates the switch from normal behaviour to the RV Tauri behaviour. The period of model 14, in its single period behaviour, was 16.0 days. In its RV Tauri mode the period was 32.0 days, made up of one period of ~ 19 days and one of ~ 13 days. There are several questions presented by this model. Firstly, when in its RV Tauri state, is it really exhibiting what is seen in the observed RV Tauri stars, or is it alternating in some other way? Then we must ask what causes this behaviour, and also what causes the alternation between two types of behaviour.

When in its RV Tauri state model 14 shows an alternation in period, a change in the shape of the light curve (the shorter period is F-type, the longer period is C-type), and an alternation in the amplitudes of both the light and velocity curves (from 1.0 mag. and 70 km/s to 2.3 mag. and 80 km/s). These changes seem to be characteristic of most observed RV Tauri behaviour (see, for example, J.P.Cox 1974; Payne-Gaposchkin 1951). The major difference is that observed RV Tauri variables have periods greater than 20 days (that is the time for one oscillation, not the period of exact

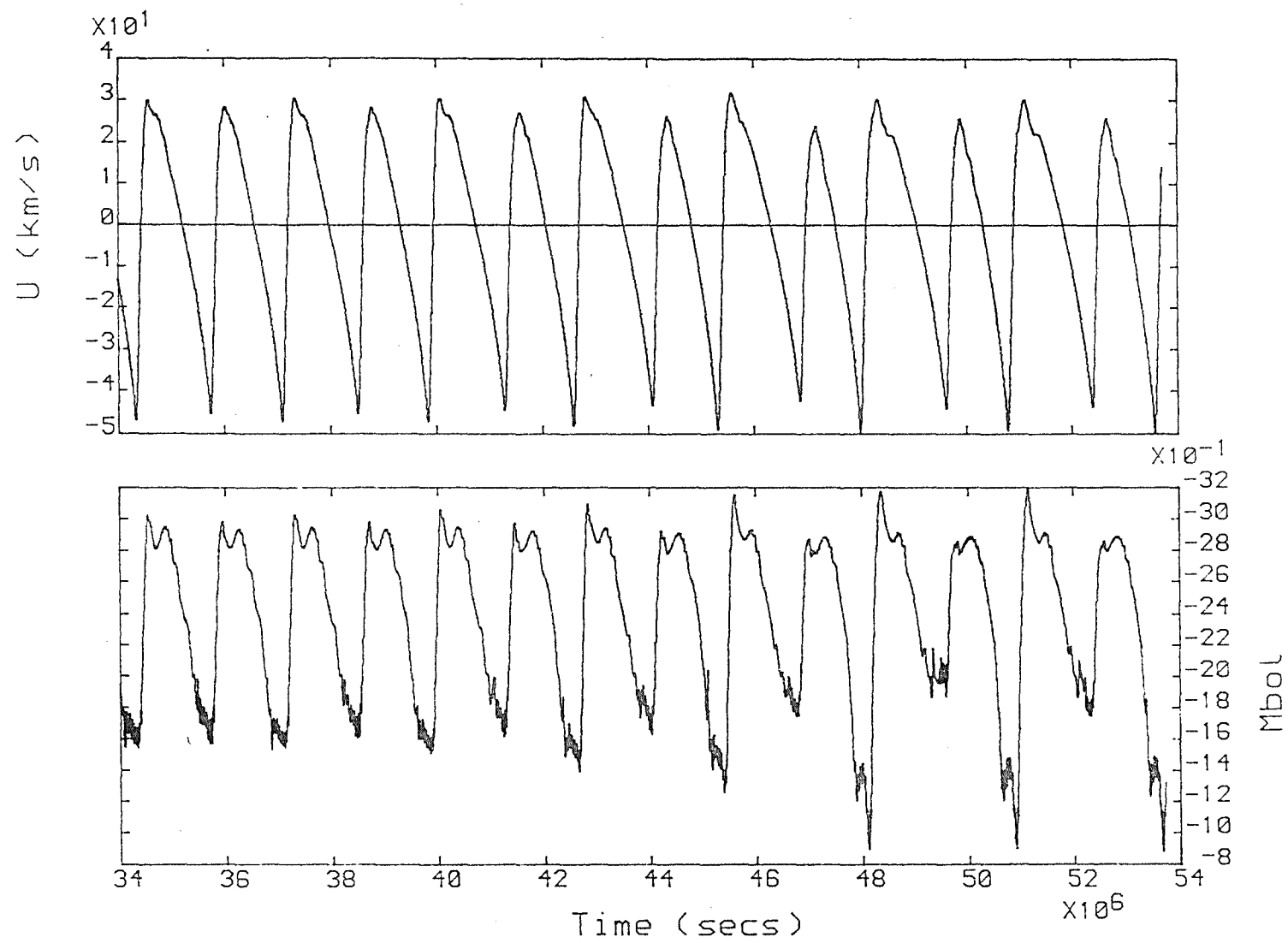


Figure 6.68 The light curve of model 14 as it switches modes

repetition). So what is seen in this (and other) models may be RV Tauri behaviour, but it might also be caused by the method of modelling used, and merely look like RV Tauri behaviour without having a real physical counterpart.

What seems to be the cause of the behaviour in the models? To help with this, two other models can be examined, numbers 20 and 24. Both show RV Tauri behaviour as described, but to a lesser extent. In both of these models, and in the RV Tauri state of model 14, the outer radius boundary is not well connected to the rest of the model; in fact it does not "return" once per period, but once every second period. On the return of the outer zone a larger velocity amplitude results. To be precise, in model 20 it is not the outer zone that is doing this, but zone N-1, since the outer zone has by now escaped the rest of the model.

Model 20 presented a very interesting case. The model reached full growth quickly, but was still irregular in its pulsation, with no consistent periodicity. After some time it settled down into the more or less reliable behaviour shown here. On examination it was discovered that, whilst showing unreliable behaviour, the outer zone was only tenuously connected to the rest of the model, and was exhibiting wildly irregular oscillations. Eventually this zone "escaped", with its outward velocity exceeding the escape velocity. At this time, with the "disturbance" of the outer zone gone, the model settled down.

The velocity history for model 20 (figure 6.63) shows the outer zone heading steadily away at above escape velocity. This seems to show that the outer zone has quite an effect on the light and velocity curves of the model. Possibly, in the case of the outer radius returning every second period, it might cause RV Tauri-like behaviour. All this of course is a possible explanation only for the events seen in the models, not in real stars. Do these descriptions have physical analogues, and is it reasonable to expect these events to occur in real stars? Firstly the loss of the outer zone is obviously "mass loss", but this is equally obviously a very crude description of any real mass loss that might occur in these stars. It is known that mass loss does occur in red variables, and might occur in RV Tauri stars.

Secondly, in reference to the RV Tauri behaviour, we might have a thin atmosphere tenuously connected to the envelope of the star. As the star pulsates, this atmosphere is pushed and pulled around, but since the connection is loose it can only follow the motion in an approximate manner. It will soon lose synchronization and wobble around in a less certain way. Whether this atmosphere would have enough energy to affect the rest of the star is another matter. What might be happening is that another oscillation of longer period is superimposed on the star, affecting the main star and the atmosphere (the latter to a greater extent because of its lower inertia). To examine these possibilities a linear analysis would be required, possibly even a non-radial pulsation analysis to look at oscillations in a tenuous atmosphere.

To conclude, it appears that the behaviour might well be "real", but highly over-estimated because of the nature of the model, which was not set up to study these effects. A more specialized modelling technique aiming at reproducing these effects might be a future step in this study.

6.13 THE EFFECTS OF VARYING MASS AND OPACITY

To gain more information about these stars and about the effects of varying some parameters, nine further models, in addition to the survey models, were produced; one for a mass $0.5 M_{\odot}$, five for a mass of $0.8 M_{\odot}$, and three using the Cox-Stewart opacities instead of the Carson opacities. Of these last three, two used the Christy formulation of the Cox-Stewart opacity (Christy 1966a) and one used the opacity table given for the King Ia mix (Cox and Tabor 1976).

For model 51, with $M/M_{\odot} = 0.5$, the other parameters used were $\log(L/L_{\odot}) = 3.0$, $\log T_e = 3.76$. Comparing this with model 18 we find little difference, except of course that model 51 has a longer period. Comparing 51 with a model of similar period, for instance model 19, we find even less difference between them. It seems that the main differences that using $M/M_{\odot} = 0.5$ would produce would be in the position of the instability strip. This is also discussed in section 2.3, where arguments for using $M/M_{\odot} = 0.6$ are discussed. Basically we see that using $M/M_{\odot} = 0.5$ would most likely not alter the survey results significantly.

The five models produced using $M/M_{\odot} = 0.8$ give a different picture. The instability strip for models of $0.8 M_{\odot}$ would be in entirely the wrong place. For instance at $\log(L/L_{\odot}) = 3.0$ and $\log T_{\text{eff}} = 3.76$, where we would expect to find a crested light curve variable, we get the light curve of model 85. In none of the five models of $0.8 M_{\odot}$ do we see a crested light curve, nor do we see a Kwee flat-topped curve, although the light curve of model 84 might be called flat-topped. The general conclusion would be that $0.8 M_{\odot}$ is too high a mass for the W Virginis variables in this period range, except possibly for any "unusual" stars that might lie in the same general area on the HR diagram. Another argument against this mass is that the He II driving is significantly greater, giving amplitudes that are far too large. As seen in section 2.2 the incorrectness of this mass is not surprising for other reasons.

These six models show that the choice of $M/M_{\odot} = 0.6$ was good. The masses of the W Virginis variables will vary, and may vary so as to produce the two Kwee classifications (as argued in section 6.6) but they will very likely lie near $0.6 M_{\odot}$.

This project has used the Carson opacities as part of its atomic data, in preference to the earlier opacities of Cox et al. of Los Alamos, and a comparison of these opacities is in order. To this end three models were calculated using the Cox opacities, in two forms. Two were calculated using the Christy formula, and one was calculated using the Cox and Tabor (1976) opacity for the King Ia mix ($Y=0.299$, $Z=0.001$).

Firstly we consider the model K1, which used the King Ia opacity. This has stellar parameters of $M/M_{\odot} = 0.6$, $\log(L/L_{\odot}) = 3.0$ and $\log T_e = 3.76$, the same as model 18. A direct comparison between these models is not possible because the King Ia mix has 30% helium to the 25% of the Carson opacity used. The periods are almost identical (16.0 days to 15.9 days), but the light and velocity curves are very different.

The light curve of model K1 is very asymmetric, showing a very rapid rise to light maximum, and also does not show the same crested light curve shape of model 18. It does not resemble the Kwee observed light curves very well at all in fact. This could be due to the increased helium abundance (which would give greater driving and thus higher asymmetry), or to the Cox-Tabor opacity. The model's work function does show a greater He II driving, and very little H driving.

Another comparison for these stellar parameters cannot be found using Cox opacities with 25% helium, because the model would be blueward of the blue edge for these opacities (see section 2.3). However the comparison can be made at other values of $\log(L/L_{\odot})$ and $\log T_e$ for 25% helium and using the Christy formulation of the Cox opacities. Models C1 and C2 do this.

Model C2, at $\log(L/L_{\odot}) = 2.9$ and $\log T_e = 3.75$ shows very different behaviour from model 13 which has the same stellar parameters, differing only in the opacity used. The period is significantly different, as are the light and velocity curves. The light curve of model 13 is undoubtedly of the crested variety, and while the light curve of model C2 has a secondary bump it is merely incipient and considerably later

in phase. In fact at similar periods in the survey models, a light curve like that of model C2 is not seen, and such a light curve is also not seen amongst the available observed stars.

On comparing the detailed velocity histories of these two stars (figures 6.55 and 6.69) we can see only some differences in the velocities. The reflected Christy "echo" is weaker and does return to the surface a little later for the Cox opacity. The asymmetry of the velocity curve is greater for model C2, having a faster rise to maximum. Why this shock front should be stronger for the Cox opacities is not obvious, though it might be caused by the higher hydrogen opacity seen in the Los Alamos opacities.

Model C1, with $\log(L/L_{\odot}) = 2.8$ and $\log T_e = 3.73$, serves as a comparison for survey model 8. Again there is a significant disparity in the periods, and the light and velocity curves do not match well at all. Model 8 is definitely not C-type, and is classified as F, but model C1 would be classified as C-type, although its light curve does not look much like Kwee's crested curves.

The general conclusions that can be made are that whilst the Carson opacities can reproduce at least the crested variety of light curves very well, using the Cox opacities for some comparable models did not produce results that were as good. A full survey using the Cox opacities would of course be necessary before firm conclusions regarding their use in these types of stars could be reached.

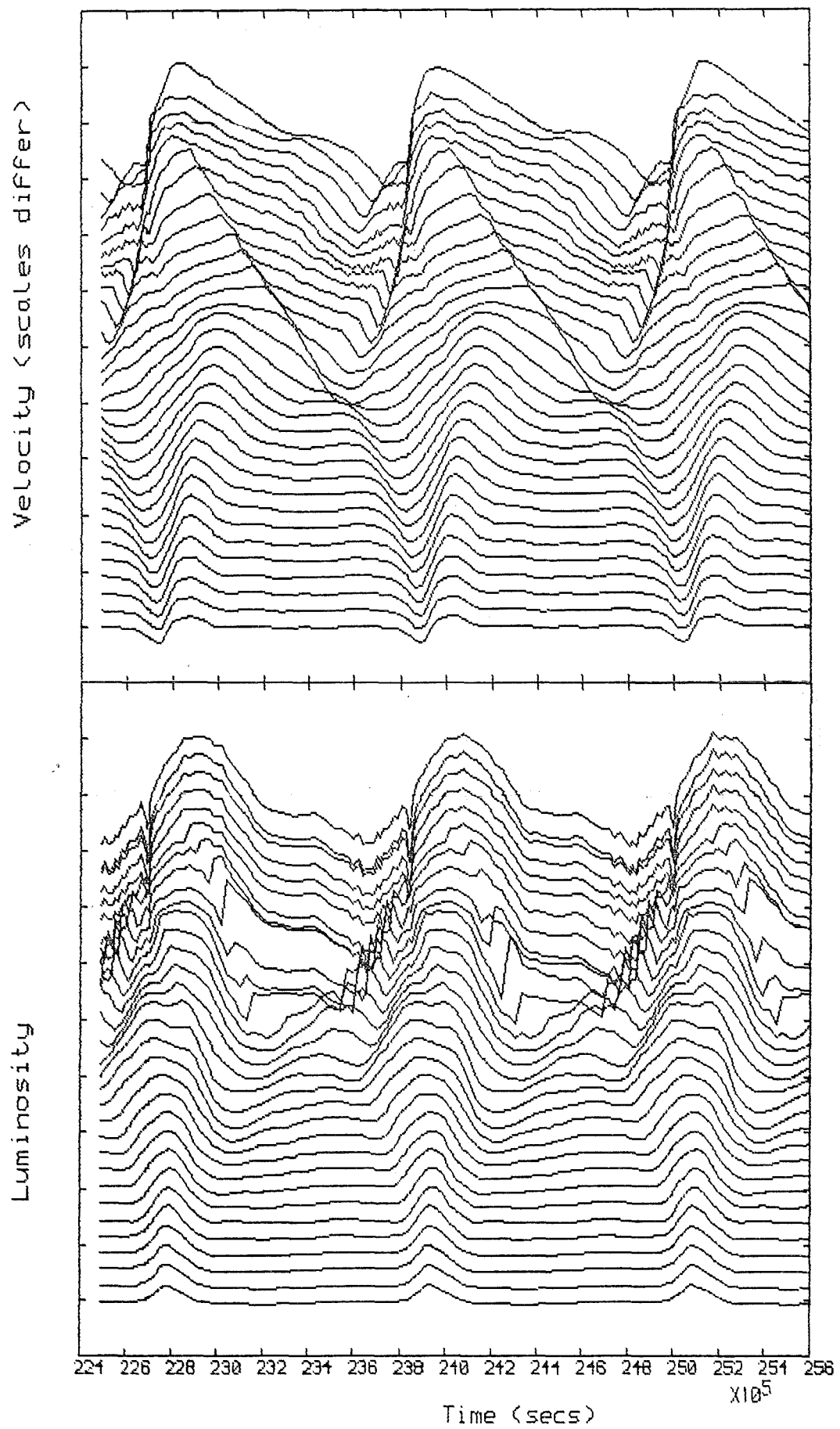


Figure 6.69 Velocity and luminosity histories of model C2

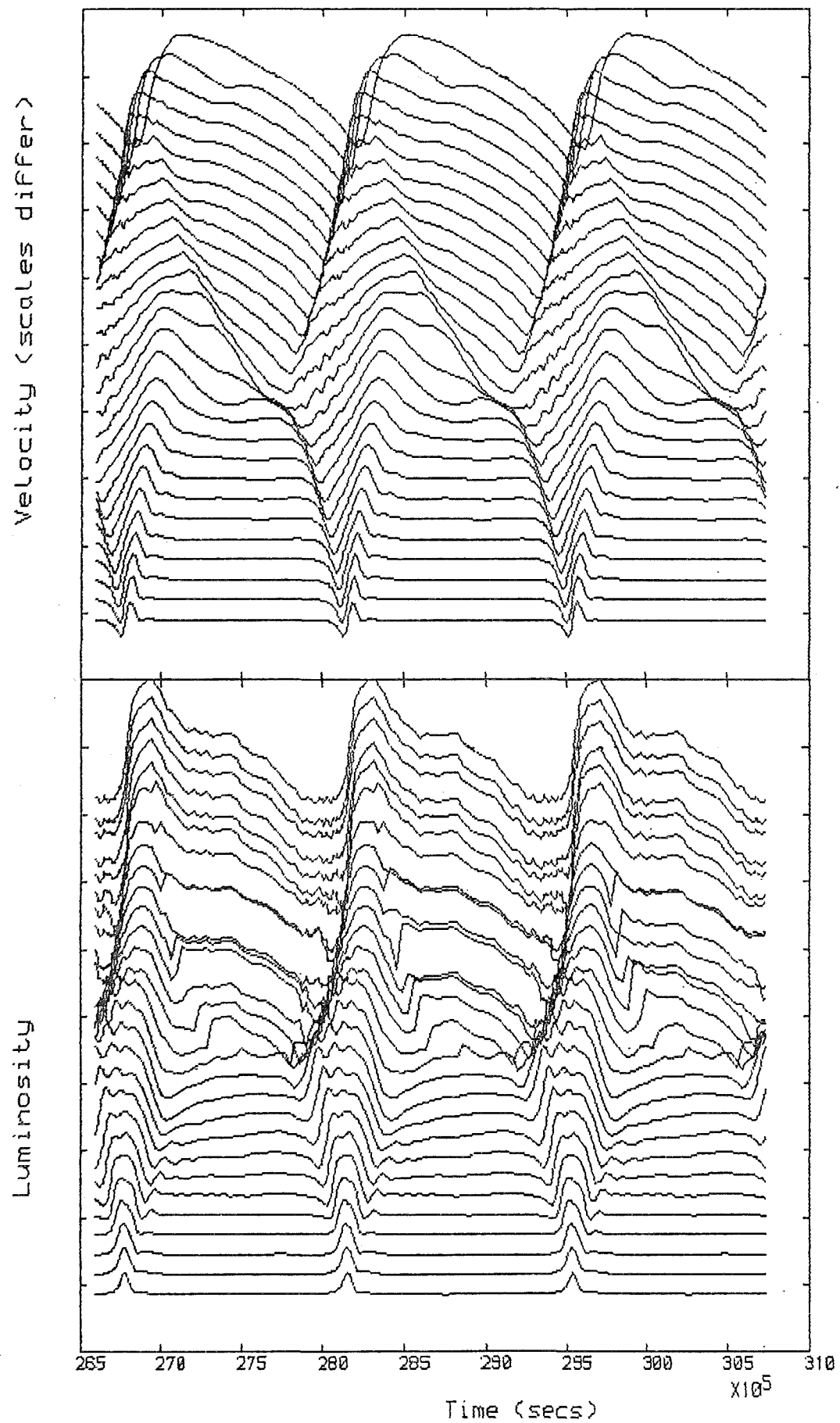


Figure 6.70 Velocity and luminosity histories of model K1

CHAPTER 7

CONCLUSION

The major aim of this work was to produce hydrodynamical models of the W Virginis variables (population II cepheids) with periods in the range ten to twenty days. In particular it was hoped that by using the Carson opacities not only could the general features of these stars be reproduced in an instability strip survey, but also that good models could be made of individual stars, simulating the light curves closely. This aim was at least partially achieved.

As detailed in section 2.2 the observed stars in this period range could be split into two main types (with a third unclassified type). The 25 survey models constructed in this work to cover some of the instability strip managed to reproduce all three of these types with varying degrees of success, as it proved much more difficult to reproduce the flat-topped variety. The general features of the observed stars - the position of the variables in the HR diagram, the periods, amplitudes and light and velocity curve shapes - were fairly well reproduced. Certainly agreement to within the observational errors is obtained. Unfortunately, observations of these stars are scarce, particularly observations of radial

velocity curves. There is some evidence that the observational period-radius relation for these stars splits into two, representing extremes of a gradation from flat-topped to crested light curves. Assuming a similar period-mass-radius relation for the two types this indicates that a range of masses may be responsible for the dichotomy. This ties in quite well with evolutionary arguments for feeding stars into the instability strip at this level. Unfortunately, the survey models produced were all of the same mass, $0.6 M_{\odot}$. Some models were constructed with differing masses, but the variation was not sufficient to add theoretical weight to this supposition. More work could be done here, using a range of masses, to check this argument.

In section 6.10, models of three observed stars were presented, CS Cassiopeia, FI Scutum and AL Virginis. The first two of these have crested light curves, and we saw that the models reproduced the pulsational features and the light curves very well. With the variation in crested light curves seen in the models it would seem that this type can be modelled very well.

AL Vir had a featureless, unclassified light curve, reproduced very well in the comparison model. This shows that the shorter period, rather characterless, observed light curves can also be modelled.

Unfortunately it has not been possible to produce an equally good model for any of the observed flat-topped light curves. Most of the modelled curves labelled as F-type still had a slight crest, or were of the wrong shape (viz. model 1). This failure could be due to many things. We expect to find

these stars at comparatively low values of $\log(L/L_{\odot})$ and $\log T_e$, and it is here that the best F-type models were constructed, and also where most of the difficulties were encountered. These difficulties may have been caused by an inadequate outer boundary condition, but the alternate cause of the problem may be excessive driving in the He II zone and (perhaps) also in the hydrogen zone. Convection in these stars may not bring about stability, but it may reduce the driving significantly, thereby perhaps making the modelling easier near the red edge. This may enable the production of a good flat-topped model light curve.

During the course of this work it was realised that RV Tauri type behaviour might be observed in some of the models. This had been seen before by Vemury and Stothers (1978) in models of classical cepheids. Indeed a suspicion of such behaviour was observed in some stars, though it may be that these stars were still settling into their final state. What was not expected was the behaviour of model 14. The very model dependent explanations of model 14 (and possible RV Tauri behaviour) would need to be explored with a far more realistic description of what happens in the outer layers of these stars, to see if there are equivalent events in the very tenuous atmospheres of these stars and also of the longer period red variables.

A comparison of the Carson opacities with the earlier opacities of Cox and his co-workers was not one of the aims of this study; however, since few published models of these stars (using the Cox opacities) exist, some comparison was done. The easiest direct comparison, changing only the opacity used, is

between model 13 and model C2. We saw here that use of the Carson opacities led to a much better agreement with observation, a conclusion also reached by CSV in their work on the BL Herculis variables. At the present time it seems that some problems may still exist in the Carson opacities; the low temperature opacities are suspect, and the helium II opacity may be over-estimated, causing excessive driving. In general, however, it seems that use of the Carson opacities produces better agreement with observations.

This study largely succeeded in its aim of modelling W Virginis stars, but has indicated in many places that more work is needed. More extensive observations of the light and velocity curves (particularly the latter) of these stars would be very useful in confirming our theoretical understanding of them. The observed velocity curves are currently too scarce to be of much use in a survey.

On the theoretical side a great deal more work can be done. The outer boundary condition normally used in hydrodynamic codes is still not very realistic, and appears to cause difficulties when used in models of stars with very tenuous outer layers. Some sort of running-wave boundary condition may well help here.

The major improvement on this work would probably be to include convection as a form of energy transport. There are now several published methods of doing this, but as yet they all involve even more "unknown" parameters, and the search for better ways to handle convection in pulsation is by no means over. The inclusion of convection would probably have little effect on most of the crested and unclassified model light

curves produced, but could well help in modelling the flat-topped variety.

Both of these improvements may help in studying the "peculiar" models (those with suspected RV Tauri behaviour), but in the light of the ideas presented it may be that something new is needed to accurately represent what is happening. Modelling the RV Tauri variables would seem to be the next step in moving up the population II instability strip, on the way across to the long period red variables.

CHAPTER 8

REFERENCES

Abt, H.A. 1954, Ap. J. Suppl. 1, 63

Aleshin, V.I. 1959, Russ. A. J. 36, 468

_____ 1964, Sov. Astron. 8, 154

Arp, H.C. 1955, A. J. 60, 1

Baker, N. 1966, in "Stellar Evolution", eds. R.F. Stein and
A.G.W. Cameron (Plenum Press) p333

Baker, N.H. and Gough, D.O. 1979, Ap. J. 234, 232

Baker, N. and Kippenhahn, R. 1962, Zeit. fur Astrophys. 54, 114

_____ 1965, Ap. J. 142, 868

Baker, N. and von Sengbusch, K. 1969, "Mitt. der Astron. Gesel."
No. 27, p162

Barker, T., Baumgart, L.D., Butler, D., Cudworth, K.M., Kemper, E.,
Kraft, R.P., Lorre, J., Rao, N.K., Reagan, G.H.,
and Soderblom, D.R. 1971, Ap. J. 165, 67

Bohm-Vitense, E. 1958, Zeit. fur Astrophys. 46, 108

_____ 1973, Astron. Astrophys. 21, 447

Bohm-Vitense, E., Szkody, P., Wallerstein, G., and Iben, I.

1974, Ap. J. 194, 125

Broglia, P. and Guerrero, G. 1973, Mem. Soc. Astron. Italiana

Nuova Ser. 44, 157

Carson, T.R. 1976, Ann. Rev. Astron. and Astrophys. 14, 95

Carson, T.R. and Hollingsworth, H. 1968, M. N. R. A. S. 141, 77

Carson, T.R., Mayers, D.F., and Stibbs, D.W.N. 1968,

M. N. R. A. S. 140, 483

Carson, T.R. and Stothers, R. 1976, Ap. J. 204, 461

_____ 1982, Ap. J. 259, 740

Carson, T.R., Stothers, R., and Vemury, S.K. 1981, Ap. J. 244, 230

Castor, J.I. 1971, Ap. J. 166, 109

Castor, J.I., Davis, C.G., and Davison, D.K. 1977, Los Alamos

Rept. LA6664

Christy, R.F. 1964, Rev. Mod. Phys. 36, 555

_____ 1966a, Ap. J. 144, 108

_____ 1966b, Ap. J. 145, 337

_____ 1966c, Ann. Rev. Astron. Astrophys. 4, 353

_____ 1967, Methods in Computational Physics 7, 191

_____ 1968, Quart. J. R. A. S. 9, 13

- Clayton, D.D. 1968, "Principles of Stellar Evolution and Nucleosynthesis", McGraw Hill
- Coutts, C.M. 1973, in "Variable Stars in Globular Clusters and Related Systems", ed. J.D.Fernie
(IAU Coll. No. 21, Reidel) p145
- Cox, A.N. 1979, Ap. J. 229, 212
- 1980, Ann. Rev. Astron. Astrophys. 18, 15
- Cox, A.N. and Stewart, J.N. 1965, Ap. J. Suppl. 11, 22
- Cox, A.N. and Tabor, J.E. 1976, Ap. J. Suppl. 31, 271
- Cox, J.P. 1955, Ap. J. 122, 286
- 1974, Rep. Prog. Phys. 37, 563
- 1980, "Theory of Stellar Pulsation" (Princeton)
- Cox, J.P., Cox, A.N., Olsen, K.H., King, D.S., and Eilers, D.D.
1966, Ap. J. 144, 1038
- Cox, J.P. and Giuli, R.T. 1968, "Principles of Stellar Structure", volumes 1 & 2 (Gordon and Breach)
- Cox, J.P. and Whitney, C.A. 1958, Ap. J. 127, 561
- Davis, C.G. 1972, Ap. J. 172, 419
- 1974, Ap. J. 187, 175
- Davis, C.G. and Davison, D.K. 1978, Ap. J. 221, 929
- Davis, C.G. and Bunker, S.S. 1975, in "Cepheid Modeling"
ed. D.Fischel and W.M.Sparks, (NASA)

Demers, S. 1969, A. J. 74, 925

Demers, S. and Harris, W.E. 1974, A. J. 79, 627

Demers, S. and Wehlau, A. 1971, A. J. 76, 916

Deupree, R.G. 1977a, Ap. J. 211, 509

————— 1977b, Ap. J. 214, 502

————— 1977c, Ap. J. 215, 232

————— 1977d, Ap. J. 215, 620

Dickens, R.J. and Carey, J.V. 1967, Roy. Obs. Bull. No. 129

Eddington, A.S. 1918a, M. N. R. A. S. 79, 2

————— 1918b, M. N. R. A. S. 79, 177

————— 1926, "The Internal Constitution of the Stars"
(Cambridge University Press)

Eggen, O.J. 1961, Roy. Obs. Bull. No. 29

Epstein, I. 1950, Ap. J. 112, 6

Fernie, J.D. 1963, A. J. 69, 258

Gingerich, O. et al. 1971, Sol. Phys. 18, 347

Gough, D.O. 1977, Ap. J. 214, 196

Hodson, S.W., Cox, A.N., and King, D.S. 1980, Spa. Sci. Rev.
27, 503

————— 1982, Ap. J. 253, 260

Hubbard, W.B. and Lampe, M. 1968, Ap. J. Suppl. Ser. 18, 297

- Iben, I. Jr. and Huchra, J. 1971, *Astron. and Astrophys.* 14, 293
- Iben, I. Jr. and Rood, R.T. 1970, *Ap. J.* 159, 605
- Joy, A.H. 1949, *Ap. J.* 110, 105
- Keller, G. and Meyerott, R.E. 1955, *Ap. J.* 122, 32
- King, D.S., Cox, A.N., and Hodson, S.W. 1981, *Ap. J.* 244, 242
- Kraft, R.P. 1972, in "Evolution of population II stars"
ed. A.G.D. Philips (Dudley Obs. Rept. No. 4)
- Kwee, K.K. 1967, *B. A. N. Suppl.* 2, 97
- 1967, *B. A. N.* 19, 260
- 1968, *B. A. N.* 19, 374
- Kwee, K.K. and Braun, L.D. 1967, *B. A. N. Suppl.* 2, 77
- Ledoux, P. and Walraven, T. 1958, *Handbuch der Physik* 51, 353
- Mengel, J.G. 1973, in "Variable stars in Globular Clusters and
related systems", ed. J.D. Fernie
(IAU Coll. No. 21, Reidel)
- Michalowska-Smak, A. and Smak, J. 1965, *Acta Astron.* 15, 333
- Mihalas, D. 1978, "Stellar Atmospheres", 2nd edition (Freeman)
- Payne-Gaposchkin, C. 1951, in "Astrophysics", ed. J.A. Hynek
(McGraw-Hill)
- 1956, *Vistas* 2, 1142
- Peterson, J.O. 1980, *Spa. Sci. Rev.* 27, 495
- Pickering, E.C. 1912, *Harvard Circ. No.* 172

Ralston, A. 1965, "A First Course in Numerical Analysis",
(McGraw-Hill)

Richtmyer, R.D. and Morton, K.M. 1967, "Difference Methods for
Initial Value Problems", 2nd ed. (Interscience)

Rosseland, S. 1949, "The Pulsation Theory of Variable Stars",
(Clarendon, also available from Dover, 1964)

Rudd, T.J. and Rosenberg, R.M. 1970, Astron. and Astrophys.
6, 193

Schwarzschild, M. 1958, "Structure and Evolution of the Stars",
(Princeton, also available from Dover, 1965)

Schwarzschild, M. and Harm, R. 1970, Ap. J. 160, 341

Shapley, H. 1914, Ap. J. 40, 448

Simon, N.R. and Schmidt, E.G. 1976, Ap. J. 205, 162

Stellingwerf, R.F. 1972, Astron. and Astrophys. 21, 91

_____ 1974, Ap. J. 192, 139

_____ 1975, Ap. J. 195, 441

_____ 1978, A. J. 83, 1184

_____ 1979, Ap. J. 227, 935

_____ 1982a, Ap. J. 262, 330

_____ 1982b, Ap. J. 262, 339

Stobie, R.S. 1969a, M. N. R. A. S. 144, 461

_____ 1969b, M. N. R. A. S. 144, 485

- _____ 1973, Observatory 93, 111
- _____ 1975, in "Multiple Periodic Variable Stars",
(IAU Coll. No. 29, Reidel) p87
- Stothers, R. 1974a, Ap. J. 194, 651
- _____ 1974b, Ap. J. 194, 695
- _____ 1976, Ap. J. 204, 853
- Stromgren, B. 1932, Zeit. fur Astrophys. 4, 118
- Sweigart, A.V. 1973, Astron. and Astrophys. 24, 459
- Tuggle, R.S. and Iben, I. Jr. 1972, Ap. J. 178, 455
- Unno, W. 1965, Publ. Astron. Soc. Japan 17, 205
- _____ 1967, Publ. Astron. Soc. Japan 19, 140
- Usher, P.D. and Whitney, C.A. 1968, Ap. J. 154, 203
- Vasiljanovskaja, O.P. and Erleksova, G.E. 1968, in "Non-periodic
Phenomena in Variable Stars" (IAU Colloquium,
Academic Press)
- Vemury, S.K. and Stothers, R. 1978, Ap. J. 225, 939
- Von Sengbusch, K. 1973, "Mitt. der Astron. Gesel." No. 32, p228
- Wallerstein, G. 1958, Ap. J. 127, 583
- _____ 1959, Ap. J. 130, 560
- Worrell, J.K. 1982a, Private communication
- _____ 1982b, Private communication

Zhevakin, S.A. 1953, Russ. A. J. 30, 161

_____ 1954a, Russ. A. J. 31, 141

_____ 1954b, Russ. A. J. 31, 335

_____ 1963, Ann. Rev. Astron. Astrophys. 1, 367